ELUCIDATING THE ROLE OF WNT INDUCED SECRETED PROTEIN 3 (WISP3) IN MITOCHONDRIAL FUNCTION

Thesis Submitted for the degree of

Doctor of Philosophy (Science)

in

Biotechnology

by

DEEPESH KUMAR PADHAN

Department of Biotechnology

University of Calcutta

2022

I dedicate this thesis to my family, teachers and friends

Acknowledgements

The first person I want to acknowledge for my research work and for this thesis is **Dr. Malini Sen,** my advisor and supervisor. I would like to express my sincere gratitude to my supervisor for recognising me as a Ph.D. student and giving me a chance to work with her. Being novice, it was my privilege to learn how to think, execute experiments and analyse data under her supervision. I specially thank her for providing me all the regents and infrastructural facility as and when needed. I am very thankful to her for providing me financial support after my fellowship tenure was over. Her immense knowledge, passion for science, perseverance and discipline kept me motivated throughout my journey.

I extend my heartfelt thanks to funding agencies for providing me financial support for 5 years of my research tenure. I was supported by CSIR fellowship and my work was funded by DST and DBT, Govt. of India.

I am also thankful to **Prof. Samit Chattopadhyay,** former Director and **Prof. Arun Bandopadhyay,** present Director of IICB for giving me a wonderful opportunity to work in this esteemed institute and providing necessary infrastructural facilities.

Beside my supervisor, I convey my regards to faculties of this institute who have been very supportive to extend their help at various phases of my research. Especially I thank **Dr. Sib Sankar Roy** and **Dr. Jayati Sengupta** for allowing me to use spectrophotometer, **Dr. Partha Chakraborti** for Chemi documentation system and Nanodrop, **Dr. Pijush Kanti Das** for electroporator and **Dr. Uday Bandopadhyay, Prof. Samit Chattopadhyay,** for providing necessary instrumental support and reagents as and when required.

I am thankful to **Department of Biotechnology, University of Calcutta** where I enrolled as a Ph.D. student. I specially thank **Prof. Koustubh Panda** for his kind help in various phases of my research and assessment.

I am extending my heartfelt thanks to **Prof. Gourisankar Ghosh**, UCSD, California, USA who not only given me critical suggestions on my research problems but also motivated me. He also helped in performing LC-MS/MS analysis.

I would like to convey thanks from depth of my heart to my teachers starting from schooling to post graduate studies. I specially thank my teachers of **Zoology Department, Kuchinda College, Kuchinda** and **School**

of Life Sciences, Sambalpur University for their constant encouragement and motivation during my entire period of research.

I gratefully acknowledge all the staffs of CSIR-IICB for helping me in many official matters which led to successful completion of my dissertation work. My special thanks to **Sounak da** and **Diptodeep da** for confocal microscopy, and **Tapas da** for helping in chemi-documentation system. I especially thank IICB Club for organizing various cultural events and picnic party which was really essential as a stress busters in my entire tenure.

I extend my regards to **Dr. Sushil Kumar Mahata**, UCSD, California, USA for performing Transmission Electron Microscope and analysis of respective data. I am thankful to **Dr. Rajeeb Kumar Swain**, ILS, Bhubaneswar for showing interest in my research work and providing me guidance in maintenance of zebrafish. Also he has given his precious time to demonstrate microinjection of zebrafish embryo in his lab and providing me an opportunity to learn by hands on practise. Also I express my thanks to **Dr. Rajesh Ramachandran**, IISER Mohali and **Dr. Jayanta Choudhury**, Managing Director, WBLDCL for their helpful suggestions related to zebrafish maintenance.

My special thanks to my friends **Paras, Anand, Kamran, Subhasis, Tanaya, Dheerendra, Koushik, Arijit, Jeet, Rajiv, Sandip, Debojyoti, Moumita, Pinaki Prasad, Rutambhara, Ashapurna, Usharani, Satyaranjan, Tikeswar, Soumya Ranjan, Sobhijit, Chinmay** and seniors **Dipayan da, Bimal da, Bhisma da , Satya da** of our institute as well as other institute for helping in various aspects in my research throughout my Ph.D tenure. I express my heartfelt thanks to **Anand Gupta** for giving his precious time during zebrafish electroporation. I am also thankful to all my friends and apologize for not mentioning your names here but you know how important you are to me. My special thanks to **Nirali Bage** and **Ratan Bage** for their constant encouragement and support during my tenure in CSIR-IICB.

As I joined lab, I was fortunate enough to come in contact with my loving and supportive seniors **Dr. Suman Kundu, Dr. Archya Sengupta, Dr Kaushiki Biswas, Dr. Milan Patra, Dr. Arijit Chakraborty,** my friends **Dr. Suborno Jati, Tresa Rani Sarraf, Indrani Das** and **Deboshruti Nath** and my juniors **Shreyasi Maity, Ananya Ganguly** and **Soham Sengupta**. I thank each and every one for experimental help, moral support and all the fun activities that we had in last 6 years. Apart from that I thank my supervisor and fellow lab mates for critically evaluating my dissertation work through repeated presentations and tolerating me in lab meetings.

Initially I started working with **Dr. Milan Patra**, who was very helpful, driven towards work, hardworking with a positive mind. I express my thanks for a great research partnership that we had during my first two years where I learnt a lot from him. His guidance and support helped me a lot.

I owe my thanks to **Dr. Archya Sengupta** for not only assisting in my research work but also providing me moral support in my tough times which driven me to complete this dissertation. He established zebrafish facility in our lab and helped me a lot in expanding my dissertation work using zebrafish as a model organism. We had a strong research partnership and without him it seems impossible to complete my thesis. I express my thanks to **Dr. Arijit Chakraborty** for providing necessary suggestions related to my work and providing moral support during my journey. I express my thanks to **Dr. Suman Kundu** for being with me in my difficult times and helping me whenever required in all possible ways. I also thank my junior **Ananya Ganguly** for assisting me in generation of knock out cell lines and maintenance of zebrafish as well as giving moral support whenever I felt down. I am thankful to **Dr. Suborno Jati** and **Shreyasi Maity** for especially helping in microscopic studies. I express my heartily thanks to my friend **Tresa Rani Sarraf** for supporting in my works as and when it was necessary and providing me suggestions related to my work and moral support during my tenure.

I also convey my regards to the interns **Sony, Nibedita, Sumela, Megha, Pritam, Arijit** who have joined in our lab and helped me in various ways. I specially thank **Pritam Chakraborty** and **Indrajit Sikdar** for giving me a helping hand in maintenance of zebrafish facility in our lab.

I am grateful to my loving and caring brothers **Dipak da, Jugal da, Ashok da** and **Shiv da** who were not only my roommates but also guided me during my ups and downs of my Ph.D journey.

Last but not the least I would like to acknowledge my family members for their constant support and encouragement in completion of my dissertation work. I bow my heads in front of my parents **Mr Gunanidhi Padhan** and **Mrs Sabita Padhan** who always stood beside me and made me strong both mentally and emotionally. Without their unconditional support it was impossible for me to stand in this position.

Deepesh Kumar Padhan

CONTENTS

ABBREVIATIONS

ACN	Acetonitrile
ATP	Adenosine triphosphate
ATP5A1	ATP synthase F1 subunit alpha
AVSD	Atrioventricular septal defects
BN-PAGE	Blue native - polyacrylamide gel electrophoresis
BSA	Bovine serum albumin
CCN	Cellular communication network
cDNA	Complementary deoxyribonucleic acid
CK	Cysteine knot
COX 4	Cytochrome c oxidase subunit 4 isoform 1
CRISPR	Clustered regularly interspaced short palindromic repeats
DMEM	Dulbecco's modified eagle media
DMSO	Dimethyl sulfoxide
DTT	Dithiothreitol
EDTA	Ethylenediaminetetraacetic acid
EGTA	Ethylene glycol-bis(β-aminoethyl ether)-N,N,N′,N′-tetraacetic acid
ER	Endoplasmic reticulum
EST	Expressed sequence tag
FBS	Fetal bovine serum
HEPES	4-(2-hydroxyethyl)-1-piperazineethanesulfonic acid
HGNC	HUGO gene nomenclature committee
HRP	Horseradish peroxidase
HUVEC	Human umbilical vein endothelial cell
IGFBP	Insulin growth factor binding protein 3
MAV	Myeloblastosis-associated virus
mRNA	Messenger RNA

MTCO1	Cytochrome c oxidase I
MTT	3-(4,5-dimethylthiazol-2-yl)-2,5-diphenyltetrazolium bromide
NADH	Nicotinamide adenine dinucleotide
NBT	Nitro blue tetrazolium chloride
NDUFB8	NADH dehydrogenase [ubiquinone] 1 beta subcomplex subunit 8
NDUFS1	NADH-ubiquinone oxidoreductase 75 kDa subunit
NHEJ	Non homologous end joining
OMIM	Online mendelian inheritance in man
OMM	Outer mitochondrial membrane
OXPHOS	Oxidative phosphorylation
PCR	Polymerase chain reaction
PPRD	Progressive pseudo rheumatoid dysplasia
PVDF	Polyvinylidene difluoride
RER	Rough endoplasmic reticulum
RGB	Red green blue
ROS	Reactive oxygen species
RT-PCR	Reverse transcriptase polymerase chain reaction
SDHB	Succinate dehydrogenase [ubiquinone] iron-sulfur subunit
SDS-PAGE	Sodium dodecyl sulfate – polyacrylamide gel electrophoresis
siRNA	Small interfering RNA
TBST	Tris-buffered saline, 0.1% Tween 20
TEM	Transmission electron microscopy
THSP1	Thrombospondin type I
UQCRC2	Cytochrome b-c1 complex subunit 2
VDAC1	Voltage-dependent anion-selective channel 1
VWC	Von willebrand factor type c
WISP	Wnt induced signaling protein
Wisp3/*wisp3*	WISP3 protein/gene nomenclature in zebrafish according to ZFIN

ABSTRACT

WISP3 (Wnt1 inducible secreted protein 3), alias CCN6 is a member of CCN family of secreted growth factors. Mutations in WISP3 leads to an incurable autosomal recessive musculoskeletal disorder PPRD (Progressive Pseudo Rheumatoid Dysplasia), which is associated with progressive cartilage loss, muscle weakness and restricted skeletal development. The underlying molecular mechanism of PPRD pathogenesis and its connection with WISP3 is not yet understood. As a multi-domain protein, WISP3 has potential to interact with other proteins to perform different functions. Previously we have observed that WISP3 localizes to mitochondria and regulates mitochondrial functions by regulating mitochondrial ROS and ATP production. In this study, we are focussed in detail on how WISP3 regulates mitochondrial function using both chondrocyte cell line and zebrafish as a model organism. It is evident from size-exclusion chromatography, BN-PAGE and 2D BN/SDS PAGE of crude mitochondria that WISP3 migrates as a high molecular weight complex and associates with different complexes of mitochondrial electron transport chain in both chondrocyte and skeletal muscle of zebrafish. Partial WISP3 depletion in chondrocyte lines causes increased Complex-I activity and assembly. CRISPR Cas9 generated WISP3 mutants show decreased Complex I assembly and activity as well as accumulation of damaged mitochondria as compared to wild type. In zebrafish moreover, depletion of Wisp3 by *wisp3* morpholino causes diminished respiratory complex activity/assembly as well as mitochondrial dysfunction in skeletal muscle. In brief, the regulatory influence of WISP3 on mitochondria can range from repression to activation, depending on its protein interaction partners, which can differ between tissue and cell types. Overall, our results suggest that WISP3 (CCN6) plays a vital role in the maintenance of mitochondrial respiration and muscle integrity. WISP3 related defects in mitochondria could be an underlying cause of muscle weakness in PPRD. This study may pave a path towards better understanding of PPRD and other musculoskeletal diseases.

CHAPTER I

INTRODUCTION

INTRODUCTION

1.1 Introducing WISP3

WISP3 (Wnt Induced Secreted Protein 3) also known as CCN6 (Cellular Communication Network Factor 6) is a member of the CCN [Cyr61 (Cysteine rich protein 61), CTGF (Connective tissue growth factor), Nov (Nephroblastoma overexpressed gene)] family proteins (Brigstock, 2003). The acronym CCN was used based on the first letter of the first members to be discovered. The family comprises of six members, Cyr61 (CCN1), CTGF (CCN2), Nov (CCN3), WISP1 (CCN4,) WISP2 (CCN5) and WISP3 (CCN6). As WISP1, WISP2 and WISP3 have high sequence homology with Cyr61, CTGF and Nov, they are also included in CCN family (Pennica *et al.*, 1998; Sen *et al.*, 2004; Holbourn, Acharya and Perbal, 2008; Perbal, 2013). CCN is now called as Cellular Communication Network Factor based on nomenclature given by HUGO Gene Nomenclature Committee (HGNC) (Perbal, Tweedie and Bruford, 2018).

WISP3 maps to chromosome 6q21–22, codes for a 354 amino acid protein, and is expressed in skeletally derived cells including human synoviocytes, articular cartilage chondrocytes and bone marrow derived mesenchymal progenitor cells (Hurvitz *et al.*, 1999). The CCN family encodes cysteine-rich secreted proteins, which modulate cell growth, survival, cell migration and differentiation. The name WISP3 is based on the homology of WISP3 with WISP1 and WISP2, which are upregulated in Wnt-1 transformed cells (Pennica *et al.*, 1998; Sen *et al.*, 2004). However, WISP3 (CCN6) has not been found to be induced by Wnt-1.

Figure I: Different structural domains of WISP3.

WISP3 has a multi-modular architecture with putative functional domains. The signal peptide domain (SP) contains signal sequence that may involve in protein secretion. The insulin-like growth factor binding protein (IGF-BP) domain may involve in physical interaction with Insulin-like growth factors. Von Willebrand factor type C (VWC) repeat domain may participate in oligomerization of extracellular membrane proteins like procollagen, glycosyalted mucins, etc. Thrombospondin type I motif repeats (THBS)

domain may be involved in the binding of CCNs to sulfated glycosaminoglycans either at cell surfaces or in the extracellular matrix. The cysteine knot (CT) domain, may participate in dimerization and receptor binding (Fig. I). The modular structure of the WISP3 and other CCN family members suggests that these proteins may have potential to execute complex functions in different cellular aspects (Engel, 2004; Schutze *et al.*, 2005; Holbourn, Acharya and Perbal, 2008; Katsube *et al.*, 2009; Perbal, 2013). Following is a brief description of CCN family of proteins.

1.2 CCN family members at a glance

The multifunctional CCN family of proteins are cysteine-rich proteins consisting of six members, designated as CCN1-CCN6. The acronym CCN was first introduced by Peter Bork in 1993 in the name of first three founding members of this family namely Cyr61 (cysteine-rich protein 61), CTGF (connective tissue growth factor) and NOV (nephroblastoma overexpressed gene) which are also named as CCN1, CCN2 and CCN3 respectively (Bork, 1993). These genes are structurally related to each other and share 38 cysteine residues conserved in the proteins of this family members. Following the discovery of CCN proteins, three additional members of this family were also identified based on sequence similarity namely Wnt-1-induced secreted protein- 1 (WISP1/CCN4), Wnt-1-induced secreted protein- 2 (WISP2/CCN5) and Wnt-1-induced secreted protein- 3 (WISP3/CCN6). These proteins were named WISP1 and WISP2 because these proteins were up regulated in Wnt-1 transformed cells (Pennica *et al.*, 1998). However, WISP3 (CCN6) has not been found to be induced by Wnt-1 but it was named so based on the sequence homology and structural similarity with WISP1 and WISP2.

The members of CCN family of proteins shares about 40-60% similarity in DNA sequence and about 30-50% similarity in overall amino acid sequence (Lau and Lam, 1999). The CCN proteins are modular proteins, overall common structure of this family proteins includes a signal peptide followed by four functional modules: insulin-like growth factor binding protein (IGFBP) domain, von Willebrand factor type C (VWC) domain, thrombospondin type 1 (TSP1) domain, and cystine-knot (CT) domain. In between VWC and TSP1 domains a hinge domain is present. As these four domains shares identity with four classes of regulatory proteins, each domain has the potential to orchestrate different function in cell biology which identifies pleiotropic function of CCN proteins (Fig. II). All CCN proteins share same type of this basic structural domains except CCN5/WISP2 which

lacks CT domain. Here is a brief description regarding discovery of CCN family of proteins.

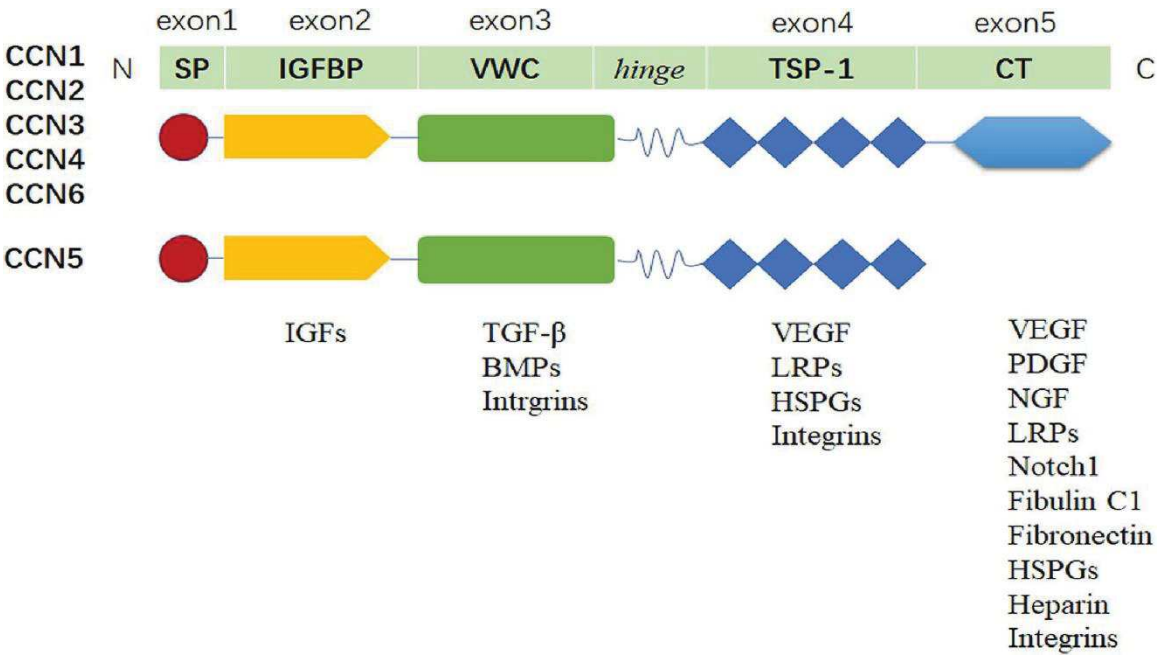

Figure II: Structure of CCN proteins. (Jia *et al.*, 2021)

Schematic representation of four conserved functional domains coded by respective exons. Below each domain, respective interacting partners are mentioned.

1.2.1 Discovery of CCN proteins

CCN1 was first identified by screening differential hybridization of cDNA library from serum-stimulated mouse fibroblast as a growth factor (Lau and Nathans, 1985). Human CCN2 was first identified in fibroblast as a mitogen and chemotactic factor in conditioned media of human umbilical vein endothelial cells (HUVECs) (Bradham *et al.*, 1991). CCN3 was identified initially as a gene overexpressed in avian nephroblastomas which is induced by chicken myeloblastosis-associated virus (MAV) (Joliot *et al.*, 1992). CCN4 was identified by researchers independently as an upregulated gene in Wnt-1 transformed mammary epithelial cell or by screening low metastatic K-1735 mouse melanoma cells (Hashimoto *et al.*, 1996). CCN5 was first identified as a gene which gets down regulated in fibroblasts of rat embryo when transformed by H-ras and inactivated p53 tumor suppressor gene (Zhang *et al.*, 1998). CCN6 was first identified as a homologous gene to CCN4 which was confirmed by screening an expressed sequence tag (EST) database with CCN4 protein sequence (Pennica *et al.*, 1998).

1.2.2 Functions of CCN family members

On account of multimodular architecture of the proteins, the CCN family of proteins performs various cellular functions such as stimulating mitosis, apoptosis, adhesion, production of extracellular matrix, arresting of growth phase and cell migration. These proteins also regulates angiogenesis, endochondrial ossification, tumour growth, implantation, placentation and embryogenesis. The target cells of these proteins includes smooth muscle cells, fibroblasts, endothelial cells, epithelial cells and neuronal cells (Moussad and Brigstock, 2000).

CCN1, CCN2 and CCN3 plays a major role in angiogenesis, osteogenesis and chondrogenesis in differentiating stem cells. CCN1 is overexpressed in aggressive human cancer making it a key player in tumorigenesis however the role of CCN2 and CCN3 are dependent on type of the tumour whereas CCN4, CCN5 and CCN6 acts as tumor supressors and inhibits cell growth (Brigstock, 2003; Zuo *et al.*, 2010; Jia *et al.*, 2021). CYR61/CCN1, CTGF/CCN2 and NOV/CCN3 also induces intracellular signaling events by binding to cell surface integrins and results in kinase activation and gene transcription (Lau and Lam, 1999; Chen, Chen and Lau, 2000, 2001; Grzeszkiewicz *et al.*, 2001; Leu, Lam and Lau, 2002; Schober *et al.*, 2002)

Impaired cardiac valvuloseptal morphogenesis was observed in CYR61/CCN1-null mice, resulting in severe atrioventricular septal defects (AVSD) as well as compromised embryonic vessel integrity leading to embryonic lethality (Babic *et al.*, 1998; Mo *et al.*, 2002). CTGF/CCN2-null mice leads to impaired chondrocyte proliferation and extracellular matrix composition resulting in skeletal dysmorphisms (Ivkovic *et al.*, 2003). NOV/CCN3 mutant mice were known to cause muscle atrophy as well as skeletal and cardiac abnormalities (Heath *et al.*, 2008). WISP1/CCN4 null mice shows impaired chondrogenesis (Yoshioka *et al.*, 2016). WISP2/CCN5 null mice leads to lipotoxic cardiomyopathy with mild obesity and diabetes (Kim *et al.*, 2018). Though WISP3/CCN6 null mice does not manifest any skeletal abnormalities (Kutz, Gong and Warman, 2005) however, mutations in WISP3/CCN6 are associated with a debilitating musculoskeletal disorder known as progressive pseudorheumatoid dysplasia (PPRD) (Hurvitz *et al.*, 1999; Dalal *et al.*, 2012; Sun *et al.*, 2012; Ekbote *et al.*, 2013; Yang, Song and Kong, 2013; Liu *et al.*, 2015; Luo *et al.*, 2015; Alawbathani *et al.*, 2018; Shahi *et al.*, 2020; Sheth *et al.*, 2021). In view of tumour suppressor function of WISP3, loss of WISP3 expression is

associated with increased metastases and resistance to apoptosis in invasive breast cancer (Kleer, Zhang and Merajver, 2007; Huang *et al.*, 2010).

1.3 WISP3/CCN6 in relation to Disease

Though there are many facets of regulation of WISP3 in cellular function starting from skeletal deformity to tumorigenesis. My focus was to elaborate the skeletal regulation of WISP3 because homozygous and compound heterozygous mutations in WISP3 gene are associated with the autosomal recessive musculoskeletal disorder, progressive pseudorheumatoid dysplasia (PPRD) (OMIM#208230 & #603400). This disease is often misdiagnosed with juvenile idiopathic arthritis and muscular dystrophy disorder (Alawbathani *et al.*, 2018; Shahi *et al.*, 2020; Liu and Chen, 2021).Till now, several mutations were identified across the domains of WISP3 leading to PPRD which implies that all the domains are essential for proper functioning of WISP3 protein (Hurvitz *et al.*, 1999; Dalal *et al.*, 2012; Ekbote *et al.*, 2013) (Fig. III).

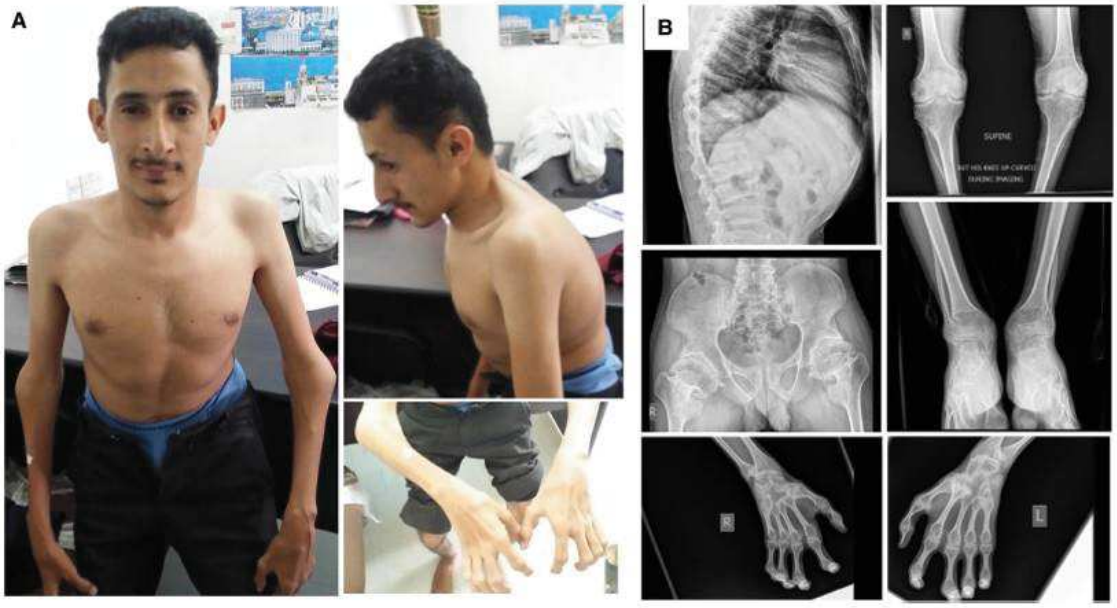

Figure III: Photo of a PPRD patient and his radiologic images. (Alawbathani *et al.*, 2018)
A) Posture of the patient is altered due to of severe joint involvement. Visible phenotype of patient includes enlargement of elbows, widening of the thoracic wall, and severe contractures of the fingers. **B)** X-ray analysis of the whole body indicating its deformities.

Symptoms of PPRD consist of stiffness and swelling of joints, widening of epiphysis and metaphysis, narrowing of joints space along with muscle wasting (Hurvitz *et al.*, 1999; Dalal *et al.*, 2012; Sun *et al.*, 2012; Ekbote *et al.*, 2013; Yang, Song and Kong, 2013; Liu *et al.*, 2015; Chouery *et al.*, 2017; Alawbathani *et al.*, 2018; Shahi *et al.*, 2020; Liu and

Chen, 2021). PPRD patients show no noticeable phenotype at birth but the disease manifests from early childhood (3-8 years age) and the patient lives a painful life throughout his/her entire lifespan. PPRD patients are found across the globe and are prevailed in certain geographical pockets where consanguineous marriages are being practised. It is reported that the frequency of PPRD patients in UK is ~1 in a million (Neerinckx *et al.*, 2015) whereas more than 1 in a million are seen in Middle- Eastern countries, USA, China, and India (Dalal *et al.*, 2012; Garcia Segarra *et al.*, 2012; Alawbathani *et al.*, 2018; Liu and Chen, 2021). Several cases were reported across different regions of India including new mutations of WISP3 gene (Dalal *et al.*, 2012; Bhavani *et al.*, 2015; Madhuri *et al.*, 2016; Rai *et al.*, 2016; Shahi *et al.*, 2020; Sheth *et al.*, 2021) which implies the seriousness of this debilitating disorder. Recently it was highlighted in several news channels (Fig. IV) that maximum population of a village called Arai situated in Poonch district of Jammu and Kashmir were affected with PPRD.

Figure IV: News of PPRD in media.
Reported in Scroll.in dated Dec 26, 2016 and Times of India dated Feb 25, 2017 respectively.

Till now more than 215 families have been reported across world out of which case series of 79 families has been documented from India (Dalal *et al.*, 2012; Bhavani *et al.*, 2015). List of various mutations reported so far pertaining to different regions of WISP3 are given in the table (Fig. V) (Dalal *et al.*, 2012). Though c.156C>A (p.Cys52Ter) is perhaps the most common recurrent variant worldwide, the most common variants in the Indian

population were found to be c.233G>A (p.Cys78Thr) and c.1010G>A (p.Cys337Thr) (Bhavani *et al.*, 2015, 2020). Looking into the molecular interaction of WISP3, so far BMP, LRP and Frizzled co-receptor are identified as few interacting partners of WISP3 which partly explain pathogenesis of PPRD progression (Nakamura *et al.*, 2007). However, till now there are not much literature regarding the study of WISP3 protein and its relationship with disease progression of PPRD making the disease an incurable one. So it is very essential to understand the basic molecular function of WISP3 protein.

Previous reports showed that WISP3 promotes expression of collagen-II in chondrocytes and restricts the production of reactive oxygen species (ROS) in cellular level suggesting that it is involved in maintenance of cartilage integrity and homeostasis (Sen *et al.*, 2004; Davis, Chen and Sen, 2006; Miller and Sen, 2007). It has also been shown that WISP3 interacts with IGF1 and acts as a negative regulator of chondrocyte

TABLE I. Mutations in *WISP3* Reported in the Literature and in Our Study

Nucleotide change[a]	Amino acid change[a]	Nucleotide change[b]	Amino acid change[b]	Location	Studied populations	Number of families	References
c.43delGC	p.Ala15fsX	c.43_44delGC	p.Ala15Thrfs*17	Exon 1	USA	1	Hurvitz et al. [1999]
g.IVS1+2insT		c.48+2dupT		Intron 1	Jordan	1	Hurvitz et al. [1999]
c.156C>A	p.Cys52X		p.Cys52*	Exon 2	Italy, France	2	Hurvitz et al. [1999]
					Lebanon, Syria	?	Delague et al., [2005]
					Turkey	1	Temiz et al. [2011]
					India	2	Our study
c.232T>C	p.Cys78Arg			Exon 2	France	1	Hurvitz et al. [1999]
c.233G>A[c]	p.Cys78Tyr			Exon 2	India	4	Our study
c.246delA	p.Pro82fsX104		p.Glu84Lysfs*21	Exon 2	Saudi Arabia	2	Hurvitz et al. [1999]
					Jordan	1	
c.248G>A	p.Gly83Glu			Exon 2	Lebanon, Syria	?	Delague et al. [2005]
					Turkey	1	Temiz et al. [2011]
					India	2	Our study
c.340T>C[c]	p.Cys114Arg			Exon 2	India	1	Our study
c.348C>A[c]			p.Tyr116*	Exon 3	India	1	Our study
c.433T>C[c]	p.Cys145Arg			Exon 3	India	2	Our study
c.434G>A	p.Cys145Tyr			Exon 3	Italy	1	Hurvitz et al. [1999]
c.536_537delGT	p.Cys179fsX		p.Cys179*	Exon 3	Syria	1	Delague et al. [2005]
c.589G>C	p.Ala197fsX201		p.Ala197Leufs*35	Exon 3	Syria	1	Delague et al. [2005]
c.624_625insA	p.Cys209fsX229	c.624_625dupA	p.Cys209Metfs*21	Exon 4	China	1	Ye et al. [2010]
c.682T>C[c]	p.Ser228Pro			Exon 4	India	1	Our study
c.727_733delGAGAAAA	p.Glu243fsX255		p.Glu243Aspfs*13	Exon 4	China	1	Ye et al. [2010]
c.739_740delTG	p.Cys247fsX277		p.Cys247Leufs*31	Exon 4	Caucasian	1	Ehl et al. [2004]
					India	1	Our study
c.802T>G[c]	p.Cys268Gly			Exon 5	India	1	Our study
c.840delT	p.Phe280fsX312		p.Phe280Leufs*33	Exon 5	China	1	Liao et al. [2004b]
c.863insAC	p.Thr288fsX313	c.862_863dupAC	p.Gln289Leufs*25	Exon 5	USA	1	Hurvitz et al. [1999]
c.866delAG	p.Gln289fsX301	c.866_867delAG	p.Ser290Leufs*12	Exon 5	Iran	1	Hurvitz et al. [1999]
c.866_867insA	p.Gln289fsX302	c.866dupA	p.Ser290Glufs*13	Exon 5	China	1	Ye et al. [2010]
c.947_951delAATTT[c]	p.Gln316fsX320		p.Gln316Argfs*5	Exon 5	India	1	Our study
c.993G>A	p.Trp331X		p.Trp331*	Exon 5	Italy	1	Hurvitz et al. [1999]
c.1000T>C	p.Ser334Pro			Exon 5	China	1	Liao et al. [2004a]
c.1010G>A[c]	p.Cys337Tyr			Exon 5	India	10	Our study

[a]Mutation description as reported in the original article.
[b]Mutation description according to the current nomenclature when it is different from the original article.
[c]Novel mutation identified in this study.

Figure V: PPRD causing mutations in WISP3 according to various literature. (Dalal *et al.*, 2012)

hypertrophy (Repudi, Patra and Sen, 2013). The modular architecture suggests WISP3 might act as a chaperone like protein, regulating the functions of other proteins by interacting with them. As it regulates cellular ROS, Calcium homeostasis as documented earlier, it might regulate mitochondrial function as well because mitochondria are the major source of ROS production in cell as a by-product of oxidative phosphorylation and calcium homeostasis. Since the focus of my thesis was to decipher the relationship between WISP3 and mitochondria, next I am going to give a brief introduction about mitochondria and its functions.

1.4 Mitochondria

Mitochondria are complex organelle that plays a key role in energy metabolism. This double membrane bound semi-autonomous organelle responsible for 95% of energy production in the form of ATP through a process called oxidative phosphorylation (OXPHOS). Besides ATP production, mitochondria plays a major role in calcium and lipid homeostasis, ROS generation and apoptosis (Brookes *et al.*, 2004; Baughman *et al.*, 2011; Friedman and Nunnari, 2014; Genova and Lenaz, 2014). In most of the eukaryotes, the process of OXPHOS carried out by 5 enzyme complexes named as Complex I (NADH:ubiquinone oxidoreductase), Complex II (Succinate:ubiquinone oxidoreductase), Complex III (ubiquinol:cytochrome c oxidoreductase), Complex IV (cytochrome c oxidase) and Complex V (ATP synthase) respectively. The schematic diagram represents different complexes in electron transport chain (Fig. VI).

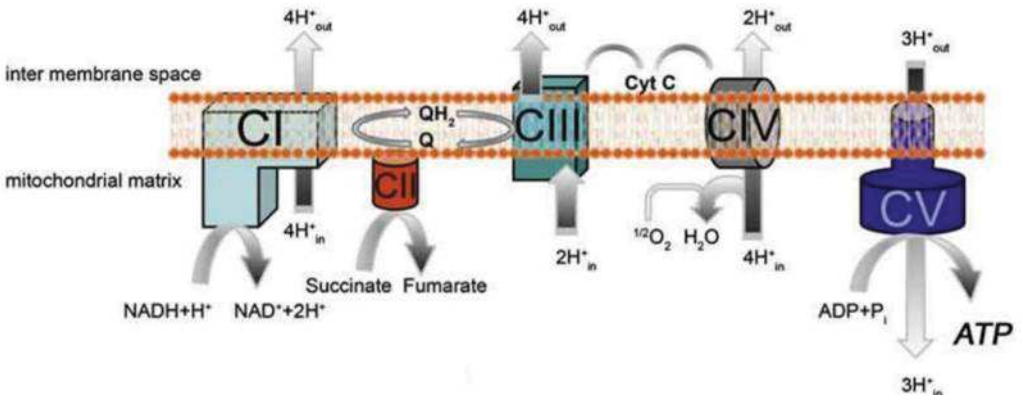

Figure VI: A schemetic model of Oxidative Phosphorylation System. (Acín-Pérez *et al.*, 2008)

Several models of OXPHOS has been proposed based on arrangement of complexes such as Fluid model (conventional model) and Solid model, but recent findings concludes a third

model called Plasticity model which states the formation of supercomplexes (Fig. VII) (Acín-Pérez *et al.*, 2008).

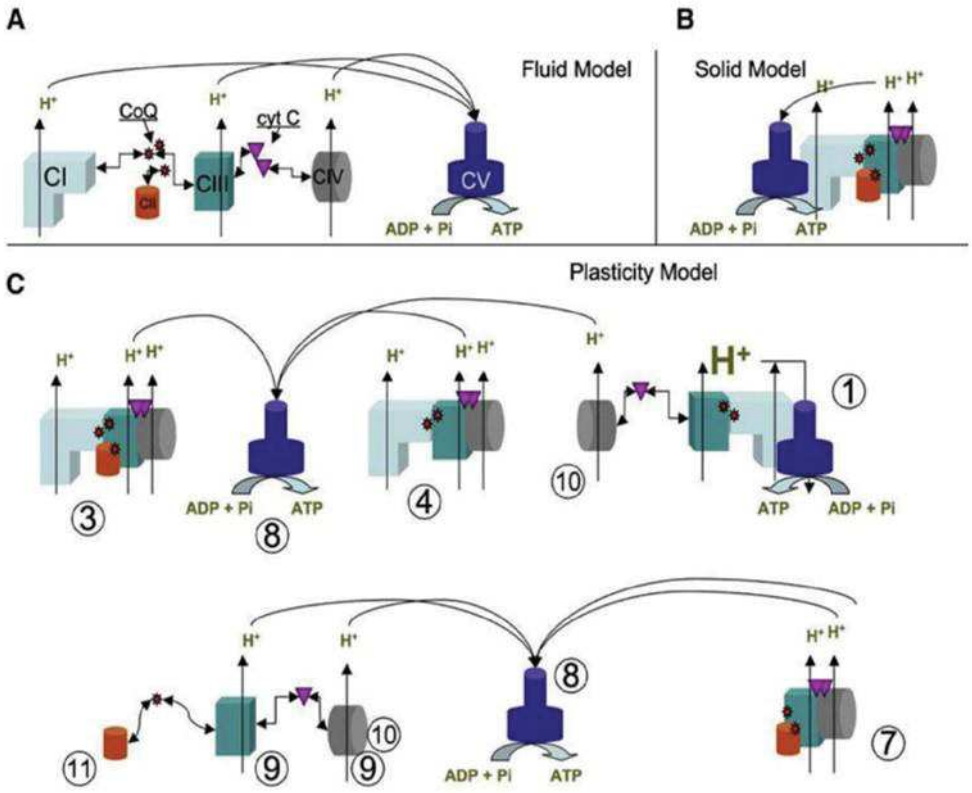

Figure VII: Schematic representations of different models of mitochondrial OXPHOS system. (Acín-Pérez *et al.*, 2008)
A) Classical Fluid model, B) Solid model and C) Plasticity model. In the plasticity model, 3 and 4 marked supercomplexes are also called as respirasomes based on its ability to transfer electron directly from NADH to oxygen.

In short the supercomplexes are formed by aggregation/ combination of two or more complexes of electron transport chain for efficient function. Supercomplex involving Complex I,II,III,IV and Complex I, III,IV are also called as respirasomes based on its functions in respiration. The reason behind formation different types of Supercomplex are not well understood however recent studies have shown that mitochondrial shape has an impact on the kinetics of biochemical events and the building of protein Supercomplexes in mitochondria (Lizana, Bauer and Orwar, 2008; Cogliati *et al.*, 2013; Mannella, Lederer and Jafri, 2013). OXPHOS system is responsible for generation of mitochondrial ROS and as WISP3 plays an important role in cellular ROS generation (Miller and Sen, 2007; Repudi, Patra and Sen, 2013), a detail insight into mitochondrial electron transport chain was essential. Though Complex I and III are responsible for generation of ROS, Complex

I being the major initiator of electron transport and subsequently ATP synthesis, a detailed knowledge of Complex I including its structure, assembly functions is essential.

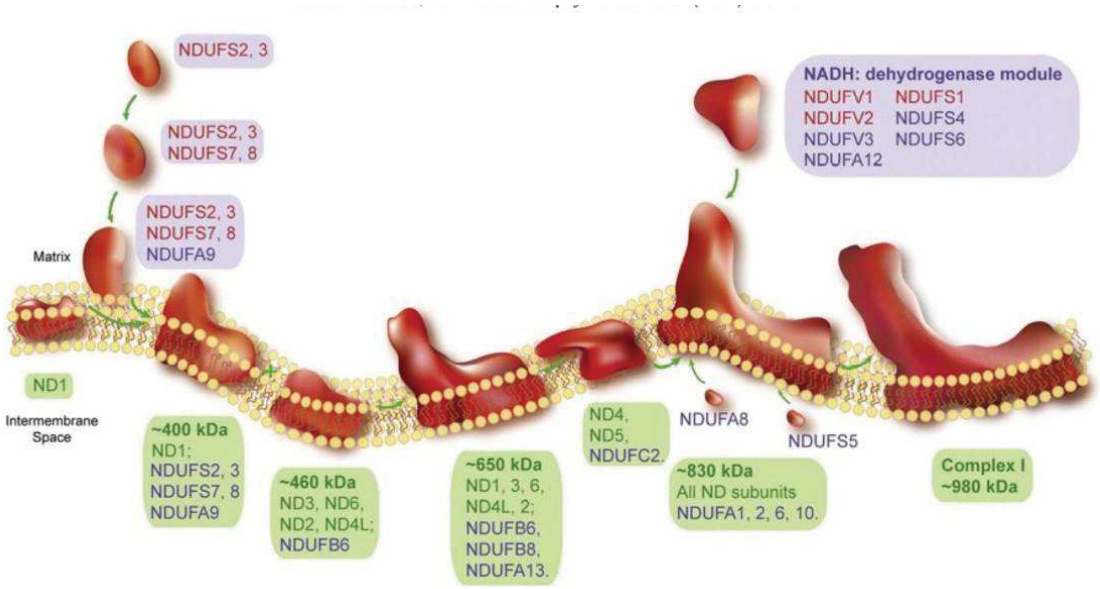

Figure VIII: Assembly model of human Complex I. (Mimaki *et al.*, 2012)
Model describing the stepwise integration of different subunits of Complex I to form a fully functional protein. Red highlighted are the core subunits, rest nuclear DNA-encoded subunits are blue highlighted. Green highlight subunits are encoded by mitochondrial DNA.

Complex I is located in the inner mitochondrial membrane and protrudes into matrix having L shaped structure in eukaryotes. Human mitochondrial Complex I consists of 45 subunits out of which 38 subunits are nuclear DNA coded, translocated to mitochondria and mitochondrial DNA (mtDNA) encodes 7 subunits which are essential for proper functioning of Complex I. The L shaped structure consists of a hydrophilic arm protruding towards matrix and a hydrophobic membrane arm present perpendicular other arm(Acín-Pérez *et al.*, 2008; Mimaki *et al.*, 2012). Assembly of all the subunits to form a functional Complex I is a multiplex process where along with subunits (nuclear and mtDNA encoded), many assembly factors and chaperons come into action after which the assembly factors and chaperons dissociates. Figure VIII represents a schematic representation of Complex I assembly (Acín-Pérez *et al.*, 2008). Nomenclature of different subunits of Complex I are based on its origin and function such as the prefix “NDU” (NADH dehydrogenase-ubiquinone) is due to nuclear encoded subunits and mtDNA-encoded subunits are given the prefix “ND” (NADH-dehydrogenase). A number of assembly factors have prefix “NDUFAF” –NADH dehydrogenase (NDU), alpha sub

complex (F), assembly factor (AF) in addition to it number is given based on its discovery (Acín-Pérez *et al.*, 2008; Mimaki *et al.*, 2012; Signes and Fernandez-Vizarra, 2018).

As healthy functioning of mitochondria is essential for proper muscle function (Sunitha *et al.*, 2016; Vincent *et al.*, 2016) and muscle wasting is observed in PPRD, it is also essential to elucidate the effect of WISP3 in maintenance of musculoskeletal health. Therefore, in addition to chondrocyte cell line I used zebrafish as a model organism.

1.5 Zebrafish as a model organism to study WISP3 in the context of PPRD

PPRD, a debilitating disorder characterized by loss of cartilage, muscle wasting and irregular bone growth in joints (Hurvitz *et al.*, 1999; Dalal *et al.*, 2012; Sun *et al.*, 2012; Ekbote *et al.*, 2013; Bhavani *et al.*, 2015; Luo *et al.*, 2015; Chouery *et al.*, 2017; Alawbathani *et al.*, 2018; Shahi *et al.*, 2020; Liu and Chen, 2021), the mechanism of disease progression is not yet clear. Looking at the multimodular domains of WISP3 and its potential to alter mitochondrial functions thereby musculoskeletal health as a whole. For functional validation of wild type WISP3 at organism level, understanding its effect in mitochondria in relation to musculoskeletal system becomes essential. Zebrafish is used as a model organism based on a previously documented result that shows defective cartilage development following Wisp3 depletion (Nakamura *et al.*, 2007). Zebrafish is a very good model organism to study broad range of human genetic disease. Another benefits of selecting zebrafish is that the zebrafish genes shows 50-80 % homology with most human sequence (Howe *et al.*, 2013) as well as shows similar basic physiology in mammals (Steele, Prykhozhij and Berman, 2014). Taking into account of the fact of using zebrafish as a model organism, the functions of WISP3 was validated using skeletal muscle of adult zebrafish to correlate the findings to pathogenesis of PPRD where muscle wasting/ muscle myopathies were a part of its manifestation. Figure IX represents the zebrafish setup we established in our lab. In this study, zebrafish WISP3 protein and gene is written as Wisp3 and *wisp3* based on ZFIN zebrafish nomenclature convention.

Figure IX: An aquarium representing zebrafish setup in our lab.

CHAPTER II

FOCUS OF THE THESIS

FOCUS OF THE THESIS

Mutations in WISP3 are associated with the autosomal recessive musculoskeletal disorder, progressive pseudorheumatoid dysplasia (PPRD)**.** Symptoms of PPRD consist of stiffness and swelling of joints, widening of epiphysis, narrowing of joints and muscle wasting. PPRD patients show no noticeable phenotype at birth and the disorder starts from early childhood (Hurvitz *et al.*, 1999; Dalal *et al.*, 2012; Alawbathani *et al.*, 2018; Shahi *et al.*, 2020; Liu and Chen, 2021). But the mechanism of the disease progression is still unknown. So knowing the basic function of WISP3 protein is very much essential. But unfortunately the function of WISP3 remains poorly understood.

WISP3 (Wnt Induced Secreted Protein 3) is a member of the CCN (Cyr61, CTGF, Nov) family proteins. The CCN family encodes cysteine-rich secreted proteins, which modulate cell growth, survival, cell migration and differentiation. WISP3 maps to chromosome 6q21–22, codes for a 354 amino acid protein, and is expressed in skeletally derived cells including human synoviocytes, articular cartilage chondrocytes and bone marrow derived mesenchymal progenitor cells (Hurvitz *et al.*, 1999; Sen *et al.*, 2004; Holbourn, Acharya and Perbal, 2008; Perbal, 2013). The name WISP3 is based on the homology of WISP3 with WISP1 and WISP2, which are upregulated in Wnt-1 transformed cells (Pennica *et al.*, 1998). However, WISP3 (CCN6) has not been found to be induced by Wnt-1. WISP3 have a multi-modular architecture with putative functional domains. The modular structure of the WISP3 suggests that it has complex functions in different cellular aspects.

Previous reports showed that WISP3 promotes expression of collagen-II in chondrocytes and restricts the production of reactive oxygen species suggesting that it is involved in maintenance of cartilage integrity and homeostasis (Sen *et al.*, 2004; Miller and Sen, 2007). It has also been shown that WISP3 interacts with IGF1 and acts as a negative regulator of chondrocyte hypertrophy (Repudi, Patra and Sen, 2013). Recently report from our lab showed that WISP3 localizes to mitochondria, and depletion of WISP3 in the chondrocyte cell line C-28/I2 by siRNA results in increased mitochondrial ROS in association with increased mitochondrial ATP synthesis, mitochondrial membrane potential and calcium (Patra *et al.*, 2016). However, how WISP3 regulates all these functions in mitochondria is not still clear. In this study, I am interested to find out the role of WISP3 in mitochondrial function in greater detail using both chondrocyte cell line and zebrafish as a model organism.

To elucidate the functions of WISP3 in mitochondria I formulated and worked on following objectives:

1) To check the association of WISP3 with mitochondrial proteins, if any.
2) To check the influence of WISP3 on mitochondrial Electron Transport System, if any.
3) To decipher the functions of mutant WISP3 generated by CRISPR Cas9 mimicking PPRD causing mutant.
4) Elucidating the function of WISP3 at organism level using zebrafish as a model organism.
5) To check its effect on musculoskeletal system of zebrafish in relation to mitochondria.

CHAPTER III

MATERIALS AND METHODS

MATERIALS AND METHODS

3.1 Cell culture

Chondrocyte cell lines C-28/I2 and C20A4 were maintained in Dulbecco Modified Eagle's Medium (DMEM) High glucose and HEK 293 cells were maintained in DMEM Low glucose supplemented with 10% Fetal Bovine Serum (FBS) (Invitrogen), 1 unit/mL of Penicillin, and 1 µg/mL of Streptomycin and 2mM Glutamine at 37°C in a humidifier chamber with 5% CO2 (Miller and Sen, 2007; Repudi, Patra and Sen, 2013; Patra *et al.*, 2016).

3.2 Cell transfection

C-28/I2 cells were transfected with WISP3-myc containing plasmid DNA using Lipofectamine LTX reagent (Invitrogen) as per manufacturer protocol. Briefly, ~ 0.5 X 10^6cells were plated in each well of 6-well tissue culture plate so that it reaches 70-80 % confluency after 14-16 hrs of plating (Repudi, Patra and Sen, 2013; Patra *et al.*, 2016). For transfection in each well of 6 well plate, 2 µg plasmid DNA was mixed with 2µl of PLUS reagent in 100µl Opti-MEM media (Invitrogen) and incubated in room temperature for 10 minutes. 6 µl Lipofectamine LTX was added to the DNA mixture and mixed well by pipetting followed by incubating it for 20 minutes in room temperature. In the meantime, the media of 6 well plate was changed with Opti-MEM media. The DNA-Lipofectamine LTX complex was added drop wise to the well, gently swirled and kept in CO_2 Incubator. After 24 hrs post transfection, the transfection media was changed with fresh DMEM complete media (10% FBS, penicillin 1 unit ml^{-1}, streptomycin 1 µg ml^{-1} and glutamine 2 mM). Cells were harvested and processed for subsequent analysis after 48 hours of transfection (Repudi, Patra and Sen, 2013; Patra *et al.*, 2016).

HEK 293 cells were transfected with WISP3-myc containing plasmid DNA by calcium phosphate method (Jordan, Schallhorn and Wurm, 1996; Kingston, Chen and Rose, 2003). Briefly, HEK 293 cells were plated 12-16 hrs prior to transfection with WISP3-myc containing plasmid DNA and calcium phosphate buffers. For transfection in each well of 6 well plate, 2 µg DNA was mixed with 90 µl Tris-EDTA buffer (10 mM Tris-Cl, 2mM EDTA, pH-7.3) and 10 µl $CaCl_2$ buffer (2.5 M $CaCl_2$, 10 mM HEPES, pH 7.2) and mixed well. The 100µl mix was then gently added to 100µl of 2x HBS buffer (273 mM NaCl, 8.8 mM KCl, 1.27 mM Na_2HPO_4, 11.1 mM Dextrose and 41.96 mM HEPES, pH 7.05) and mixed well. The reaction mix was incubated for 30 minutes in room temperature. In the

meantime the media of 6 well plates were changed with fresh DMEM low glucose media. After incubation, the transfection mix was added drop wise to the well and mixed by gentle swirling and kept in humidified CO_2 incubator at 37°C with 5%CO_2. The media was changed 24 hours post transfection and the cells were harvested after 48 hours post transfection and processed for subsequent analysis.

C-28/I2 and C20A4 chondrocyte cells were transfected separately with WISP3 siRNA (50 nM) and Control siRNA (50 nM) (Dharmacon) using RNAimax as transfection reagent (Invitrogen) following previously published protocol (Patra *et al.*, 2016). Briefly, 0.5 X 10^6 cells (C-28/I2 or C20A4) were plated in each well of 6 well plate 14-16hrs prior to transfection. Transfection of siRNA was performed on 70-80% confluent cells. For each single well of 6 well plate, required amount of WISP3 siRNA or Control siRNA and 5µl of RNAimax was mixed separately with 150µl of Opti-MEM (Gibco, Thermo Fisher Scientific). After which the siRNA-Opti-MEM mix was slowly added to the RNAimax-Opti-MEM solution and mixed well gently by pipetting. The siRNA and RNAimax mixture solution (300µl) was incubated for 20 minutes following which the mixture solution was added drop wise to the well. The plate was gently swirled for even distribution of solution and kept in CO_2 incubator. Transfected cell media was changed at 24 hours post-transfection. Cells were harvested after 60-63 hours of transfection and processed for subsequent analysis.

3.3 Zebrafish maintenance

Adult zebrafish (AB strain) were purchased from local vendors and kept in 1 month quarantine period. Further, the fishes were kept in 30-L fish tanks where 14:10 hour light/dark cycle was maintained at 26 $\pm$ 2 °C temperature. Continuous flow of filtered water was maintained in the tanks and were aerated by air pump so as to keep the water oxygenated. Fishes were fed twice a day in an interval of 9-10 hour with fish food pellets (Optimum micro pellet). During the course of feeding, the filter pump were switched off for at least 15 minutes. All experiments were performed following CPCSEA approved guidelines, Govt. of India.

3.4 Confocal microscopy

Confocal microscopy was used to visualize the localization of WISP3 in mitochondria of C-28/I2 cells. Briefly, the chondrocyte cells were transfected with WISP3-myc or cultured without any treatment on 8-well chambered slides (Millipore, USA). Prior to processing

for antibody staining, the cells were incubated with mitotracker green (200nM) for 30 minutes in CO_2 incubator at 37°C. The cells were further fixed with chilled methanol followed by blocking for 1 hour with 2.5% BSA in PBST (PBS containing 0.1% Tween 20). The chambered slides were incubated overnight with primary antibodies: anti-myc antibody (1:500) and anti-WISP3 (1:200) at 4°C. After incubation with primary antibody, the cells were washed twice with PBST followed by incubating for 2 hours at 4°C with either Alexa Fluor 546 conjugated anti-rabbit antibody (1:2000) or Alexa Fluor 546 conjugated anti-goat antibody (1:2000). Nucleus of the cells were stained with DAPI followed by washing of slides and mounting of slide with 60% glycerol. Andor Revolution XD Spinning Disk Microscope with Andor ixon 897 EMCCD camera was used in this confocal microscopy. Image J software (NIH) was used to generate RGB intensity plot from the co-localization image.

3.5 Localization analysis of WISP3 in mitochondria

Protease protection assay was performed to validate the sub-mitochondrial localization of WISP3. Briefly, mitochondria from C-28/I2 cells were isolated following earlier described procedure. Mitoplast was prepared from the isolated mitochondria by osmotically rupturing the outer membrane of mitochondria by addition of MOPS buffer [10 mM MOPS and 1 mM EDTA, pH-7.2] (Mick *et al.*, 2012). Mitoplasts of C-28/I2 cells were then subjected to digestion by adding different concentrations of proteinase K in increasing order (1, 5 and 25 $\mu g\ ml^{-1}$) followed by incubation on ice for 10-15 minutes. Action of proteinase K on mitoplast was blocked by adding 1mM PMSF to the reaction mixture after incubation (Mick *et al.*, 2012). Membranous fraction and soluble fraction of mitochondria were separated by using carbonate buffer. In brief, the mitochondria were isolated from $WISP3^{myc}$ transfected HEK 293 cells followed by incubation in carbonate buffer (100 mM Na_2CO_3, pH-11.5) for 30 minutes at 4°C. Following incubation, the carbonate buffer containing mitochondria was centrifuged at 45000g for 45 minutes at 4°C. The obtained pellet after centrifugation represents the membranous fraction whereas the supernatant represents soluble fraction of mitochondria (Mick *et al.*, 2012).

3.6 Morpholino treatment

Translation of *wisp3* gene of zebrafish was blocked locally by injecting morpholino. Zebrafish *wisp3*-specific morpholino oligo was designed and ordered from Gene Tools (United States). The sequence of *wisp3* morpholino used is 5′-GTAGTGATAGCA

TCATACACGGCTT-3′, parallelly, standard control morpholino having the sequence 5′-C CTCTTACCTCAGTTACAATTTATA-3′ was used as a negative control (Stainier *et al.*, 2017). Adult fish of 9–12 months of age were selected for injection. To inject into skeletal muscle of adult fish, morpholinos were reconstituted in sterile water to make a final concentration of 200 mM. Briefly, each fish was either anesthetized with MS222 (0.168 mg/mL, pH 7.5) or subjected to cold shock following internationally approved guidelines (Reed and Jennings, 2010). Using a 30-gauge Hamilton syringe, 4 µl of morpholino solution was injected in each fish just above the dorsal fin on the left dorsal muscle followed by electroporation using a tweezer electrode with three pulses with 5 seconds intervals. The current was set at 50 Volt for 50 milli seconds (Fausett, Gumerson and Goldman, 2008). In order to avoid dehydration and proper respiration, the gills of the fish was irrigated with aerated water during the entire process of injection and electroporation. The fish were immediately moved into the water tanks having temperature 26 $\pm$ 2°C and kept for 65 hours followed by collection of skeletal muscle after sacrifice. The injected site of left dorsal muscle was dissected out and labeled as "*wisp3*/Control morpholino injected" whereas the right ventral side muscle of the same fish dissected and labeled as "uninjected".

3.7 Isolation of RNA and cDNA preparation

Total cellular RNA was isolated using Trizol (Invitrogen) following manufacturer protocol. In brief, 0.2 volume of chloroform was added to the total cellular Trizol extract followed by shaking of the tube so that the choloroform and Trizol mixes well. The tube was centrifuged at high speed (12000 g) for 10 minutes at 4°C to obtain a transparent aqueous layer on the top of the tube. The aqueous layer was aspirated slowly by pipetting and transferred it to another tube. 0.3 volume of Isopropanol was added to the same tube, mixed well and kept for 10 minutes in room temperature. Further, the tube was centrifuged at 12000 g for 10 minutes at 4°C to obtain the RNA pellet. The supernatant was discarded and the RNA pellet was washed with 600µl of 70% ethanol to remove residual salts. The RNA pellet was air dried in room temperature followed by dissolving it in DEPC treated water at 50°C for 10 minutes. Isolated RNA was quantified using UV-Vis spectrophotometer and proceeded for cDNA preparation. cDNA synthesis kit (BioBharati Lifescience) was used to prepare cDNA from total cellular RNA.

3.8 Gene expression analysis by RT-PCR

Following isolation of cDNA, expression of the respective genes were analyzed by reverse transcription PCR (RT-PCR) using cDNA, specific primers and Taq Polymerase (BioBharati Lifescience). Primers used were WISP3 primers (forward 5′-ACCAAA GCTGGCTGGCAGTC-3′ and reverse 5′-TCTCCAGGTTCTCTGCAGTTTC-3′), GAPDH primers (forward 5′-ACCACAGTCCATGCCATCAC-3′ and reverse 5′-TC CACCACCCTGTTGCTGTA-3′), NDUFB8 primers (forward 5′-GTGAAGATGGCGG TGGCC-3′ and reverse 5′-GATCTCATAGTGAACCACCC-3′) and NDUFS1 primers (forward 5′-TCCAACACATGAATTGTGGAG-3′ and reverse 5′-GCATATACATATA TACACAC-3′). The PCR products were separated using agarose gel electrophoresis and the DNA bands were visualized under UV trans-illuminator and documented.

3.9 Variant analysis of WISP3

Variants of WISP3 in C-28/I2 cell line were analyzed by isolating total cellular RNA followed by RT-PCR. On the basis of NCBI, Variant 1 mRNA (Ref. Seq- NM_003880.4) and Variant 3 mRNA (Ref. Seq-NM_198239.2) specific primers were designed. Forward primer for WISP3 variant 1, 5′-GAGTCCCGGGAGGAAAGTGC-3′ and variant 3, 5′-GGAGCAATGAACAAGCGGCGA-3′ were used with reverse primers matching exons 2,3,4 and 5 respectively. Reverse primers used for the analysis are Exon 2: 5′-CACA CACTCCAGTCTCGTACC-3′, Exon 3: 5′-GTAGCTTGTTGAAAGCTGCTGTA-3′, Exon 4: 5′-CTGTCGCAAGGCTGAATGTAAC-3′ and Exon 5: 5′-CTTGAGCTCAGA AAATATATCTCC-3′.

3.10 Preparation of cell/tissue lysate and immunoblotting

For whole cell lysate, chondrocyte cells were harvested by scraping the cells in PBS followed by centrifugation at 2000 rpm for 5 minutes at 4°C. The obtained cell pellet was lysed with cell lysis buffer [20 mM Tris-HCl (pH 7.5), 500 mM NaCl, 1% Triton X-100, 1 mM EDTA, 10% Glycerol, 50 mM dithiothreitol, 2 mM phenylmethylsulfonyl fluoride, and 1% protease inhibitor cocktail]. The cell lysate was passed through 1 ml syringe for 10 times after which it was centrifuged at 12000 g at 4°C to obtain a clear lysate as supernatant and debris as pellet. The lysate was then transferred to a separate tube and used in further assays. Similarly, adult zebrafish skeletal muscle tissue was homogenized with a motorized dounce homogenizer using tissue lysis buffer [50 mM Tris (pH 8.0), 150 mM NaCl, 0.1% SDS, 50 mM DTT, 2 mM PMSF, 1 mM EDTA, 5% glycerol, 5 mM NaF, 2

mM sodium orthovanadate, 0.5% sodium deoxycholate, and 1% Triton-X]. Total protein concentrations of lysates were measured using Bradford reagent (Bio-Rad).

Immunoblotting was carried out by following previously published protocols (Repudi, Patra and Sen, 2013; Patra *et al.*, 2016). Briefly, the lysates were separated either by sodium dodecyl sulfate polyacrylamide gel electrophoresis (SDS-PAGE) or Blue Native polyacrylamide gel electrophoresis (BN-PAGE) followed by transfer of proteins to PVDF membrane.The membrane was kept in blocking solution [5% BSA in Tris-buffered saline with 0.1% Tween 20 (TBST)] for 2 hrs followed by incubation for execution of different experiments with respective primary antibody overnight at 4°C. Primary antibodies used are anti-WISP3 antibody (custom synthesis by BioBharati Lifescience), zebrafish specific anti-Wisp3 and anti-Ndufb8 antibody (custom synthesis by BioBharati Lifescience), anti-β-actin antibody (Cat. no- SC-47778, Santa Cruz), anti-OXPHOS cocktail comprising mitochondrial respiratory complex subunits (Cat. no- MS604, Abcam), anti-NDUFB8 antibody (Cat. no- 459210, Invitrogen), anti-NDUFS1 antibody (Cat. no- PA5-22309, Invitrogen), anti-VDAC1 antibody (Cat. no- ab15895, Abcam), anti-UQCRC2 antibody (Cat. no- SC-292924, Santa Cruz), anti-ATP5A1 antibody (Cat. no- 459240, Invitrogen), anti-HSP60 antibody (Cat. no-MA3-012, Invitrogen), anti-Myc antibody (Cat. no-BB-AB0045, BioBharati Lifescience), anti-WISP3 N-18 antibody (Cat. no-SC-8871, Santa Cruz) and anti-COX 4 antibody (Cat. no- 11967, Cell Signaling Technology). Following primary antibody incubation, Horseradish Peroxidase (HRP) - conjugated respective secondary antibodies were used for visualization with chemiluminescence reagent (Millipore). Chemi documentation system of Azure Biosystems, Model-C400 was used to capture images. Densitometric analysis of immunoblot bands was performed using GelQuant.NET software provided by biochemlabsolutions.com.

3.11 Antibody generation

Customised polyclonal antibodies are generated against human WISP3, zebrafish Wisp3 and zebrafish Ndufb8 by outsourcing it to BioBharati Lifescience. Human WISP3 antibody was generated targeting residues 201 aa to 372 aa of human WISP3 protein. Zebrafish Wisp3 antibody was generated targeting residue 320 aa to 335 aa of zebrafish Wisp3 protein, the sequence of peptide is “VCQRKCSNADDMFSELC”. Zebrafish specific NDUFB8 antibody was generated targeting peptide “KQYPYNNLYLERGGD” of zebrafish NDUFB8 protein.

3.12 Sub-cellular fractionation

Mitochondria and cytosol were isolated separately from Chondrocyte cells and zebrafish skeletal muscle by following previously published protocols (Wieckowski *et al.*, 2009). To isolate mitochondria from chondrocyte cells, cells were scraped, pelleted down and suspended in Isolation buffer 1 [225 mM mannitol, 75 mM sucrose, 0.1 mM EGTA, and 30 mM Tris-HCl (pH-7.4)] and for zebrafish, flash frozen muscle tissue stored in -80°C was thawed on ice and incubated in Isolation buffer 1. Following incubation, chondrocyte cells were homogenized manually by dounce homogenizer whereas zebrafish muscle tissues were homogenized using a motorized homogenizer. The homogenization continued for 3 minutes followed by 5 minutes incubation in ice and this process was repeated three times. The homogenates of chondrocyte cells or zebrafish muscles were centrifuged at 600 g for 5 minutes at 4°C. The supernatant was proceeded further whereas the pellets were discarded as it contains unbroken cells/tissues and nuclei. Supernatants were further centrifuged at 7,000 g for 10 minutes at 4°C to obtain mitochondria enriched pellet and the cytosolic supernatant. The mitochondria containing pellet were washed with Isolation buffer 2 [225 mM mannitol, 75 mM sucrose, and 30 mM Tris–HCl (pH 7.4)] and centrifuged at 10,000 g for 5 minutes at 4°C. Mitochondria resuspension buffer [250 mM mannitol, 0.5 mM EGTA, and 5 mM HEPES (pH 7.4)] was used to resuspend the crude mitochondria pellets which was obtained after centrifugation. For BN-PAGE, resuspended mitochondria was stored in -80°C and for SDS-PAGE, mitochondria were lysed with mitochondria lysis buffer [50 mM Tris-HCl (pH 7.5), 150 mM NaCl, 0.1 mM EDTA, 1% Triton X-100, and 2 mM 6-amino hexanoic acid]. Bradford reagent was used to quantify protein.

3.13 Size exclusion chromatography

Size exclusion chromatography of C-28/I2 cell mitochondrial lysate and endogenous zebrafish muscle mitochondria lysate was carried out using sephacryl S-300 resin. Initially, the column was packed with sephacryl s-300 resin to 30 ml bed volume. The column was equilibrated by running equilibration buffer [50 mM Tris-chloride (pH 8.0), 150 mM NaCl and 1 mM EDTA] for several times. Thereafter, the column was calibrated by using Thyroglobulin (Sigma-Aldrich) and a molecular weight marker kit (Sigma-Aldrich) followed by generation of column calibration curve which determines the elution volume of molecular weight standards. The calibration curve was used as a reference scale for calculating molecular weight of protein based on the elution volume. Briefly, 300 µg of

mitochondria lysate was loaded into the column and for each run, 90 nos of fractions were collected of volume 330µl each. Each fractions were precipitated using 20% TCA solution followed by washing of obtained pellet with acetone. Samples were dissolved in protein loading dye and denatured by boiling at 95°C. Further, the samples were subjected to SDS-PAGE and immunoblotting according to earlier described protocol.

3.14 BN-PAGE and 2D BN/SDS-PAGE

Frozen resuspended mitochondria were thawed on ice and protein was estimated by Bradford reagent. 25 µg of mitochondria was centrifuged at 10,000 g for 10 min at 4°C, the obtained pellet was solubilized by incubating with 20 µl of solubilization buffer [50 mM NaCl, 2 mM 6-aminohexanoic acid, 1 mM EDTA, and 50 mM imidazole–HCl (pH 7.0)] and 1 µl of 20% dodecyl maltoside for 10 min on ice. The sample was centrifuged at 20,000 g for 20 min at 4°C, resultant supernatant was mixed with 1.5 µl of 50% glycerol and 1 µl of native loading dye (5% G250 Coomassie Blue in 500 mM 6-aminohexanoic acid). Prepared samples were loaded in 3-13% gradient native gel and were run for 8 hrs at 80 volt in cold room (Wittig, Braun and Schägger, 2006). Immunoblotting was carried out after running BN-PAGE. Briefly, proteins from BN-PAGE were transferred to PVDF membrane using semi dry transfer system (Hoefer) at 30 volt for 90 min in room temperature. The coomassie dye attached to the membrane after transfer were removed by rinsing the membrane in methanol followed by rinsing in transfer buffer and processed for immunoblotting according to the protocol described earlier.

For 2D BN/SDS PAGE, the protein loaded lane of BN-PAGE was cut as a strip and incubated in denaturing solution [1% SDS and 1% β-Mercaptoethanol (β-ME)] for 30 min. Following incubation, Traces of β-ME was removed from the gel strip by rinsing repeatedly with distilled water. The gel strip was set on a 12% denaturing SDS-PAGE in second dimension (Acín-Pérez *et al.*, 2008) followed by immunoblotting as per procedure described earlier.

3.15 In gel Complex I activity assay

In-gel Complex I activity of mitochondria was visualized on gel following BN-PAGE. Briefly, the gel after BN-PAGE was incubated in a buffer containing 0.1 M Tris-HCL (pH 7.4), 1 mg/ml of Nitrotetrazolium Blue Chloride (Sigma-Aldrich) and 0.14 mM NADH (Sigma-Aldrich) at room temperature for about 1 hr (Díaz, Barrientos and Fontanesi, 2009). Formazan is formed at the reaction site leading to development of blue/purple colour after

which the gel was washed with distilled water and fixed with 30% methanol and 10% acetic acid solution. The gel was subsequently documented by scanning the image and the band intensities were quantified by using GelQuant.NET software provided by biochemlabsolutions.com.

3.16 Measurement of complex I activity

Complex I activity of isolated mitochondria was measured according to the previously published protocols (Spinazzi *et al.*, 2012) with minor modification. Briefly, freshly isolated mitochondria resuspended in mitochondria resuspension buffer were estimated spectrophotometrically by Bradford reagent. Both from control and experimental samples, equal amount of mitochondria was pelleted down by centrifugation at 10,000 g for 10 minutes at 4°C. The obtained mitochondria pellet was resuspended in ice cold 10 mM hypotonic Tris buffer (pH-7.6) and subjected to three cycles of freeze thaw in liquid nitrogen so as to rupture the mitochondrial membranes. The sample was further suspended in assay buffer (50 mM potassium phosphate buffer [pH-7.5], 3 mg/ml of BSA and 3 mM sodium azide) to which 100µM NADH and 100µM ubiquinone were added. Reduction of NADH (extinction coefficient- 6.22 mM^{-1} cm^{-1}) was measured by correlating the decrease in absorbance of NADH (340nm) at different time points recorded for 5 minutes. Complex I activity (nmoL min^{-1} mg^{-1}) was calculated as (Δ Absorbance/min × 1000)/[(Extinction coefficient × Volume of sample used in ml) × (Sample protein concentration in mg ml^{-1})] (Spinazzi *et al.*, 2012). Percent change in Complex I activity was calculated considering activity of control sample as 100.

3.17 Measurement of mitochondrial ATP synthesis

Mitochondrial ATP synthesis was measured by a bioluminescence assay. Based on published literature (Mittal, Babu and Roy, 2009; Patra *et al.*, 2016), freshly isolated mitochondria (100 mg/mL) was energized by incubating in respiration buffer [0.6 M sorbitol, 1 mM MgCl2, 1 mM EDTA, 25 mM succinate, 5 mM ADP, and 25 mM potassium phosphate buffer (pH 7.0)] for 15 min at 37°C. ATP determination kit (Thermo Fisher Scientific) was used to quantify the generated ATP in mitochondria following the manufacturer's protocol. Luminescence was measured by using HIDEX Sense Multimode Micro Plate Reader 425-301 (HIDEX).

3.18 Liquid chromatography and mass spectrometry

In Gel Digest: The gel slices were cut to 1 mm by 1 mm cubes and destained three times by first washing with 100 µL of 100 mM ammonium bicarbonate for 15 minutes, followed by addition of the same volume of acetonitrile (ACN) for 15 minutes. The supernatant was discarded and samples (gel pieces) were dried in a speedvac. Samples were then reduced by mixing with 200 µL of 100 mM ammonium bicarbonate and 10 mM DTT and incubated at 56°C for 30 minutes. Following liquid removal, 200 µL of 100 mM ammonium bicarbonate-55 mM iodoacetamide was added to gel pieces and incubated at room temperature in the dark for 20 minutes. After the removal of the solvent and one wash with 100 mM ammonium bicarbonate for 15 minutes, same volume of ACN was added to dehydrate the gel pieces. After solvent removal, the samples were dried in a speedvac. For digestion, enough solution of ice-cold trypsin (0.01 µg µL−1) in 50 mM ammonium bicarbonate was added to cover the gel pieces for 30 minutes on ice. After complete rehydration, the excess trypsin solution was removed, replaced with fresh 50 mM ammonium bicarbonate, and left overnight at 37°C. The peptides were extracted twice by the addition of 50 µL of 0.2% formic acid and 5% ACN and vortex mixing at room temperature for 30 minutes. The combined extractions are analyzed directly by liquid chromatography (LC) in combination with tandem mass spectroscopy (MS/MS) using electrospray ionization.

LC-MS-MS: Trypsin-digested peptides were analyzed by ultra-high pressure liquid chromatography (UPLC) coupled with tandem mass spectroscopy (LC-MS/MS) using nano-spray ionization. The nanospray ionization experiments were performed using a Orbitrap fusion Lumos hybrid mass spectrometer (Thermo Fisher Scientific, Waltham, MA, USA) interfaced with nano-scale reversed-phase UPLC (Thermo Dionex UltiMate 3000 RSLC nano System) using a 25 cm, 75-micron ID glass capillary packed with 1.7-µm C18 (130) BEH beads (Waters corporation, Milford, MA, USA). Peptides were eluted from the C18 column into the mass spectrometer using a linear gradient (5-80%) of ACN (Acetonitrile) at a flow rate of 375 µL min−1 for 1 hour. The buffers used to create the ACN gradient were: Buffer A (98% H2O, 2% ACN, 0.1% formic acid) and Buffer B (100% ACN, 0.1% formic acid). Mass spectrometer parameters were as follows; an MS1 survey scan using the orbitrap detector of mass range (m/z): 400-1500 (using quadrupole isolation), 120 000 resolution setting, spray voltage of 2200 V, ion transfer tube temperature of 275°C, AGC target of 400 000, and maximum injection time of 50 ms was

followed by data-dependent scans (top speed for most intense ions, with charge state set to only include + 2-5 ions, and 5 second exclusion time, while selecting ions with minimal intensities of 50 000 in which the collision event was carried out with high energy collision energy of 30%), and the fragment masses where analyzed in the ion trap mass analyzer (with ion trap scan rate of turbo, first mass m/z 100, AGC Target 5000 and maximum injection time of 35 ms). Protein identification and label free quantitation was carried out using Peaks Studio 8.5 (Bioinformatics solutions Inc).

3.19 Electron microscopy

C-28/I2 chondrocyte line was fixed with 2.5% glutaraldehyde and 2% paraformaldehyde in 0.15 M cacodylate buffer. Post fixing, cells incubated with 1% OsO4 in 0.1 M cacodylate buffer on ice for 1 hour. Subsequent staining en bloc was with 2%-3% uranyl acetate for 1 hour on ice. Graded series of ethanol (20%-100%) on ice was used to dehydrate the cells. This was followed by one wash with 100% ethanol and two washes with acetone (15 min each). Embedding was done with Durcupan. Sections were cut at 50 to 60 nm on a Leica UCT ultramicrotome, and picked up on Formvar and carbon-coated copper grids. Sections were stained with 2% uranyl acetate for 5 minutes and Sato's lead stain for 1 minute. Finally grids were viewed using a JEOL 1200EX II (JEOL) TEM and photographed using a Gatan digital camera (Gatan).

3.20 WISP3 mutant generation

CRISPR Cas9 technology was used to generate Exon 5 specific WISP3 mutants. Guide RNA having minimum off target and maximum on target was designed online using CHOPCHOP tool (Montague *et al.*, 2014). The guide RNA oligo was cloned into pSpCas9 (BB) 2A-Puro (PX458) vector (Addgene). Briefly, the primer pair, for forward strand 5′-C ACCGCATTTAAATGACCCCTCATT-3′, and for reverse strand 5′-AAACAATGAG GGGTCATTTAAATGC-3′ were annealed, phosphorylated with polynucleotide kinase (Thermo Fisher scientific) and ligated to BbsI digested vector using T7 ligase (NEB). The positive clone was confirmed by Sanger sequencing and are used to transfect C-28/I2 cells using Lipofectamine 2000 (Invitrogen) as per manufacturer's protocol. In brief, C-28/I2 cells were plated 12-14 hours prior to transfection at a density of $0.5X10^6$ cells per well in each well of six well plate. For each well of six-well plate, 5 µL of Lipofectamine 2000 and 2 µg of plasmid DNA were mixed separately with 150 µL of Opti-MEM. The plasmid DNA and Opti-MEM mixture solution was poured slowly to Lipofectamine-Opti-MEM

solution and mixed well. The resultant mixture (300µl) was incubated for 30 minutes in room temperature following which the solution was added drop wise to the well. The plate was swirled gently for even distribution of transfecting mixture before keeping inside the CO_2 incubator. Media of transfected cells was replaced after 24 hours post-transfection with fresh DMEM high glucose complete medium. After 48 hrs of transfection, Puromycin (1.5 µg/ml) was added for selection of transfected cells and further incubated for 48 hrs, fresh media was added thereafter. The surviving cells were pooled, diluted and plated in 12 well plates so as to obtain single cell in each well. The single cell colonies were screened further by checking WISP3 expression in whole cell level and by Sanger sequencing to check insertion or deletion of bases in genome. Colonies having mutations and showing decreased expression of mutant WISP3 were propagated further and harvested for assays related to mitochondrial function.

3.21 Genomic DNA isolation and sequencing

Genomic DNA was isolated from both wild type and mutant C-28/I2 cells. In brief, cells were harvested by scraping the cells in PBS followed by spin down at 2000 rpm. The obtained cell pellet was resuspended in digestion buffer having composition 100 mM NaCl, 10 mM Tris (pH 8.0), 25 mM EDTA (pH 8.0), 0.5% SDS and 0.1 mg mL−1 of proteinase K and incubated overnight at 50°C in dry bath. Following digestion, equal volume of phenol/chloroform/isoamyl alcohol was added and centrifuged at 12000 g for 10 minutes. The aqueous layer was gently transferred to a separate tube. To the aqueous layer, two volumes of ethanol was added and mixed by turning upside down. The solution was centrifuged at 12000 g for 10 minutes to obtain genomic DNA pellet (Koh, 2013). The target region of genomic DNA (exon 5 region) was then subjected to PCR amplification by Pfu Plus DNA Polymerase (BioBharati Lifescience) using primers Exon 5 Fw 5′-GCCTCCAAATACTCAGATTTG-3′ (forward) and Exon 5 Rv 5′-GTAGTGATCTGAG AATAGGCA-3′ (reverse). The PCR product was separated on a 1.5% Agarose gel, band containing DNA was excised from gel and purified by using PureLink™ quick gel extraction kit (Thermo Fisher Scientific). The purified PCR product was sent for sanger sequencing (1st Base Sequencing Service) to determine insertion and deletion in the the genome followed by comparing mutant and wild type sequence using Clustal Omega program (Madeira *et al.*, 2019).

3.22 MTT assay

Cell viability of wild type versus mutant C-28/I2 cells was performed by MTT (Dimethylthiazol-diphenyl tetrazolium bromide) assay. For MTT assay, cells were plated in a 96-well flat bottom culture plate. Under standard tissue culture conditions, cells were plated at a density of 10^4 cells per well. 10µl of MTT (5 mg/ml) (Sigma-Aldrich) was added to each well at desired time points and incubation continued for 4 hours at 37°C, 5% CO2. The culture media was removed followed by addition of 200 µl of DMSO was added to each well. dissolve The formazan crystals gets dissolved by mixing DMSO and absorbance was measured at 595 nm in a micro plate reader (Bio-Rad) as described in previously published protocol (van Meerloo, Kaspers and Cloos, 2011).

3.33 Histology and immunofluorescence

Left dorsal skeletal muscle of zebrafish was dissected out and 10% buffered formalin was used to fix the tissue by incubating it overnight. The muscle sample was then dehydrated in graded alcohol and embedded in paraffin. Tissue was sectioned at a thickness of 3 µm using a microtome and subjected to histology and immunofluorescence. Mayer's albumin-coated glass slides was used to mount the tissue sections and stained with haematoxylin–eosin for histological studies following published procedure (Feldman and Wolfe, 2014). Tissue sections were mounted on poly-L-lysine-coated glass slides and processed for immunofluorescence study following previously reported protocol (Scanziani, 1998; Joshi and Yu, 2017). For heat-induced antigen retrieval from tissue sections, the slides were immersed in Tris-EDTA buffer [10 mM Tris base, 1 mM EDTA, 0.05% Tween 20 (pH 9.0)] and placed in a pressure cooker. The slides were bought to room temperature and blocked with 10% normal serum and 1% BSA in TBS. Tissue sections slides were kept in moist chamber and incubated overnight at 4°C with primary antibody (anti-Vdac1, anti-Wisp3, or anti-Cox4). Next day, the slides were incubated with fluorophore-conjugated secondary antibody [Alexa Fluor 546 anti-rabbit antibody or Alexa Fluor 488 anti-mouse antibody (Thermo Fisher Scientific)] for 1 hour followed by visualization of slides under fluorescence microscope (Leica, DMI 3000B) and confocal microscope (Leica, TCS SP8).

3.34 Analysis of swimming behaviour

After the administration of *wisp3* or control morpholino, the swimming behaviour of zebrafish was analysed following reported procedure of "startle response" (Eddins *et al.*, 2010; Miller *et al.*, 2012), with minor modifications. Briefly, following morpholino

injection, individual fish was kept in a small transparent rectangular tank (28 cm length, 20 cm width and 10 cm height) with 4 L of water. After 48 or 72 h post-morpholino injection, stimulus was given by a "single tap" on the tank. Following the single tap, swimming behaviour was recorded for up to 4 min with a video camera placed at the top of the tank. Uninjected fish was used as a reference in this experiment. Filmora 9, a video editing software was used to analyse the video recordings. The distance covered and turns taken per minute by each fish was calculated and plotted as graph by using GraphPad Prism software.

3.35 Statistical analysis

All the data were presented as the mean $\pm$ SEM and p value was calculated by Student's *t* test; *$p \leq 0.05$, **$p \leq 0.005$, ***$p \leq 0.0005$. Percentage of damaged mitochondria in TEM was analysed by one-way ANOVA followed by multiple comparison tests. Three to five zebrafish were used in each group for a particular point of data. The difference between the experimental and control groups were evaluate thereafter. For experiments involving zebrafish mitochondria, about 10 fish represents each pool, and at least three pools represents any one data point. GraphPad Prism software was used for all the statistical analysis and graphical presentation of data.

CHAPTER IV

RESULTS

RESULTS

4.1 WISP3 localizes to mitochondria

WISP3 is a multimodular protein having potential to interact with other proteins (Hurvitz *et al.*, 1999; Brigstock, 2003; Engel, 2004; Davis, Chen and Sen, 2006; Miller and Sen, 2007; Perbal, 2013; Repudi, Patra and Sen, 2013). WISP3 plays a major role as a regulator of basal mitochondrial metabolism by regulating ATP production and calcium uptake in mitochondria (Patra *et al.*, 2016). Taking into account of regulation of mitochondrial metabolism by WISP3, it was interesting to check its localization in mitochondria. Presence of WISP3 in mitochondria of C-28/I2 cells was evident from immunoblotting of subcellular fractionation as depicted in figure 1A where COX IV is used as a marker protein of mitochondria (Dolga *et al.*, 2014). Protease protection assay was performed to validate the sub-mitochondrial localization of WISP3 in C-28/I2 cell line.

Figure 1

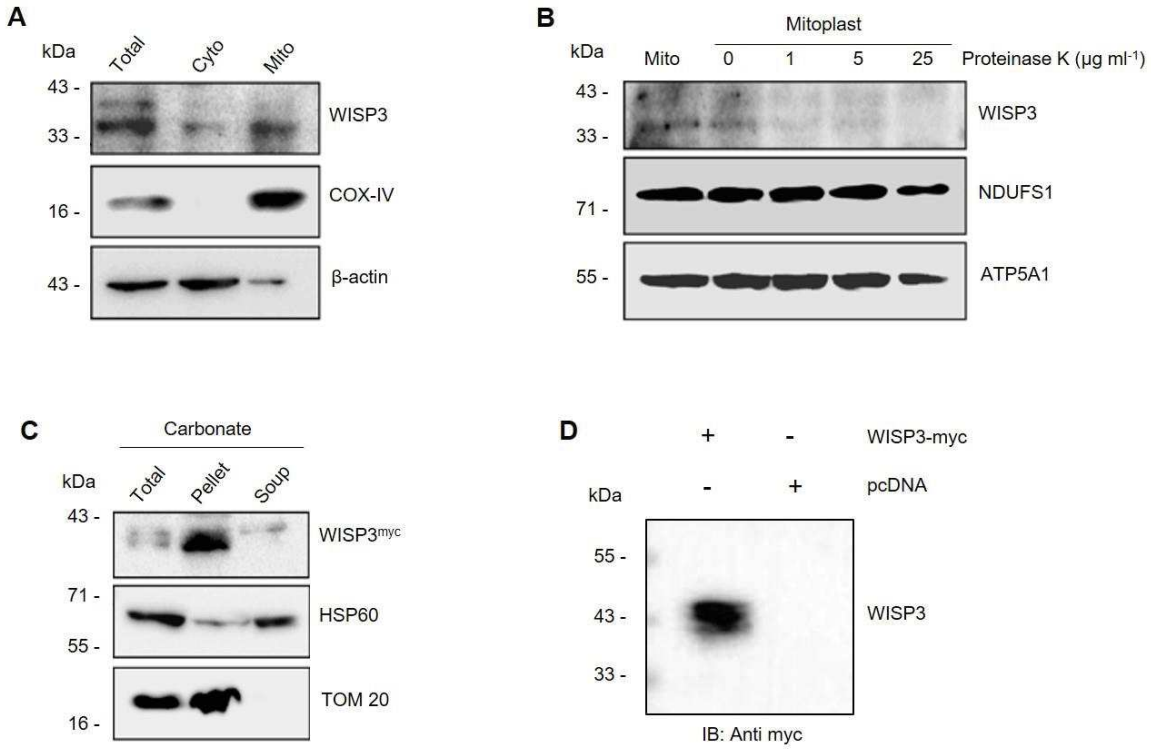

Figure 1: WISP3 localizes to mitochondria.

(A) Immunoblot depicting the presence of WISP3 in mitochondrial fraction (Mito), cytosolic fraction (Cyto) and whole cell lysate (Total) of C-28/I2 cells. β-actin and COX-IV were used as loading control of cytosolic and mitochondrial fractions respectively. (B) Immunoblot of mitochondria and proteinase K treated mitoplast indicates sub-mitochondrial localization of WISP3. Respiratory complex proteins NDUFS1 and ATP5A1 are used as marker of inner mitochondrial compartment. (C) Immunoblot of Na_2CO_3 incubated mitochondria of $WISP3^{myc}$ transfected HEK293 cells depicting association of WISP3 with membrane fraction (pellet), soluble

fraction (soup) of mitochondria. Total indicates the whole mitochondria, TOM20 is used as marker of outer mitochondrial membrane, HSP60 is used as an indicator of inner mitochondrial membrane and mitochondrial matrix. (D) Immunoblot of WISP3^{myc} and pcDNA transfected HEK293 cells depicting the transfection efficiency of WISP3^{myc} DNA.

Mitoplast was prepared from isolated mitochondria of chondrocyte cell and subjected to proteinase K digestion at different time interval followed by immunoblotting with anti-WISP3 antibody and antibody against mitochondrial inner compartment marker proteins (NDUFS1 and ATP5A1). It was observed that a significant amount of WISP3 protein was accessible to proteinase K digestion whereas a notable fraction was resistant to protease digestion figure 1B. In order to further validate the sub-cellular localization of WISP3 in mitochondria, membranous fraction and soluble fraction of mitochondria were separated from mitochondria of WISP3^{myc} transfected HEK293 cells in carbonate buffer (Zhou *et al.*, 2008; Mick *et al.*, 2012). Both the membranous fraction and soluble fractions were subjected to immunoblotting using anti-Myc antibody to detect WISP3, anti-HSP60 antibody as an inner membrane/matrix marker and anti-TOM20 antibody as an outer membrane marker. Immunoblot suggests that most of mitochondrial WISP3 is associated with membrane of mitochondria while a portion is also present in soluble fraction as depicted in figure 1C (Sun *et al.*, 2006; De Vos *et al.*, 2012). Over expression of WISP3 by transfecting WISP3^{myc} DNA in HEK293 cells was validated by immunoblotting using anti-myc antibody to lysate of transfected cells (figure 1D).

Localization of WISP3 in mitochondria of C-28/I2 cells was also demonstrated by confocal microscopy. It was observed that endogenous as well as over-expressed WISP3 co-localizes with mitochondria stained with mitotracker green (Figure 2A, B). The extent of co-localization of WISP3 and mitotracker green in both endogenous level and WISP3^{myc} over-expressed level was estimated by both RGB plot and Pearson's coefficient (Figure 2 C-E). These results indicates that the regulation of mitochondrial metabolism by WISP3 (Patra *et al.*, 2016) is due to its physical association with mitochondrial proteins. This paves path to explore more on the role of mitochondrial WISP3 and its regulation in maintaining mitochondrial respiratory complexes. Taking into account the multimodular nature of WISP3, led us to investigate its interacting partners in mitochondria and its subsequent regulation of electron transport chain complexes.

Figure 2

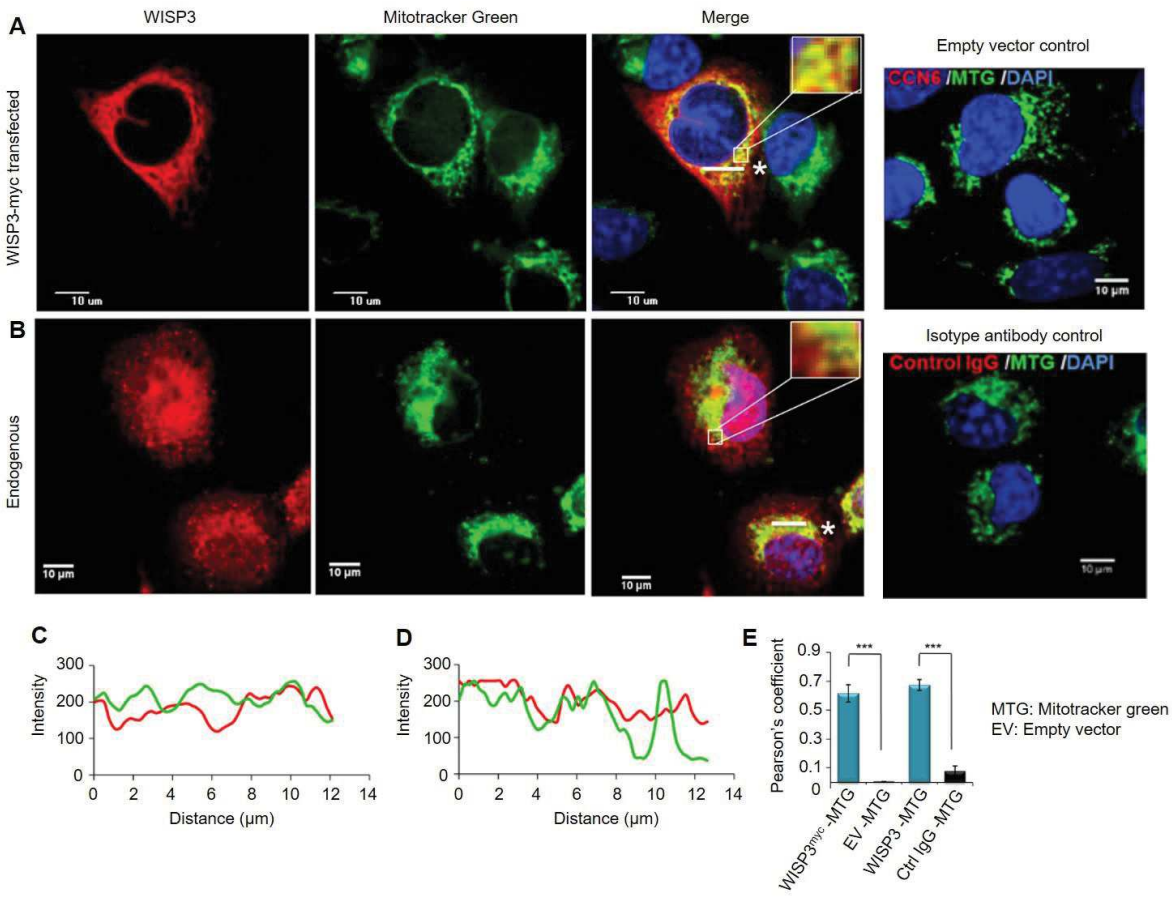

Figure 2: WISP3 is present in mitochondria.

(A&B) Confocal microscopy of WISP3^{myc} transfected C-28/I2 cells and endogenous cell revealing co-localization of WISP3 with mitochondria. Mitotracker green dye is used to stain mitochondria and WISP3 is stained as red. Yellow colour in the merge image indicates co-localization of WISP3 and mitochondria. (C&D) RGB intensity plot of confocal images depicting co-localization in WISP3^{myc} transfected and endogenous cell respectively. (E) Pearson's coefficient of co-localization was calculated from the confocal images as depicted in A&B.

4.2 WISP3 remains associated with the mitochondrial respiratory complex

Considering multimodular architecture of WISP3, its potential to interact with other proteins and regulating mitochondrial functions (Hurvitz *et al.*, 1999; Patra *et al.*, 2016) it is important to look into the mechanism of its regulation. In this regard we were interested to find whether WISP3 remains associated with mitochondrial respiratory chain complexes. In order to achieve our objective, initially we isolated mitochondria from C-28/I2 chondrocyte cell line to perform two-dimensional gel electrophoresis. Briefly, mitochondrial protein was first run on BN-PAGE. Then SDS-PAGE and immunoblotting with anti-WISP3 antibody and anti-mitochondrial cocktail antibody were performed in the

second dimension to detect different subunits of mitochondrial respiratory chain complexes existing in the functional domain (Wittig, Braun and Schägger, 2006; Acín-Pérez *et al.*, 2008; Mimaki *et al.*, 2012). It was observed that although WISP3 is present in its own molecular weight form whereas a significant portion remains associated with mitochondrial respiratory Complex I, Super Complex and other respiratory complex intermediates comprising Complex III, Complex IV and Complex V.

WISP3 was detected in accordance with NDUFB8 (Complex I subunit), ATP5A1 (Complex V subunit), UQCRC2 (Complex III subunit), and MTCO1 (Complex IV subunit) and also in the form of Super Complexes, which comprise Complex I and other respiratory complex intermediates as depicted in figure 3A.

Dotted lines on the blots denote skewed protein migration due to two dimensional BN/SDS-PAGE. In chondrocyte cell line, the presence of mitochondrial Complex I in the Super Complex region and the existence of other mitochondrial respiratory complexes in that region are in line with the previously published literature (Acín-Pérez *et al.*, 2008; Mimaki *et al.*, 2012; Moreno-Lastres *et al.*, 2012; D *et al.*, 2017). Mitochondria lysate was run on BN-PAGE, the region encompassing Super Complex and Complex I region were excised (excision mark of each region in highlighted in red box) (Figure 3B) and were subjected to liquid chromatography followed by mass spectrophometry. Presence of different respiratory complex intermediate proteins as well as certain respiratory complex assembly factors were also detected by mass spectrophotometric analysis of BN-PAGE taking Super Complex and Complex I region (Figure 3C). However, WISP3 remained undetected perhaps due to its incompatibility with the peptide detection system of mass spectrometer.

Further validation of association of mitochondrial WISP3 with mitochondrial respiratory complexes was confirmed by size exclusion chromatography followed by immunoblotting. The fractions collected by size exclusion chromatography of total mitochondria lysate was immunoblotted using anti-WISP3 antibody and certain subunits of mitochondrial respiratory chain. Also in this case, it was observed that WISP3 remained in high molecular weight complex by being associated with subunits of Complex I (NDUFB8, NDUFS1) and other subunits like UQCRC2, MTCO1 and ATP5A1 which comes in the range of Complex I/Super Complex and other intermediates of respiratory complexes as depicted in figure 4.

Figure 3

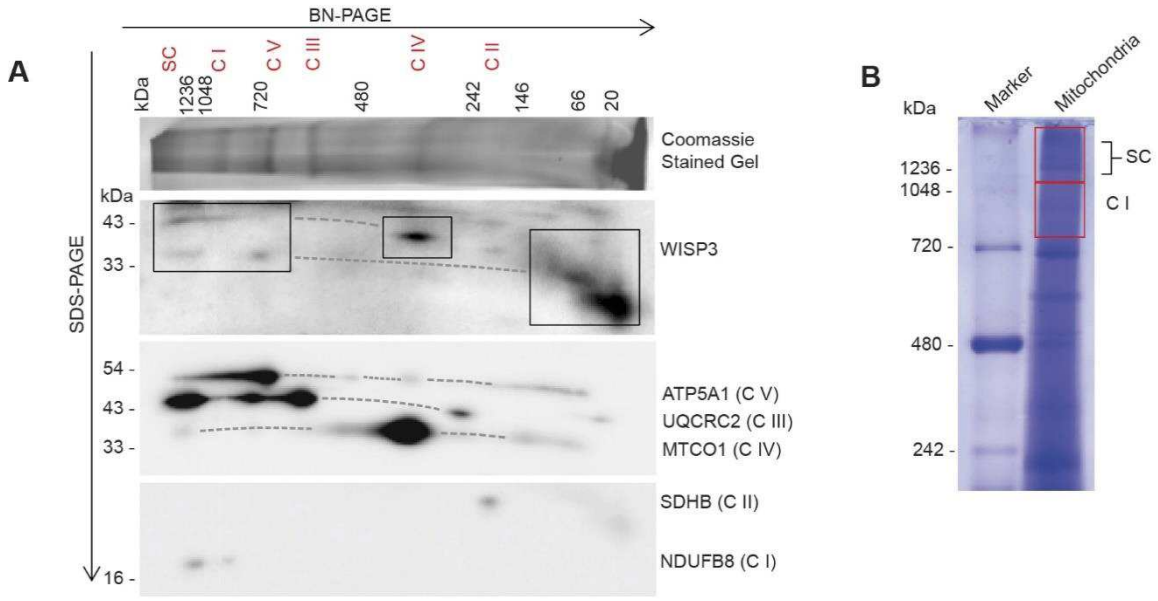

SC : Super Complex, C I : Complex I, C II : Complex II, C III : Complex III, C IV : Complex IV, C V : Complex V

C

Description of proteins	Number of peptides	
	SC region	C I region
NADH-ubiquinone oxidoreductase 75kDa subunit (NDUFS1)	40	39
NADH dehydrogenase [ubiquinone] iron-sulfur protein 2 (NDUFS2)	34	33
NADH dehydrogenase [ubiquinone] flavoprotein 1 (NDUFV1)	25	22
NADH dehydrogenase [ubiquinone] 1 beta subcomplex subunit 8 (NDUFB8)	7	5
NADH dehydrogenase [ubiquinone] 1 alpha subcomplex subunit 9 (NDUFA9)	24	24
NADH dehydrogenase [ubiquinone] iron-sulfur protein 3 (NDUFS3)	14	18
NADH dehydrogenase [ubiquinone] 1 alpha subcomplex subunit 8 (NDUFA8)	12	11
Cytochrome b-c1 complex subunit 1 (UQCRC1)	39	20
Cytochrome b-c1 complex subunit 2 (UQCRC2)	30	17
Cytochrome b-c1 complex subunit Rieske (UQCRFS1)	17	5
Cytochrome b-c1 complex subunit 7 (UQCRB)	11	6
Cytochrome c oxidase subunit 4 isoform 1 (COX4I1)	7	7
Cytochrome c oxidase subunit 2 (MTCO2)	5	5
Cytochrome c oxidase subunit 5A (COX5A)	8	5
Cytochrome c oxidase subunit 5B (COX5B)	6	2
Cytochrome c oxidase assembly protein COX15 homolog (COX15)	6	6
ATP synthase subunit alpha (ATP5A1)	25	49
ATP synthase subunit beta (ATP5B)	25	53
ATP synthase F(0) complex subunit B1 (ATP5F1)	7	15
ATP synthase subunit d (ATP5H)	7	15
ATP synthase subunit O (ATP5O)	7	13
Complex I assembly factor TIMMDC1 (TIMMDC1)	4	9
NADH dehydrogenase [ubiquinone] 1 alpha assembly factor 3 (NDUFAF3)	2	7
Complex I intermediate-associated protein 30 (NDUFAF1)	2	11

SC : Super Complex, C I : Complex I

Figure 3: WISP3 remains associated with respiratory complex of mitochondria.

(A) WISP3 is detected in immunoblot of 2D BN-SDS-PAGE of mitochondria at high molecular weight region along with Super complex/Complex I along with other intermediates of mitochondrial respiratory chain. Presence of WISP3 is highlighted in black box, dotted lines in the blot indicates skewing in protein migration (B) Coomassie stained gel of mitochondria lysate of C-28/I2 cell. Red box highlights the Super Complex and Complex I region excised for LC-MS/MS. (C) Sorted list of proteins detected in Super Complex and Complex I region by LC-MS/MS.

These results suggest that the association of WISP3 with mitochondrial respiratory complex may be a key player in regulation of mitochondrial function as described earlier (Patra *et al.*, 2016). This led us to investigate the role of WISP3 in mitochondrial respiratory complex assembly and activity.

Figure 4

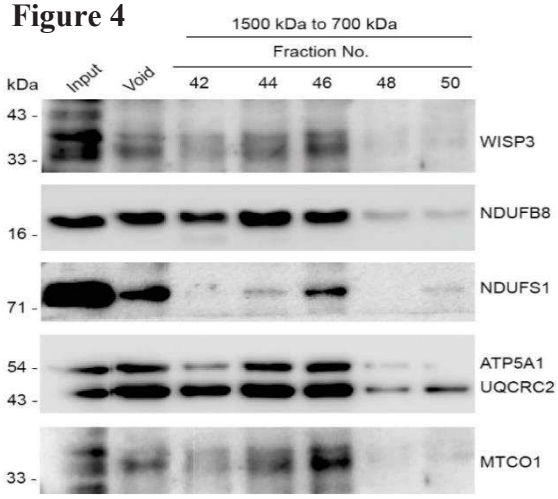

Figure 4: WISP3 exists as high molecular weight complex. Immunoblot of mitochondrial lysate by size exclusion chromatography depicting migration of WISP3 with subunits of

4.3 Partial reduction of WISP3 alters mitochondrial respiratory complex activity and assembly

Mitochondrial respiratory complex activity and assembly was evaluated to determine the effect of WISP3. Here, mitochondrial Complex I was taken for study as it the initiator of electron transport chain of mitochondria and plays an important role in ATP synthesis as well as it exists in equilibrium as Super Complexes (Acín-Pérez *et al.*, 2008; Mimaki *et al.*, 2012; Moreno-Lastres *et al.*, 2012; D *et al.*, 2017; Signes and Fernandez-Vizarra, 2018). In order to assess the influence of WISP3 on mitochondrial respiratory complex activity and assembly, knockdown of WISP3 was essential in both C-28/I2 and C20A4 (chondrocyte) cell line. In chondrocyte cell line, mitochondrial Complex I / Super Complex assembly and activity was evaluated after partial depletion of WISP3 by siRNA transfection. Reduction in WISP3 expression about 35% in protein and 50% in mRNA was confirmed by densitometry of band intensities as depicted in figure 5A, B.

Figure 5

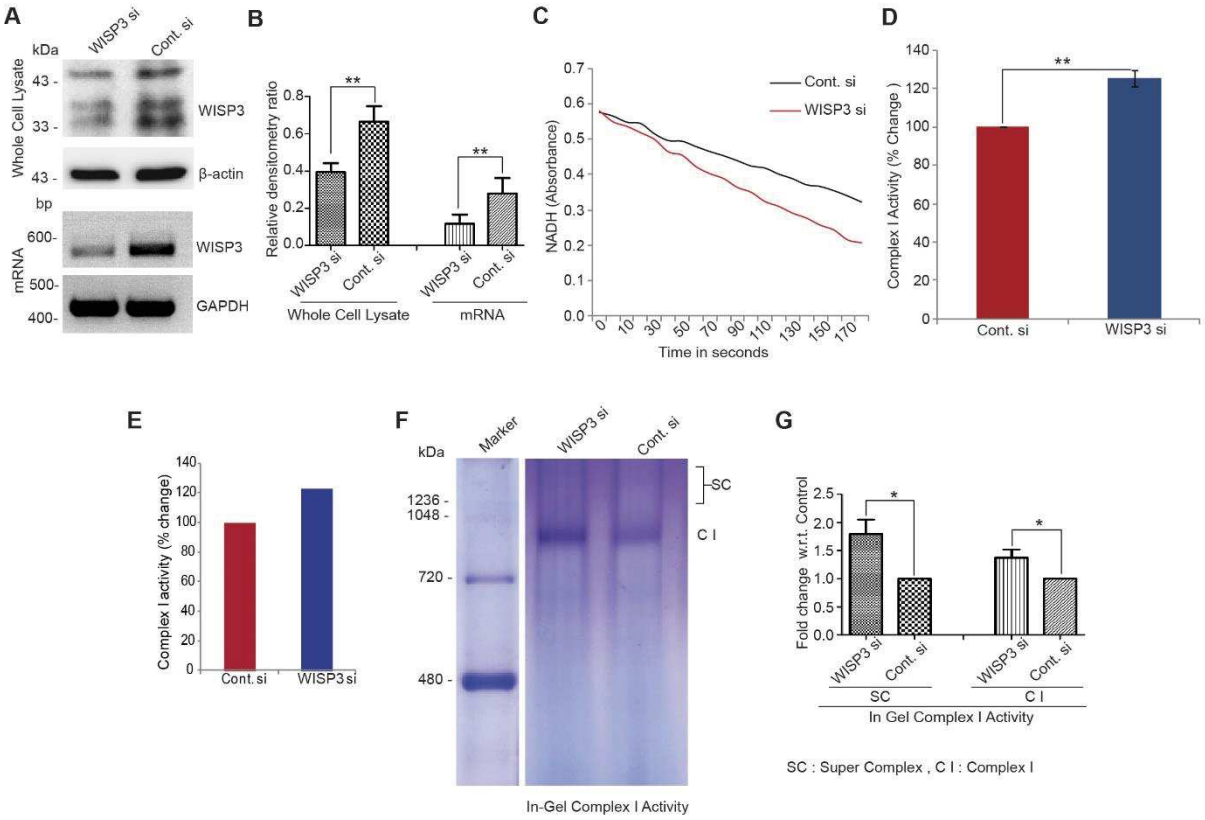

Figure 5: Complex I activity is increased in WISP3 depleted cells.

(A&B) Immunoblotting of lysate of WISP3 depleted cells by siRNA followed by quantification of band intensities by densitometry in bar graph demonstrating reduction of WISP3 in whole cell lysate and in mRNA. (C) Depletion of WISP3 increases Complex I activity as represented by higher rate of decrease of NADH absorbance as compared with control. (D&E) Bar graph showing percent change in Complex I activity in WISP3 depleted cells compared to control (taking control as 100). (F&G) BN-PAGE in-gel Complex I activity assay followed by quantification of band intensities by densitometry shows increased activity in WISP3 siRNA transfected cells when compared with control. Data are presented as mean $\pm$ SEM $*p < 0.05$, $**p < 0.01$ (Student's t- test).

This moderate reduction of WISP3 leads to increase in Complex I activity in both C-28/I2 and C20A4 chondrocyte cell line. Increase in complex I activity was measured based on oxidation of NADH by mitochondria in WISP3 siRNA treated sets vs. control sets. Oxidation of NADH correlates with decrease in absorbance of NADH at 340nm which are displayed in term of time kinetics spanning a period of 180 seconds (Figure 5C). The percent change in Complex I activity in both C-28/I2 and C20A4 chondrocyte cell line are depicted in Figure 5D & E respectively. Further, in order to validate this result, mitochondria of WISP3 depleted cells were subjected to BN- PAGE followed by in-gel assessment of Complex I activity. In-gel Complex I activity assay was performed based on published protocols (Acín-Pérez *et al.*, 2008; Díaz, Barrientos and Fontanesi, 2009). Here as well, the reduction of NBT by NADH was significantly more in mitochondria of WISP3

depleted cells than corresponding control (Figure 5F) as revealed by densitometry of band intensities (Figure 5G).

Figure 6

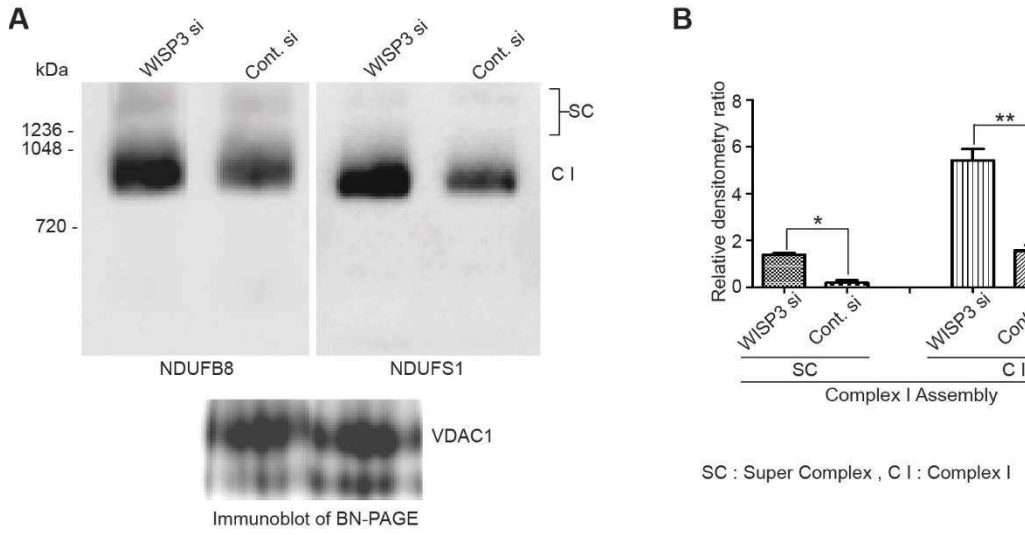

Figure 6: Assembly of Complex I is increased in WISP3 depleted cells.

(A) Immunoblotting of BN-PAGE with anti -NDUFB8 & NDUFS1 (Complex I subunits) antibodies shows increased Complex I and Super Complex assembly. (B) Quantification of band intensities by densitometry indicates increased assembly in ComplexI/Supercomplex region. Data are presented as mean $\pm$ SEM $*p < 0.05$, $**p < 0.01$ (Student's t- test).

In order to dig deep into the cause of increase in Complex I activity, we predicted that this might be due to either NADH oxidation in a more efficient manner by Complex I or more assembled form of Complex I so that the NADH is oxidised relatively faster in WISP3 siRNA treated cells. Interestingly, it was found that the increase in Complex I activity is due to the increase in assembled form of Complex I/ Super complex which was clear from immunoblot after BN-PAGE of total mitochondrial lysate using antibodies against NDUFB8 and NDUFS1 (subunits of Complex I) (Figure 6A). As a loading control, anti-VDAC1 antibody was used. Corresponding band intensities were quantified by densitometry and relative densitometry ratio of WISP3 siRNA and control siRNA are plotted in graph as depicted in Figure 6B. From these results it is clear that moderate reduction of WISP3 leads to increase in assembled form of Complex I in respiratory complexes.

It was also observed that the NDUFB8 level in whole cell lysate was also 50% more in WISP3 siRNA transfected cells as seen in immunoblot of SDS-PAGE whereas there was no change in mRNA level as seen by RT-PCR. However, upon WISP3 depletion, there was

no change in NDUFS1 expression in both protein and mRNA level as depicted in densitometry of corresponding band intensities (Figure 7A & B). These results suggests that WISP3 level plays an important role in both stability and assembly of subunits of Complex I and mitochondrial respiratory chain complexes.

Figure 7

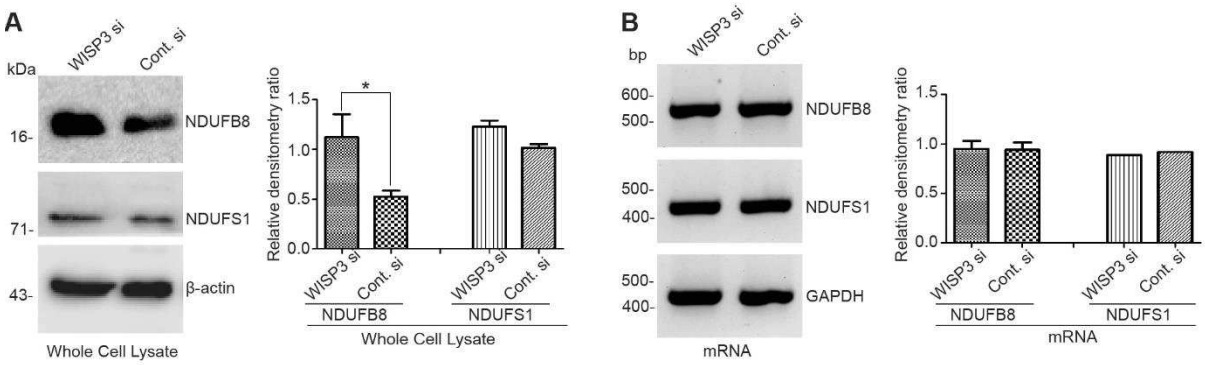

Figure 7: (A&B) Immunoblot of whole cell lysate of WISP3 depleted cells shows increased expression of NDUFB8 protein but not in mRNA of C-28/I2 cells. However no significant change is seen in both protein and mRNA level of NDUFS1. The bar graphs represents relative densitometric ratios of bands. Data are presented as mean $\pm$ SEM $*p < 0.05$ (Student's t- test).

4.4 Moderate depletion of WISP3 increases its mitochondrial localization

In order to substantiate how the effect of moderate WISP3 depletion in whole cell level in C-28/I2 and C20A4 cell line correlates with the mitochondrial WISP3 level, we assessed the distribution of WISP3 in mitochondria and cytosol. Interestingly, it was observed that the increase in Complex I / Super complex activity and assembly was correlated with increased mitochondrial localization of WISP3 as compared to its cytosol in both C-28/I2 and C20A4 chondrocyte cell line (Figure 8A). Moderate depletion of WISP3 was visible in the cytosol but more amount of WISP3 was harboured in mitochondria of WISP3 depleted cells compared to corresponding control. The ratio of WISP3 expression in mitochondria:cytosol of WISP3 depleted cells is quantified densitometrically and plotted in Figure 8B.

Figure 8

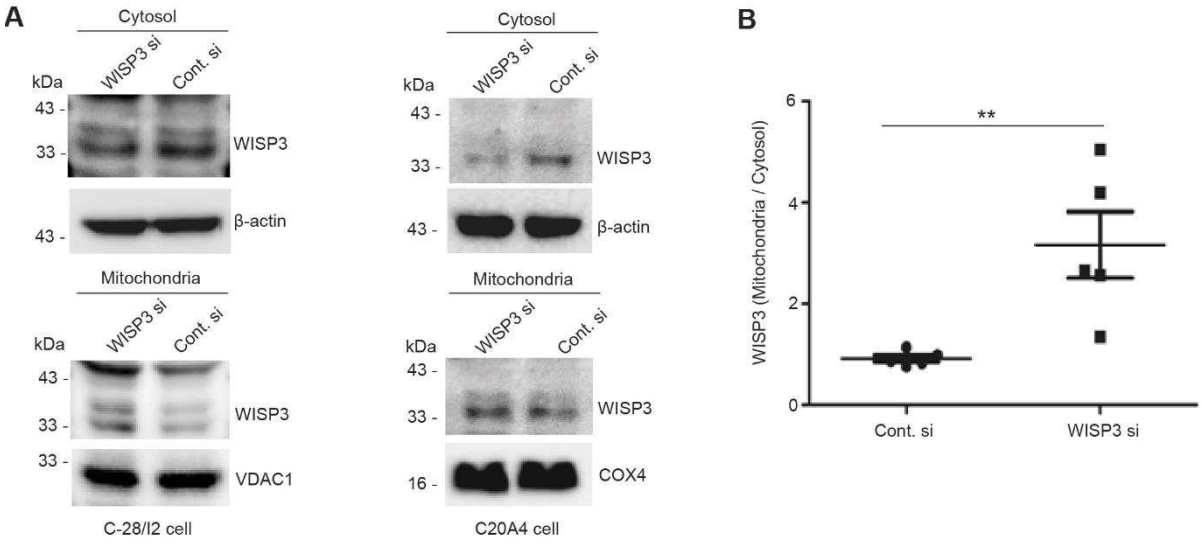

Figure 8: WISP3 depletion by siRNA alters mitochondrial distribution of WISP3.

(A) Immunoblots showing decreased cytosolic but increased mitochondrial distribution of WISP3 in both C28/I2 and C20A4 chondrocyte lines. β-actin and VDAC1/COX4 are shown as loading controls for cytosol and mitochondria respectively. (B) Densitometric plot of relative WISP3 level (mitochondria/cytosol). Data are presented as mean ± SEM $**p < 0.01$(Student's t- test).

This relative increase in mitochondrial WISP3 in WISP3 depleted condition correlated with notable decrease in RER (rough ER)-OMM (outer mitochondrial membrane) distance as visualized by transmission electron microscopy (Figure 9A). Distance between RER-Mitochondria was measured by morphometric analysis and the distribution plot (Figure 9B) shows that the distance is reduced in WISP3 depleted condition. The mechanism of altered WISP3 distribution in mitochondria is not clear at this stage.

Figure 9

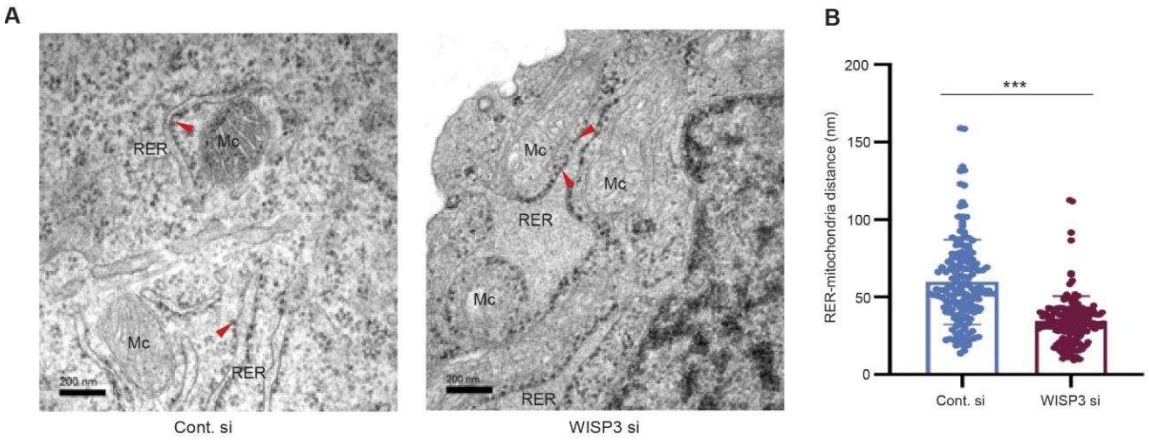

Figure 9: Depletion of WISP3 alters RER-Mitochondria distance.

(A) Transmission Electron micrographs showing closer association of rough endoplasmic reticulum (RER) ribosome with outer mitochondrial membrane (OMM) in WISP3 depleted cells compared to controls. Mc denotes mitochondria. Red arrowheads indicate ribosomes. Scale bar, 200nm. (B) Distribution plot with mean value showing morphometric analysis of the distance between RER and OMM. RER-OMM distance was calculated in more than 150 points. Data are presented as mean ± SEM ***$p < 0.001$(Student's t- test).

However the decrease in WISP3 protein level disturbs RER-mitochondria distance leading to bring ribosomes close to mitochondria. This may facilitate incorporation of ribosome translated WISP3 and other mitochondrial protein to enter into mitochondria leading to its increased localization thereby increased respiratory complex assembly and activity. These results suggest that WISP3 plays a vital role in maintenance of ideal RER-mitochondria distance which is required for flow of proteins into the mitochondria in a well-balanced manner. Previous publications also suggests that ER – mitochondria distance is essential in proper functioning of respiration in cells (Csordás *et al.*, 2006; de Brito and Scorrano, 2010).

4.5 Mutations in WISP3 result in disruption in respiratory complex assembly and activity leading to accumulation of abnormal mitochondria and cell viability

Mutations in WISP3 leads to a debilitating skeletal disorder called PPRD, which is marked by loss of normal chondrocyte in cartilage growth plate (Hurvitz *et al.*, 1999). There are several cases where PPRD is caused due to truncation in exon 5 of WISP3 (Trp 349 stop in variant 3 and Trp 331 stop in variant 1) (Garcia Segarra *et al.*, 2012; Sailani *et al.*, 2018). We wanted to check the effect of this mutation on mitochondrial function by generating truncated WISP3 mutant (Trp 349 stop) by CRISPR Cas9 technology (Ran *et al.*, 2013). As the chondrocyte cell line we use expresses variant 3 predominantly (Figure 10A) hence we focused on variant 3 of WISP3. A guide RNA was designed targeting exon 5 region of WISP3 followed by cloning it in a puromycin resistant plasmid vector, pSpCas9 (BB)-2A-Puro (PX459). The clone was then transfected into C-28/I2 cell line followed by puromycin selection. After transfection, cells were diluted and grown so as to obtain single cell colonies. Mutant cell populations were selected on the basis of diminished WISP3 expression in immunoblot using anti-WISP3 antibody which recognizes the protein beyond the target region of the mutation (Figure 10B, C). Of the selected clones, M1, M2 and M3 were sequenced and found to have frame shift mutation at amino acid residues 339 (M1), 338 (M2), and 339 (M3) leading to stop codon at 353,341 and 344 respectively (Figure 10D). This implies that the truncated proteins are produced in all three mutants which was

different from wild type. Slight difference in molecular weight (2-3 kDa) of mutant WISP3 was not visible by immunoblotting probably due to post translational modifications.

Figure 10

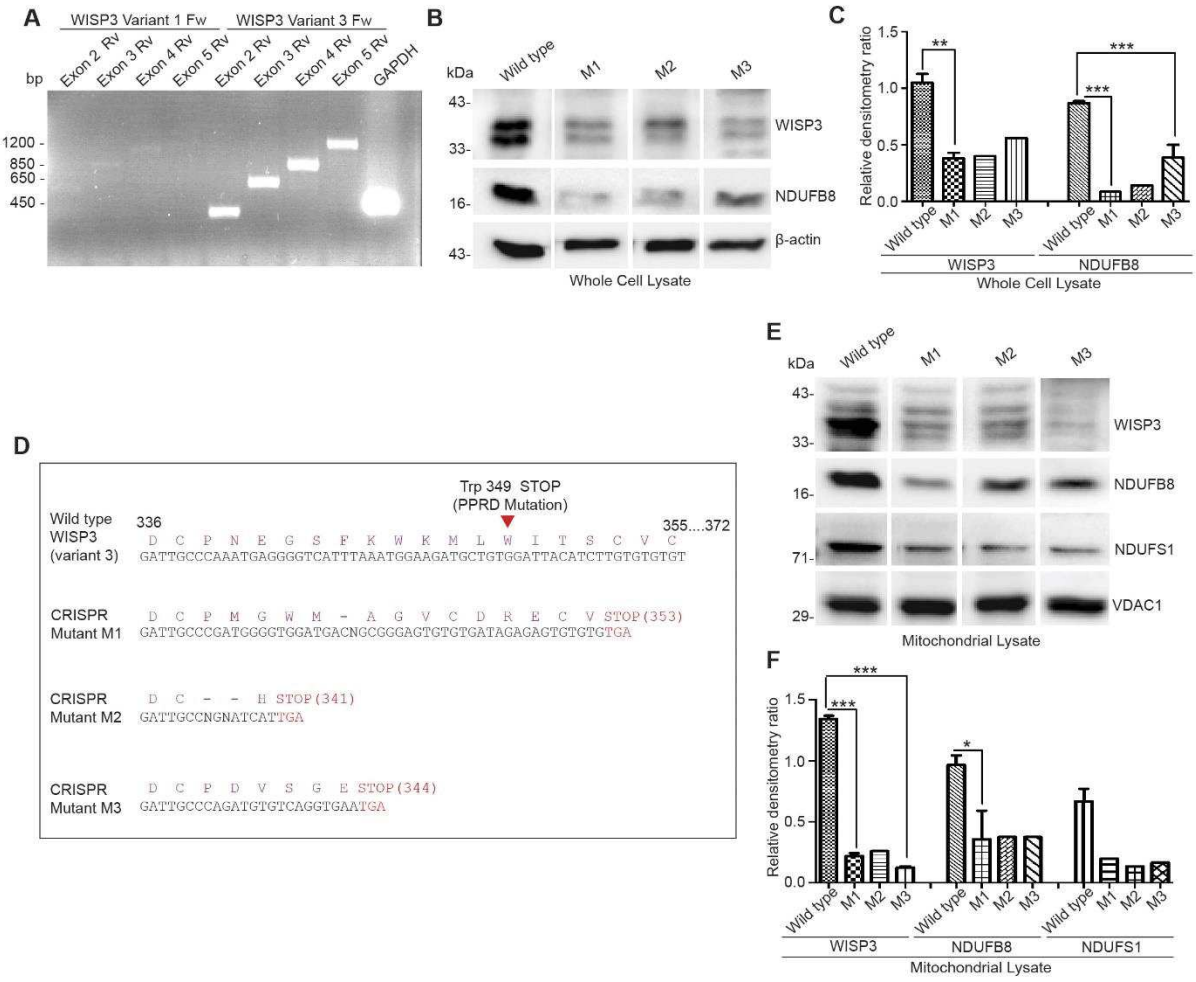

Figure 10: WISP3 mutant generation by CRISPR Cas9 technology.

(A) DNA gel of WISP3 variant analysis by PCR confirms the predominance of variant 3 over variant 1 in C-28/I2 chondrocyte cells. (B&C) WISP3 mutant lines (M1, M2 & M3) showing reduced expression of mutant WISP3 (>60%) and diminished expression of NDUFB8 (Complex I subunit) (65-90%) as demonstrated by immunoblotting followed by quantification of band intensities by densitometry. (D) DNA sequence obtained by Sanger sequencing showing truncation of WISP3; respective amino acids are mentioned above the sequence on codon basis. (E) Immunoblotting followed by quantification of band intensities showing decreased expression of mutant WISP3, NDUFB8 and NDUFS1 in the mitochondria of the WISP3 mutant lines M1, M2 and M3 as compared to wild type. VDAC1 is used as loading control of mitochondria. Data are represented as mean $\pm$ SEM $*p < 0.05$, $**p < 0.01$ (Student's t- test).

However, expression of WISP3 was significantly reduced in mitochondria of mutants where VDAC1 was used as loading control. Level of NDUFB8 and NDUFS1 were also decreased (about 60-70%) in both whole cell and mitochondrial lysate (Figure 10B,C &

D,F) in mutant cell as compared to wild type. This diminished expression of NDUFB8 and NDUFS1 is possibly due to defect in protein interaction pattern of mutant WISP3.

Figure 11

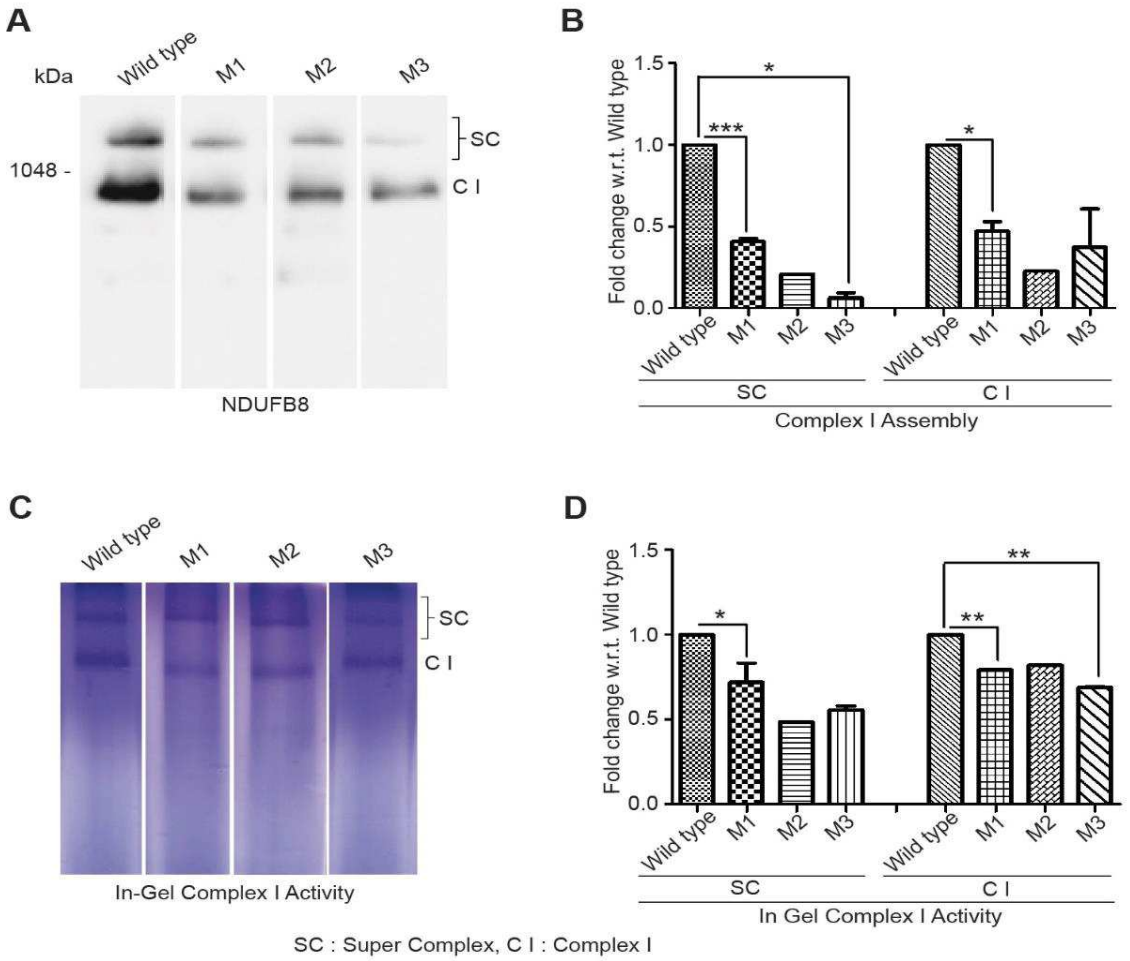

Figure 11: Mutations in WISP3 alter respiratory complex assembly and activity.

(A&B) Immunoblot of BN-PAGE probed with anti-NDUFB8 antibody followed by quantification of band intensities by densitometry showing reduced Complex I / Super Complex assembly in WISP3 mutant lines in comparison with wild type. (C&D) In-gel Complex I activity assay and corresponding quantification of band intensity showing altered Complex I/Super Complex activity in WISP3 mutant lines M1, M2 and M3 in comparison with wild type. Data are represented as mean $\pm$ SEM $*p < 0.05$, $**p < 0.01$ (Student's t- test).

Reduced expression level in these subunits in mitochondria correlated with defective in assembly of Complex I/Super complex as depicted from immuunoblot of BN-PAGE and its respective densitometry (Figure 11A, B). BN-PAGE of mitochondria of WISP3 mutants followed by in-gel Complex I activity shows markedly altered Complex I/ Super complex activity (Figure 11C, D). The defect in respiratory complex assembly and activity in WISP3

mutants (M1, M2 and M3) leads to accumulation of damaged/abnormal mitochondria as seen in transmission electron microscope (Figure 12A, B). Due to the accumulation of damaged/abnormal mitochondria in mutants, they are less viable as compared to wild type cells as demonstrated by MTT assay (Figure 12C). Overall these experimental results indicated that mutations in WISP3 disrupts mitochondrial respiratory chain assembly and activity. Disrupted assembly and assembly of mitochondrial respiratory chain correlates with accumulation of damaged mitochondria and loss of cell viability. Hence, WISP3 plays a vital role in maintenance of mitochondrial health.

Figure 12

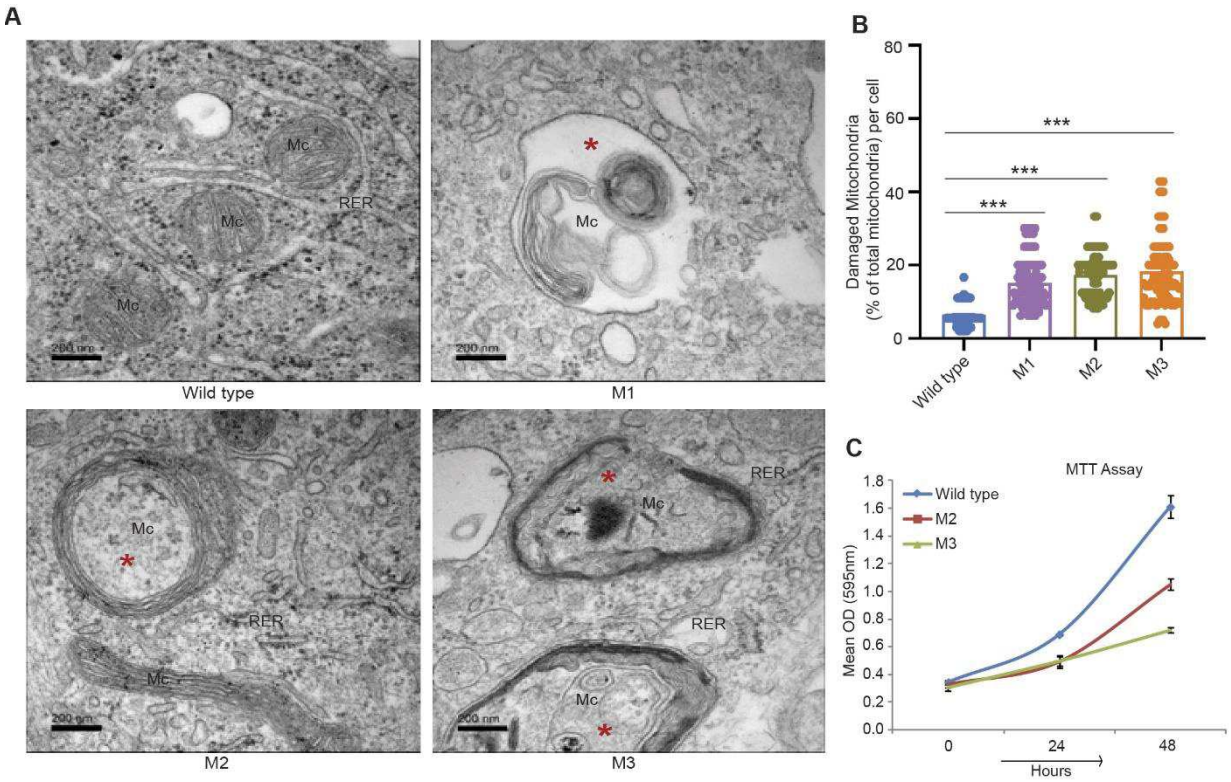

Figure 12: Mutations in WISP3 induce accumulation of damaged mitochondria and loss of cell viability. (A) Transmission electron micrographs of WISP3 mutant cells showing damaged/abnormal mitochondrial morphology in WISP3 mutant lines M1, M2, M3 as compared to wild type. Mc indicates mitochondria and * (Red asterisks) indicates damaged/abnormal mitochondria, RER indicates rough endoplasmic reticulum. Scale bar: 200 nm. B) Distribution plot with mean value showing percent of damaged mitochondria per cell in mutant lines and wild type. Scoring was done by counting more than 100 cells for each set. Data were analysed by one-way ANOVA followed by multiple comparison test (**$p < 0.01$, ***$p < 0.001$). (C) MTT assay showing less viability of WISP3 mutant lines as compared to wild type. Data are plotted as Mean $\pm$ SE of 8 replicates.

4.6 Wisp3 exists as an integral part of mitochondrial respiratory complexes in skeletal muscle of zebrafish

As per our earlier studies in chondrocyte cell line, WISP3 is present in mitochondria and regulates mitochondrial ATP production (Patra *et al.*, 2016). Our recent findings in two different chondrocyte cell lines also state that WISP3 is associated with mitochondrial respiratory complexes and regulates its activity and assembly thereby maintaining overall mitochondrial health. As WISP3 mutations are linked to PPRD which are associated with muscle weakness and muscle wasting (Alawbathani *et al.*, 2018; Al Kaissi *et al.*, 2020; Shahi *et al.*, 2020; Liu and Chen, 2021), we decided to study the function of WISP3 in mitochondria in relation to musculoskeletal system using zebrafish as a model organism. Here in this study, we used adult zebrafish to elucidate the function of Wisp3 in skeletal muscle.

Figure 13

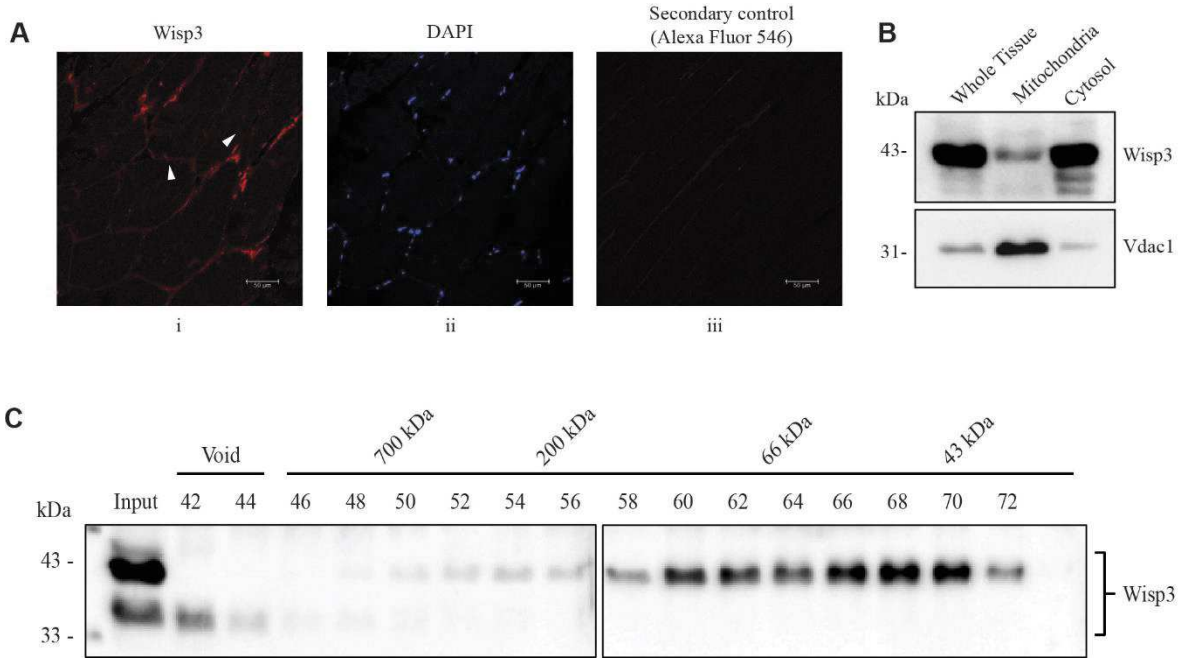

Figure 13: Wisp3 is expressed in skeletal muscle of zebrafish and present in mitochondria of skeletal muscle.

(A) Immunostaining and confocal microscopy demonstrating Wisp3 expression in zebrafish skeletal muscle. (i) Wisp3 expression in fiber lining near sarcolemma and in patches in intermyofibril spaces as shown by arrows, (ii) DAPI stain showing nuclei, (iii) only secondary antibody control. **(B)** Wisp3 expression in skeletal muscle mitochondria in comparison with whole tissue and cytosol. Vdac1 is used as reference as a mitochondrial protein. **(C)** Immunoblot of mitochondrial lysate after size exclusion chromatography using Sephacryl S- 300 beads demonstrating presence of Wisp3 in high molecular weight complexes.

Presence of Wisp3 was validated in the skeletal muscle of zebrafish by immunostaining and immunoblotting using custom synthesized zebrafish specific anti-Wisp3 antibody. Distribution of Wisp3 in mitochondria with respect to whole tissue was evaluated by tissue section staining and immunoblotting as shown in Figure 13A, B. Similar to distribution of mitochondrial WISP3 in C28/I2 cells, here as well, mitochondrial Wisp3 of adult zebrafish muscle was found in high molecular weight complexes by immunoblotting of fractions collected from size exclusion chromatography of whole mitochondria lysate (Figure 13C). BN-PAGE of muscle mitochondria of zebrafish and its immunoblot with anti-Wisp3 antibody validated the presence of Wisp3 in high molecular weight complexes by partly associating with subunits of different respiratory chain complexes such as Ndufb8 (Complex I subunit), Uqcrc2 (Complex III subunit), Cox4 (Complex IV subunit) and Atp5A1 (Complex V subunit) (Figure 14A panel i-vi). These subunits are widely used to study respiratory complexes of mitochondria (Csordás *et al.*, 2006; Wittig, Braun and Schägger, 2006; Acín-Pérez *et al.*, 2008; Moreno-Lastres *et al.*, 2012). Panel vii of figure 12A shows in-gel complex I activity which validated activity of assembled Complex I. Association of Wisp3 with mitochondrial respiratory complexes was further validated by immunostaining. Wisp3 was found to be associated with Cox4, co-localization of Cox4 with Wisp3 indicates its association with mitochondria which are present in both sarcolemma and in inter-myofibril space (Percival *et al.*, 2013; Lee *et al.*, 2016) (Figure 14B). These results suggest that the association of Wisp3 with mitochondrial respiratory complex might be due to the multi-modular architecture (Hurvitz *et al.*, 1999) which makes Wisp3 a key player in regulation of mitochondrial function. This led us to investigate the role of Wisp3 in stabilization of mitochondrial respiratory complex assembly and activity by its chaperon like activity.

4.7 Depletion of Wisp3 in Zebrafish skeletal muscle leads to reduced mitochondrial respiratory complex activity and assembly

In the previous experiment it was clear that Wisp3 is also present in mitochondria of skeletal muscle of zebrafish and it is associated at least partly with respiratory complexes. Here we were interested to investigate whether Wisp3 regulates mitochondrial respiratory complex assembly and activity. In order to determine the specific role of Wisp3 in mitochondria of skeletal muscle, it was essential to deplete Wisp3 therein. Expression of Wisp3 was knocked down in adult zebrafish skeletal muscle by injecting *wisp3* specific

Figure 14

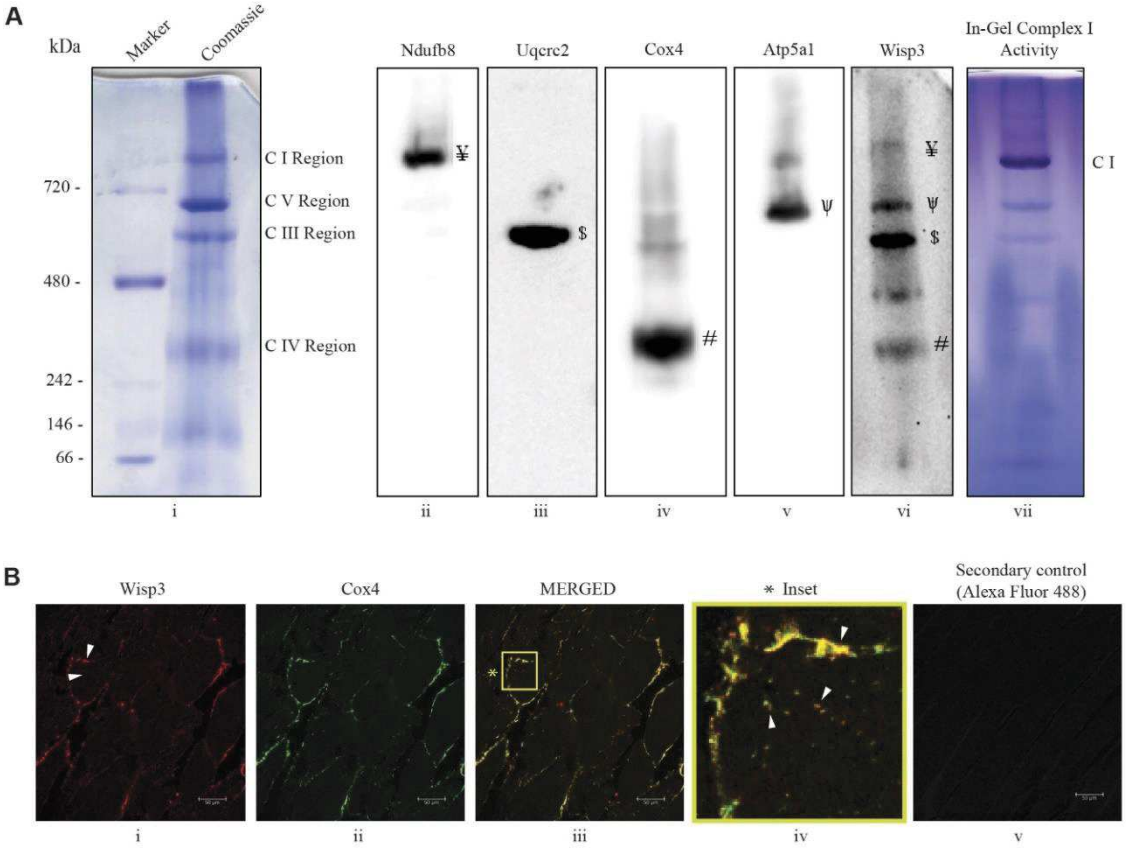

Figure 14: Wisp3 is present in association with mitochondrial respiratory complexes.

(A) A coomassie stained gel of Blue Native (BN)-PAGE of muscle mitochondria (panel i) and immunoblotting separately with antibodies to Ndufb8 of Complex I (panel ii), Uqcrc2 of Complex III (panel iii), Cox4 of Complex IV (panel iv), Atp5a1 of Complex V (panel v) and Wisp3 (panel vi). Symbols on the blots (panel ii, iii, iv & v) denote positions of different complexes corresponding with Wisp3 bands in panel vi. In gel NBT assay after BN-PAGE of mitochondria demonstrates activity of assembled Complex I (panel vii). (B) Immunostaining demonstrating colocalization of Wisp3 with mitochondrial respiratory complex. (i) Wisp3 expression, (ii) Cox4, representing mitochondrial respiratory Complex IV expression, (iii) Merged view showing colocalization of Wisp3 with Cox4, (iv) Magnified view (inset) of colocalization (arrow heads) (v) Secondary antibody control for Cox4. Presented data are representative of 3 independent experiments.

morpholino (4µl of 200µM morpholino solution) into the dorsal side muscle of zebrafish followed by electroporation using tweezer electrode. Equal concentration of non-targeting morpholino was injected as negative control. After ~65 hours of electroporation muscle tissues were collected by sacrificing the fish. Muscle tissue excised from injected left dorsal side taken as experimental and right ventral side of the same fish was taken as respective uninjected set. Immunoblotting with zebrafish specific anti-Wisp3 antibody and corresponding densitometry shows about 60% reduction in Wisp3 expression upon

morpholino injection but not in non-targeting (control) morpholino set (Figure 15A) and its respective densitometric graph of blots shows significant reduction in *wisp3* morpholino set than its respective uninjected whereas no significant differences were observed in control set (Figure 15B). Decrease in expression of Wisp3 by *wisp3* morpholino was also visualised by immunofluorescence of the skeletal muscle tissue (Figure 15C).

Figure 15

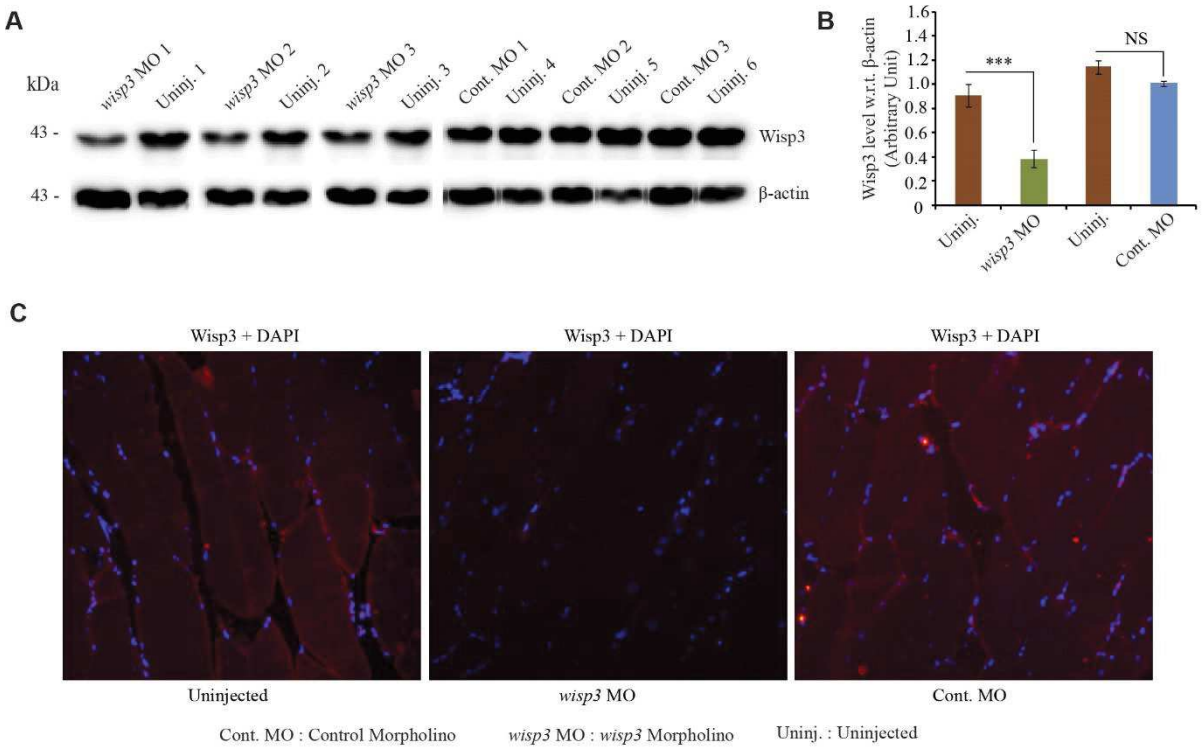

Figure 15: Wisp3 depletion in skeletal muscle by morpholino injection.

(A&B) Immunoblotting of total muscle lysate, and corresponding band densitometry demonstrating about 60% reduction in Wisp3 expression by *wisp3* morpholino but not control morpholino, as compared to the corresponding uninjected control. β-actin is used as a loading control. (C) Fluorescence microscopy of muscle sections stained with anti-Wisp3 antibody and counterstained with DAPI showing significant reduction of Wisp3 expression in *wisp3* morpholino injected tissue compared to control morpholino injected or uninjected.

In order to evaluate the effect of Wisp3 depletion on mitochondrial respiratory chain complexes, skeletal muscle mitochondrial lysate was subjected to BN-PAGE followed by immunoblotting with antibodies against subunits of respiratory chain complexes. Significant reduction in assembly of mitochondrial complex I, III, IV and V in mitochondria of zebrafish muscle were observed. This experiment was demonstrated by taking equal amount of mitochondria of skeletal muscles from experimental set (*wisp3*

morpholino injected) and control set (non-targeting morpholino and uninjected) followed by subjecting it to BN-PAGE and western blot analysis using antibody of respective subunits of mitochondrial respiratory complexes (complex I: Ndufb8, complex III: Uqcrc2, complex IV: Cox4, and complex V: Atp5a1) (Figure 16A, B). However, no changes in assembly were seen in control morpholino injected set (Figure 16C, D) which confirms the specific effect of *wisp3* morpholino on mitochondrial respiratory complexes assembly. A mitochondrial structural protein, Vdac1 was taken as loading control in these experiments.

Figure 16

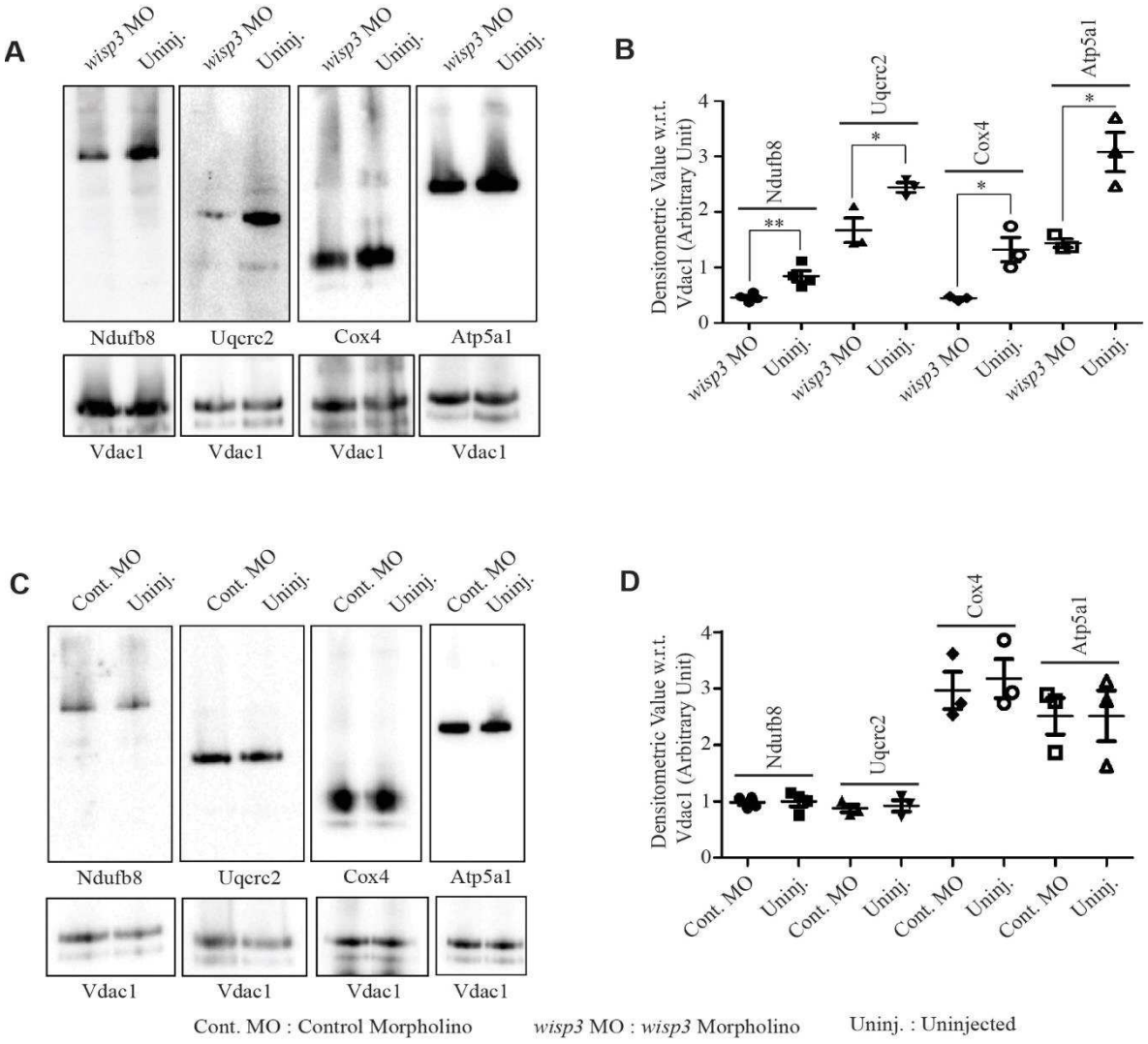

Figure 16: Depletion of Wisp3 inhibits mitochondrial respiratory complex assembly in zebrafish muscle.

(A, C) BN-PAGE of muscle mitochondrial lysate followed by immunoblotting separately with antibodies to Ndufb8 (Complex I), Uqcrc2 (Complex III), Cox4 (Complex IV), Atp5a1 (Complex V) and (B, D) corresponding band densitometry projected by distribution plot, demonstrating that *wisp3* morpholino, but

not control morpholino inhibits respiratory complex assembly as compared to respective uninjected. Vdac1 is used as loading control. Data are presented as mean ± SEM of at least 3 independent experiments. *p < 0.05, **p < 0.01, (Student's t- test)

Defect in respiratory complex assembly resulted in significant reduction in Complex I activity. Decrease in complex I activity was measured based on decrease in oxidation rate of NADH by skeletal muscle mitochondria of *wisp3* morpholino injected compared to control sets (non-targeting morpholino and uninjected). Oxidation of NADH correlates with decrease in absorbance of NADH at 340nm which are displayed in term of time kinetics spanning a period of 300 seconds (Figure 17A). The percent change in Complex I activity were significantly less in mitochondria of *wisp3* morpholino injected muscle as compared to control morpholino injected and uninjected as depicted in Figure 17B.

Figure 17

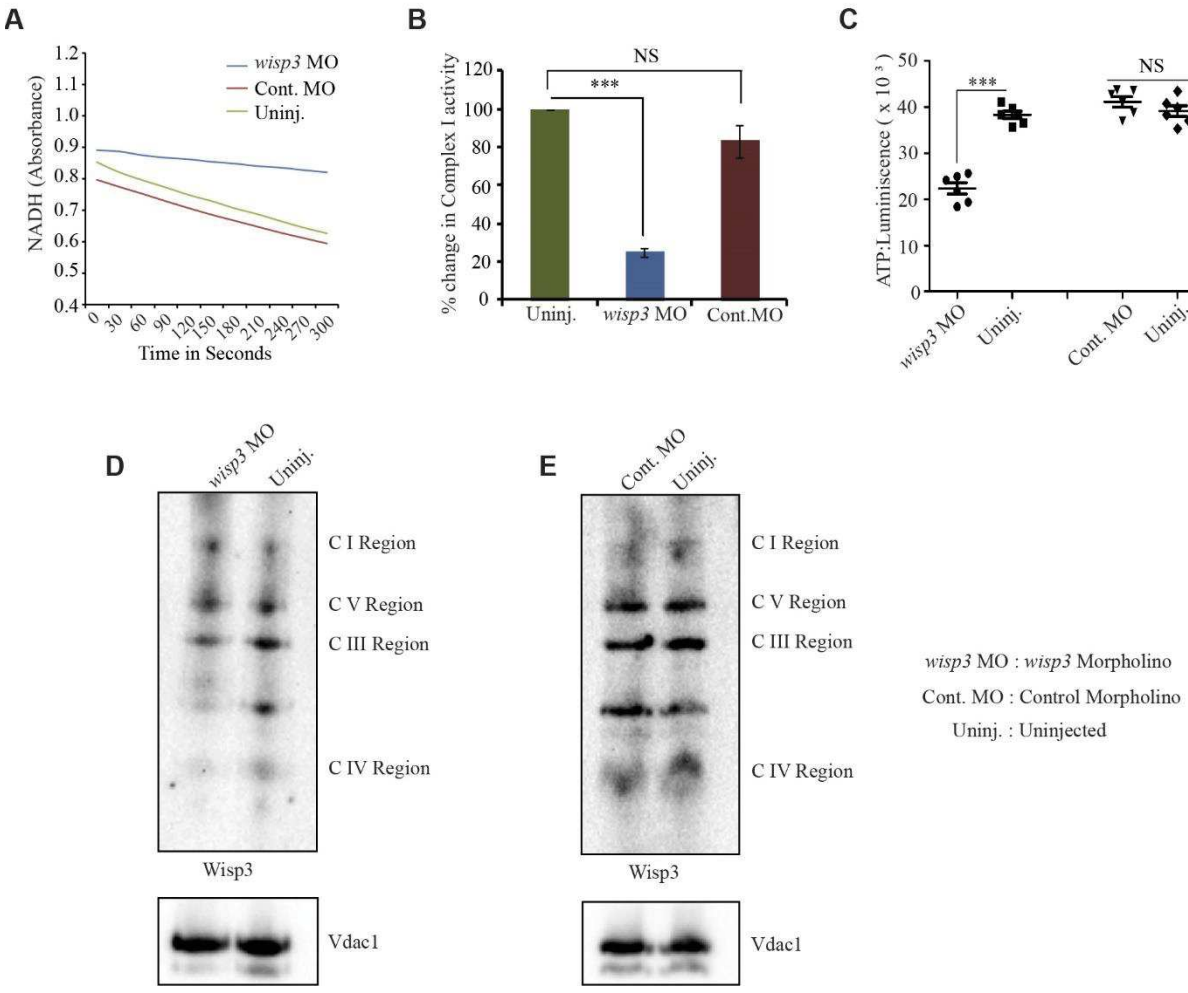

Figure 17: Depletion of Wisp3 inhibits mitochondrial respiratory complex activity in zebrafish muscle.

(A) Depletion of Wisp3 by morpholino injection increases Complex I activity as represented by higher rate of decrease of NADH absorbance measured by spectrophotometer as compared with control morpholino injected and uninjected. (B) Bar graph showing percent change in Complex I activity in mitochondria of

Wisp3 depleted tissues compared to uninjected (taking uninjected as 100). (C) Plotted graph of ATP measurement assay demonstrating decrease in ATP synthesis in mitochondria of *wisp3* morpholino injected tissue but not in control morpholino injection as compared to uninjected control. (D&E) BN-PAGE of zebrafish muscle mitochondrial lysate and subsequent immunoblotting with Wisp3 antibody demonstrates less Wisp3 protein as well as alteration in its distribution among the respiratory complexes in *wisp3* morpholino injected but not in control morpholino injected as compared to the corresponding uninjected controls. Data are presented as mean $\pm$ SEM of at least 3 independent experiments. ***$p < 0.001$, NS-Not Significant (Student's t- test).

These findings are in line with involvement of mitochondrial complex III-V in proper functioning of Complex I as described in published literature (Mimaki *et al.*, 2012; Moreno-Lastres *et al.*, 2012; D *et al.*, 2017; Signes and Fernandez-Vizarra, 2018). Reduced Complex I activity upon depletion of Wisp3 is linked with significant decrease in mitochondrial ATP synthesis as illustrated in Figure 17C. This changes in mitochondrial upon Wisp3 depletion in skeletal muscle of zebrafish alters its distribution among different mitochondrial respiratory complexes. BN-PAGE of zebrafish muscle mitochondrial lysate and subsequent immunoblotting with anti-Wisp3 antibody demonstrates less expression of Wisp3 protein as well as alteration in its distribution among the respiratory complexes in the skeletal muscle mitochondria of *wisp3* morpholino injected fish but not in control morpholino injected fish as compared to the corresponding un-injected controls (Figure 17D&E). Overall, these results suggest that the level of Wisp3 in the mitochondria of skeletal muscles plays an important role in regulating the stability, activity and assembly of mitochondrial respiratory complexes and thereby respiration. This led us to investigate the influence of Wisp3 in maintaining integrity of mitochondria and skeletal muscle physiology.

4.8 Wisp3 depletion in skeletal muscle of zebrafish affects mitochondrial integrity leading to abnormal muscle organization

Muscle weakness and muscle wasting are characteristics feature of PPRD progression. In order to better understand the influence of Wisp3 on mitochondria and musculoskeletal system in organism level, zebrafish was used as a model organism (Howe *et al.*, 2013; Steele, Prykhozhij and Berman, 2014). It is clear from the previous mentioned experiments that depletion of Wisp3 by morpholino causes loss in mitochondrial respiratory complex assembly and activity in zebrafish skeletal muscle (Figure 16&17). Hence it was very interesting to investigate the role of Wisp3 in maintenance of mitochondrial integrity and muscle physiology. Healthy mitochondria play a very important role in proper functioning

of muscle (Sunitha *et al.*, 2016; Vincent *et al.*, 2016). Here I used Vdac1, a mitochondrial structural protein as an indicator of mitochondrial integrity in adult zebrafish muscle.

Figure 18

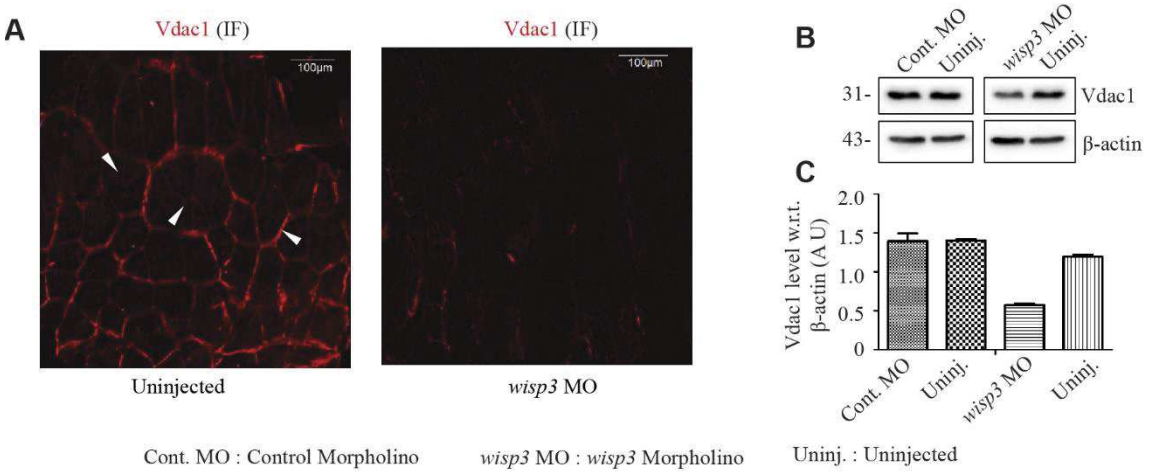

Figure 18: Wisp3 depletion causes loss in muscle mitochondrial abundance.

(A) Immunofluorescence of muscle sections of *wisp3* morpholino injected and uninjected zebrafish demonstrating loss in Vdac1 (representing structural protein of mitochondria) expression upon Wisp3 depletion. Arrow marks denote the presence of mitochondria along muscle fiber edges near the sarcolemma and in patches in the inter-myofibril spaces. (B) Immunoblot of muscle lysate and corresponding densitometry showing reduction in Vdac1 levels in *wisp3* morpholino but not control morpholino injected fish as compared to uninjected control. β-actin is used as a loading control.

Immunofluorescence microscopy carried out on microtomed tissue sections using anti-Vdac1 antibody revealed loss of mitochondrial abundance in Wisp3 morpholino injected tissue as compared to uninjected tissue (Figure 18A). This finding was also supported by immunoblotting of whole tissue lysate following SDS-PAGE where there was about 50% reduction in protein level of Vdac1 in Wisp3 morpholino injected muscle but no significant changes were seen in respective control morpholino injected and uninjected samples (Figure 18B) as depicted in the densitometric graph with respect beta actin (Figure 18C). Thus reduced assembly and activity of mitochondrial respiratory complex upon Wisp3 depletion was due to loss of mitochondria which in turn results in disruption in mitochondria integrity.

Taking into account the importance of mitochondrial function on muscle physiology (Sunitha *et al.*, 2016; Vincent *et al.*, 2016), we were interested to find whether loss of mitochondria in skeletal muscles in Wisp3 depleted condition leads to change in structure and function of muscles. Interestingly, hematoxylene and eosin stained microtome tissue sections of *wisp3* morpholino injected muscle shows broaden interstitial space between

muscle fibres and inflammatory infiltrates (Figure 19). These are the characteristic features linked to muscle wasting as documented in various PPRD cases (Alawbathani *et al.*, 2018; Shahi *et al.*, 2020; Liu and Chen, 2021). In control morpholino injected samples, a very minor variation in interstitial space is observed which is may be due to injury caused during electroporation or naturally occurring difference in tissue architecture. These results confirmed and strengthen in elucidating the specific role of Wisp3 in maintenance of muscle integrity in skeletal muscle of zebrafish.

Figure 19

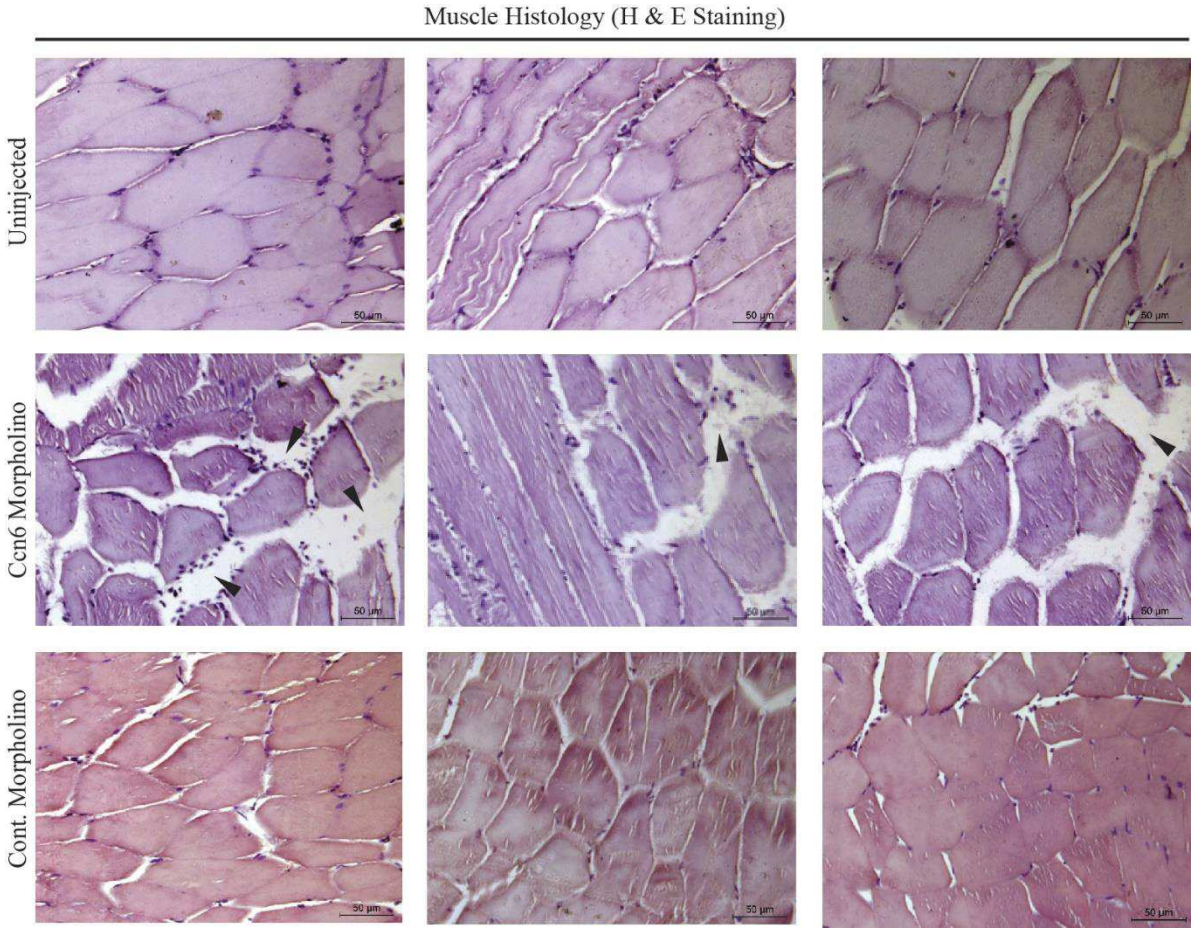

Figure 19: Depletion of Wisp3 causes alteration in muscle organization.

Hematoxylin & Eosin stained histological sections of muscles demonstrates increase in interstitial gaps and presence of inflammatory infiltrates (arrow marks) in *wisp3* morpholino injected muscle compared to control morpholino injected and uninjected fish.

4.9 Wisp3 knock down in skeletal muscle hinders locomotion in zebrafish

As depletion of Wisp3 by morpholino affects muscle integrity, we wanted to see whether if it affects locomotion in zebrafish. Interestingly, it was found that altered skeletal muscle structure formed by depletion of Wisp3 correlated with hindered locomotion.

Figure 20

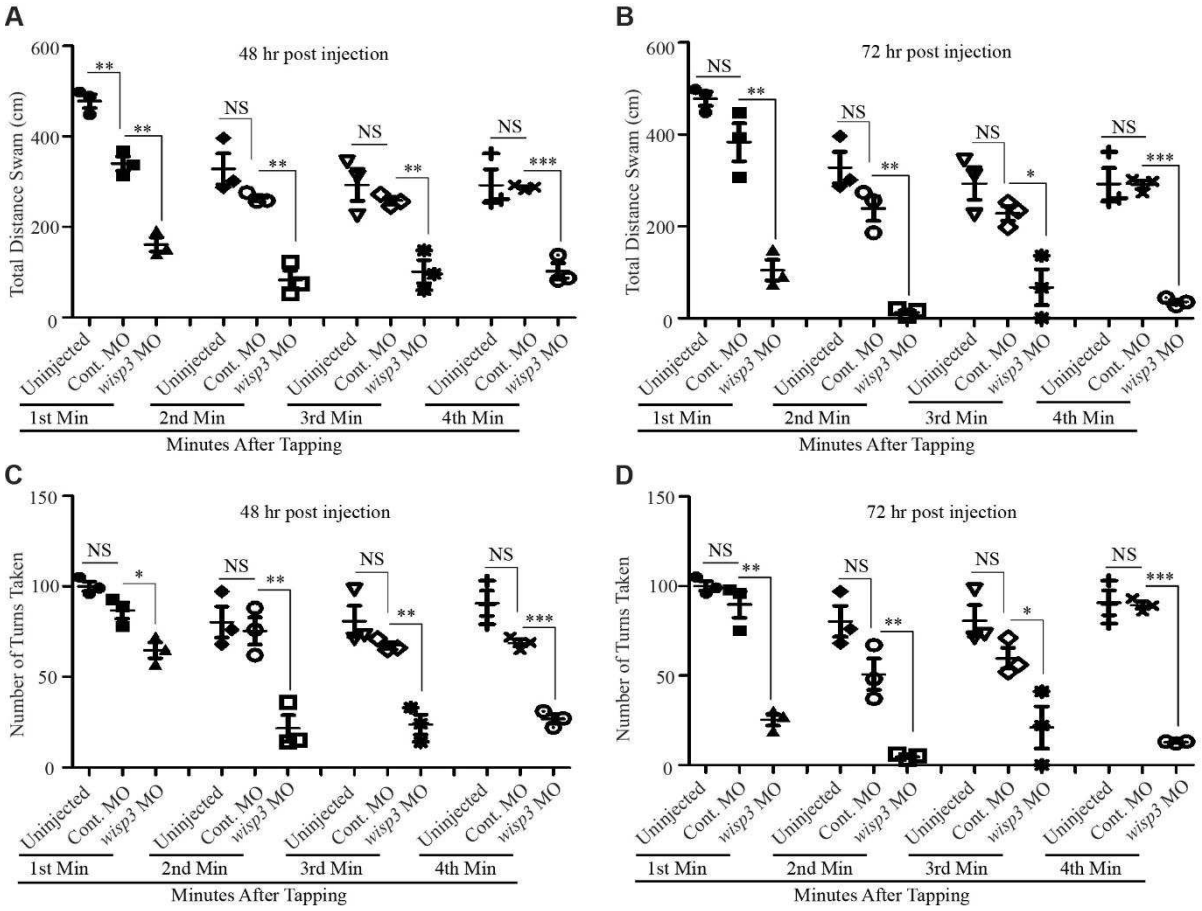

Figure 20: Depletion of Wisp3 in skeletal muscle hinders locomotion in response to stimulus.

(A & B) Depletion of Wisp3 in skeletal muscle by *wisp3* morpholino restricts distance covered by zebrafish in response to stimulus after 48 and 72 hours post injection as compared to corresponding controls (control morpholino injected and uninjected) n=3. (C & D) Plotted graphs indicates number of turns taken by *wisp3* morpholino injected fish was significantly less as compared to corresponding controls measured after 48 and 72 hours post injection, n=3. Data are presented as mean $\pm$ SEM *p < 0.05, **p < 0.01, ***p < 0.001, NS- Not Significant (Student's t- test).

To evaluate the locomotion of zebrafish, 'startle response experiment' was conducted after *wisp3* or Control morpholino administration based on published literature (Miller *et al.*, 2012; Lebold *et al.*, 2013). Locomotion in zebrafish was evaluated by measuring two parameters such as total distance covered (in centimetres) and the number of turns taken after stimulus. After being subjected to a startle, given by single tap on one side of the fish

tank it was observed that *wisp3* morpholino injected fishes in both 48 and 72 hrs post injection were unable to travel same distance as covered by control morpholino injected and uninjected (Figure 20A, B). Number of turns taken after stimulus were significantly less in *wisp3* morpholino injected zebrafish as compared to respective control morpholino injected and uninjected (Figure 20C, D).

For each fish, after tapping the distance covered and turns taken were measured at first, second, third and fourth minutes and plotted in respective graph. A schematic diagram of "startle response experiment" is illustrated in Figure 21. Overall, our results indicate the importance of Wisp3 in maintaining skeletal muscle organization and function by influencing mitochondrial respiratory complex assembly and activity.

Figure 21

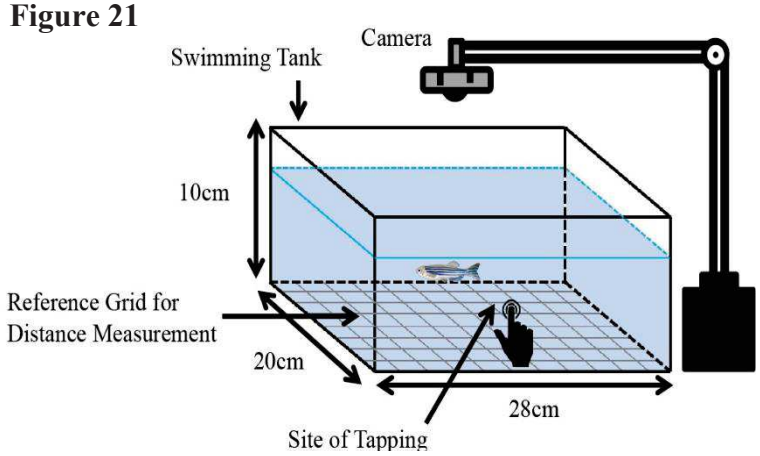

Figure 21: Schematic representation of set up for Startle response experiment.

4.10 Distribution pattern of Wisp3 in organs of zebrafish

In order to unravel the underneath mechanism of manifestation of specific defects caused by PPRD in skeletal muscle but not in other tissue type, it was quite interesting to investigate the different forms of Wisp3 in mitochondria of various tissues. For comparing the expression pattern in different mitochondrial rich tissues of zebrafish, here we have taken skeletal muscle, brain and heart. Immunoblot of isolated mitochondria from skeletal muscle, brain and heart indicates that Wisp3 is present in different forms in different tissue type as depicted in figure 22A. Skeletal muscle mitochondria harbours mainly 43 kDa form of Wisp3, heart mitochondria harbours mostly 33 kDa form whereas mitochondria of brain harbours both 33kDa and 43kDa forms.

Figure 22

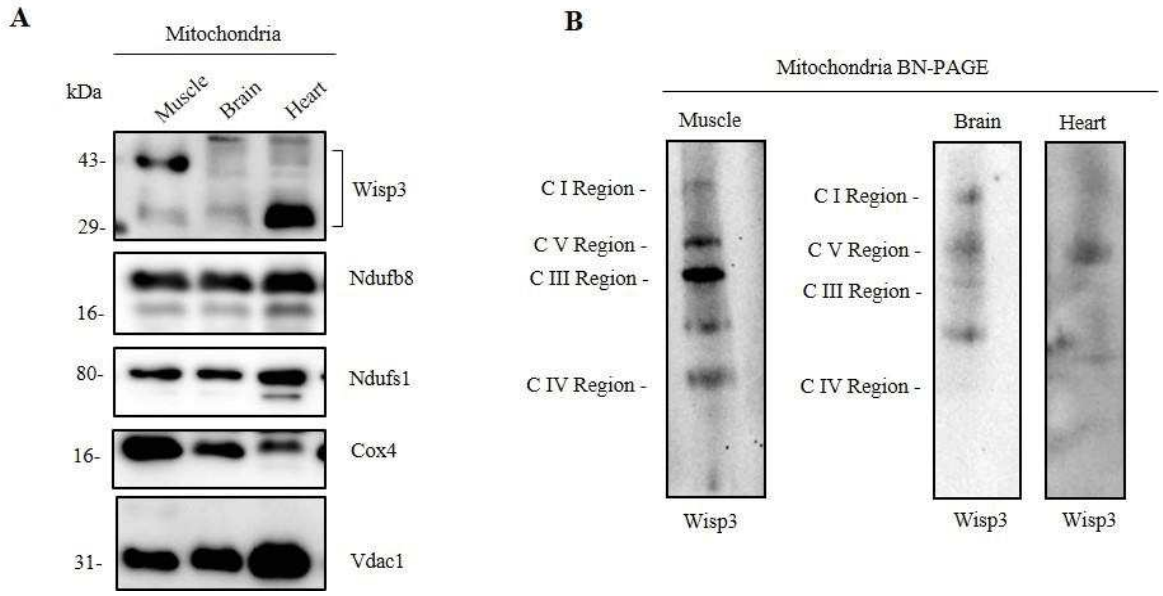

Figure 22: Distribution pattern in forms of Wisp3 in zebrafish is tissue specific.

(A) Immunoblot of mitochondrial lysate of different tissue sections (muscle, brain, heart) shows varied expression level of Wisp3 (43kDa and 33kDa) with respect to Ndufb8 and Ndufs1 (Complex I subunits), Cox4 (Complex IV subunit) and Vdac1 (mitochondrial structural protein). (B) BN-PAGE and subsequent immunoblots of mitochondrial lysates of muscle, brain and heart of zebrafish showing different distribution pattern of Wisp3 in the mitochondrial respiratory complexes.

The mechanism and function of these variants of Wisp3 is not studied well, studying this aspects may pave a better path in better understanding of Wisp3 function. However, distribution pattern of Wisp3 in mitochondria was analysed by immunoblotting following BN-PAGE. It was observed that distribution of Wisp3 was more prominent in skeletal muscle as compared to brain and heart (Figure 22B).

CHAPTER V

DISCUSSION

DISCUSSION

Having established the role of WISP3 as a growth and differentiation factor in cells of mesenchymal origin, we found indications of its potential to perform various functions due to its multimodular architecture. Mutations in WISP3 are linked with PPRD, a debilitating musculoskeletal disorder characterised with joint stiffness, swelling of joints, widening of epiphysis, narrowing of joints space by periarticular calcification along with muscle wasting (Hurvitz *et al.*, 1999; Dalal *et al.*, 2012; Ekbote *et al.*, 2013; Bhavani *et al.*, 2015; Chouery *et al.*, 2017; Alawbathani *et al.*, 2018; Shahi *et al.*, 2020; Liu and Chen, 2021). It is known that due to a lack of a fully functioning WISP3 protein, chondrocytes in the growth plate and articular cartilage undergo premature and uncontrolled hypertrophic differentiation. Studies have shown in chondrocyte that WISP3 regulates expression of collagen II, transcription factor SOX9 and aggrecan expression, promotes superoxide dismutase activity and regulating accumulation of cellular reactive oxygen species (ROS) which indicates its vital role in maintenance of cartilage integrity (Sen *et al.*, 2004; Davis, Chen and Sen, 2006; Miller and Sen, 2007; Repudi, Patra and Sen, 2013). As the major site of ROS generation in cell is mitochondria and the role of mitochondria is established in maintenance of cartilage and musculoskeletal integrity (Sunitha *et al.*, 2016; Vincent *et al.*, 2016), it is very important to understand the connection between WISP3 and mitochondrial function in both cellular and organismal level. In the current study, I found that WISP3 localizes to mitochondria in both chondrocyte cell line and muscle of zebrafish and plays a significant role in controlling mitochondrial metabolism and thereby regulating skeletal architecture and functions which might correlate with progression of PPRD pathogenesis.

Previous findings related to functions of WISP3 in maintenance of cartilage homeostasis states that WISP3 stimulates the expression of cartilage-specific proteins collagen-II and aggrecan, regulates metalloprotease expression and controls the build-up of reactive oxygen species (ROS) (Sen *et al.*, 2004; Davis, Chen and Sen, 2006; Miller and Sen, 2007; Baker *et al.*, 2012). Also, WISP3 interacts with BMP and Wnt1 signalling pathway components such as LRP6 and Fz8, according to other studies (Nakamura *et al.*, 2007). Taking into account the modular architecture of WISP3 protein, it has an IGF1 binding motif, which is necessary for growth of cartilage and bone, besides WISP3 also interacts with IGF1 and controls ROS accumulation in hypertrophic chondrocyte (Wang, Zhou and Bondy, 1999; Wu *et al.*, 2008; Repudi, Patra and Sen, 2013) suggesting chaperones like activity of WISP3. In line with the previous findings that regulation of cellular ROS by

WISP3 in chondrocyte cell line, it was quite interesting to dig into the mechanism of ROS generation and subsequent effect of WISP3 at molecular level.

As mitochondria are the primary source of reactive oxygen species (ROS), especially Complex I and Complex III (Boveris, Oshino and Chance, 1972; Bell *et al.*, 2007; Murphy, 2009), WISP3 may have a role in mitochondrial ROS regulation by regulating mitochondria respiratory complexes. In order to validate this hypothesis, together with Dr. Milan Patra, I found that knockdown of WISP3 enhances mitochondrial ROS production, ATP synthesis and Ca^{2+} uptake in chondrocyte cell line. This study also shows for the first time that the amount of WISP3-mediated effects on mitochondrial electron transport regulates the expression and activity of PGC1, a crucial transcriptional co-activator for mitochondrial biogenesis and oxidative phosphorylation (Patra *et al.*, 2016). These findings paved a clear path for investigating the role of WISP3 in regulating mitochondrial functions in greater detail.

Further, working in association with Dr. Archya Sengupta, I studied the mechanism of WISP3 mediated regulation of mitochondrial function in maintenance of cartilage and musculoskeletal system using both chondrocyte cell line and zebrafish as an animal model. A previous report of poor cartilage formation following morpholino-mediated WISP3 reduction encouraged this choice of organism (Nakamura *et al.*, 2007). Present study in cell line demonstrates that WISP3 localizes to mitochondria (Fig. 1&2) in both chondrocyte cell line and $WISP3^{myc}$ transfected HEK293 cell line thereby regulating mitochondrial functions. However how WISP3 enters to mitochondria without having a strict mitochondria targeting sequence (MTS) is still unknown. WISP3 has a simple stretch of amino acid ØXXØØ (Ø is a hydrophobic residue and X is any residue) that works as MTS on occasion as it do not adhere to strict consensus. Without direct investigation is difficult to determine if WISP3 uses any MTS for mitochondrial entrance or is imported to mitochondria through any other indirect method (Doyle *et al.*, 2013). Within mitochondria, WISP3 is found to be associated with subunits of mitochondrial respiratory complexes (Fig. 3&4). In this study, subunits of respiratory chain complexes were studied as a reference of respective complexes. NDUFB8 and NDUFS1 as subunits of Complex I, UQCRC2 as a subunit of Complex III, MTCO1 as a subunit of Complex IV and ATP5A1 as a Complex V subunit. In order to evaluate the cause of mitochondrial ROS generation and ATP synthesis it was essential to evaluate the activity and assembly of mitochondrial respiratory chain complexes in WISP3 depleted condition. Here the status of mitochondrial

Complex I was focused based on its role as an initiator of electron transport chain and ATP synthesis (Acín-Pérez *et al.*, 2008; Mimaki *et al.*, 2012; Moreno-Lastres *et al.*, 2012; D *et al.*, 2017). Assembly and activity of respiratory Complex I, a 45-subunit entity that can also be found as a part of Super Complexes which are crucial for electron transport (Acín-Pérez *et al.*, 2008; Mimaki *et al.*, 2012; D *et al.*, 2017). Out of these 45 subunits, 38 are nuclear encoded and 7 subunits are mitochondrial DNA encoded. Moderate reduction of WISP3 by siRNA leads to increase in Complex I/ Super complex activity in both C-28/I2 and C20A4 chondrocyte cells (Fig. 5) evaluated on the basis of oxidising NADH. The increase in activity of respiratory complex was either due to more efficient functioning of Complex I or due to presence of increased amount of Complex I proteins. Results shows that upon moderate reduction of WISP3 the assembly of respiratory complex proteins, in particular Complex I/ Super Complex is increased in C-28/I2 cells as depicted in figure 6. In keeping with the observation that depletion of WISP3 leads to increased Complex I activity/assembly, it was quite essential to check the mitochondrial distribution of WISP3 in its depleted condition. Interestingly it was found that there was relatively more distribution of WISP3 in mitochondria of WISP3 depleted cells as compared to controls in both C-28/I2 and C20A4 cell line. However, there was significant decrease in WISP3 expression in cytosol (Fig. 8). Based on the multimodular architecture of WISP3, it might be possible that WISP3 could be a part of tethers or plays a role in maintaining RER-mitochondrial distance (Csordás *et al.*, 2006; de Brito and Scorrano, 2010). Electron micrographs of partial WISP3 depleted chondrocyte cell reveals that the distance between RER and mitochondria collapses, drawing RER in close proximity of mitochondria (Fig.9). Probably due to this reason, the ribosomes of RER facilitates the co-translational import of mitochondrial proteins including WISP3 to mitochondria (Lesnik *et al.*, 2014; Gold *et al.*, 2017). These results suggests that RER/ribosome-mitochondria distance which is required for controlled distribution of mitochondrial proteins including WISP3 thereby regulating respiratory complex assembly and activity.

PPRD, debilitating skeletal disorder is caused by homozygous mutation of WISP3 gene. Several mutations were identified across the domains of WISP3, leads to PPRD which implies that all the domains are essential for proper functioning of WISP3 protein (Hurvitz *et al.*, 1999; Dalal *et al.*, 2012; Bhavani *et al.*, 2015). In order to mimic the biological outcome of PPRD, C-terminal truncated mutants were generated in C-28/I2 cell line using CRISPR Cas9 technology (Ran *et al.*, 2013). Our main intention was to see the effect of

WISP3 mutants in maintaining mitochondrial function and integrity. Our results demonstrated that the generated truncated mutant cells had significant loss in mitochondrial respiratory complex activity and assembly as compared to wild type cells (Fig. 10&11). These defects in assembly and activity of respiratory complexes are associated with accumulation of degrading mitochondria as seen in electron micrographs of mutants resulting in poor survival as compared to healthy wild type cells (Fig. 12). Interrelation between respiratory complex assembly/activity and mitochondrial structural integrity has already been reported in relation to Complex I assembly deficiency in muscle myopathies (Sunitha *et al.*, 2016; Vincent *et al.*, 2016). Overall our results from chondrocyte cell line suggests that WISP3 is an essential protein in maintaining its critical functions in mitochondria though it is also present in cytosol and nucleus of chondrocytes.

Functions of WISP3 was further elaborated by validating its effect using zebrafish as a model organism. Taking into account of the musculoskeletal disease PPRD, we performed experiments mainly on skeletal muscle of adult zebrafish. Here it was observed that Wisp3 is partly present in mitochondria of skeletal muscle as a complex with different subunits of mitochondrial respiratory chain complexes (Complex I, III, IV, V) as depicted in figure 13&14. Functional aspects of Wisp3 in zebrafish skeletal muscle was determined by down regulating Wisp3 expression by localised administration of *wisp3* morpholino and compared with non-targeting/control morpholino. It was demonstrated that depletion of Wisp3 by 60% leads to loss in mitochondrial respiratory complex assembly and activity in skeletal muscle of zebrafish (Fig. 15-17) thereby loss of mitochondrial abundance as depicted in immuno-fluorescence images (Fig. 18). Concomitantly, haematoxylin and eosin stained histological sections of skeletal muscles showed widening of interstitial spaces between the muscle fibres. These features of change in tissue architecture upon *wisp3* morpholino administration indicates the involvement of Wisp3 in muscle wasting (Rayavarapu *et al.*, 2013; Yang *et al.*, 2019). These results confirm the specific function of Wisp3 in maintenance of integrity of skeletal muscle in zebrafish. Probably due to altered skeletal muscle structure caused by depletion of Wisp3, the normal locomotion and swimming pattern of zebrafish gets hampered as compared to corresponding controls (Fig. 19&20) suggesting the importance of Wisp3 in maintenance of musculoskeletal health.

Given that most tissues and cell types require functional mitochondria to survive, it is unclear that PPRD-related abnormalities caused by Wisp3 mutations are mainly seen in skeletal tissues (Hurvitz *et al.*, 1999; Dalal *et al.*, 2012; Garcia Segarra *et al.*, 2012; Ekbote

et al., 2013; Alawbathani *et al.*, 2018; Sailani *et al.*, 2018; Shahi *et al.*, 2020; Liu and Chen, 2021). Perhaps the distribution pattern of Wisp3 in mitochondria differs by cell and tissue type, and hence the impact of *wisp3* mutations is more prominent in skeletal tissues than in others. Indeed our results indicates that the distribution pattern and forms of Wisp3 in mitochondria of skeletal muscle, brain and heart was distinctly different from each other (Fig. 22). Although the mechanism behind this regulation was not understood, the distribution pattern of Wisp3 in respiratory complexes of mitochondria of skeletal muscle was more prominent as compared to brain and heart. The association of Wisp3 with respiratory complexes in skeletal tissues might be the reason behind susceptibility to the detrimental consequence of *wisp3* mutations. Also, as the mechanism of tissue specificity of WISP3 in connection to mitochondrial function is unknown, various tissue specific mitochondrial abnormalities have been documented (Pacheu-Grau, Rucktäschel and Deckers, 2018). However, because Wisp3 is found in subcellular organelles other than mitochondria (Fig. 13), skeletal muscle injury caused by Wisp3 mutations or depletion may occur independently of the mitochondria.

Taken together, our study on both chondrocyte cell line (C-28/I2 & C20A4) and zebrafish unveils the detailed function of WISP3 in a new direction. In a nutshell, our results suggests that WISP3 as a multimodular protein performs essential functions, though it may have functions in cytosol and nucleus, its function in mitochondria is critical and inevitable. Moderate reduction of WISP3 in chondrocytes alters mitochondrial mass and thereby mitochondrial functions by increasing complex I activity and assembly to a certain extent; whereas in contradiction to this depletion of Wisp3 in zebrafish by morpholino significantly reduces mitochondrial abundance, thus decreasing complex I activity and assembly. However, generated WISP3 mutants, analogous to PPRD mu tants shows poor survival rates due to compromised mitochondrial function. In zebrafish as well, the effects were similar causing mitochondrial dysfunction and ultimately altered musculoskeletal functions making Wisp3 a key protein regulator in mitochondrial respiration and maintenance of muscle integrity. The variation in regulation pattern of WISP3 in chondrocyte and zebrafish seems contradictory which might be due to WISP3's ability to interact with numerous proteins. The regulatory influence on mitochondria can range from repression to activation, depending on its protein interaction partners, which can differ between tissue and cell types. Overall findings indicate that a fully functional WISP3 protein is required in chondrocyte and adult zebrafish muscle for maintenance of

mitochondrial health and muscle integrity. The findings of this new line of research could pave the way for significant advancements in the diagnosis and understanding of PPRD and other musculoskeletal diseases.

CHAPTER VI

FUTURE PERSPECTIVES

FUTURE PERSPECTIVES

From the results of my findings from chondrocyte cell lines and zebrafish it is assumed that WISP3 plays a major role in regulation of mitochondrial respiratory complex assembly and activity and thereby maintaining mitochondrial integrity and mitochondrial function. Partial depletion of Wisp3 in skeletal muscle of zebrafish leads to abnormal mitochondrial function results in disruption of tissue architecture and hinders locomotion in adult zebrafish. This results explains the localized effect of *wisp3* morpholino. However, depletion of Wisp3 in whole zebrafish will impart more knowledge in understanding the biology of Wisp3 regulation. Experiments that needs to be done in this line on zebrafish are as follows:

1- To examine mechanistically whether the regulation of mitochondrial function controlled by Wisp3 is through transcriptional regulation. Based on the presence of its putative nuclear localization signal, it might go to nucleus and perform certain transcription of mitochondrial genes along with others. This can be done by whole tissue transcriptome analysis by RNA sequencing.

2- To examine the effect of *wisp3* morpholino in different developmental stages of zebrafish embryo which can be achieved by microinjection of *wisp3* specific morpholino in single cell stage of fertilized egg.

3- To generate PPRD causing Wisp3 mutants in zebrafish by CRISPR Cas9 technology and to evaluate the deleterious effect of Wisp3 depletion at organism level. Parameters like muscle architecture, skeletal deformities and mitochondrial regulations should be taken into account.

REFERENCES

REFERENCES

Acín-Pérez, R. *et al.* (2008) 'Respiratory active mitochondrial supercomplexes', *Molecular Cell*, 32(4), pp. 529–539. doi:10.1016/j.molcel.2008.10.021.

Al Kaissi, A. *et al.* (2020) 'Skeletal phenotype/genotype in progressive pseudorheumatoid chondrodysplasia', *Clinical Rheumatology*, 39(2), pp. 553–560. doi:10.1007/s10067-019-04783-z.

Alawbathani, S. *et al.* (2018) 'Late diagnosis of a truncating WISP3 mutation entails a severe phenotype of progressive pseudorheumatoid dysplasia', *Cold Spring Harbor Molecular Case Studies*, 4(1), p. a002139. doi:10.1101/mcs.a002139.

Babic, A.M. *et al.* (1998) 'CYR61, a product of a growth factor-inducible immediate early gene, promotes angiogenesis and tumor growth', *Proceedings of the National Academy of Sciences of the United States of America*, 95(11), pp. 6355–6360. doi:10.1073/pnas.95.11.6355.

Baker, N. *et al.* (2012) 'Dual regulation of metalloproteinase expression in chondrocytes by Wnt-1-inducible signaling pathway protein 3/CCN6', *Arthritis and Rheumatism*, 64(7), pp. 2289–2299. doi:10.1002/art.34411.

Baughman, J.M. *et al.* (2011) 'Integrative genomics identifies MCU as an essential component of the mitochondrial calcium uniporter', *Nature*, 476(7360), pp. 341–345. doi:10.1038/nature10234.

Bell, E.L. *et al.* (2007) 'The Qo site of the mitochondrial complex III is required for the transduction of hypoxic signaling via reactive oxygen species production', *The Journal of Cell Biology*, 177(6), pp. 1029–1036. doi:10.1083/jcb.200609074.

Bhavani, G.S. *et al.* (2015) 'Novel and recurrent mutations in WISP3 and an atypical phenotype', *American Journal of Medical Genetics. Part A*, 167A(10), pp. 2481–2484. doi:10.1002/ajmg.a.37164.

Bhavani, G.S. *et al.* (2020) 'Progressive Pseudorheumatoid Dysplasia', in Adam, M.P. et al. (eds) *GeneReviews®*. Seattle (WA): University of Washington, Seattle. Available at: http://www.ncbi.nlm.nih.gov/books/NBK327267/ (Accessed: 25 April 2022).

Bork, P. (1993) 'The modular architecture of a new family of growth regulators related to connective tissue growth factor', *FEBS letters*, 327(2), pp. 125–130. doi:10.1016/0014-5793(93)80155-n.

Boveris, A., Oshino, N. and Chance, B. (1972) 'The cellular production of hydrogen peroxide', *The Biochemical Journal*, 128(3), pp. 617–630. doi:10.1042/bj1280617.

Bradham, D.M. *et al.* (1991) 'Connective tissue growth factor: a cysteine-rich mitogen secreted by human vascular endothelial cells is related to the SRC-induced immediate early gene product CEF-10', *The Journal of Cell Biology*, 114(6), pp. 1285–1294. doi:10.1083/jcb.114.6.1285.

Brigstock, D.R. (2003) 'The CCN family: a new stimulus package', *The Journal of Endocrinology*, 178(2), pp. 169–175. doi:10.1677/joe.0.1780169.

de Brito, O.M. and Scorrano, L. (2010) 'An intimate liaison: spatial organization of the endoplasmic reticulum-mitochondria relationship', *The EMBO journal*, 29(16), pp. 2715–2723. doi:10.1038/emboj.2010.177.

Brookes, P.S. *et al.* (2004) 'Calcium, ATP, and ROS: a mitochondrial love-hate triangle', *American Journal of Physiology. Cell Physiology*, 287(4), pp. C817-833. doi:10.1152/ajpcell.00139.2004.

Chen, C.C., Chen, N. and Lau, L.F. (2001) 'The angiogenic factors Cyr61 and connective tissue growth factor induce adhesive signaling in primary human skin fibroblasts', *The Journal of Biological Chemistry*, 276(13), pp. 10443–10452. doi:10.1074/jbc.M008087200.

Chen, N., Chen, C.C. and Lau, L.F. (2000) 'Adhesion of human skin fibroblasts to Cyr61 is mediated through integrin alpha 6beta 1 and cell surface heparan sulfate proteoglycans', *The Journal of Biological Chemistry*, 275(32), pp. 24953–24961. doi:10.1074/jbc.M003040200.

Chouery, E. *et al.* (2017) 'Progressive pseudorheumatoid dysplasia in North and West Africa: Clinical description in ten patients with mutations of WISP3', *Egyptian Journal of Medical Human Genetics*, 18(3), pp. 299–303. doi:10.1016/j.ejmhg.2016.11.004.

Cogliati, S. *et al.* (2013) 'Mitochondrial cristae shape determines respiratory chain supercomplexes assembly and respiratory efficiency', *Cell*, 155(1), pp. 160–171. doi:10.1016/j.cell.2013.08.032.

Csordás, G. *et al.* (2006) 'Structural and functional features and significance of the physical linkage between ER and mitochondria', *The Journal of Cell Biology*, 174(7), pp. 915–921. doi:10.1083/jcb.200604016.

D, M. *et al.* (2017) 'The Enigma of the Respiratory Chain Supercomplex', *Cell metabolism*, 25(4). doi:10.1016/j.cmet.2017.03.009.

Dalal, A. *et al.* (2012) 'Analysis of the WISP3 gene in Indian families with progressive pseudorheumatoid dysplasia', *American Journal of Medical Genetics. Part A*, 158A(11), pp. 2820–2828. doi:10.1002/ajmg.a.35620.

Davis, L., Chen, Y. and Sen, M. (2006) 'WISP-3 functions as a ligand and promotes superoxide dismutase activity', *Biochemical and Biophysical Research Communications*, 342(1), pp. 259–265. doi:10.1016/j.bbrc.2006.01.132.

De Vos, K.J. *et al.* (2012) 'VAPB interacts with the mitochondrial protein PTPIP51 to regulate calcium homeostasis', *Human Molecular Genetics*, 21(6), pp. 1299–1311. doi:10.1093/hmg/ddr559.

Díaz, F., Barrientos, A. and Fontanesi, F. (2009) 'Evaluation of the mitochondrial respiratory chain and oxidative phosphorylation system using blue native gel electrophoresis', *Current Protocols in Human Genetics*, Chapter 19, p. Unit19.4. doi:10.1002/0471142905.hg1904s63.

Dolga, A.M. *et al.* (2014) 'Subcellular expression and neuroprotective effects of SK channels in human dopaminergic neurons', *Cell Death & Disease*, 5, p. e999. doi:10.1038/cddis.2013.530.

Doyle, S.R. *et al.* (2013) 'Evidence of evolutionary constraints that influences the sequence composition and diversity of mitochondrial matrix targeting signals', *PloS One*, 8(6), p. e67938. doi:10.1371/journal.pone.0067938.

Eddins, D. *et al.* (2010) 'Zebrafish provide a sensitive model of persisting neurobehavioral effects of developmental chlorpyrifos exposure: comparison with nicotine and pilocarpine effects and relationship to dopamine deficits', *Neurotoxicology and Teratology*, 32(1), pp. 99–108. doi:10.1016/j.ntt.2009.02.005.

Ekbote, A.V. *et al.* (2013) 'A descriptive analysis of 14 cases of progressive-psuedorheumatoid-arthropathy of childhood from south India: review of literature in comparison with juvenile idiopathic arthritis', *Seminars in Arthritis and Rheumatism*, 42(6), pp. 582–589. doi:10.1016/j.semarthrit.2012.09.001.

Engel, J. (2004) 'Role of oligomerization domains in thrombospondins and other extracellular matrix proteins', *The International Journal of Biochemistry & Cell Biology*, 36(6), pp. 997–1004. doi:10.1016/j.biocel.2003.12.009.

Fausett, B.V., Gumerson, J.D. and Goldman, D. (2008) 'The proneural basic helix-loop-helix gene ascl1a is required for retina regeneration', *The Journal of Neuroscience: The Official Journal of the Society for Neuroscience*, 28(5), pp. 1109–1117. doi:10.1523/JNEUROSCI.4853-07.2008.

Feldman, A.T. and Wolfe, D. (2014) 'Tissue processing and hematoxylin and eosin staining', *Methods in Molecular Biology (Clifton, N.J.)*, 1180, pp. 31–43. doi:10.1007/978-1-4939-1050-2_3.

Friedman, J.R. and Nunnari, J. (2014) 'Mitochondrial form and function', *Nature*, 505(7483), pp. 335–343. doi:10.1038/nature12985.

Garcia Segarra, N. *et al.* (2012) 'The diagnostic challenge of progressive pseudorheumatoid dysplasia (PPRD): a review of clinical features, radiographic features, and WISP3 mutations in 63 affected individuals', *American Journal of Medical Genetics. Part C, Seminars in Medical Genetics*, 160C(3), pp. 217–229. doi:10.1002/ajmg.c.31333.

Genova, M.L. and Lenaz, G. (2014) 'Functional role of mitochondrial respiratory supercomplexes', *Biochimica Et Biophysica Acta*, 1837(4), pp. 427–443. doi:10.1016/j.bbabio.2013.11.002.

Gold, V.A. *et al.* (2017) 'Visualization of cytosolic ribosomes on the surface of mitochondria by electron cryo-tomography', *EMBO reports*, 18(10), pp. 1786–1800. doi:10.15252/embr.201744261.

Grzeszkiewicz, T.M. *et al.* (2001) 'CYR61 stimulates human skin fibroblast migration through Integrin alpha vbeta 5 and enhances mitogenesis through integrin alpha vbeta 3, independent of its carboxyl-terminal domain', *The Journal of Biological Chemistry*, 276(24), pp. 21943–21950. doi:10.1074/jbc.M100978200.

Hashimoto, Y. *et al.* (1996) 'Identification of genes differentially expressed in association with metastatic potential of K-1735 murine melanoma by messenger RNA differential display', *Cancer Research*, 56(22), pp. 5266–5271.

Heath, E. *et al.* (2008) 'Abnormal skeletal and cardiac development, cardiomyopathy, muscle atrophy and cataracts in mice with a targeted disruption of the Nov (Ccn3) gene', *BMC developmental biology*, 8, p. 18. doi:10.1186/1471-213X-8-18.

Holbourn, K.P., Acharya, K.R. and Perbal, B. (2008) 'The CCN family of proteins: structure-function relationships', *Trends in Biochemical Sciences*, 33(10), pp. 461–473. doi:10.1016/j.tibs.2008.07.006.

Howe, K. *et al.* (2013) 'The zebrafish reference genome sequence and its relationship to the human genome', *Nature*, 496(7446), pp. 498–503. doi:10.1038/nature12111.

Huang, W. *et al.* (2010) 'Blockade of CCN6 (WISP3) Activates Growth Factor–Independent Survival and Resistance to Anoikis in Human Mammary Epithelial Cells', *Cancer Research*, 70(8), pp. 3340–3350. doi:10.1158/0008-5472.CAN-09-4225.

Hurvitz, J.R. *et al.* (1999) 'Mutations in the CCN gene family member WISP3 cause progressive pseudorheumatoid dysplasia', *Nature Genetics*, 23(1), pp. 94–98. doi:10.1038/12699.

Ivkovic, S. *et al.* (2003) 'Connective tissue growth factor coordinates chondrogenesis and angiogenesis during skeletal development', *Development (Cambridge, England)*, 130(12), pp. 2779–2791. doi:10.1242/dev.00505.

Jia, Q. *et al.* (2021) 'CCN Family Proteins in Cancer: Insight Into Their Structures and Coordination Role in Tumor Microenvironment', *Frontiers in Genetics*, 12. Available at: https://www.frontiersin.org/article/10.3389/fgene.2021.649387 (Accessed: 22 April 2022).

Joliot, V. *et al.* (1992) 'Proviral rearrangements and overexpression of a new cellular gene (nov) in myeloblastosis-associated virus type 1-induced nephroblastomas', *Molecular and Cellular Biology*, 12(1), pp. 10–21. doi:10.1128/mcb.12.1.10-21.1992.

Jordan, M., Schallhorn, A. and Wurm, F.M. (1996) 'Transfecting mammalian cells: optimization of critical parameters affecting calcium-phosphate precipitate formation', *Nucleic Acids Research*, 24(4), pp. 596–601. doi:10.1093/nar/24.4.596.

Joshi, S. and Yu, D. (2017) 'Chapter 8 - Immunofluorescence', in Jalali, M., Saldanha, F.Y.L., and Jalali, Mehdi (eds) *Basic Science Methods for Clinical Researchers*. Boston: Academic Press, pp. 135–150. doi:10.1016/B978-0-12-803077-6.00008-4.

Katsube, K. *et al.* (2009) 'Role of CCN, a vertebrate specific gene family, in development', *Development, Growth & Differentiation*, 51(1), pp. 55–67. doi:10.1111/j.1440-169X.2009.01077.x.

Kim, J. *et al.* (2018) 'CCN5 knockout mice exhibit lipotoxic cardiomyopathy with mild obesity and diabetes', *PloS One*, 13(11), p. e0207228. doi:10.1371/journal.pone.0207228.

Kingston, R.E., Chen, C.A. and Rose, J.K. (2003) 'Calcium phosphate transfection', *Current Protocols in Molecular Biology*, Chapter 9, p. Unit 9.1. doi:10.1002/0471142727.mb0901s63.

Kleer, C.G., Zhang, Y. and Merajver, S.D. (2007) 'CCN6 (WISP3) as a New Regulator of the Epithelial Phenotype in Breast Cancer', *Cells Tissues Organs*, 185(1–3), pp. 95–99. doi:10.1159/000101308.

Koh, C.M. (2013) 'Isolation of genomic DNA from mammalian cells', *Methods in Enzymology*, 529, pp. 161–169. doi:10.1016/B978-0-12-418687-3.00013-6.

Kutz, W.E., Gong, Y. and Warman, M.L. (2005) 'WISP3, the gene responsible for the human skeletal disease progressive pseudorheumatoid dysplasia, is not essential for

skeletal function in mice', *Molecular and Cellular Biology*, 25(1), pp. 414–421. doi:10.1128/MCB.25.1.414-421.2005.

Lau, L.F. and Lam, S.C. (1999) 'The CCN family of angiogenic regulators: the integrin connection', *Experimental Cell Research*, 248(1), pp. 44–57. doi:10.1006/excr.1999.4456.

Lau, L.F. and Nathans, D. (1985) 'Identification of a set of genes expressed during the G0/G1 transition of cultured mouse cells', *The EMBO journal*, 4(12), pp. 3145–3151.

Lebold, K.M. *et al.* (2013) 'Chronic vitamin E deficiency promotes vitamin C deficiency in zebrafish leading to degenerative myopathy and impaired swimming behavior', *Comparative biochemistry and physiology. Toxicology & pharmacology: CBP*, 157(4), pp. 382–389. doi:10.1016/j.cbpc.2013.03.007.

Lee, H. *et al.* (2016) 'Mitochondrial oxidative phosphorylation complexes exist in the sarcolemma of skeletal muscle', *BMB reports*, 49(2), pp. 116–121. doi:10.5483/bmbrep.2016.49.2.232.

Lesnik, C. *et al.* (2014) 'OM14 is a mitochondrial receptor for cytosolic ribosomes that supports co-translational import into mitochondria', *Nature Communications*, 5, p. 5711. doi:10.1038/ncomms6711.

Leu, S.-J., Lam, S.C.-T. and Lau, L.F. (2002) 'Pro-angiogenic activities of CYR61 (CCN1) mediated through integrins alphavbeta3 and alpha6beta1 in human umbilical vein endothelial cells', *The Journal of Biological Chemistry*, 277(48), pp. 46248–46255. doi:10.1074/jbc.M209288200.

Liu, L. *et al.* (2015) 'Novel WISP3 mutations causing spondyloepiphyseal dysplasia tarda with progressive arthropathy in two unrelated Chinese families', *Joint Bone Spine*, 82(2), pp. 125–128. doi:10.1016/j.jbspin.2014.10.005.

Liu, Z. and Chen, X. (2021) 'Progressive pseudorheumatoid dysplasia: a case series report', *Translational Pediatrics*, 10(7), pp. 1932–1939. doi:10.21037/tp-21-152.

Lizana, L., Bauer, B. and Orwar, O. (2008) 'Controlling the rates of biochemical reactions and signaling networks by shape and volume changes', *Proceedings of the National*

Academy of Sciences of the United States of America, 105(11), pp. 4099–4104. doi:10.1073/pnas.0709932105.

Luo, H. *et al.* (2015) 'A novel compound WISP3 mutation in a Chinese family with progressive pseudorheumatoid dysplasia', *Gene*, 564(1), pp. 35–38. doi:10.1016/j.gene.2015.03.029.

Madeira, F. *et al.* (2019) 'The EMBL-EBI search and sequence analysis tools APIs in 2019', *Nucleic Acids Research*, 47(W1), pp. W636–W641. doi:10.1093/nar/gkz268.

Madhuri, V. *et al.* (2016) 'WISP3 mutational analysis in Indian patients diagnosed with progressive pseudorheumatoid dysplasia and report of a novel mutation at p.Y198', *Bone & Joint Research*, 5(7), pp. 301–306. doi:10.1302/2046-3758.57.2000520.

Mannella, C.A., Lederer, W.J. and Jafri, M.S. (2013) 'The connection between inner membrane topology and mitochondrial function', *Journal of Molecular and Cellular Cardiology*, 62, pp. 51–57. doi:10.1016/j.yjmcc.2013.05.001.

van Meerloo, J., Kaspers, G.J.L. and Cloos, J. (2011) 'Cell sensitivity assays: the MTT assay', *Methods in Molecular Biology (Clifton, N.J.)*, 731, pp. 237–245. doi:10.1007/978-1-61779-080-5_20.

Mick, D.U. *et al.* (2012) 'MITRAC links mitochondrial protein translocation to respiratory-chain assembly and translational regulation', *Cell*, 151(7), pp. 1528–1541. doi:10.1016/j.cell.2012.11.053.

Miller, D.S. and Sen, M. (2007) 'Potential role of WISP3 (CCN6) in regulating the accumulation of reactive oxygen species', *Biochemical and Biophysical Research Communications*, 355(1), pp. 156–161. doi:10.1016/j.bbrc.2007.01.114.

Miller, G.W. *et al.* (2012) 'Zebrafish (Danio rerio) fed vitamin E-deficient diets produce embryos with increased morphologic abnormalities and mortality', *The Journal of Nutritional Biochemistry*, 23(5), pp. 478–486. doi:10.1016/j.jnutbio.2011.02.002.

Mimaki, M. *et al.* (2012) 'Understanding mitochondrial complex I assembly in health and disease', *Biochimica Et Biophysica Acta*, 1817(6), pp. 851–862. doi:10.1016/j.bbabio.2011.08.010.

Mittal, N., Babu, M.M. and Roy, N. (2009) 'The efficiency of mitochondrial electron transport chain is increased in the long-lived mrg19 Saccharomyces cerevisiae', *Aging Cell*, 8(6), pp. 643–653. doi:https://doi.org/10.1111/j.1474-9726.2009.00518.x.

Mo, F.-E. *et al.* (2002) 'CYR61 (CCN1) is essential for placental development and vascular integrity', *Molecular and Cellular Biology*, 22(24), pp. 8709–8720. doi:10.1128/MCB.22.24.8709-8720.2002.

Montague, T.G. *et al.* (2014) 'CHOPCHOP: a CRISPR/Cas9 and TALEN web tool for genome editing', *Nucleic Acids Research*, 42(Web Server issue), pp. W401-407. doi:10.1093/nar/gku410.

Moreno-Lastres, D. *et al.* (2012) 'Mitochondrial complex I plays an essential role in human respirasome assembly', *Cell Metabolism*, 15(3), pp. 324–335. doi:10.1016/j.cmet.2012.01.015.

Moussad, E.E. and Brigstock, D.R. (2000) 'Connective tissue growth factor: what's in a name?', *Molecular Genetics and Metabolism*, 71(1–2), pp. 276–292. doi:10.1006/mgme.2000.3059.

Murphy, M.P. (2009) 'How mitochondria produce reactive oxygen species', *The Biochemical Journal*, 417(1), pp. 1–13. doi:10.1042/BJ20081386.

Nakamura, Y. *et al.* (2007) 'The CCN family member Wisp3, mutant in progressive pseudorheumatoid dysplasia, modulates BMP and Wnt signaling', *The Journal of Clinical Investigation*, 117(10), pp. 3075–3086. doi:10.1172/JCI32001.

Neerinckx, B. *et al.* (2015) 'A homozygous deletion of exon 1 in WISP3 causes progressive pseudorheumatoid dysplasia in two siblings', *Human Genome Variation*, 2(1), pp. 1–3. doi:10.1038/hgv.2015.49.

Pacheu-Grau, D., Rucktäschel, R. and Deckers, M. (2018) 'Mitochondrial dysfunction and its role in tissue-specific cellular stress', *Cell Stress*, 2(8), pp. 184–199. doi:10.15698/cst2018.07.147.

Patra, M. *et al.* (2016) 'CCN6 regulates mitochondrial function', *Journal of Cell Science*, 129(14), pp. 2841–2851. doi:10.1242/jcs.186247.

Pennica, D. *et al.* (1998) 'WISP genes are members of the connective tissue growth factor family that are up-regulated in wnt-1-transformed cells and aberrantly expressed in human colon tumors', *Proceedings of the National Academy of Sciences of the United States of America*, 95(25), pp. 14717–14722. doi:10.1073/pnas.95.25.14717.

Perbal, B. (2013) 'CCN proteins: A centralized communication network', *Journal of Cell Communication and Signaling*, 7(3), pp. 169–177. doi:10.1007/s12079-013-0193-7.

Perbal, B., Tweedie, S. and Bruford, E. (2018) 'The official unified nomenclature adopted by the HGNC calls for the use of the acronyms, CCN1–6, and discontinuation in the use of CYR61, CTGF, NOV and WISP 1–3 respectively', *Journal of Cell Communication and Signaling*, 12(4), pp. 625–629. doi:10.1007/s12079-018-0491-1.

Percival, J.M. *et al.* (2013) 'Defects in mitochondrial localization and ATP synthesis in the mdx mouse model of Duchenne muscular dystrophy are not alleviated by PDE5 inhibition', *Human Molecular Genetics*, 22(1), pp. 153–167. doi:10.1093/hmg/dds415.

Rai, E. *et al.* (2016) 'Whole Exome Screening Identifies Novel and Recurrent WISP3 Mutations Causing Progressive Pseudorheumatoid Dysplasia in Jammu and Kashmir-India', *Scientific Reports*, 6, p. 27684. doi:10.1038/srep27684.

Ran, F.A. *et al.* (2013) 'Genome engineering using the CRISPR-Cas9 system', *Nature Protocols*, 8(11), pp. 2281–2308. doi:10.1038/nprot.2013.143.

Rayavarapu, S. *et al.* (2013) 'Idiopathic inflammatory myopathies: pathogenic mechanisms of muscle weakness', *Skeletal Muscle*, 3(1), p. 13. doi:10.1186/2044-5040-3-13.

Reed, B. and Jennings, M. (2010) *Guidance on the housing and care of Zebrafish (Danio rerio)*. Royal Society for the Prevention of Cruelty to Animals (RSPCA), UK.

Repudi, S.R., Patra, M. and Sen, M. (2013) 'WISP3-IGF1 interaction regulates chondrocyte hypertrophy', *Journal of Cell Science*, 126(Pt 7), pp. 1650–1658. doi:10.1242/jcs.119859.

Sailani, M.R. *et al.* (2018) 'WISP3 mutation associated with pseudorheumatoid dysplasia', *Cold Spring Harbor Molecular Case Studies*, 4(1), p. a001990. doi:10.1101/mcs.a001990.

Scanziani, E. (1998) 'Immunohistochemical staining of fixed tissues', *Methods in Molecular Biology (Clifton, N.J.)*, 104, pp. 133–140. doi:10.1385/0-89603-525-5:133.

Schober, J.M. *et al.* (2002) 'Identification of integrin alpha(M)beta(2) as an adhesion receptor on peripheral blood monocytes for Cyr61 (CCN1) and connective tissue growth factor (CCN2): immediate-early gene products expressed in atherosclerotic lesions', *Blood*, 99(12), pp. 4457–4465. doi:10.1182/blood.v99.12.4457.

Schutze, N. *et al.* (2005) 'Differential expression of CCN-family members in primary human bone marrow-derived mesenchymal stem cells during osteogenic, chondrogenic and adipogenic differentiation', *Cell communication and signaling: CCS*, 3(1), p. 5. doi:10.1186/1478-811X-3-5.

Sen, M. *et al.* (2004) 'WISP3-dependent regulation of type II collagen and aggrecan production in chondrocytes', *Arthritis and Rheumatism*, 50(2), pp. 488–497. doi:10.1002/art.20005.

Shahi, P. *et al.* (2020) 'Delayed-onset progressive pseudorheumatoid dysplasia with secondary synovial chondromatosis', *BMJ case reports*, 13(5), p. e234461. doi:10.1136/bcr-2020-234461.

Sheth, H. *et al.* (2021) 'Case Report: Recurrent Variant c.298 TA in CCN6 Gene Found in Progressive Pseudorheumatoid Dysplasia Patients From Patni Community of Gujarat: A Report of Three Cases', *Frontiers in Genetics*, 12, p. 724824. doi:10.3389/fgene.2021.724824.

Signes, A. and Fernandez-Vizarra, E. (2018) 'Assembly of mammalian oxidative phosphorylation complexes I-V and supercomplexes', *Essays in Biochemistry*, 62(3), pp. 255–270. doi:10.1042/EBC20170098.

Spinazzi, M. *et al.* (2012) 'Assessment of mitochondrial respiratory chain enzymatic activities on tissues and cultured cells', *Nature Protocols*, 7(6), pp. 1235–1246. doi:10.1038/nprot.2012.058.

Stainier, D.Y.R. *et al.* (2017) 'Guidelines for morpholino use in zebrafish', *PLoS genetics*, 13(10), p. e1007000. doi:10.1371/journal.pgen.1007000.

Steele, S.L., Prykhozhij, S.V. and Berman, J.N. (2014) 'Zebrafish as a model system for mitochondrial biology and diseases', *Translational Research: The Journal of Laboratory and Clinical Medicine*, 163(2), pp. 79–98. doi:10.1016/j.trsl.2013.08.008.

Sun, F.-C. *et al.* (2006) 'Localization of GRP78 to mitochondria under the unfolded protein response', *The Biochemical Journal*, 396(1), pp. 31–39. doi:10.1042/BJ20051916.

Sun, J. *et al.* (2012) 'Novel and recurrent mutations of WISP3 in two Chinese families with progressive pseudorheumatoid dysplasia', *PloS One*, 7(6), p. e38643. doi:10.1371/journal.pone.0038643.

Sunitha, B. *et al.* (2016) 'Muscle biopsies from human muscle diseases with myopathic pathology reveal common alterations in mitochondrial function', *Journal of Neurochemistry*, 138(1), pp. 174–191. doi:10.1111/jnc.13626.

Vincent, A.E. *et al.* (2016) 'The Spectrum of Mitochondrial Ultrastructural Defects in Mitochondrial Myopathy', *Scientific Reports*, 6, p. 30610. doi:10.1038/srep30610.

Wang, J., Zhou, J. and Bondy, C.A. (1999) 'Igf1 promotes longitudinal bone growth by insulin-like actions augmenting chondrocyte hypertrophy', *FASEB journal: official publication of the Federation of American Societies for Experimental Biology*, 13(14), pp. 1985–1990. doi:10.1096/fasebj.13.14.1985.

Wieckowski, M.R. *et al.* (2009) 'Isolation of mitochondria-associated membranes and mitochondria from animal tissues and cells', *Nature Protocols*, 4(11), pp. 1582–1590. doi:10.1038/nprot.2009.151.

Wittig, I., Braun, H.-P. and Schägger, H. (2006) 'Blue native PAGE', *Nature Protocols*, 1(1), pp. 418–428. doi:10.1038/nprot.2006.62.

Wu, S. *et al.* (2008) 'Stimulatory effects of insulin-like growth factor-I on growth plate chondrogenesis are mediated by nuclear factor-kappaB p65', *The Journal of Biological Chemistry*, 283(49), pp. 34037–34044. doi:10.1074/jbc.M803754200.

Yang, Q. *et al.* (2019) 'Leptin induces muscle wasting in a zebrafish kras-driven hepatocellular carcinoma (HCC) model', *Disease Models & Mechanisms*, 12(2), p. dmm038240. doi:10.1242/dmm.038240.

Yang, X., Song, Y. and Kong, Q. (2013) 'Diagnosis and surgical treatment of progressive pseudorheumatoid dysplasia in an adult with severe spinal disorders and polyarthropathy', *Joint Bone Spine*, 80(6), pp. 650–652. doi:10.1016/j.jbspin.2013.03.006.

Yoshioka, Y. *et al.* (2016) 'CCN4/WISP-1 positively regulates chondrogenesis by controlling TGF-β3 function', *Bone*, 83, pp. 162–170. doi:10.1016/j.bone.2015.11.007.

Zhang, R. *et al.* (1998) 'Identification of rCop-1, a new member of the CCN protein family, as a negative regulator for cell transformation', *Molecular and Cellular Biology*, 18(10), pp. 6131–6141. doi:10.1128/MCB.18.10.6131.

Zhou, C. *et al.* (2008) 'The kinase domain of mitochondrial PINK1 faces the cytoplasm', *Proceedings of the National Academy of Sciences of the United States of America*, 105(33), pp. 12022–12027. doi:10.1073/pnas.0802814105.

Zuo, G.-W. *et al.* (2010) 'The CCN proteins: important signaling mediators in stem cell differentiation and tumorigenesis', *Histology and Histopathology*, 25(6), pp. 795–806. doi:10.14670/HH-25.795.

PUBLICATIONS

PUBLICATIONS

Research Articles

1. **Padhan DK**, Sengupta A, Patra M, Ganguly A, Mahata SK, and Sen M (2020) CCN6 regulates mitochondrial respiratory complex assembly and activity. FASEB J. 34, 12163–12176. doi: 10.1096/fj.202000405RR
2. Sengupta A, **Padhan DK**, Ganguly A and Sen M (2021) CCN6 Is Required for Mitochondrial Integrity and Skeletal Muscle Function in Zebrafish. Front. Cell Dev. Biol. 9:627409. doi: 10.3389/fcell.2021.627409
3. Patra M, Mahata S K, **Padhan D K**, and Sen M (2016) CCN6 regulates mitochondrial function. J. Cell Sci. 129, 2841–2851. doi: 10.1242/jcs.186247

Abstract

1. **Padhan DK**, Sengupta A, Patra M, Mahata SK, Ganguly A and Sen M (2020) CCN6 REGULATES MITOCHONDRIAL RESPIRATORY COMPLEX ASSEMBLY AND ACTIVITY. FASEB Journal, Volume-34, Issue S1, Experimental Biology 2020 meeting abstract. https://doi.org/10.1096/fasebj.2020.34.s1.02868

Received: 21 February 2020 | Revised: 26 June 2020 | Accepted: 29 June 2020

DOI: 10.1096/fj.202000405RR

RESEARCH ARTICLE

THE FASEB JOURNAL

CCN6 regulates mitochondrial respiratory complex assembly and activity

Deepesh Kumar Padhan[1] | **Archya Sengupta**[1] | **Milan Patra**[2] | **Ananya Ganguly**[1] | **Sushil Kumar Mahata**[3] | **Malini Sen**[1]

[1]Cancer Biology and Inflammatory Disorder Division, CSIR-Indian Institute of Chemical Biology, Kolkata, India

[2]Hadassah Medical School, Hebrew University of Jerusalem, Jerusalem, Israel

[3]VA San Diego Healthcare System, University of California, San Diego, CA, USA

Correspondence
Malini Sen, Cancer Biology and Inflammatory Disorder Division, CSIR-Indian Institute of Chemical Biology, 4, Raja S.C. Mullick Road, Jadavpur, Kolkata, West Bengal, India
Email: msen@iicb.res.in, msen648@gmail.com

Funding information
Department of Biotechnology , Ministry of Science and Technology (DBT), Grant/Award Number: BT/PR24244/MED/12/764/2017 and Research Associateship; Council of Scientific and Industrial Research (CSIR), Grant/Award Number: Research Fellowship; University Grants Commission (UGC), Grant/Award Number: Research Fellowship; U.S. Department of Veterans Affairs (VA), Grant/Award Number: Research Career Scientist Award

Abstract

Cellular communication network factor 6 (CCN6) mutations are linked with Progressive Pseudo Rheumatoid Dysplasia (PPRD) a debilitating musculoskeletal disorder. The function of CCN6 and the mechanism of PPRD pathogenesis remain unclear. Accordingly, we focused on the functional characterization of CCN6 and CCN6 mutants. Using size exclusion chromatography and native polyacrylamide gel electrophoresis we demonstrated that CCN6 is present as a component of the mitochondrial respiratory complex in human chondrocyte lines. By means of siRNA-mediated transfection and electron microscopy we showed that moderate reduction in CCN6 expression decreases the RER– mitochondria inter-membrane distance. Parallel native PAGE, immunoblotting and Complex I activity assays furthermore revealed increase in both mitochondrial distribution of CCN6 and mitochondrial respiratory complex assembly/activity in CCN6 depleted cells. CCN6 mutants resembling those linked with PPRD, which were generated by CRISPR-Cas9 technology displayed low level of expression of mutant CCN6 protein and inhibited respiratory complex assembly/activity. Electron microscopy and MTT assay of the mutants revealed abnormal mitochondria and poor cell viability. Taken together, our results indicate that CCN6 regulates mitochondrial respiratory complex assembly/activity as part of the mitochondrial respiratory complex by controlling the proximity of RER with the mitochondria, and CCN6 mutations disrupt mitochondrial respiratory complex assembly/activity resulting in mitochondrial defects and poor cell viability.

Abbreviations: ACN, acetonitrile; ATP, adenosine triphosphate; ATP5A1, ATP synthase F1 subunit alpha; BN-PAGE, blue native-polyacrylamide gel electrophoresis; BSA, bovine serum albumin; CCN6, cellular communication network factor 6; CK, cysteine knot; COX 4, cytochrome c oxidase subunit 4 isoform 1; CRISPR, clustered regularly interspaced short palindromic repeats; DMEM, dulbecco's modified eagle media; DMSO, dimethyl sulfoxide; DTT, dithiothreitol; EDTA, ethylenediaminetetraacetic acid; EGTA, ethylene glycol-bis(β-aminoethyl ether)-N,N,N′,N′-tetraacetic acid; ER, endoplasmic reticulum; FBS, fetal bovine serum; HEPES, 4-(2-hydroxyethyl)-1-piperazineethanesulfonic acid; HRP, horseradish peroxidase; IGFBP, insulin-like growth factor binding protein; MTCO1, cytochrome c oxidase I; MTT, 3-(4,5-dimethylthiazol-2-yl)-2,5-diphenyltetrazolium bromide; NADH, nicotinamide adenine dinucleotide; NDUFB8, NADH dehydrogenase [ubiquinone] 1 beta subcomplex subunit 8; NDUFS1, NADH-ubiquinone oxidoreductase 75 kDa subunit; NHEJ, non homologous end joining; OMM, outer mitochondrial membrane; PCR, polymerase chain reaction; PPRD, progressive pseudo rheumatoid dysplasia; PVDF, polyvinylidene difluoride; RER, rough endoplasmic reticulum; ROS, reactive oxygen species; SDHB, succinate dehydrogenase complex iron sulfur subunit B; SDS-PAGE, sodium dodecyl sulfate-polyacrylamide gel electrophoresis; TBST, Tris-buffered saline, 0.1% Tween 20; TEM, transmission electron microscopy; THSP1, thrombospondin type I; UQCRC2, cytochrome b-c1 complex subunit 2; VDAC1, voltage-dependent anion-selective channel 1; VWC, von willebrand factor type c; WISP3, wnt-1–induced signaling protein 3.

KEYWORDS
chondrocyte, mitochondria, PPRD

1 | INTRODUCTION

Wnt-1–Induced Signaling Protein 3 (WISP3) or CCN6 belongs to the CCN (CYR61, CTGF, and NOV) family of cell growth modulators that have long been known for their significant involvement in connective tissue growth/differentiation and maintenance. CYR61 (CCN1), CTGF (CCN2), NOV (CCN3), WISP1 (CCN4), and WISP2 (CCN5) are intrinsically associated with a diverse array of functions ranging from extracellular matrix remodeling during angiogenesis and wound healing to controlling fibrosis in the maintenance of musculoskeletal homeostasis.[1-7] Interestingly, although CCN6 bears the "Wnt-1 Induced Signaling Protein" nomenclature based on its sequence homology to WISP1 and WISP2, which are known to be induced by Wnt-1,[2] Wnt-1 mediated induction of CCN6 has not been documented thus far. CCN6 appears to be present in both secreted as well as cell associated forms.[8,9] Like the other CCN family members, CCN6 is of a multi-modular nature, carrying the potential for interaction with other proteins. At the N-terminus of CCN6 is a signal peptide, followed by the Insulin-like Growth Factor Binding Protein (IGFBP) domain, the Von Willebrand Factor type C (VWC) domain, the Thrombospondin type I (THSP1) domain and the Cysteine knot (CK) domain, which can potentially interconnect with other proteins through the formation of disulfide bonds and oligomerization.[10,11]

The connective tissue function of CCN6 appears to rest mainly on skeletal cartilage and muscle. Mutations in the CCN6 gene are linked to a debilitating yet neglected skeletal disorder termed Progressive Pseudo Rheumatoid Dysplasia (PPRD), where cartilage loss is associated with irregular limb development related deformities and muscle wasting.[12-19] Functional characterization of CCN6 and its mutants, however, remains incomplete. For a comprehensive analysis of the outcome of CCN6 mutations and a basic understanding of PPRD progression, it is essential to have a clear knowledge of the function of CCN6 and the defects of CCN6 mutants in relation to the wild type.

Previously, we demonstrated that CCN6 regulates the production of reactive oxygen species (ROS) and localizes to mitochondria.[20,21] In the current study, we demonstrated using chondrocyte lines that CCN6 controls the assembly and activity of mitochondrial respiratory Complex I, an entity of 45 subunits present also in the form of Super Complexes, and crucial for mitochondrial electron transport.[22-24] The level of cell associated CCN6 protein and its mitochondrial distribution are important for the regulation of mitochondrial respiratory complex assembly and activity. Mutations in CCN6 resembling those linked to PPRD disrupt respiratory complex assembly/activity, resulting in the accumulation of abnormal mitochondria and loss of cell viability.

2 | MATERIALS AND METHODS

2.1 | Cell culture maintenance

Dulbecco Modified Eagle's Medium (DMEM) (Gibco, Thermo Fisher Scientific, Waltham, MA, USA) supplemented with 10% FBS (Gibco, Thermo Fisher Scientific, Waltham, MA, USA), 1 unit mL^{-1} of penicillin, 1 μg mL^{-1} of streptomycin (Gibco, Thermo Fisher Scientific, Waltham, MA, USA), and 2 mM glutamine (Gibco, Thermo Fisher Scientific, Waltham, MA, USA) was used to maintain C-28/I2 and C20A4 chondrocyte cell lines. The cell lines were maintained in a humidified incubator at 37°C with 5% CO_2.

2.2 | Cell transfection

C-28/I2 and C20A4 chondrocyte cells were transfected separately with CCN6 siRNA (50 nM) and Control siRNA (50 nM) (Dharmacon, Horizon Discovery) using RNAimax transfection reagent (Invitrogen, Thermo Fisher Scientific, Waltham, MA, USA) following previously published protocol.[21] In brief, the required amount of each of RNAimax and siRNA was mixed separately with 150 μL of Opti-MEM (Gibco, Thermo Fisher Scientific, Waltham, MA, USA) following which the siRNA mix was slowly added to the RNAimax solution and mixed well. Incubation was continued for 20 minutes. The resulting 300 μL mix was then added drop wise to each well of plated cells in a six-well tissue culture plate. Media of transfected cells was changed at 24 hours post-transfection and incubation continued. After 60-63 hours post transfection, cells were harvested and processed for subsequent analysis.

2.3 | Preparation of RNA/cDNA and PCR

Total cellular RNA was isolated using Trizol (Invitrogen, Thermo Fisher Scientific, Waltham, MA, USA) following the protocol provided by the manufacturer. Briefly, RNA, which separated in the aqueous layer after treatment of the Trizol-homogenate with chloroform was precipitated with isopropanol. RNA was quantified before proceeding to the

cDNA preparation step. cDNA was prepared from total RNA using cDNA synthesis kit (BioBharati Lifescience, Kolkata, West Bengal, India) following instructions provided by the manufacturer. Gene expression was analyzed following PCR of cDNA with specific primers using Taq Polymerase (BioBharati Lifescience, Kolkata, West Bengal, India). Primers used were CCN6 primers (forward 5′-ACCAAAGCTGGCTGGCAGTC-3′ and reverse 5′-TCTCCAGGTTCTCTGCAGTTTC-3′), GAPDH primers (forward 5′-ACCACAGTCCATGCCATCAC-3′ and reverse 5′-TCCACCACCCTGTTGCTGTA-3′), NDUFB8 primers (forward 5′-GTGAAGATGGCGGTGGCC-3′ and reverse 5′-GATCTCATAGTGAACCACCC-3′) and NDUFS1 primers (forward 5′-TCCAACACATGAATTGTGGAG-3′ and reverse 5′-GCATATACATATATACACAC-3′).

2.4 | Variant analysis of CCN6

Variant analysis of CCN6 in C-28/I2 cell line was done by RT-PCR after isolation of RNA. Primers were designed on the basis of NCBI Variant 1 mRNA (Ref. Seq- NM_003880.4) and Variant 3 mRNA (Ref. Seq-NM_198239.2). CCN6 variant 1 forward primer 5′-GAGTCCCGGGAGGAAAGTGC-3′ and variant 3 forward primer 5′-GGAGCAATGAACAAGCGGCGA-3′ were used with reverse primers matching exons 2, 3, 4 & 5. Exon 2 reverse primer: 5′-CACACACTCCAGTCTCGTACC-3′, Exon 3 reverse primer: 5′-GTAGCTTGTTGAAAGCTGCTGTA-3′, Exon 4 reverse primer: 5′-CTGTCGCAAGGCTGAATGTAAC-3′ and Exon 5 reverse primer: 5′-CTTGAGCTCAGAAAATATATCTCC-3′ were used for the analysis.

2.5 | Preparation of cell lysate and immunoblotting

Cell lysis buffer (20 mM Tris-HCl [pH 7.5], 500 mM NaCl, 1% Triton X-100, 1 mM EDTA, 10% Glycerol, 50 mM dithiothreitol, 2 mM phenylmethylsulfonyl fluoride, and 1% protease inhibitor cocktail) was applied to harvested cells for preparing whole cell lysate. Prior to immunoblotting, total protein concentration was determined using Bradford reagent (Bio-Rad, Hercules, CA, USA).

Immunoblotting was performed following previously published procedures.[9,21] In brief, for each experiment, the protein was transferred to PVDF membrane after separation through sodium dodecyl sulfate-polyacrylamide gel electrophoresis (SDS-PAGE) and thereafter blocked for 2 hours with 5% BSA in Tris-buffered saline with 0.1% Tween 20 (TBST). Blots generated were incubated at 4°C overnight with the primary antibodies appropriate for the different experiments executed: anti-CCN6 (custom synthesis targeting residues 201 aa to 372 aa of CCN6, from BioBharati Lifescience, Kolkata, West Bengal, India), anti-β-actin (Santa Cruz, Dallas, TX, USA), anti-OXPHOS cocktail comprising mitochondrial respiratory complex subunits (Abcam, Cambridge, MA, USA), anti-NDUFB8 (Invitrogen, Thermo Fisher Scientific, Waltham, MA, USA), anti-NDUFS1 (Invitrogen, Thermo Fisher Scientific, Waltham, MA, USA), anti-VDAC1 antibody (Abcam, Cambridge, MA, USA) and anti-COX 4 antibody (Abcam, Cambridge, MA, USA). Following primary antibody incubation, Horseradish Peroxidase (HRP)-conjugated matching secondary antibodies were used for visualization with chemiluminescence reagent (Millipore, Burlington, MA, USA), using Chemi documentation system of Azure Biosystems, Model-C400. Densitometric analysis of immunoblot bands was performed using GelQuant.NET software provided by biochemlabsolutions.com.

2.6 | Subcellular fractionation

In order to separately isolate mitochondria and cytosol, we followed instructions provided in previously published protocols.[25] Chondrocyte cells were initially resuspended in Isolation buffer 1 (225 mM mannitol, 75 mM sucrose, 0.1 mM EGTA, and 30 mM Tris-HCl [pH-7.4]) and homogenized with dounce homogenizer following which unbroken cells and nuclei were discarded after centrifugation at 600 g for 5 minutes. The collected supernatant was further subjected to centrifugation at 7000 g for 10 minutes to obtain the mitochondrial pellet and cytosolic fraction (supernatant). The mitochondrial pellet was resuspended in mitochondrial resuspension buffer (250 mM mannitol, 0.5 mM EGTA and 5 mM HEPES [pH-7.4]) after washing with Isolation Buffer 2 (225 mM mannitol, 75 mM sucrose and 30 mM Tris-HCl [pH-7.4]). Isolated mitochondria were either lysed for immunoblotting purpose with mitochondria lysis buffer (50 mM Tris-HCl [pH-7.5], 150 mM NaCl, 0.1 mM EDTA, 1% Triton X 100, and 2 mM 6-Amino Hexanoic Acid) or stored in resuspension buffer in frozen condition for blue native-poly acrylamide gel electrophoresis (BN-PAGE) analysis. To the cytosolic fraction, 1% protease inhibitor cocktail was added. Bradford reagent was used to measure the protein concentration of both mitochondria and cytosol.

2.7 | Gel filtration chromatography

Gel filtration chromatography of mitochondrial lysate was performed using Sephacryl S-300 resin. First, the column was packed carefully with the resin to bed volume 30 mL and then equilibrated with equilibration buffer (50 mM Tris-chloride [pH 8.0], 150 mM NaCl and 1 mM EDTA). Thereafter, the

packed column was calibrated using Thyroglobulin (Sigma-Aldrich, St. Louis, MO, USA) and a molecular weight marker kit (Sigma-Aldrich, St. Louis, MO, USA). The calibration curve was used as a reference scale for different experiments. About 300 μg of mitochondrial lysate was loaded onto the column and for each experimental run 90 no of fractions were collected (330 μL each). After fraction collection, proteins were precipitated from each fraction using 20% TCA and washed with acetone. Samples were subsequently subjected to SDS-PAGE and immunoblotting following the methodology described earlier.

2.8 | Blue Native (BN)-PAGE & 2D BN/SDS-PAGE

Purified mitochondria suspended in resuspension buffer were centrifuged at 10 000 *g* for 10 minutes at 4°C following which the pellet was incubated with 20 μL of solubilization buffer (50 mM NaCl, 2 mM 6-aminohexanoic acid, 1 mM EDTA, and 50 mM imidazole-HCl [pH-7.0]) and 1 μL of Dodecyl maltoside (20%) on ice for 10 minutes. Following solubilization, the sample was subjected to centrifugation for 20 minutes at 20 000 *g* at 4°C.[26] The clear supernatant was loaded onto a 3%-13% gradient gel after mixing with 1.5 μL of 50% glycerol and 1 μL of native loading dye (5% G250 coomassie blue in 500 mM 6-aminohexanoic acid). The gel was run for about 8 hours at 80 volt in cold room. For immunoblotting after BN-PAGE, the proteins were transferred to PVDF membrane using a semi-dry transfer system (Hoefer) for 90 minutes at 30 volt in room temperature. Following transfer, the membrane was rinsed with methanol to remove attached coomassie dye and processed for respective antibody staining and protein detection following the procedure described earlier.

For 2D gel electrophoresis, the protein-loaded lane of BN-PAGE was cut as a strip and incubated in denaturing solution (1% SDS and 1% β-Mercaptoethanol [β-ME]) for about 30 minutes. The gel piece was subsequently washed with distilled water to remove traces of β-ME and set on a second dimensional 12% denaturing SDS-PAGE.[22] After SDS-PAGE immunoblotting was performed following already described procedure.

2.9 | In-gel Complex I activity assay

Gel of BN-PAGE was incubated in 0.1 M Tris-HCL (pH 7.4) containing 1 mg mL^{-1} of Nitrotetrazolium Blue Chloride (Sigma-Aldrich, St. Louis, MO, USA) and 0.14 mM NADH (Sigma-Aldrich, St. Louis, MO, USA) at room temperature for 1 hour based on information garnered from previous publication.[27] Subsequently, after development of blue/purple color, indicating deposition of formazan the gel was washed with distilled water and fixed with 30% methanol and 10% acetic acid solution. The gel was subsequently scanned for documentation of image.

2.10 | Measurement of Complex I activity

Mitochondrial Complex I (NADH dehydrogenase) activity was measured following published protocols [28] with minor modifications. Briefly, protein estimation of freshly isolated mitochondria was done by Bradford method. Equal amount of mitochondria from experimental and control samples was pelleted down in cold centrifuge at 10 000 *g* for 10 minutes. Mitochondria pellet was resuspended in 10 mM ice-cold hypotonic Tris buffer (pH-7.6) and subjected to three cycles of freeze-thawing followed by suspension in assay buffer (50 mM potassium phosphate buffer [pH-7.5], 3 mg mL^{-1} of BSA and 3 mM sodium azide) to which 100 μM NADH and 100 μM ubiquinone were added. Reduction of NADH (extinction coefficient- 6.22 mM^{-1} cm^{-1}) was monitored by following decrease in absorbance of NADH (340 nm) at different time points. Complex I activity (nmoL min^{-1} mg^{-1}) was calculated as (Δ Absorbance/min × 1000)/([Extinction coefficient × Volume of sample used in mL] × [Sample protein concentration in mg mL^{-1}]).[28] Percent change of activity was calculated considering activity of control sample as 100.

2.11 | Liquid chromatography and mass spectrometry

In Gel Digest: The gel slices were cut to 1 mm by 1 mm cubes and destained three times by first washing with 100 μL of 100 mM ammonium bicarbonate for 15 minutes, followed by addition of the same volume of acetonitrile (ACN) for 15 minutes. The supernatant was discarded and samples (gel pieces) were dried in a speedvac. Samples were then reduced by mixing with 200 μL of 100 mM ammonium bicarbonate-10 mM DTT and incubated at 56°C for 30 minutes. Following liquid removal, 200 μL of 100 mM ammonium bicarbonate-55 mM iodoacetamide was added to gel pieces and incubated at room temperature in the dark for 20 minutes. After the removal of the solvent and one wash with 100 mM ammonium bicarbonate for 15 minutes, same volume of ACN was added to dehydrate the gel pieces. After solvent removal, the samples were dried in a speedvac. For digestion, enough solution of ice-cold trypsin (0.01 μg μL^{-1}) in 50 mM ammonium bicarbonate was added to cover the gel pieces for 30 minutes on ice. After complete rehydration, the excess trypsin solution was removed, replaced with fresh 50 mM ammonium bicarbonate, and left overnight at 37°C. The peptides were extracted twice by the addition of

50 μL of 0.2% formic acid and 5% ACN and vortex mixing at room temperature for 30 minutes. The combined extractions are analyzed directly by liquid chromatography (LC) in combination with tandem mass spectroscopy (MS/MS) using electrospray ionization.

LC-MS-MS: Trypsin-digested peptides were analyzed by ultra-high pressure liquid chromatography (UPLC) coupled with tandem mass spectroscopy (LC-MS/MS) using nano-spray ionization. The nanospray ionization experiments were performed using a Orbitrap fusion Lumos hybrid mass spectrometer (Thermo Fisher Scientific, Waltham, MA, USA) interfaced with nano-scale reversed-phase UPLC (Thermo Dionex UltiMate 3000 RSLC nano System) using a 25 cm, 75-micron ID glass capillary packed with 1.7-μm C18 (130) BEH beads (Waters corporation, Milford, MA, USA). Peptides were eluted from the C18 column into the mass spectrometer using a linear gradient (5-80%) of ACN (Acetonitrile) at a flow rate of 375 μL min^{-1} for 1 hour. The buffers used to create the ACN gradient were: Buffer A (98% H_2O, 2% ACN, 0.1% formic acid) and Buffer B (100% ACN, 0.1% formic acid). Mass spectrometer parameters were as follows; an MS1 survey scan using the orbitrap detector of mass range (m/z): 400-1500 (using quadrupole isolation), 120 000 resolution setting, spray voltage of 2200 V, ion transfer tube temperature of 275°C, AGC target of 400 000, and maximum injection time of 50 ms was followed by data-dependent scans (top speed for most intense ions, with charge state set to only include + 2-5 ions, and 5 second exclusion time, while selecting ions with minimal intensities of 50 000 in which the collision event was carried out with high energy collision energy of 30%), and the fragment masses where analyzed in the ion trap mass analyzer (with ion trap scan rate of turbo, first mass m/z 100, AGC Target 5000 and maximum injection time of 35 ms). Protein identification and label free quantitation was carried out using Peaks Studio 8.5 (Bioinformatics solutions Inc Waterloo, ON, Canada).

2.12 | Electron microscopy

About 2.5% glutaraldehyde and 2% paraformaldehyde in 0.15 M cacodylate buffer were used to fix the C-28/I2 chondrocyte line. Post fixing of cells with 1% OsO_4 in 0.1 M cacodylate buffer was performed on ice for 1 hour. Subsequent staining *en bloc* was with 2%-3% uranyl acetate for 1 hour on ice. Graded series of ethanol (20%-100%) on ice was used to dehydrate the cells. This was followed by one wash with 100% ethanol and two washes with acetone (15 min each). Embedding was done with Durcupan. Sections were cut at 50 to 60 nm on a Leica UCT ultramicrotome, and picked up on Formvar and carbon-coated copper grids. Sections were stained with 2% uranyl acetate for 5 minutes and Sato's lead stain for 1 minute. Finally grids were viewed using a JEOL 1200EX II (JEOL, Peabody, MA, USA) TEM and photographed using a Gatan digital camera (Gatan, Pleasanton, CA, USA).

2.13 | CCN6 mutant generation

Exon 5-specific mutant CCN6 was generated using CRISPR Cas9 technology. Guide RNA having maximum on target and minimum off target was designed using CHOPCHOP tool.[29] The guide RNA was cloned into pSpCas9 (BB) 2A-Puro vector (Addgene, Watertown, MA, USA). The primer pair, forward strand 5′-CACCGCATTTAAATGACCCCTCATT-3′, and reverse strand 5′-AAACAATGAGGGGTCATTTAAATGC-3′ were annealed, phosphorylated with polynucleotide kinase (Thermo Fisher Scientific, Waltham, MA, USA) and ligated to the BbsI digested vector pSpCas9 (BB)-2A-Puro (PX458) using T7 ligase (NEB, Ipswich, MA, USA). The sequenced positive clone was used to transfect C-28/I2 cells using Lipofectamine 2000 (Invitrogen, Thermo Fisher Scientific, Waltham, MA, USA).[30] C-28/I2 cells were plated in six-well plates 12-14 hours prior to transfection. Transfection was carried out using Lipofectamine 2000 as per manufacturer's protocol. Briefly, for each well of six-well plates, 5 μL of Lipofectamine 2000 and 2 μg of plasmid DNA were mixed separately with 150 μL of Opti-MEM. The two were combined and the 300 μL mix was incubated for 30 minutes in room temperature. Subsequently, the mix was added drop wise on the plated cells. After 24 hours post transfection, the medium with transfection mix was replaced with fresh complete DMEM High Glucose medium. Puromycin (1.5 μg mL^{-1}) (Gibco, Thermo Fisher Scientific, Waltham, MA, USA) was added to each well 24 hours thereafter, following which incubation was continued for another 48 hours. Finally, Puromycin was removed and fresh complete medium was added to cells continuing incubation for another 24 hours. Untransfected cells, which died after puromycin treatment served as negative control. The surviving cells were pooled, plated in 12-well plates at a dilution of about a single cell in each well. The growing colonies were passaged further for checking CCN6 expression and sequencing. Colonies that harbored CCN6 mutations and displayed diminished expression of the mutant protein were harvested for mitochondria-related assays.

2.14 | Genomic DNA isolation and sequencing

Both wild type and mutant cells were harvested and resuspended in digestion buffer (100 mM NaCl, 10 mM Tris [pH 8.0], 25 mM EDTA [pH 8.0], 0.5% SDS and 0.1 mg mL^{-1} of

proteinase K) and incubated overnight at 50°C in dry bath. DNA was extracted with phenol/chloroform/isoamyl alcohol and the aqueous layer was collected by centrifugation. Two volumes of ethanol were added to precipitate the genomic DNA from the aqueous layer.[31] To determine the insertion/deletion in the target region of genome, isolated DNA was PCR amplified by Pfu Plus DNA Polymerase (BioBharati Lifescience, Kolkata, West Bengal, India) using primers 5′-GCCTCCAAATACTCAGATTTG-3′ (forward) and 5′-GTAGTGATCTGAGAATAGGCA-3′ (reverse) spanning the targeted exon 5 region of CCN6. Resulting PCR product was gel extracted and sent for Sanger sequencing (1st Base Sequencing Service, Singapore science park, Singapore). Sequences of mutants were compared with wild type sequence using Clustal Omega Program [32] and deletion/mutation of the sequences was noted.

2.15 | MTT assay

For MTT (Dimethylthiazol-diphenyl tetrazolium bromide) assay, cells were plated in a 96-well flat bottom culture plate at a density of 10^4 cells per well and allowed to adhere under standard tissue culture conditions. Ten microliter of MTT (5 mg mL^{-1}) (Sigma-Aldrich, St. Louis, MO, USA) was added to each well at stipulated time points and incubation continued for 4 hours at 37°C, 5% CO_2. After incubation, the culture medium was removed and 200 μL of DMSO was added into each well to dissolve the formazan crystals. Absorbance was measured at 595 nm in a micro plate reader (Bio-Rad, Hercules, California, USA) based on previously published protocol.[33]

2.16 | Statistical analysis

Student's *t* test was used for statistical analysis of Complex I activity, densitometry units, MTT assay absorbance values and RER-mitochondria distance measurement (TEM). Percentage of damaged mitochondria in TEM was analyzed by one-way ANOVA followed by multiple comparison tests. GraphPad Prism (La Jolla, CA, USA) was used for all the analyses and graphical presentation of data.

3 | RESULTS

3.1 | CCN6 is associated with the mitochondrial respiratory complex

In view of the mitochondrial localization of CCN6 and its potential to interact with several proteins,[10,21] we became interested in examining whether CCN6 remains associated at least partly with mitochondrial respiratory complexes. Accordingly, two-dimensional gel electrophoresis of freshly prepared mitochondria from the chondrocyte cell line C-28/I2 was performed, where the total mitochondrial protein was subjected first to BN-PAGE followed by SDS-PAGE separation of the active entity in the second dimension, and then to immunoblotting with anti-CCN6 and anti-mitochondrial cocktail antibody separately to detect components present in the active entity.[22,26] Using this procedure we demonstrated that while a portion of the mitochondria localized CCN6 protein (denoted by rectangle) is present in its original low molecular weight form, a significant fraction of it is also present in association with mitochondrial respiratory Complex I, Super Complexes ([Complex I + Complex III + Complex IV], [Complex I + Complex III + Complex V]) and other respiratory complex intermediates comprising Complexes III, IV and V. SDS-PAGE following BN-PAGE skewed protein migration to some extent as denoted by dotted lines. Clearly, SDS-PAGE/immunoblot-mediated detection of CCN6 in line with NDUFB8 (Complex I subunit), ATP5A1 (Complex V subunit), UQCRC2 (Complex III subunit), and MTCO1 (Complex IV subunit) corresponded with the high molecular weight regions encompassing respiratory Super Complexes, Complex I and respiratory complex intermediates in BN-PAGE (Figure 1A). The existence of Complex I as a part of mitochondrial Super Complex(s) and the occurrence of different respiratory complex intermediates in the chondrocyte line are in accordance with contemporary literature.[22-24,34] Presence of respiratory complex subunits in the BN-PAGE regions depicted as encompassing Complex I, Super Complexes and other respiratory complex intermediates was validated by mass spectrometry (Figure 1B, Supporting Table S1). CCN6, however, was not detected by mass spectrometry probably on account of its incompatibility with the peptide detection system. Association of mitochondrial CCN6 with the mitochondrial respiratory complexes was corroborated by gel filtration of total mitochondrial protein and subsequent immunoblotting of collected fractions with anti-CCN6 and anti-mitochondrial cocktail antibodies separately (Figure 1C). Here too, CCN6 was present in association with Complex I subunits (NDUFB8, NDUFS1) and the other respiratory complex subunits UQCRC2, ATP5A1 and MTCO1 in a high molecular weight range, which encompasses mitochondrial Complex I, Super Complex and other respiratory complex intermediates. These results suggested that the association of CCN6 with mitochondrial respiratory complexes may be key to its influence on mitochondrial function, as described previously[21] and led us to investigate if CCN6 is important for mitochondrial respiratory complex assembly and activity.

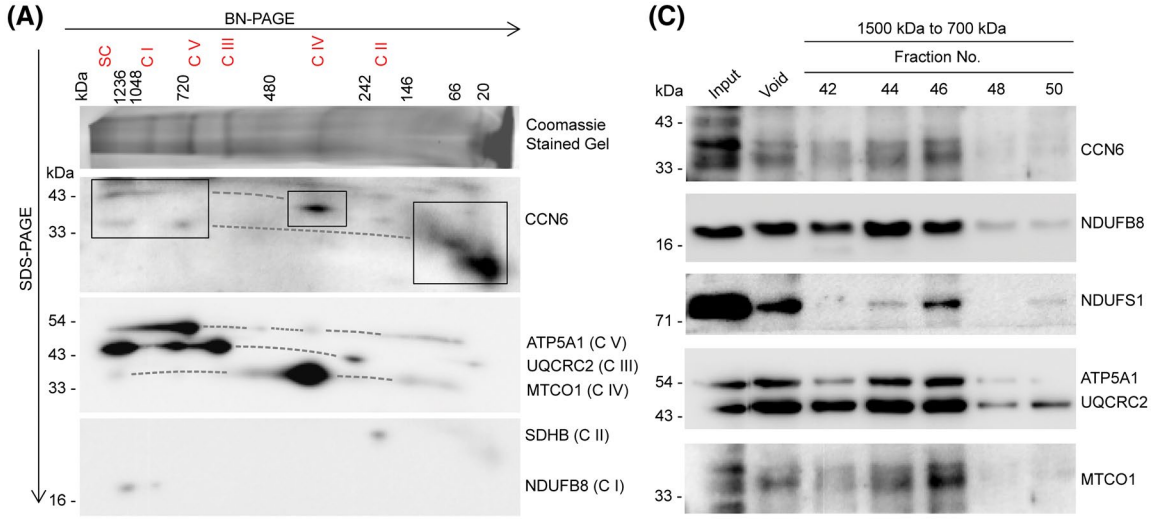

(B)

Description of proteins	Number of peptides	
	SC region	C I region
NADH-ubiquinone oxidoreductase 75kDa subunit (NDUFS1)	40	39
NADH dehydrogenase [ubiquinone] iron-sulfur protein 2 (NDUFS2)	34	33
NADH dehydrogenase [ubiquinone] flavoprotein 1 (NDUFV1)	25	22
NADH dehydrogenase [ubiquinone] 1 beta subcomplex subunit 8 (NDUFB8)	7	5
Cytochrome b-c1 complex subunit 1 (UQCRC1)	39	20
Cytochrome b-c1 complex subunit 2 (UQCRC2)	30	17
ATP synthase subunit alpha (ATP5A1)	25	49
ATP synthase subunit beta (ATP5B)	25	53
Cytochrome c oxidase subunit 4 isoform 1 (COX4I1)	7	7
Cytochrome c oxidase subunit 2 (MTCO2)	5	5

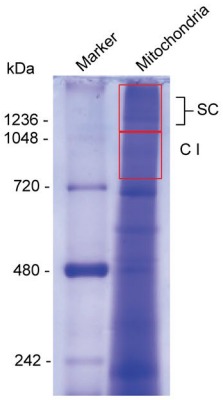

SC : Super Complex, C I : Complex I, C II : Complex II, C III : Complex III, C IV : Complex IV, C V : Complex V

FIGURE 1 CCN6 remains associated with mitochondrial respiratory complex. A, CCN6 is detected in 2D BN-SDS-PAGE immunoblot at higher molecular weight region along with mitochondrial respiratory Complex I/Super Complex and other respiratory complex intermediates. Black box highlights presence of CCN6 and the dotted lines indicate skewing in protein migration. B, Detection of respiratory complex subunits in regions encompassing Complex I/Super Complex by LC-MS/MS. C, Migration of CCN6 with respiratory complex subunits in higher molecular weight complex is observed in size exclusion chromatography of mitochondrial lysate. Presented data in (A, C) are representative of three independent experiments

3.2 | Moderate reduction in CCN6 level augments mitochondrial respiratory complex assembly and activity

In order to evaluate the influence of CCN6 on mitochondrial respiratory complex assembly and activity, we focused on mitochondrial Complex I on account of its role as an initiator of mitochondrial electron transport and ATP synthesis, keeping in mind that it exists in equilibrium as Super Complex(s).[22-24,34] Accordingly, we examined the effect of siRNA-mediated partial depletion of CCN6 on Complex I/Super Complex assembly as well as Complex I-specific NADH dehydrogenase activity in the mitochondria of the C-28/I2 (chondrocyte) cell line. As depicted in Figure 2, a moderate reduction of CCN6 expression, about 35% in protein and 50% in mRNA (Figure 2A) led to considerable increase in mitochondrial Complex I activity, as displayed both in terms of time kinetics (Figure 2B), and the level of total activity spanning a period of 180 seconds (Figure 2C). Similar results were also obtained with another chondrocyte line C20A4 (Supporting Figure S1). This result was corroborated by an analogous increase in in-gel Complex I activity in the mitochondria of CCN6 depleted cells. Clearly, in-gel NBT reduction of NADH after BN-PAGE of total mitochondrial protein extract was significantly more in the CCN6 depleted cells as compared to the corresponding control as revealed by densitometry of band intensities (Figure 2D). The assay for in-gel activity was performed following already published protocols.[22-24,27,34] Increase in in-gel Complex I activity mediated by the moderate level of CCN6 depletion was in accordance with augmented Complex I/Super Complex assembly as documented by immunoblotting with antibodies against NDUFB8 and NDUFS1 (subunits of Complex I) following BN-PAGE of total mitochondrial protein, and

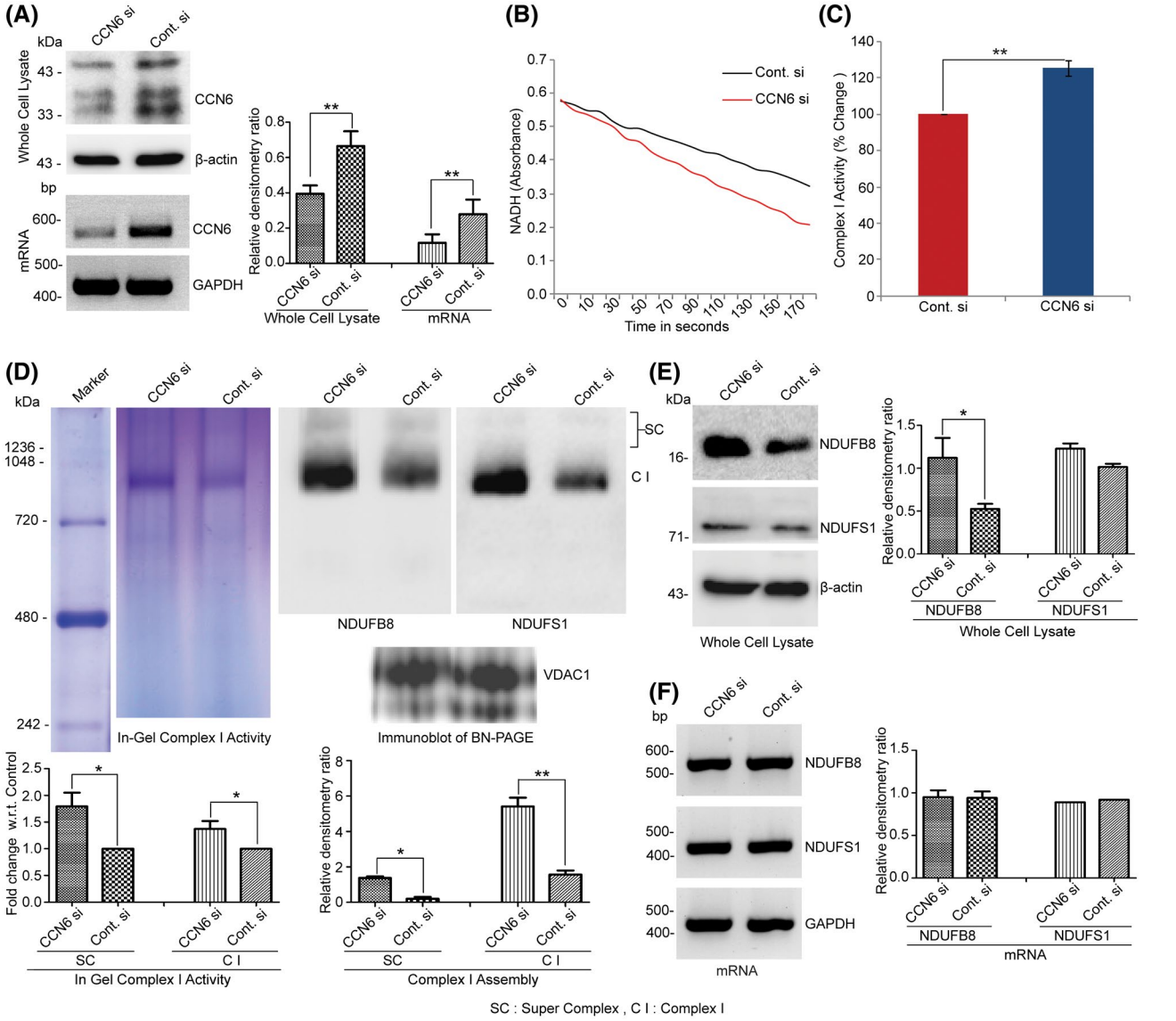

FIGURE 2 Complex I assembly and activity increase in CCN6 depleted cells. A, Immunoblotting followed by quantitation of band intensities by densitometry (bar graph) demonstrating reduction of CCN6 in whole cell lysate (35%) and in mRNA (50%) by siRNA transfection. B, Depletion of CCN6 by siRNA increases Complex I activity as represented by higher rate of decrease of NADH absorbance in comparison to control as measured spectrophotometrically. C, Bar graph showing percent change in Complex I activity in CCN6 depleted cells compared to control (taking control as 100). D, BN-PAGE in-gel Complex I activity assay followed by quantitation showing increased activity in CCN6 siRNA transfected cells compared to control. Increased Complex I and Super Complex assembly is also evident from immunoblotting of BN-PAGE with anti - NDUFB8 & NDUFS1 (Complex I subunits) antibodies followed by quantification of band intensities by densitometry. VDAC1 was used as a loading control in BN-PAGE. E, Level of NDUFB8 protein but not mRNA is increased ~ 50% in whole cell after CCN6 depletion by siRNA. No significant change is seen in NDUFS1. Data are presented as mean ± SEM $*P < .05$, $**P < .01$ (Student's *t* test)

quantitation of the corresponding band intensities by densitometry (Figure 2D). VDAC1 (porin), a mitochondrial structural protein was used as loading control for these experiments. These results suggested that the observed increase in Complex I activity upon moderate reduction of CCN6 is caused by increased levels of at least some Complex I subunits such as NDUFB8 and NDUFS1 in the assembled respiratory complex. The level of NDUFB8 was in fact about 50% more at the protein level in the total lysate of the CCN6 siRNA transfected cells with reference to control as demonstrated by SDS-PAGE/immunoblotting, but not at the mRNA level as demonstrated by RT-PCR. There was no significant change, however, in NDUFS1 either at the protein or mRNA level upon siRNA-mediated CCN6 depletion (Figure 2E,F). These results imply that the level of the CCN6 protein serves as an important determinant of both the stability of Complex I subunit(s) and the level of assembly of mitochondrial respiratory complexes.

To verify how the outcome of moderate CCN6 depletion at the whole cell level fits with the level of mitochondrial CCN6, we estimated CCN6 in both the mitochondria and the cytosol after fractionation. Quite interestingly, increase in Complex I/Super Complex assembly and Complex I activity upon siRNA-mediated CCN6 depletion correlated with increase in the mitochondrial distribution of CCN6 protein relative to its cytosolic content in both C-28/I2 and C20A4 chondrocyte lines (Figure 3A). While the siRNA-mediated moderate depletion of CCN6 was reflected in the cytosol, the mitochondria of CCN6 depleted cells harbored relatively more CCN6 protein than the corresponding controls. A quantitative estimate of the mitochondria: cytosol ratio of the CCN6 protein in CCN6 depleted C-28/I2 and C20A4 cells in comparison to the corresponding controls is represented in Figure 3B. The relative increase in the mitochondrial pool of CCN6 upon CCN6 depletion clearly correlated with notable decrease in the RER (rough ER)–OMM (outer mitochondrial membrane) distance and the concurrent close proximity of the mitochondria with ribosomes as visualized by transmission electron microscopy (Figure 3C,D). We are unclear at this stage about the mechanism of altered sub-cellular distribution of CCN6 at a situation where the overall level of CCN6 is moderately reduced. Perhaps a moderate decrease in CCN6 protein level disrupts the mitochondria-RER inter organelle intervals drawing ribosomes of RER into close apposition with the mitochondria. This may result in facilitated incorporation of ribosome-translated CCN6 and other proteins into the mitochondria leading to increase in respiratory complex assembly and activity.

Taken together, our results suggested that CCN6 contributes to the maintenance of optimal RER-mitochondria

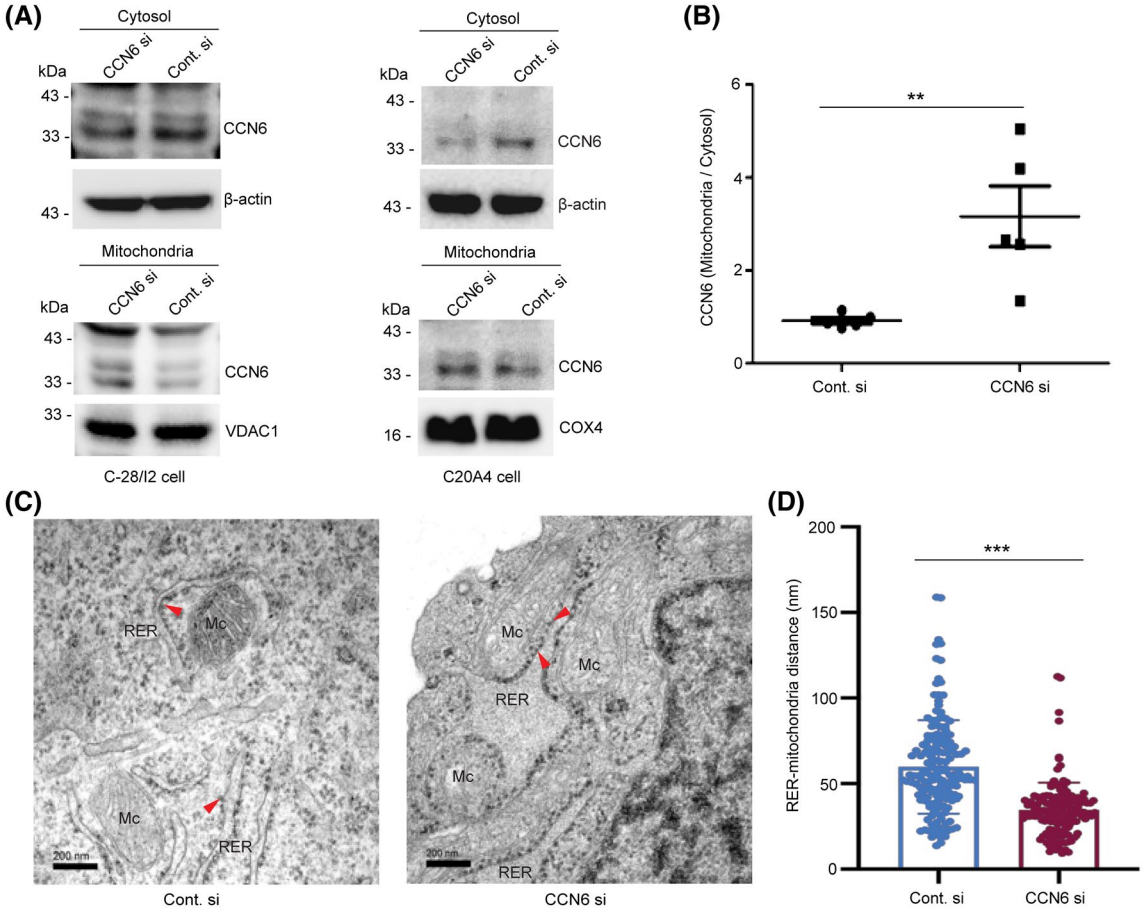

FIGURE 3 Moderate CCN6 depletion alters mitochondrial distribution of CCN6 and RER-mitochondria distance. A, Immunoblots showing decreased cytosolic but increased mitochondrial distribution of CCN6 in both C-28/I2 and C20A4 chondrocyte lines. β-actin and VDAC1/COX4 are shown as loading controls for cytosol and mitochondria, respectively. B, Densitometry of relative CCN6 level (mitochondria/cytosol). Data are presented as mean ± SEM $^{**}P < .01$(Student's *t* test). C, Transmission Electron micrographs showing closer association of rough endoplasmic reticulum (RER) ribosome with outer mitochondrial membrane (OMM) in CCN6 depleted cells (CCN6 si) as compared to control (Cont. si). Mc denotes mitochondria. Red arrowheads indicate ribosomes. Scale bar, 200 nm. D, Distribution plot with mean value showing morphometric analysis of the distance between RER and OMM. RER-OMM distance was calculated in more than 150 points. Data are presented as mean ± SEM $^{***}P < .001$(Student's *t* test)

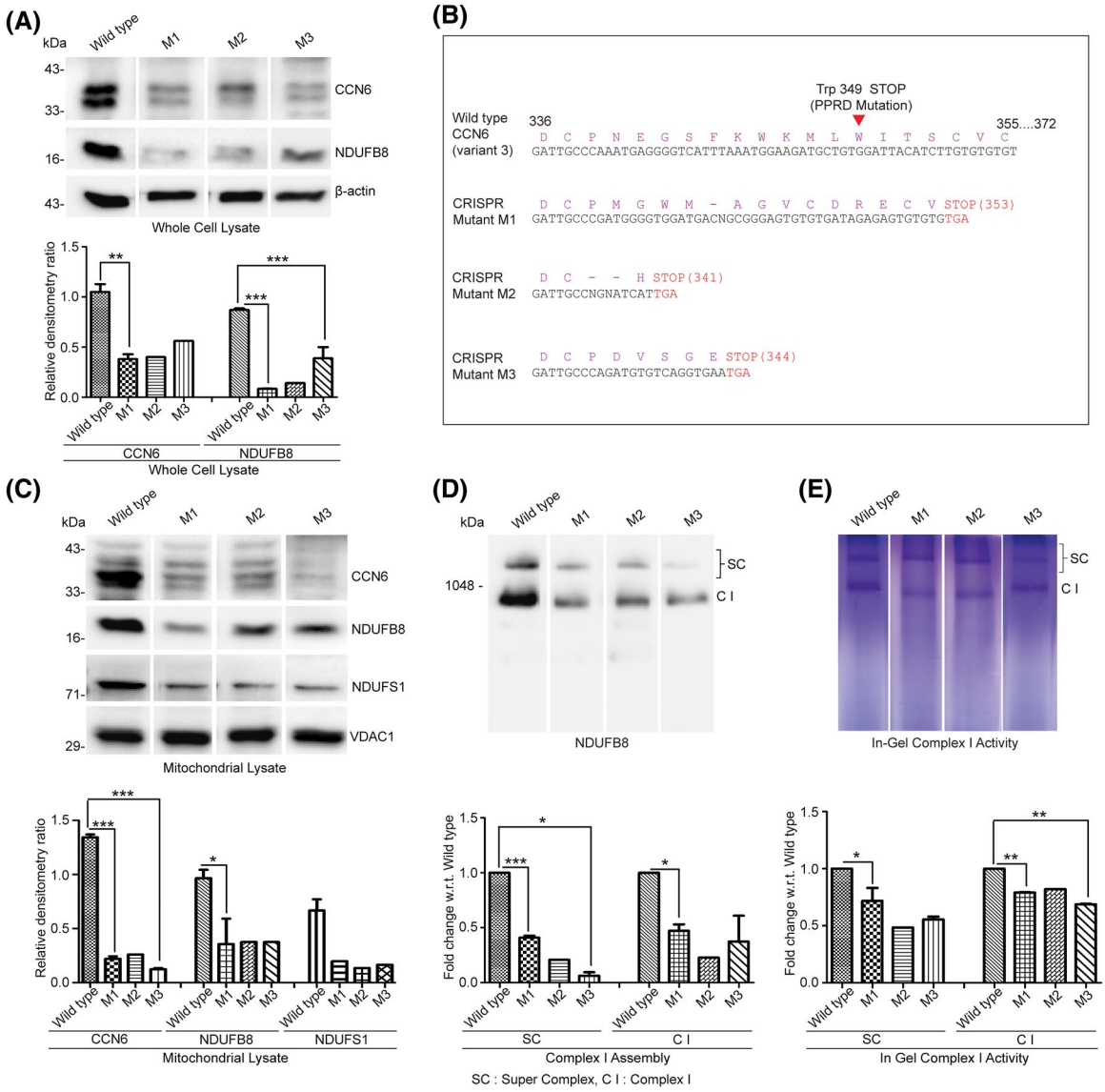

FIGURE 4 Mutations in CCN6 alter respiratory complex assembly and activity. A, CCN6 mutant lines (M1, M2 & M3) showing reduced expression of mutant CCN6 (>60%) and diminished expression of NDUFB8 (Complex I subunit) (65%-90%) as demonstrated by immunoblotting followed by quantitation of band intensities by densitometry. B, DNA sequence showing truncation of CCN6; amino acids mentioned above the sequence on codon basis. C, Immunoblotting followed by quantitation of band intensities showing decreased expression of mutant CCN6, NDUFB8, and NDUFS1 in the mitochondria of the CCN6 mutant lines M1, M2, and M3 as compared to wild type. VDAC1 is used as loading control of mitochondria. D, Immunoblot of BN-PAGE probed with anti-NDUFB8 antibody followed by quantitation of band intensities by densitometry showing reduced Complex I/Super Complex assembly in CCN6 mutant lines in comparison with wild type. E, In-gel Complex I activity assay and corresponding quantitation of band intensity showing altered Complex I/Super Complex activity in CCN6 mutant lines M1, M2, and M3 in comparison with wild type. Data are represented as mean ± SEM $*P < .05$, $**P < .01$ (Student's *t* test)

intervals, which may be required for a balanced flow of mitochondrial proteins inclusive of CCN6 into the mitochondria and an optimal level of respiratory complex assembly and activity. Thus, a moderate reduction in the level of CCN6 is sufficient to lead to decrease in RER-mitochondria distance and increase in respiratory complex assembly/activity. The importance of mitochondria–ER distance in the preservation of vital cell functions such as respiration has been previously discussed.[35,36]

3.3 | CCN6 mutations disrupt respiratory complex assembly and activity, leading to accumulation of abnormal mitochondria and loss of cell viability

Cellular communication network factor 6 mutations have been linked to a debilitating skeletal disorder termed PPRD, which is characterized by loss of normal chondrocyte clusters in the cartilage growth plate.[10] In light of the fact that

CCN6 (variant 3) exon 5 truncation mutation Trp 349 stop (equivalent to Trp 331 stop mutation in variant 1) is linked to PPRD[14,37] we used CRISPR-Cas9 NHEJ methodology[30] to generate truncation mutations similar to Trp 349 stop in CCN6 for investigating if such mutations have any deleterious effects on mitochondrial respiratory complex assembly/activity, and thus cell viability. We focused on CCN6 variant 3 because the chondrocyte line used in this study expresses this variant predominantly (Supporting Figure S2). A guide RNA targeting exon 5 of CCN6 variant 3 was designed and cloned into the puromycin selection vector pSpCas9 (BB)-2A-Puro (PX459), which was then used to transfect C-28/I2 cells. Following transfection and puromycin selection, mutant lines were screened by limited dilution focusing on significantly diminished level of mutant protein expression as compared to wild type. Diminished expression of mutant protein was expected on the basis of anticipated protein instability due to frame shift induced truncation mutation. Detection of the mutant protein was performed by immunoblotting with an antibody that recognized CCN6 beyond the targeted region of mutation. The selected mutants M1, M2, and M3 were sequenced using CCN6-specific primer and found to have frame shifts at amino acid residues 339 (M1), 338 (M2), and 339 (M3), yielding stop codon-mediated truncations at residues 353, 341, and 344, respectively. This suggested that the entire pool of expressed CCN6 in the mutant lines was generated from truncated proteins. Indeed, the level of expression of the CCN6 mutants was distinctly different from that of the wild type, based on the level of expression of β-actin (housekeeping protein), although the expected 2-3 kDa difference in molecular weight was not discernible by immunoblotting possibly due to post translational modifications (Figure 4A,B). Reduced expression of the CCN6 mutants was also reflected in the mitochondria, where VDAC1 was used as loading control, as revealed by densitometry of band intensities. Incidentally, the levels of the mitochondrial respiratory complex subunits NDUFB8 and NDUFS1 also decreased significantly (60%-70%) in the CCN6 mutant lines in the whole cell level and the mitochondrial level as compared to the wild type (Figure 4A,C). Possibly, defects in protein interaction patterns of the CCN6 mutants compounded with their significantly decreased level of expression lowered the stability of the respiratory complex subunits such as NDUFB8 and NDUFS1 resulting in their diminished level of expression. Decreased levels of the respiratory complex subunits in the mitochondria of the mutant lines correlated with poor assembly of Complex I/Super Complex (Figure 4D). Defective Complex I/Super Complex assembly was accompanied by markedly altered Complex I activity as depicted by in-gel assays (Figure 4E).

Altered respiratory complex assembly and activity in the CCN6 mutant chondrocyte lines (M1, M2, and M3) correlated with accumulation of damaged/abnormal mitochondria as exhibited in transmission electron micrographs of samples processed from both the wild-type and mutant lines (Figure 5A). Clearly, the level of abnormal or damaged mitochondria, projected as percent of total mitochondria per cell, was significantly higher in the CCN6 mutant lines M1, M2, and M3 as compared to the wild type. In accordance with the high level of buildup of abnormal mitochondria per cell, the CCN6 mutant lines were significantly less viable than the wild type as demonstrated by MTT assay. Wild type CCN6 expressing cells produced much higher numbers of MTT reducing equivalents in MTT assay than the mutant CCN6 expressing cells (Figure 5B).

Overall our experimental results indicated that CCN6 mutations cause disruption in the assembly and activity of mitochondrial respiratory complexes. Poor assembly/activity of respiratory complexes is associated with accumulation of damaged mitochondria and loss of cell viability.

4 | DISCUSSION

Being a growth and differentiation factor in cells of mesenchymal origin, CCN6 is associated with musculoskeletal health. In view of the link of CCN6 mutations with PPRD, a musculoskeletal disorder, and the role of mitochondria in the preservation of musculoskeletal integrity,[38,39] connection of CCN6 with mitochondrial respiratory complex activity and electron transport constitutes an important, yet not enough explored theme of contemporary research.

In a previously published article, we demonstrated that CCN6 regulates mitochondrial membrane potential, ROS and ATP synthesis. Thus, we described it as acting as a brake on mitochondrial respiration[21] and further investigated the mechanism of CCN6 mediated regulation of mitochondrial function. In the current study, we established that moderate depletion of CCN6 leads to increased mitochondrial Complex I/Super Complex assembly and activity (Figure 2). Interestingly, in this study we demonstrated that the moderate depletion (35%) of total cell associated CCN6 protein not only did not diminish the level of CCN6 in the mitochondria, but in fact led to its relatively increased mitochondrial distribution as compared to the control state where CCN6 was not depleted (Figure 3). Although CCN6 does not harbor any obvious mitochondrial localization sequence, its entry into the mitochondria could be influenced at least in part by intermolecular interactions with other proteins for example, mitochondrial respiratory complex subunits on account of its multi-modular nature.[10] Such a scenario is quite likely based on our demonstration in the current study that CCN6 is present as a part of the mitochondrial respiratory complex (Figure 1). Due to inter protein interactions CCN6 could also be part of the tethers that link mitochondria with the RER/ER.[35,36] Upon moderate depletion of CCN6, perhaps these

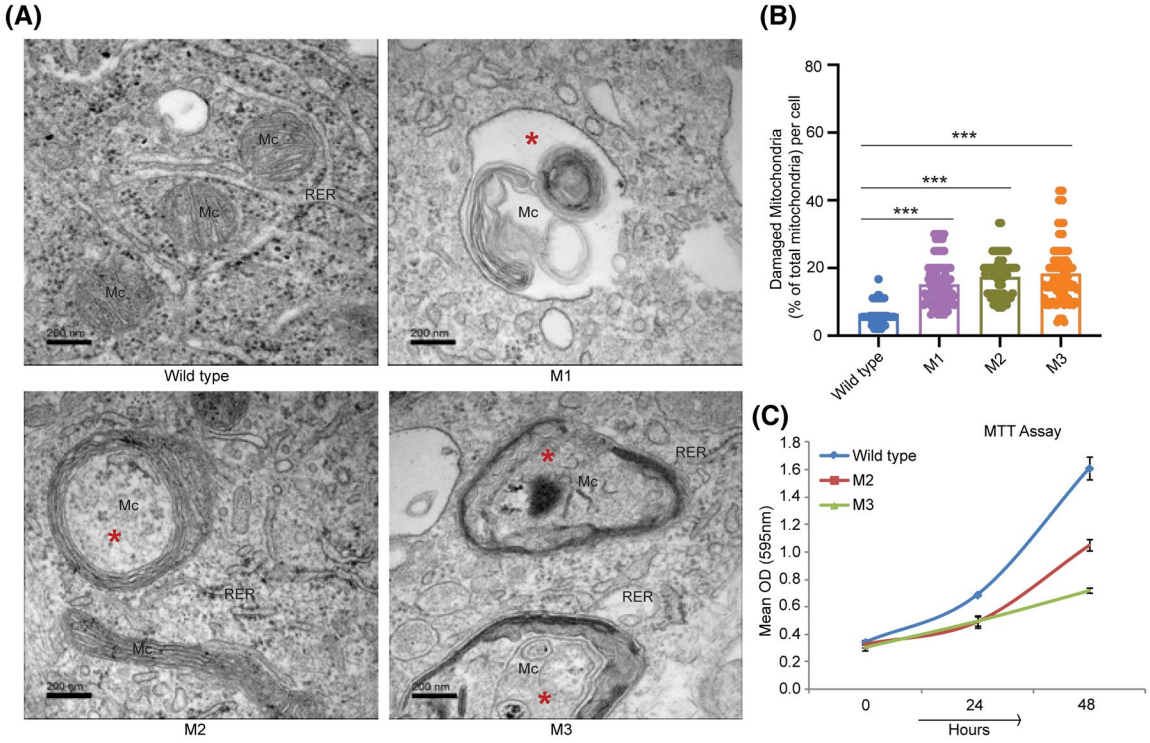

FIGURE 5 Mutations in CCN6 induce accumulation of damaged mitochondria and loss of cell viability. A, Transmission electron micrographs of CCN6 mutant cells showing damaged/abnormal mitochondrial morphology in CCN6 mutant lines M1, M2, and M3 as compared to wild type. Mc indicates mitochondria and * (Red asterisks) indicate damaged/abnormal mitochondria. Scale bar: 200 nm. B, Distribution plot with mean value showing percent of damaged mitochondria per cell in mutant lines and wild type. Scoring was done by counting more than 100 cells for each set. Data were analysed by one-way ANOVA followed by multiple comparison test (**$P < .01$, ***$P < .001$). C, MTT assay showing less viability of CCN6 mutant lines as compared to wild type. Data are plotted as Mean ± SE of eight replicates

tethers collapse, drawing ribosomes of RER in close proximity to the mitochondria (Figure 3) and thereby facilitating mitochondrial transport of ribosome-translated mitochondrial proteins[40,41] that also include CCN6. Augmented mitochondrial distribution of CCN6 may facilitate organization of respiratory complex subunits into assembled complexes promoting their activity (Figures 2 and 3). Our results suggest that CCN6 determines the RER/ribosome-mitochondria intervals that constitute a fundamental element in the regulation of respiratory complex assembly and activity through controlled distribution of mitochondrial proteins that include CCN6. Accordingly, CCN6 acts as a brake on mitochondrial respiration by regulating the mitochondria–RER distance and its own mitochondrial translocation. Such a detailed concept of mitochondrial respiration by CCN6 remained unexplained in our previous study although we observed closer association of mitochondria with the ER in CCN6 depleted cells.[21]

Generation of a CCN6 knock out cell line for evaluating how essential CCN6 is for mitochondrial function was difficult. However, we generated cell lines expressing CCN6 C-terminal truncation mutants similar to those linked with PPRD so as to decipher the effect of these mutants on mitochondrial function and integrity. We demonstrated that cells expressing the CCN6 C-terminal truncation mutants led to significant loss in respiratory complex assembly and activity when compared to those expressing wild type CCN6. Defective respiratory complex assembly and activity were associated with accumulation of degrading mitochondria (Figures 4 and 5). Such interrelation between respiratory complex assembly/activity and mitochondrial structural integrity has been reported in relation to Complex I assembly deficiency in muscle myopathies.[38,39] CCN6 mutant directed defects in respiratory complex assembly/activity and mitochondrial damage led to poor viability of the cells (Figure 5), corroborating that CCN6 is vital for mitochondrial respiration.

In view of the fact that the mitochondrial respiration defective CCN6 mutants used in this study can be treated as analogous to those linked to PPRD, it may be proposed that the skeletal deformities that are manifested during progression of PPRD may at least in part be due to defects in mitochondrial respiration. However, why anomalous mitochondrial respiration would be manifested in only components of the skeletal system is unclear at this stage of our understanding of PPRD pathogenesis. If the involvement of CCN6 in mitochondrial respiration is relatively more pronounced in skeletal tissues the effect of CCN6 mutations may be more prominent in skeletal tissues than in other tissues. Although

the mechanism of tissue specificity in relation to mitochondrial function remains vague, several tissue specific phenotypes of mitochondrial defects have in fact been reported.[42] A more comprehensive diagnosis and understanding of the different features of PPRD may aid in relating mitochondrial defects to this disease.

Worthy of note is the finding that while limited reduction of CCN6 level by CCN6 siRNA enhances its mitochondrial distribution and respiratory complex assembly, abolition of expression of wild-type CCN6 through the effect of mutations results in the collapse of respiratory complex assembly, alteration of complex activity and degeneration of mitochondrial integrity. Such regulation of mitochondrial respiration by optimization of mitochondrial protein distribution, in this case CCN6, has not been documented so far and opens up an as yet unexplored avenue of regulation of protein function.

Our results suggest that CCN6 is an essential protein and although it might have functions in the cytosol and nucleus, its function in the mitochondria is critical. Moderate reduction of CCN6 perhaps sends an SOS signal pushing the cell to put all its effort to survive through mitochondrial respiratory activity. However, when wild-type levels are too low as in the case of CCN6 mutations then the cell fails to survive on account of severely compromised mitochondrial function. Overall, our study indicates that CCN6 is required for the regulation of mitochondrial respiratory complex assembly/activity in chondrocytes and mutations in CCN6 that disrupt mitochondrial respiratory complex assembly/activity are detrimental for chondrocyte viability.

ACKNOWLEDGMENTS

LC-MS/MS was carried out in Mass Spectrometry Facility, UCSD, CA. Transmission Electron Microscopy was conducted at the Cellular & Molecular Medicine Electron Microscopy core Facility, UCSD. We thank J. Sengupta for the use of spectrophotometer and G. Ghosh for insightful comments. This work is supported by a grant from the Department of Biotechnology, Government of India and institutional funding. D. K. P and A.G are supported by the Council of Scientific and Industrial Research (CSIR) fellowship and the University Grants Commission fellowship respectively from the Government of India. A.S is supported by a research associate grant (DBT-RA Programme) from the Department of Biotechnology, Govt. of India. A research career scientist award from the Department of Veterans Affairs supports SKM.

CONFLICT OF INTEREST

The authors declare that they have no conflict of interest.

AUTHOR CONTRIBUTIONS

M. Sen designed research, analyzed the data, and wrote the paper. D. K. Padhan performed research, analyzed data, and assisted in writing the paper. A. Sengupta performed research, analyzed data, and assisted in writing the paper. M. Patra performed research. A. Ganguly performed research. S. K. Mahata performed EM and analyzed the data.

REFERENCES

1. Perbal B. CCN proteins: a centralized communication network. *J Cell Commun Signal*. 2013;7:169-177.
2. Pennica D, Swanson TA, Welsh JW, et al. WISP genes are members of the connective tissue growth factor family that are up-regulated in wnt-1-transformed cells and aberrantly expressed in human colon tumors. *Proc Natl Acad Sci U S A*. 1998;95:14717-14722.
3. Katsube K, Sakamoto K, Tamamura Y, Yamaguchi A. Role of CCN, a vertebrate specific gene family, in development. *Dev Growth Differ*. 2009;51:55-67.
4. Holbourn KP, Acharya KR, Perbal B. The CCN family of proteins: structure-function relationships. *Trends Biochem Sci*. 2008;33:461-473.
5. Schutze N, Noth U, Schneidereit J, Hendrich C, Jakob F. Differential expression of CCN-family members in primary human bone marrow-derived mesenchymal stem cells during osteogenic, chondrogenic and adipogenic differentiation. *Cell Commun Signal*. 2005;3:5.
6. Takigawa M, Nakanishi T, Kubota S, Nishida T. Role of CTGF/HCS24/ecogenin in skeletal growth control. *J Cell Physiol*. 2003;194:256-266.
7. Sen M, Cheng Y-H, Goldring MB, Lotz MK, Carson DA. WISP3-dependent regulation of type II collagen and aggrecan production in chondrocytes. *Arthritis Rheum*. 2004;50:488-497.
8. Davis L, Chen Y, Sen M. WISP-3 functions as a ligand and promotes superoxide dismutase activity. *Biochem Biophys Res Commun*. 2006;342:259-265.
9. Repudi SR, Patra M, Sen M. WISP3-IGF1 interaction regulates chondrocyte hypertrophy. *J Cell Sci*. 2013;126:1650-1658.
10. Hurvitz JR, Suwairi WM, Van Hul W, et al. Mutations in the CCN gene family member WISP3 cause progressive pseudorheumatoid dysplasia. *Nat Genet*. 1999;23:94-98.
11. Engel J. Role of oligomerization domains in thrombospondins and other extracellular matrix proteins. *Int J Biochem Cell Biol*. 2004;36:997-1004.
12. Dalal A, Bhavani GSL, Togarrati PP, et al. Analysis of the WISP3 gene in Indian families with progressive pseudorheumatoid dysplasia. *Am J Med Genet A*. 2012;158A:2820-2828.
13. Sun J, Xia W, He S, et al. Novel and recurrent mutations of WISP3 in two Chinese families with progressive pseudorheumatoid dysplasia. *PLoS One*. 2012;7:e38643.
14. Garcia Segarra N, Mittaz L, Campos-Xavier AB, et al. The diagnostic challenge of progressive pseudorheumatoid dysplasia (PPRD): a review of clinical features, radiographic features, and WISP3 mutations in 63 affected individuals. *Am J Med Genet C Semin Med Genet*. 2012;160C:217-229.
15. Yang X, Song Y, Kong Q. Diagnosis and surgical treatment of progressive pseudorheumatoid dysplasia in an adult with severe spinal disorders and polyarthropathy. *Jt Bone Spine Rev Rhum*. 2013;80:650-652.
16. Ekbote AV, Danda D, Kumar S, Danda S, Madhuri V, Gibikote S. A descriptive analysis of 14 cases of progressive-psuedorheumatoid-arthropathy of childhood from south India: review of literature

in comparison with juvenile idiopathic arthritis. *Semin Arthritis Rheum*. 2013;42:582-589.
17. Luo H, Shi C, Mao C, et al. A novel compound WISP3 mutation in a Chinese family with progressive pseudorheumatoid dysplasia. *Gene*. 2015;564:35-38.
18. Liu L, Li N, Zhao Z, Li W, Xia W. Novel WISP3 mutations causing spondyloepiphyseal dysplasia tarda with progressive arthropathy in two unrelated Chinese families. *Jt Bone Spine Rev Rhum*. 2015;82:125-128.
19. Alawbathani S, Kawalia A, Karakaya M, Altmüller J, Nürnberg P, Cirak S. Late diagnosis of a truncating WISP3 mutation entails a severe phenotype of progressive pseudorheumatoid dysplasia. *Cold Spring Harb Mol Case Stud*. 2018;4.
20. Miller DS, Sen M. Potential role of WISP3 (CCN6) in regulating the accumulation of reactive oxygen species. *Biochem Biophys Res Commun*. 2007;355:156-161.
21. Patra M, Mahata SK, Padhan DK, Sen M. CCN6 regulates mitochondrial function. *J Cell Sci*. 2016;129:2841-2851.
22. Acín-Pérez R, Fernández-Silva P, Peleato ML, Pérez-Martos A, Enriquez JA. Respiratory active mitochondrial supercomplexes. *Mol Cell*. 2008;32:529-539.
23. Mimaki M, Wang X, McKenzie M, Thorburn DR, Ryan MT. Understanding mitochondrial complex I assembly in health and disease. *Biochim Biophys Acta*. 2012;1817:851-862.
24. Moreno-Lastres D, Fontanesi F, García-Consuegra I, et al. Mitochondrial complex I plays an essential role in human respirasome assembly. *Cell Metab*. 2012;15:324-335.
25. Wieckowski MR, Giorgi C, Lebiedzinska M, Duszynski J, Pinton P. Isolation of mitochondria-associated membranes and mitochondria from animal tissues and cells. *Nat Protoc*. 2009;4:1582-1590.
26. Wittig I, Braun H-P, Schägger H. Blue native PAGE. *Nat Protoc*. 2006;1:418-428.
27. Díaz F, Barrientos A, Fontanesi F. Evaluation of the mitochondrial respiratory chain and oxidative phosphorylation system using blue native gel electrophoresis. *Curr Protoc Hum Genet*. 2009;63:hg1904s63.
28. Spinazzi M, Casarin A, Pertegato V, Salviati L, Angelini C. Assessment of mitochondrial respiratory chain enzymatic activities on tissues and cultured cells. *Nat Protoc*. 2012;7:1235-1246.
29. Montague TG, Cruz JM, Gagnon JA, Church GM, Valen E. CHOPCHOP: a CRISPR/Cas9 and TALEN web tool for genome editing. *Nucleic Acids Res*. 2014;42:W401-W407.
30. Ran FA, Hsu PD, Wright J, Agarwala V, Scott DA, Zhang F. Genome engineering using the CRISPR-Cas9 system. *Nat Protoc*. 2013;8:2281-2308.
31. Koh CM. Isolation of genomic DNA from mammalian cells. *Methods Enzymol*. 2013;529:161-169.
32. Madeira F, Park YM, Lee J, et al. The EMBL-EBI search and sequence analysis tools APIs in 2019. *Nucleic Acids Res*. 2019;47:W636-W641.
33. van Meerloo J, Kaspers GJL, Cloos J. Cell sensitivity assays: the MTT assay. *Methods Mol Biol*. 2011;731:237-245.
34. Milenkovic D, Blaza JN, Larsson N-G, Hirst J. The enigma of the respiratory chain supercomplex. *Cell Metab*. 2017;25:765-776.
35. Csordás G, Renken C, Várnai P, et al. Structural and functional features and significance of the physical linkage between ER and mitochondria. *J Cell Biol*. 2006;174:915-921.
36. de Brito OM, Scorrano L. An intimate liaison: spatial organization of the endoplasmic reticulum-mitochondria relationship. *EMBO J*. 2010;29:2715-2723.
37. Sailani MR, Chappell J, Jingga I, et al. WISP3 mutation associated with pseudorheumatoid dysplasia. *Cold Spring Harb Mol Case Stud*. 2018;4:a001990.
38. Sunitha B, Gayathri N, Kumar M, et al. Muscle biopsies from human muscle diseases with myopathic pathology reveal common alterations in mitochondrial function. *J Neurochem*. 2016;138:174-191.
39. Vincent AE, Ng YS, White K, et al. The spectrum of mitochondrial ultrastructural defects in mitochondrial myopathy. *Sci Rep*. 2016;6.
40. Lesnik C, Cohen Y, Atir-Lande A, Schuldiner M, Arava Y. OM14 is a mitochondrial receptor for cytosolic ribosomes that supports co-translational import into mitochondria. *Nat Commun*. 2014;5:5711.
41. Gold VA, Chroscicki P, Bragoszewski P, Chacinska A. Visualization of cytosolic ribosomes on the surface of mitochondria by electron cryo-tomography. *EMBO Rep*. 2017;18:1786-1800.
42. Pacheu-Grau D, Rucktäschel R, Deckers M. Mitochondrial dysfunction and its role in tissue-specific cellular stress. *Cell Stress*. 2018;2:184-199.

SUPPORTING INFORMATION

Additional Supporting Information may be found online in the Supporting Information section.

How to cite this article: Padhan DK, Sengupta A, Patra M, Ganguly A, Mahata SK, Sen M. CCN6 regulates mitochondrial respiratory complex assembly and activity. *The FASEB Journal*. 2020;00:1–14. https://doi.org/10.1096/fj.202000405RR

frontiers in Cell and Developmental Biology

BRIEF RESEARCH REPORT
published: 11 February 2021
doi: 10.3389/fcell.2021.627409

Ccn6 Is Required for Mitochondrial Integrity and Skeletal Muscle Function in Zebrafish

*Archya Sengupta, Deepesh Kumar Padhan, Ananya Ganguly and Malini Sen**

Division of Cancer Biology & Inflammatory Disorder, CSIR-Indian Institute of Chemical Biology, Kolkata, India

Mutations in the *CCN6* (*WISP3*) gene are linked with a debilitating musculoskeletal disorder, termed progressive pseudorheumatoid dysplasia (PPRD). Yet, the functional significance of CCN6 in the musculoskeletal system remains unclear. Using zebrafish as a model organism, we demonstrated that zebrafish Ccn6 is present partly as a component of mitochondrial respiratory complexes in the skeletal muscle of zebrafish. Morpholino-mediated depletion of Ccn6 in the skeletal muscle leads to a significant reduction in mitochondrial respiratory complex assembly and activity, which correlates with loss of muscle mitochondrial abundance. These mitochondrial deficiencies are associated with notable architectural and functional anomalies in the zebrafish muscle. Taken together, our results indicate that Ccn6-mediated regulation of mitochondrial respiratory complex assembly/activity and mitochondrial integrity is important for the maintenance of skeletal muscle structure and function in zebrafish. Furthermore, this study suggests that defects related to mitochondrial respiratory complex assembly/activity and integrity could be an underlying cause of muscle weakness and a failed musculoskeletal system in PPRD.

Keywords: CCN6, PPRD, muscle, mitochondria, respiratory complex, zebrafish

OPEN ACCESS

Edited by:
Eleonora Napoli,
University of California, Davis,
United States

Reviewed by:
Steffen Just,
Ulm University Medical Center,
Germany
Emy Basso,
Institute of Neuroscience, National Research Council (CNR), Italy

****Correspondence:***
Malini Sen
msen@iicb.res.in;
msen648@gmail.com

Specialty section:
This article was submitted to Cellular Biochemistry, a section of the journal Frontiers in Cell and Developmental Biology

Received: *09 November 2020*
Accepted: *05 January 2021*
Published: *11 February 2021*

Citation:
Sengupta A, Padhan DK, Ganguly A and Sen M (2021) Ccn6 Is Required for Mitochondrial Integrity and Skeletal Muscle Function in Zebrafish. Front. Cell Dev. Biol. 9:627409. doi: 10.3389/fcell.2021.627409

INTRODUCTION

CCN6 (WISP3), a CCN (Cyr61, CTGF, NOV) family member, is a multi-domain protein that is expressed in most cells of mesenchymal origin. Similar to other members of the CCN family, the signal peptide at the N terminus of CCN6 is followed by the insulin growth factor binding protein (IGFBP)-like domain, von Willebrand factor type C (VWR)-like domain, thrombospondin type I (THBS)-like domain, and cysteine knot (CK)-like domain, which have potential for binding to different proteins or peptides and dimerization *via* inter-protein disulfide bond formation (Engel, 2004; Schutze et al., 2005; Holbourn et al., 2008; Katsube et al., 2009; Perbal, 2013). Given the potential of CCN6 to interact with several proteins, it can be expected that loss of CCN6 function resulting from *CCN6* gene mutations or depletion would have diverse effects on cellular functions. In fact, mutations in the *CCN6* gene, which span across the entire length of the protein coding sequence, are linked with a musculoskeletal disorder termed progressive pseudorheumatoid dysplasia (PPRD) (Hurvitz et al., 1999).

Progressive pseudorheumatoid dysplasia, an incurable debilitating disorder, is characterized by loss of cartilage, muscle weakness, and irregular bone growth especially in the joints (Hurvitz et al., 1999; Dalal et al., 2012; Sun et al., 2012; Ekbote et al., 2013; Yang et al., 2013; Liu et al., 2015; Luo et al., 2015; Chouery et al., 2017; Alawbathani et al., 2018; Shahi et al., 2020). But how *CCN6* gene

mutations lead to defects in cartilage and muscle remains unclear at the molecular level. In order to gain an in-depth understanding of how PPRD initiates and progresses, one must have a clear picture of the function of the wild-type CCN6 protein and how it interacts with other proteins in different cellular contexts.

Previous reports have demonstrated that CCN6 is present in adult cartilage, mostly in chondrocytes of the mid-zone to the superficial zone and in the fetal growth plate. In chondrocytes, CCN6 maintains the expression of cartilage-specific matrix proteins, such as collagen II and aggrecan, and regulates the production of reactive oxygen species and hypertrophy (Sen et al., 2004; Davis et al., 2006; Miller and Sen, 2007; Repudi et al., 2013). Furthermore, we recently reported that CCN6 localizes to the mitochondria and controls mitochondrial respiratory complex assembly/activity and ATP production (Patra et al., 2016; Padhan et al., 2020). In view of the fact that all the functional assays with reference to CCN6 were performed using cell lines, we wanted to examine the function of CCN6 at the organism level. Accordingly, for a thorough understanding of CCN6 function in the mitochondria and its relation to the musculoskeletal system, we have used zebrafish as our study platform. This choice of organism was prompted by a prior report of a defective cartilage development following morpholino-mediated Ccn6 depletion (Nakamura et al., 2007).

In the current manuscript, we have demonstrated that in the mitochondria of adult zebrafish skeletal muscle, a significant fraction of the total Ccn6 protein is present as a component of the mitochondrial respiratory complexes. Morpholino-mediated depletion of Ccn6 in zebrafish skeletal muscle leads to a considerable reduction in respiratory complex assembly and activity and to a loss of mitochondrial integrity. These mitochondrial defects are associated with abnormal muscle architecture and a diminished muscle function in zebrafish. Our results indicate that defects in the mitochondrial respiratory complex assembly/activity and loss of mitochondrial integrity may constitute an underlying cause of muscle weakness associated with PPRD.

MATERIALS AND METHODS

Animal Maintenance

Adult zebrafish (AB strain) were kept in 30-L fish tanks maintained at 26 ± 2°C temperature in 14:10-h light/dark cycle. All fish tanks were supplied with filtered water. Aeration through an air pump and continuous circulatory flow of water were retained in all the tanks as described in the literature (Avdesh et al., 2012). Fish were fed twice a day with commercially available fish food pellets. Age-matched groups including both males and females were used for experiments. All experiments were performed following internationally approved guidelines (Reed and Jennings, 2010).

Morpholino Treatment

Zebrafish *ccn6*-specific morpholino oligo was designed and procured from Gene Tools (United States) to block *ccn6* translation. The sequence of the morpholino used is 5′-GTA GTGA TAGCATCA TACACGGCTT-3′. A universal standard control morpholino having the sequence 5′-CCT CTT ACC TCA GTT ACA ATT TAT A-3′ was also procured for use as a negative control (Stainier et al., 2017). Each morpholino oligo was reconstituted in sterile water to make a final concentration of 200 μM for injection into adult fish. For morpholino injection, adult fish of 9–12 months of age were selected. Each fish was either anesthetized with MS222 (0.168 mg/mL, pH 7.5) or subjected to cold shock following internationally approved guidelines (Reed and Jennings, 2010). Subsequently, each fish was injected with 4 μL of morpholino solution at the left dorsal muscle just above the dorsal fin using a 30-gauge Hamilton syringe. After injection, each fish was subjected to electroporation using a tweezer electrode with three pulses of a 50-V current, 50 ms each with 5-s intervals to ensure intracellular delivery of morpholino (Fausett et al., 2008). During injection and electroporation, aerated water was used to irrigate fish gill for avoiding dehydration and ensuring proper respiration. After electroporation, the fish were immediately moved into the water tanks and maintained for ∼65 h at 26 ± 2°C for collection of skeletal muscle following sacrifice. The left dorsal muscle around the injection site was dissected out and labeled as "*ccn6*/Control morpholino injected." Muscle from the right ventral side of the same fish was also dissected and labeled as "uninjected."

Tissue Lysate Preparation and Immunoblotting

Tissue was homogenized with a motorized dounce homogenizer using tissue lysis buffer [50 mM Tris (pH 8.0), 150 mM NaCl, 0.1% SDS, 50 mM DTT, 2 mM PMSF, 1 mM EDTA, 5% glycerol, 5 mM NaF, 2 mM sodium orthovanadate, 0.5% sodium deoxycholate, and 1% Triton-X]. Total protein concentration was measured using Bradford reagent. Following sodium dodecyl sulfate polyacrylamide gel electrophoresis (SDS-PAGE), the proteins were transferred to a polyvinylidene fluoride (PVDF) membrane and kept in a blocking solution [5% bovine serum albumin (BSA) in Tris-buffered saline (TBS) with 0.1% Tween-20] for 2 h. Membranes were then incubated with specific primary antibodies overnight at 4°C [primary antibodies used: zebrafish-specific anti-Ccn6 and anti-Ndufb8 antibody (BioBharati Life Sciences), anti-β-actin antibody (Santa Cruz), anti-Ndufs1 antibody (Thermo Fisher Scientific), anti-Cox-IV antibody (Cell Signaling), anti-Vdac1 antibody (Abcam), anti-Atp5a1 antibody (Thermo Fisher Scientific), and anti-Uqcrc2 antibody (Thermo Fisher Scientific)]. Using appropriate horseradish peroxidase (HRP)-conjugated secondary antibodies, anti-rabbit and anti-mouse IgG (Sigma), the membranes were visualized with a chemiluminescence reagent (Millipore) and the chemiluminescence corresponding to each antibody was documented in a chemi-documentation system.

Mitochondria Isolation

Mitochondria were isolated from the skeletal muscle tissue of zebrafish by following previously published protocols (Spinazzi et al., 2012; Patra et al., 2016; Padhan et al., 2020). The tissue samples, flash frozen in liquid nitrogen and stored in a -80°C

freezer, were thawed on ice. Next, the samples were incubated in isolation buffer 1 [225 mM mannitol, 75 mM sucrose, 0.1 mM EGTA, and 30 mM Tris-HCl (pH 7.4)] and homogenized on ice using a motorized dounce homogenizer for 3 min, followed by 5 min ice incubation. The homogenization and incubation process was repeated three times. The homogenate was then collected and centrifuged at 600 × *g* for 5 min at 4°C. The pellets containing unbroken tissue and nuclei were discarded and the supernatant was further centrifuged at 7,000 × *g* for 10 min to obtain a mitochondria-containing pellet and a cytosolic supernatant. This pellet was washed with isolation buffer 2 [225 mM mannitol, 75 mM sucrose, and 30 mM Tris–HCl (pH 7.4)] and centrifuged at 10,000 × *g* for 10 min at 4°C. The isolated crude mitochondrial pellet was resuspended in mitochondrial resuspension buffer [250 mM mannitol, 0.5 mM EGTA, and 5 mM HEPES (pH 7.4)] and either stored for blue native PAGE (BN-PAGE) analysis or lysed for immunoblotting with mitochondria lysis buffer [50 mM Tris-HCl (pH 7.5), 150 mM NaCl, 0.1 mM EDTA, 1% Triton X-100, and 2 mM 6-amino hexanoic acid]. The protein content was estimated by Bradford reagent.

Size Exclusion Chromatography

Size exclusion chromatography of endogenous muscle mitochondria was performed using Sephacryl S-300 resin packed with 30 mL bed volume. The column was first washed with buffer containing 50 mM Tris–HCl (pH 8), 150 mM NaCl, and 1 mM EDTA several times and then calibrated with specific molecular weight markers (Sigma). A column calibration curve was prepared using the elute volume of the molecular weight markers and used as a reference scale for each experimental sample elution. Of the mitochondrial lysate, 300 μg was run through the column and fractions were collected (330 μL each). From each fraction, protein was precipitated using 20% TCA and washed with acetone. Dried precipitated samples were then processed for SDS-PAGE and immunoblotting following the protocol described earlier.

Blue Native PAGE

Frozen mitochondria suspended in resuspension buffer was thawed on ice and estimated by Bradford reagent. About 25 μg of mitochondria was centrifuged at 10,000 × *g* for 10 min at 4°C, after which the pellet was incubated with 20 μl solubilization buffer [50 mM NaCl, 2 mM 6-aminohexanoic acid, 1 mM EDTA, and 50 mM imidazole–HCl (pH 7.0)] and 1 μl dodecyl maltoside (20%) on ice for 10 min. The sample was then subjected to centrifugation for 20 min at 20,000 × *g* at 4°C. The clear supernatant was mixed with 1.5 μL 50% glycerol and 1 μl native loading dye (5% G250 Coomassie Blue in 500 mM 6-aminohexanoic acid) before loading onto a 3–13% gradient gel (Wittig et al., 2006). The gel was run in a cold room for about 8 h at 80 V. After BN-PAGE, the gel was processed for immunoblotting. Briefly, the proteins were transferred to a PVDF membrane for 90 min at 30 V at room temperature using a semi-dry transfer system (Hoefer). Following transfer, the attached Coomassie dye on the membrane was removed by rinsing it with methanol. Finally, the membrane was processed for antibody staining and protein detection following the immunoblotting procedure described earlier.

Measurement of Complex I Activity

Mitochondrial complex I (NADH dehydrogenase) activity was measured from the isolated mitochondria by following published protocol (Spinazzi et al., 2012; Patra et al., 2016; Padhan et al., 2020), with minor modifications. Briefly, the protein was estimated from freshly isolated mitochondria by the Bradford method. Accordingly, equal amounts of mitochondria from the experimental and control samples were taken and centrifuged at 10,000 × *g* for 10 min at 4°C to obtain mitochondria pellet. The pellet was resuspended in 10 mM ice-cold hypotonic Tris buffer (pH 7.6) and subjected to three cycles of freeze–thawing. Subsequently, the sample was mixed with an assay buffer [50 mM potassium phosphate buffer (pH 7.5), 3 mg/mL BSA, and 3 mM sodium azide], to which 100 μM NADH and 100 μM ubiquinone were added. NADH reduction (extinction coefficient, 6.22 mM^{-1} cm^{-1}) was correlated with a decrease in the absorbance of NADH (340 nm) at different time points over a course of 5 min. Complex I activity (nmol min^{-1} mg^{-1}) was calculated as: (ΔAbsorbance/min × 1,000)/[(extinction coefficient × volume of sample used in mL) × (sample protein concentration in mg mL^{-1})] (Spinazzi et al., 2012). Percent change of activity was calculated considering activity of the control sample as 100.

Measurement of Mitochondrial ATP Synthesis

Mitochondrial ATP synthesis was measured by a bioluminescence assay. Briefly, freshly isolated mitochondria (100 μg/mL) from frozen tissue was energized by incubating in a respiration buffer [0.6 M sorbitol, 1 mM $MgCl_2$, 1 mM EDTA, 25 mM succinate, 5 mM ADP, and 25 mM potassium phosphate buffer (pH 7.0)] for 15 min at 37°C, based on published literature (Mittal et al., 2009; Patra et al., 2016). The ATP generated was quantified by using an ATP determination kit (Thermo Fisher Scientific) following the manufacturer's protocol. Luminescence was measured by using HIDEX Sense Multimode Micro Plate Reader 425-301 (HIDEX).

Histology and Immunofluorescence

Skeletal muscle was dissected out and fixed in 10% buffered formalin overnight. The sample was then dehydrated in graded alcohol, embedded in paraffin, sectioned using a microtome at a thickness of 3 μM, and subjected to routine histology and immunofluorescence. For histological study, the sections were mounted in Mayer's albumin-coated glass slides and stained with hematoxylin–eosin following standard procedure (Feldman and Wolfe, 2014). For immunofluorescence study, the tissue sections were mounted on poly-L-lysine-coated glass slides and processed accordingly following standard protocol (Scanziani, 1998; Joshi and Yu, 2017). The prepared slides were immersed in Tris-EDTA buffer [10 mM Tris base, 1 mM EDTA, 0.05% Tween 20 (pH 9.0)] and placed in a pressure cooker for heat-induced antigen retrieval. The slides were then incubated with primary

antibody (anti-Vdac1, anti-Ccn6, or anti-Cox4) overnight at 4°C after blocking with 10% normal serum and 1% BSA in TBS. An appropriate fluorophore-conjugated secondary antibody [Alexa Fluor 546 anti-rabbit antibody or Alexa Fluor 488 anti-mouse antibody (Thermo Fisher Scientific)] was used to detect the signal under a confocal microscope (**Figures 1A,E**, **3A**) and a fluorescence microscope (**Supplementary Figure 1**).

Analysis of Swimming Behavior

The swimming behavior of zebrafish after the administration of morpholino was analyzed following published protocol of "startle response" (Eddins et al., 2010; Miller et al., 2012), with slight modifications. After injection, individual fish was kept in a small white rectangular tank (28 cm length × 20 cm width × 10 cm height) with 4 L of system water. After 48 or 72 h post-morpholino injection, a "single tap" on the tank was used to create stimulus. Swimming behavior after tapping was recorded up to 4 min with a digital video camera fixed at the top of the tank. Uninjected fish was also used as a reference. Captured video recordings were analyzed with video analysis software (Filmora9) to determine the distance covered and the turns taken per minute by each fish.

Statistical Analysis

All the data were presented as the mean ± SEM. Statistical analysis was performed using GraphPad Prism software, and *p* value was calculated by Student's *t* test. For the evaluation of differences between the experimental and control groups, three to five fish were used for each group for a particular data point. For experiments involving mitochondria, where samples were pooled, each pool represented about 10 fish, and any one data point represented at least three pools. For the analysis of immunoblot band intensity, statistical analysis was done after densitometry using GelQuant.NET software provided by biochemlabsolutions.com.

RESULTS

Ccn6 Is Present as a Component of Mitochondrial Respiratory Complexes in Zebrafish Skeletal Muscle

Earlier studies using human cell lines demonstrated that CCN6 is associated with the mitochondria, regulates respiratory complex assembly and activity, and controls ATP production (Patra et al., 2016; Padhan et al., 2020). Since mitochondrial assembly and activity are essential for muscle function (Vincent et al., 2016), we wanted to decipher whether Ccn6 is in any way associated with the respiratory complexes of muscle mitochondria. This study was particularly important for understanding CCN6 function in the context of PPRD, where *CCN6* mutations are associated with muscle fatigue and wasting (Alawbathani et al., 2018; Al Kaissi et al., 2019). Accordingly, we used zebrafish as a model organism for our study.

Initially, we demonstrated that Ccn6 is expressed in zebrafish skeletal muscle both by immunostaining and immunoblotting with an anti-Ccn6 antibody. Mitochondrial distribution of Ccn6 with respect to whole tissue was also evaluated [**Figures 1A(i–iii),B**]. Subsequently, we observed that Ccn6 is present not only in its native molecular weight form but also in the form of high-molecular-weight complexes in the range of 66–1,000 kDa and beyond in zebrafish skeletal muscle mitochondria. This was demonstrated by size exclusion chromatography of the zebrafish skeletal muscle mitochondrial lysate followed by immunoblotting of the collected fractions with the anti-Ccn6 antibody (**Figure 1C**). BN-PAGE of the zebrafish muscle mitochondria (**Figure 1D**, panel i) and immunoblotting using the same anti-Ccn6 antibody validated that, in zebrafish muscle mitochondria, a significant fraction of Ccn6 exists as high-molecular-weight complexes (**Figure 1D**, panel vi). Additional immunoblotting after BN-PAGE, separately with antibodies against mitochondrial respiratory complex subunits, revealed that the high-molecular-weight fraction of Ccn6 is at least partially present in association with complex I (panel ii: Ndufb8), complex III (panel iii: Uqcrc2), complex IV (panel iv: Cox4), and complex V (panel v: Atp5a1). Antibodies against the NDUFB8 subunit (complex I), UQCRC2 subunit (complex III), COX4 subunit (complex IV), and the ATP5A1 subunit (complex V) have been widely used for verifying mitochondrial respiratory complexes (Wittig et al., 2006; Acín-Pérez et al., 2008; Padhan et al., 2020). Complex I activity, as depicted in panel vii of **Figure 1D** by in-gel nitro blue tetrazolium chloride (NBT) assay (Padhan et al., 2020) validated complex assembly. The association of Ccn6 with mitochondrial respiratory complexes was furthermore verified by immunostaining, where Ccn6 was found to co-localize with Cox4. The co-localization of Ccn6 and Cox4 along the edges of the muscle fibers and in small patches, as depicted by arrow marks, was indicative of their association with the mitochondria, which are present both in connection with the sarcolemma and in inter-myofibril spaces (**Figure 1E**, i–iv; Percival et al., 2013; Lee et al., 2016). Given the potential of CCN6 for inter-protein interactions by virtue of its modular architecture (Hurvitz et al., 1999), these results led us to investigate whether Ccn6 stabilizes the assembly and activity of mitochondrial respiratory complexes through chaperone-like activity.

Ccn6 Depletion in Zebrafish Skeletal Muscle Leads to Diminished Mitochondrial Respiratory Complex Assembly and Activity

Having demonstrated that Ccn6 is associated with mitochondrial respiratory complexes in zebrafish skeletal muscle, we investigated whether Ccn6 controls mitochondrial respiratory complex assembly and activity therein. In this context, the effect of Ccn6 depletion was assessed. Depletion of Ccn6 was obtained by injecting *ccn6*-specific morpholino (4 μL of 200 μM morpholino solution in water) into the dorsal side of zebrafish muscle followed by electroporation. For each morpholino-injected muscle tissue sample excised from the left dorsal side of a fish, an uninjected sample of equal size was excised from the right ventral side as a negative control. A similar procedure was exercised with an equal concentration

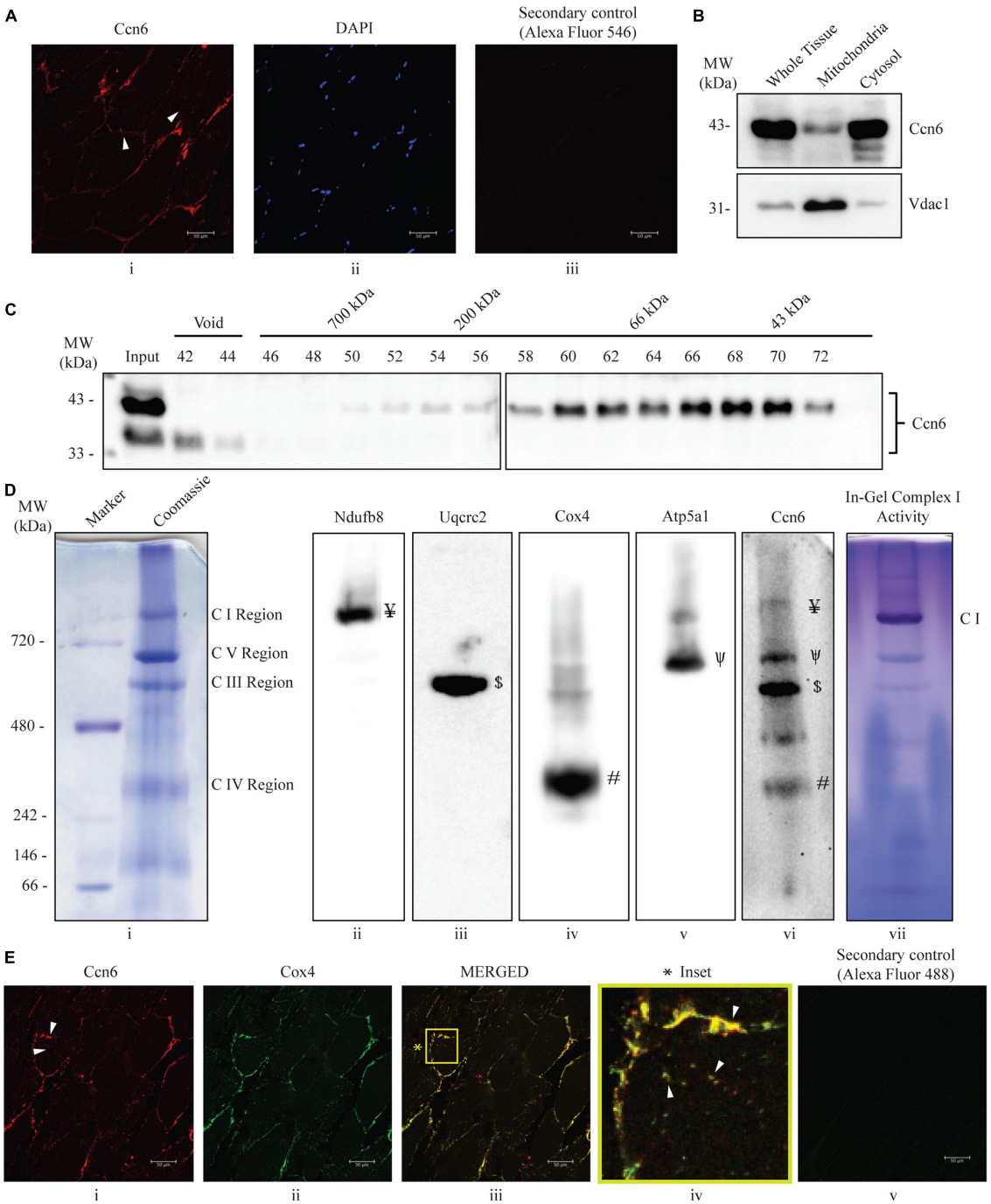

FIGURE 1 | Ccn6 is expressed in zebrafish skeletal muscle and remains associated with mitochondrial respiratory complexes. **(A)** Immunostaining and confocal microscopy demonstrating Ccn6 expression in zebrafish skeletal muscle. **(i)** Ccn6 expression in the fiber lining near the sarcolemma and in patches in inter-myofibril spaces, as shown by *arrows*; **(ii)** DAPI stain showing nuclei; **(iii)** only secondary antibody control. **(B)** Ccn6 expression in skeletal muscle mitochondria in comparison with whole tissue and cytosol. Vdac1 is used as a reference as a mitochondrial protein. **(C)** Sephacryl S-300 gel filtration of zebrafish muscle mitochondrial lysate demonstrating the presence of Ccn6 in high molecular weights encompassing those of mitochondrial respiratory complexes. **(D)** Blue native (BN)-PAGE of muscle mitochondria **(i)** and immunoblotting separately with antibodies to Ndufb8 of complex I **(ii)**, Uqcrc2 of complex III **(iii)**, Cox4 of complex IV **(iv)**, Atp5a1 of complex V **(v)**, and Ccn6 **(vi)**. *Symbols on the blots* **(ii–v)** denote the positions of different complexes corresponding with the Ccn6 bands in panel **(vi)**. In-gel nitro blue tetrazolium chloride (NBT) assay after BN-PAGE of the mitochondria demonstrates the activity of assembled complex I **(vii)**. **(E)** Immunostaining demonstrating the co-localization of Ccn6 with the mitochondrial respiratory complex. **(i)** Ccn6 expression; **(ii)** Cox4, representing mitochondrial respiratory complex IV expression; **(iii)** merged view showing the co-localization of Ccn6 with Cox4; **(iv)** magnified view (*inset*) of the co-localization (*arrowheads*); and **(v)** secondary antibody control for Cox4. The presented data **(A,E)** are representative of three independent experiments. For pooled experiments **(B–D)**, the number of fish used were 3, 25, and 10, respectively.

of a non-targeted morpholino as an additional negative control. All experimental and control samples were collected about 65 h post-electroporation after sacrificing the fish.

Figure 2A (immunoblotting with Ccn6 antibody) and **Figure 2B** (corresponding densitometry) depict that an average of about 60% depletion of Ccn6 expression in the skeletal muscle of individual fish was obtained by *ccn6* morpholino, but not the non-targeted (control) morpholino injection, with reference to the uninjected control. Depletion of Ccn6 by morpholino administration was also demonstrated by immunostaining of the skeletal muscle tissue (**Supplementary Figure 1**).

ccn6-specific morpholino-mediated depletion of Ccn6 in zebrafish skeletal muscle resulted in a significant reduction in the assembly of complexes I, III, IV, and V in zebrafish muscle mitochondria. Non-targeted (control) morpholino injection did not result in a similar change in the respiratory complex assembly, confirming the specific effect of *ccn6* morpholino on mitochondrial respiratory complexes. This was demonstrated by BN-PAGE of equal amounts of skeletal muscle mitochondria from the experimental (*ccn6* morpholino) and control (non-targeted morpholino and uninjected) samples, followed by immunoblotting separately with antibodies to mitochondrial respiratory complex subunits (complex I: Ndufb8, complex III: Uqcrc2, complex IV: Cox4, and complex V: Atp5a1) and subsequent densitometry. Vdac1 (mitochondrial porin), a mitochondrial structural protein, was used as the reference in the analysis (**Figures 2C–F**). Defective assembly of the respiratory complexes upon Ccn6 depletion moreover resulted in a significant drop in complex I activity (**Figures 2G,H**). This finding is in accordance with the already reported involvement of complexes III–V in complex I function (Mimaki et al., 2012; Moreno-Lastres et al., 2012; Milenkovic et al., 2017). The inhibited complex I activity upon Ccn6 depletion was also linked with a marked reduction in mitochondrial ATP synthesis (**Figure 2I**), indicating a blockade in mitochondrial respiration. The observed changes in the mitochondrial respiratory complex assembly/activity and ATP synthesis upon Ccn6 depletion were associated with the altered distribution of Ccn6 itself among the different respiratory complexes, validating that Ccn6 regulates mitochondrial respiration as a component of the different respiratory complexes. Clearly, *ccn6* morpholino-injected but not control morpholino-injected muscle had overall less mitochondrial Ccn6 protein as well as alteration in its relative distribution among the different mitochondrial respiratory complexes as compared to the uninjected control (**Supplementary Figure 2**).

Defective Mitochondrial Respiratory Complex Assembly and Activity in Ccn6-Depleted Skeletal Muscle Dampens Mitochondrial Integrity, Causing Anomalous Muscle Organization and Function

We were interested in investigating how loss of mitochondrial respiratory complex assembly and activity in zebrafish skeletal muscle upon Ccn6 depletion, as described in **Figure 2**, influences mitochondrial integrity and muscle physiology. This was particularly important on account of the need of a functional mitochondria for proper muscle function (Sunitha et al., 2016; Vincent et al., 2016).

Microtome sections generated from *ccn6* morpholino-injected experimental and matched control zebrafish skeletal muscle samples were prepared for immunofluorescence microscopy with antibody against Vdac1, which, being a mitochondrial structural protein, serves as an indicator of mitochondrial integrity (Padhan et al., 2020). Vdac1 stain was visible both along the edges of the muscle fibers and in patches denoting inter-myofibril spaces, as depicted for Ccn6 and Cox4 in **Figure 1**. The markedly low level of Vdac1 in the sections prepared from Ccn6-depleted muscle samples as opposed to the controls indicated loss of mitochondrial abundance (**Figure 3A**). This result was corroborated by immunoblotting muscle lysates obtained from *ccn6* morpholino/control morpholino-injected and uninjected fish with Vdac1 antibody (**Figure 3B**). As depicted by densitometry with reference to β-actin, while there was about a 50% reduction in Vdac1 level in *ccn6* morpholino-injected muscle as compared to the uninjected muscle, no significant difference was noted between the uninjected and control morpholino-injected muscle samples. Thus, the marked reduction in respiratory complex assembly and activity in zebrafish skeletal muscle upon Ccn6 depletion was associated with loss of mitochondria, indicating a decline in mitochondrial integrity.

In light of the fact that muscle physiology is dependent on mitochondrial function (Vincent et al., 2016), we examined whether the loss of mitochondria in zebrafish skeletal muscle due to Ccn6 depletion correlated with alterations in skeletal muscle structure and function. Accordingly, microtome sections generated from *ccn6* morpholino-injected experimental and matched control zebrafish muscle samples were prepared for histology (hematoxylin and eosin staining). As depicted in **Figure 3C**, histology revealed that the mitochondrial defects in zebrafish muscle observed upon Ccn6 depletion are associated with a widening of the interstitial spaces between the muscle fibers and inflammatory infiltrates, features which have been linked with muscle wasting (Rayavarapu et al., 2013; Yang et al., 2019). Unlike the *ccn6* morpholino-treated muscle samples, the control morpholino samples appeared more or less like the uninjected samples in the histology. The very minor variations in the interstitial spaces that were observed in some control morpholino samples were perhaps due to injury during electroporation or were just naturally occurring differences in the tissue architecture of different fish. These results confirmed a specific role of Ccn6 in the maintenance of muscle integrity.

The altered skeletal muscle structure upon Ccn6 depletion was reflected in the hindered locomotion in the experimental fish as compared to the corresponding controls in response to stimulus. As depicted in **Figure 4**, *ccn6* morpholino-injected zebrafish, at both 48 and 72 h post-injection, were unable to travel the same distance and perform as many turns as the controls (uninjected and control morpholino-injected zebrafish) after being subjected to a startle, generated by a single tap on the fish tank. The

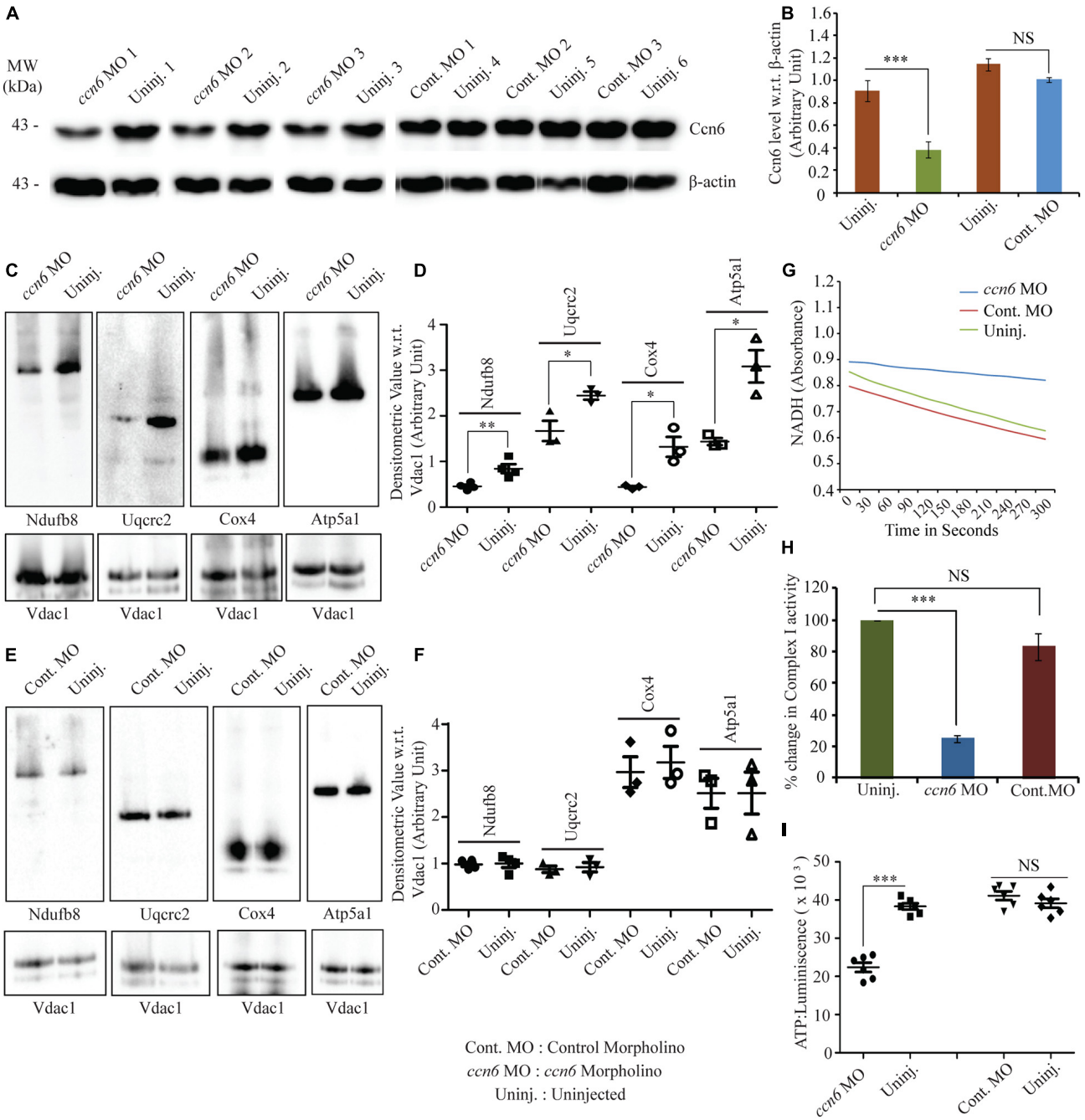

FIGURE 2 | Ccn6 depletion inhibits mitochondrial respiratory complex assembly and activity in zebrafish muscle. **(A,B)** Immunoblotting of the total muscle lysate and corresponding band densitometry demonstrating about 60% reduction in Ccn6 expression by *ccn6* morpholino, but not control morpholino, as compared to the corresponding uninjected control. β-actin is used as a reference for the estimation of Ccn6 expression. **(C–F)** Blue native (BN)-PAGE of the muscle mitochondrial lysate followed by **(i)** immunoblotting separately with antibodies to Ndufb8 (complex I), Uqcrc2 (complex III), Cox4 (complex IV), and Atp5a1 (complex V) and **(ii)** corresponding band densitometry projected by a distribution plot, demonstrating that *ccn6* morpholino, but not non-targeted morpholino, inhibits respiratory complex assembly as compared to no injection. Vdac1 expression from equal amounts of mitochondrial protein is used as a reference for this estimation. **(G,H)** Spectrophotometric and bar graph representation of the decrease in complex I activity upon Ccn6 depletion by *ccn6* morpholino, but not control morpholino. No injection is a reference for this estimation. **(I)** ATP measurement assay demonstrating the decrease in ATP synthesis upon *ccn6* morpholino (MO), but not control MO injection, as compared to the uninjected control. Data are presented as the mean ± SEM of at least three independent experiments. $^{*}p < 0.05$, $^{**}p < 0.01$, $^{***}p < 0.001$; *NS*, not significant (Student's *t*-test). For pooled experiments **(C–I)**, the number of fish used were 10, 10, 10, and 5, respectively, in each experimental group.

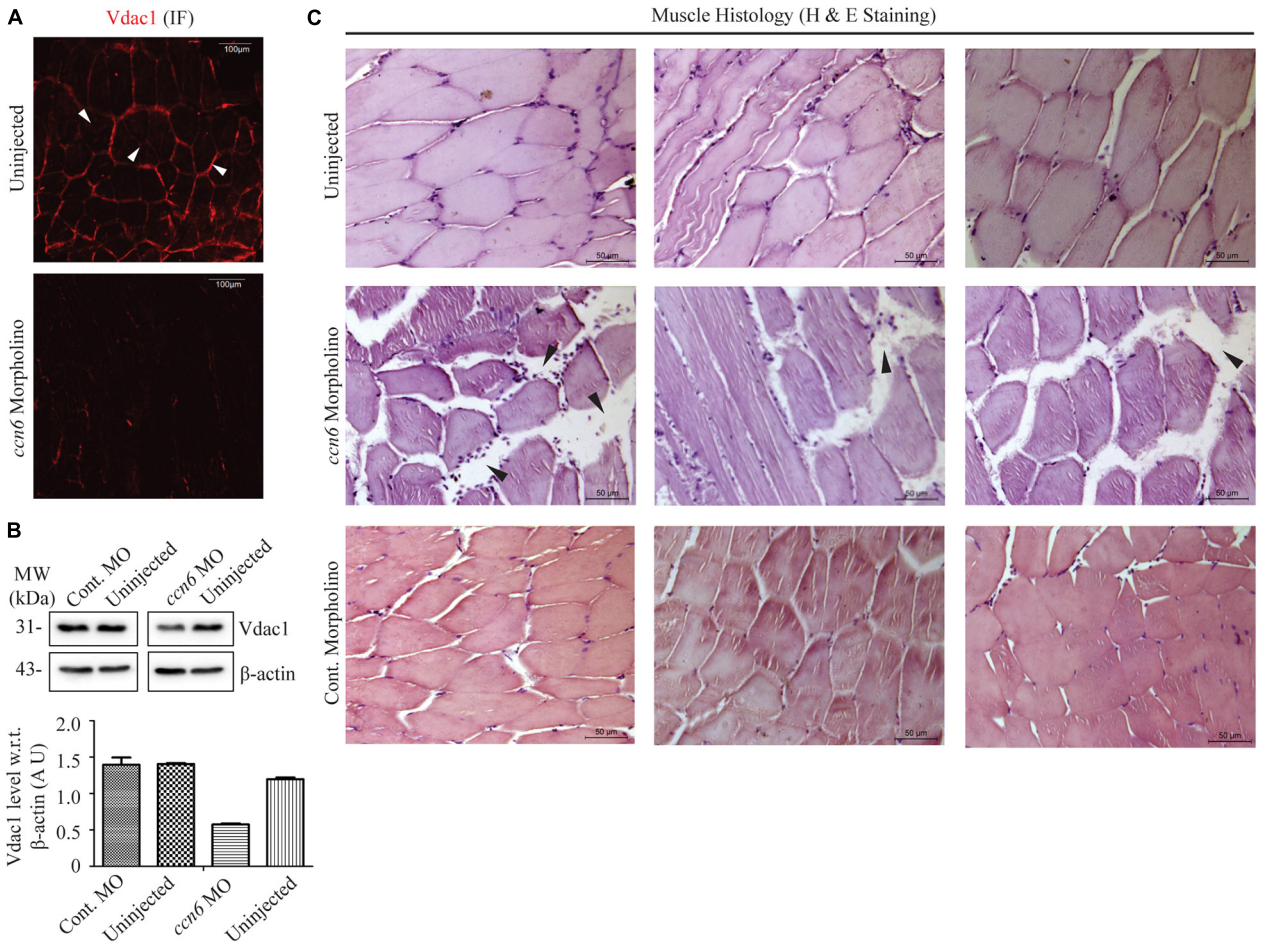

FIGURE 3 | Ccn6 depletion causes loss of muscle mitochondrial abundance and alterations in muscle organization. **(A)** Immunofluorescence of the muscle sections of *ccn6* morpholino-injected and uninjected zebrafish using anti-Vdac1 antibody with Alexa Fluor 546 rabbit secondary antibody, demonstrating loss of Vdac1 (mitochondrial structural protein) expression upon Ccn6 depletion: representation of three different experimental sets. *Arrow marks* denote the presence of mitochondria along the muscle fiber edges near the sarcolemma and in patches in the inter-myofibril spaces. **(B)** Immunoblot of the muscle lysate and corresponding densitometry showing a reduction in Vdac1 levels in *ccn6* morpholino, but not control morpholino-injected fish, as compared to the uninjected control. β-actin is used as a reference protein for this estimation. Data are presented from two independent experiments; tissue was pooled from 10 fish in each experiment. **(C)** Histology (hematoxylin and eosin staining) of the muscle sections from *ccn6* morpholino/control morpholino-injected and uninjected zebrafish demonstrating an increase in the interstitial gaps and presence of inflammatory infiltrates (*arrow marks*) in *ccn6* morpholino-injected muscle: representation of five different experimental sets.

distance covered was measured separately for each fish after the first, second, third, and fourth minutes following tapping (**Figures 4A–D**). The setup of the "startle response experiment" adapted from contemporary literature (Miller et al., 2012; Lebold et al., 2013) is described in **Figure 4E**.

Overall, our results indicate that Ccn6 regulates skeletal muscle organization and function through its influence on the mitochondrial respiratory complex assembly and activity.

DISCUSSION

Based on studies in human chondrocyte lines demonstrating that CCN6 localizes to the mitochondria and regulates mitochondrial respiratory complex assembly and activity, we intended to validate the function of CCN6 at the organism level. Therefore, we characterized Ccn6 with respect to mitochondrial function using zebrafish as a model organism. We found that Ccn6 is present partly as a component of mitochondrial respiratory complexes in zebrafish skeletal muscle tissue and that depletion of Ccn6 in the skeletal muscle damages respiratory complex assembly/activity along with mitochondrial integrity. Moreover, loss of mitochondria due to Ccn6 depletion is associated with defects in skeletal muscle morphology and locomotion in zebrafish.

Prior studies describing the role of CCN6 in mitochondrial function using human chondrocyte lines revealed that about 35% depletion of CCN6 elevates mitochondrial mass and raises mitochondrial respiratory complex assembly and activity (Patra et al., 2016; Padhan et al., 2020). This result may seem contradictory to the current finding where about 60% Ccn6 depletion in skeletal muscle tissue leads to loss in mitochondrial

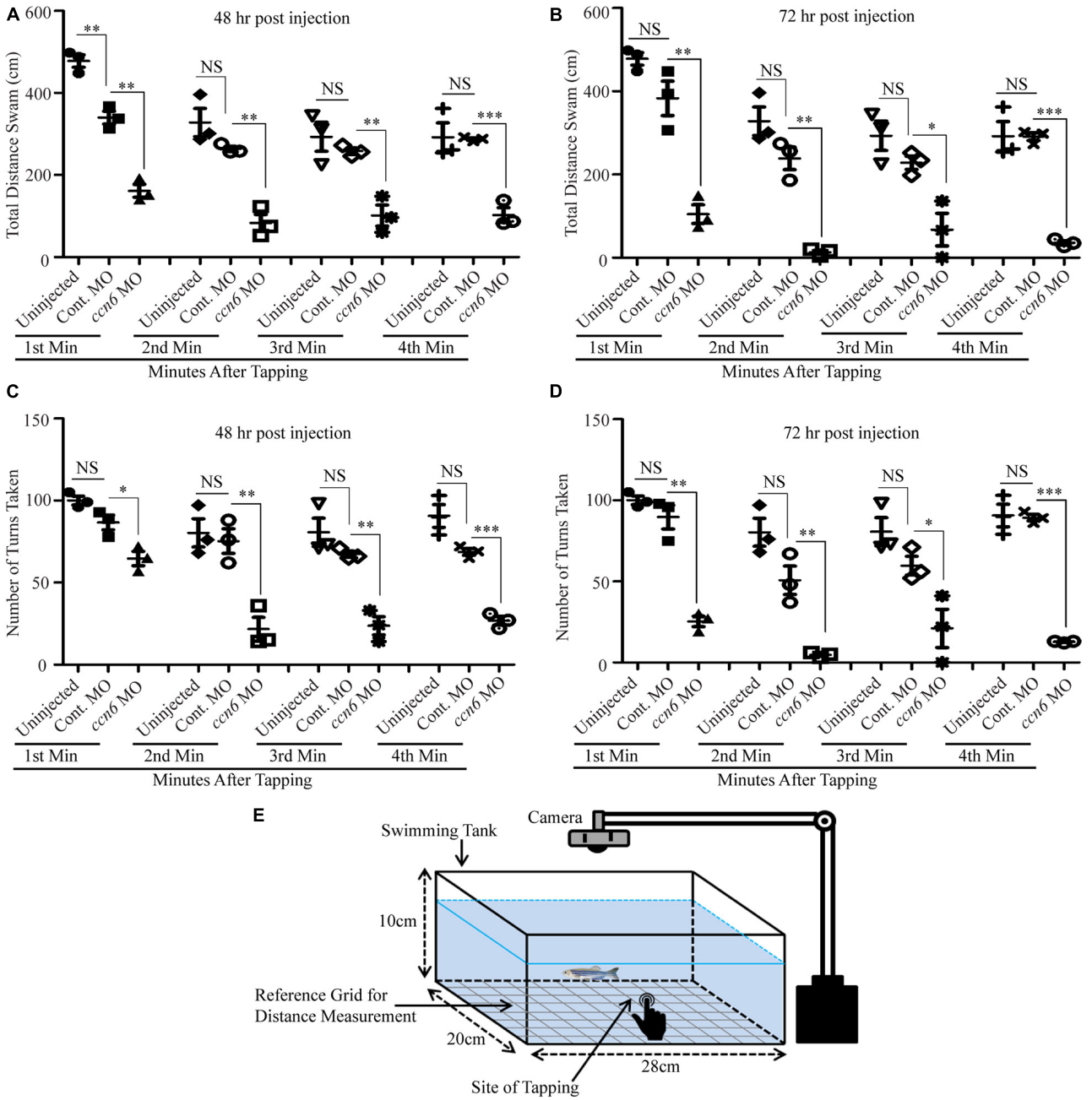

FIGURE 4 | Depletion of Ccn6 expression in zebrafish skeletal muscle inhibits locomotion in response to stimulus. **(A,B)** Ccn6 depletion in skeletal muscle by *ccn6* morpholino restricts the distance covered by zebrafish in response to stimulus as compared to the corresponding controls (control morpholino-injected and uninjected) at 48 and 72 h post-injection ($n = 3$). **(C,D)** Significantly less number of turns by *ccn6* morpholino-injected fish as compared to the corresponding controls at 48 and 72 h post-injection ($n = 3$). Data are presented as the mean ± SEM. $^{*}p < 0.05$, $^{**}p < 0.01$, $^{***}p < 0.001$; *NS*, not significant (Student's *t* test). **(E)** Representation of the experimental setup.

abundance as well as respiratory complex assembly and activity. It must be noted, however, that on account of the potential of CCN6 to interact with multiple proteins, its regulatory influence on the mitochondria may include both repression and activation, depending on its protein interacting partners, which may vary between tissue and cell types. Thus, the extent of CCN6 depletion may have different effects on the mitochondria. While about 35% depletion of CCN6 in cartilage chondrocytes may abolish the formation of CCN6-associated repressor complexes, leading to an overall increase in mitochondrial function (Patra et al., 2016; Padhan et al., 2020), more than 60% depletion of Ccn6 in zebrafish muscle tissue may very likely produce a

more global effect on Ccn6 activities, causing mitochondrial dysfunction. Accordingly, *CCN6* mutations that are similar to those associated with PPRD lead to loss of mitochondrial activity in chondrocytes, possibly on account of a totally collapsed CCN6 function (Padhan et al., 2020).

Since most tissues and cell types need a functional mitochondria for survival, one may wonder why PPRD-related defects due to *CCN6* mutations are manifested only in skeletal tissues (Hurvitz et al., 1999; Dalal et al., 2012; Garcia Segarra et al., 2012; Sun et al., 2012; Ekbote et al., 2013; Yang et al., 2013; Liu et al., 2015; Luo et al., 2015; Shahi et al., 2020). Perhaps the mitochondrial distribution pattern of Ccn6 varies among the different cell and tissue types, and accordingly, the influence of *ccn6* mutations is more marked in skeletal tissues as compared to others. From **Supplementary Figure 3**, it is in fact clear that the Ccn6 distribution patterns in the mitochondria of the skeletal muscle, brain, and heart of zebrafish are distinctly different. **Supplementary Figure 3A** demonstrates the relative levels of the Ccn6 protein in the mitochondria of the muscle, brain, and heart in relation to Vdac1 (mitochondrial structural protein) and subunits of the mitochondrial respiratory complexes (Ndufb8, Ndufs1: complex I; Cox4: complex IV). It appears that the levels of Ccn6 are different in the mitochondria of these tissues, with muscle containing the most. Also importantly, the mitochondria of these tissues have different forms of Ccn6. While the muscle mitochondria harbor mostly a 43-kDa form of Ccn6, the heart mitochondria harbor mostly a 33-kDa form. The brain mitochondria, on the other hand, harbor almost equal amounts of both forms. Although not clearly understood how, Ccn6 distribution among the different respiratory complexes is clearly more prominent in zebrafish skeletal muscle as compared to the brain and heart (**Supplementary Figure 3B**). Ccn6 protein distribution in the mitochondria of other skeletal tissues could be the same as in skeletal muscle, thus rendering the skeletal system more susceptible to the deleterious effects of *ccn6* mutations. It is not to be ruled out, however, that in view of the distribution of Ccn6 in subcellular organelles other than the mitochondria (**Figure 1B**), skeletal muscle damage due to Ccn6 mutations or depletion may also occur independent of the mitochondria.

Taken together, our study on zebrafish reveals a crucial role of Ccn6 in mitochondrial respiration and the maintenance of muscle integrity. In light of the fact that *CCN6* mutations cause muscle weakness in PPRD (Hurvitz et al., 1999; Dalal et al., 2012; Garcia Segarra et al., 2012; Sun et al., 2012; Ekbote et al., 2013; Yang et al., 2013; Liu et al., 2015; Luo et al., 2015; Alawbathani et al., 2018; Shahi et al., 2020), our findings open up a new theme in the study of CCN6 in the context of PPRD pathogenesis. The results garnered from this new direction of research may lead to significant progress in the diagnosis and understanding of PPRD and similar musculoskeletal disorders.

DATA AVAILABILITY STATEMENT

The raw data supporting the conclusions of this article will be made available by the authors, without undue reservation.

ETHICS STATEMENT

Ethical review and approval was not required for the animal study because Zebrafish does not fall under the purview of the Committee for the Purpose of Control and Supervision of Experiments on Animals (CPCSEA), Govt. of India. Nevertheless, all experiments were performed following internationally approved guidelines.

AUTHOR CONTRIBUTIONS

MS conceptualized the research, analyzed the data, and wrote the manuscript. AS performed research, analyzed data, and assisted in writing the manuscript. DP performed research, analyzed data, and assisted in writing the manuscript. AG provided expert technical assistance. All authors contributed to the article and approved the submitted version of the manuscript.

FUNDING

This work was supported by the Science and Engineering Research Board (SERB), Govt. of India, grant no. CRG/2019/001933 and institutional funding from the Council of Scientific and Industrial Research (CSIR), Govt. of India.

ACKNOWLEDGMENTS

Thanks are due to A. K. Gupta for helping in electroporation procedure. We thank J. Sengupta for the use of spectrophotometer. We also thank S. Jati and S. Maity for helping in microscopic study, and T. Roychoudhury, P. Prasad, and S. S. Roy for providing some reagents. We are also thankful to R. Ramachandran for helpful suggestions. AS is supported by a research associate grant (DBT-RA Programme) from the Department of Biotechnology, Govt. of India. DP and AG are supported by the Council of Scientific and Industrial Research (CSIR) fellowship and the University Grants Commission fellowship respectively from the Government of India.

SUPPLEMENTARY MATERIAL

The Supplementary Material for this article can be found online at: https://www.frontiersin.org/articles/10.3389/fcell.2021.627409/full#supplementary-material

REFERENCES

Acín-Pérez, R., Fernández-Silva, P., Peleato, M. L., Pérez-Martos, A., and Enriquez, J. A. (2008). Respiratory active mitochondrial supercomplexes. *Mol. Cell* 32, 529–539. doi: 10.1016/j.molcel.2008.10.021

Al Kaissi, A., Kenis, V., Jemaa, L. B., Sassi, H., Shboul, M., Grill, F., et al. (2019). Skeletal phenotype/genotype in progressive pseudorheumatoid chondrodysplasia. *Clin. Rheumatol.* 39, 553–560. doi: 10.1007/s10067-019-04783-z

Alawbathani, S., Kawalia, A., Karakaya, M., Altmüller, J., Nürnberg, P., and Cirak, S. (2018). Late diagnosis of a truncating WISP3 mutation entails a severe phenotype of progressive pseudorheumatoid dysplasia. *Cold Spring Harb. Mol. Case Stud.* 4, a002139. doi: 10.1101/mcs.a002139

Avdesh, A., Chen, M., Martin-Iverson, M. T., Mondal, A., Ong, D., Rainey-Smith, S., et al. (2012). Regular care and maintenance of a zebrafish (*Danio rerio*) laboratory: an introduction. *J. Vis. Exp.* 69, e4196. doi: 10.3791/4196

Chouery, E., Corbani, S., Dahmen, J., Zouari, L., Gribaa, M., Leban, N., et al. (2017). Progressive pseudorheumatoid dysplasia in North and West Africa: Clinical description in ten patients with mutations of WISP3. *Egypt. J. Med. Hum. Genet.* 18, 299–303. doi: 10.1016/j.ejmhg.2016.11.004

Dalal, A., Bhavani, G. S. L., Togarrati, P. P., Bierhals, T., Nandineni, M. R., Danda, S., et al. (2012). Analysis of the WISP3 gene in Indian families with progressive pseudorheumatoid dysplasia. *Am. J. Med. Genet. A* 158A, 2820–2828. doi: 10.1002/ajmg.a.35620

Davis, L., Chen, Y., and Sen, M. (2006). WISP-3 functions as a ligand and promotes superoxide dismutase activity. *Biochem. Biophys. Res. Commun.* 342, 259–265. doi: 10.1016/j.bbrc.2006.01.132

Eddins, D., Cerutti, D., Williams, P., Linney, E., and Levin, E. D. (2010). Zebrafish provide a sensitive model of persisting neurobehavioral effects of developmental chlorpyrifos exposure: comparison with nicotine and pilocarpine effects and relationship to dopamine deficits. *Neurotoxicol. Teratol.* 32, 99–108. doi: 10.1016/j.ntt.2009.02.005

Ekbote, A. V., Danda, D., Kumar, S., Danda, S., Madhuri, V., and Gibikote, S. (2013). A descriptive analysis of 14 cases of progressive-psuedorheumatoid-arthropathy of childhood from south India: review of literature in comparison with juvenile idiopathic arthritis. *Semin. Arthritis Rheum.* 42, 582–589. doi: 10.1016/j.semarthrit.2012.09.001

Engel, J. (2004). Role of oligomerization domains in thrombospondins and other extracellular matrix proteins. *Int. J. Biochem. Cell Biol.* 36, 997–1004. doi: 10.1016/j.biocel.2003.12.009

Fausett, B. V., Gumerson, J. D., and Goldman, D. (2008). The proneural basic helix-loop-helix gene Ascl1a is required for retina regeneration. *J. Neurosci.* 28, 1109–1117. doi: 10.1523/JNEUROSCI.4853-07.2008

Feldman, A. T., and Wolfe, D. (2014). "Tissue processing and hematoxylin and eosin staining," in *Histopathology: Methods and Protocols Methods in Molecular Biology*, ed. C. E. Day (New York, NY: Springer), 31–43. doi: 10.1007/978-1-4939-1050-2_3

Garcia Segarra, N., Mittaz, L., Campos-Xavier, A. B., Bartels, C. F., Tuysuz, B., Alanay, Y., et al. (2012). The diagnostic challenge of progressive pseudorheumatoid dysplasia (PPRD): a review of clinical features, radiographic features, and WISP3 mutations in 63 affected individuals. *Am. J. Med. Genet. C Semin. Med. Genet.* 160C, 217–229. doi: 10.1002/ajmg.c.31333

Holbourn, K. P., Acharya, K. R., and Perbal, B. (2008). The CCN family of proteins: structure-function relationships. *Trends Biochem. Sci.* 33, 461–473. doi: 10.1016/j.tibs.2008.07.006

Hurvitz, J. R., Suwairi, W. M., Van Hul, W., El-Shanti, H., Superti-Furga, A., Roudier, J., et al. (1999). Mutations in the CCN gene family member WISP3 cause progressive pseudorheumatoid dysplasia. *Nat. Genet.* 23, 94–98. doi: 10.1038/12699

Joshi, S., and Yu, D. (2017). "Chapter 8 – immunofluorescence," in *Basic Science Methods for Clinical Researchers*, eds M. Jalali, F. Y. L. Saldanha, and M. Jalali (Boston: Academic Press), 135–150. doi: 10.1016/B978-0-12-803077-6.00008-4

Katsube, K., Sakamoto, K., Tamamura, Y., and Yamaguchi, A. (2009). Role of CCN, a vertebrate specific gene family, in development. *Dev. Growth Differ.* 51, 55–67. doi: 10.1111/j.1440-169X.2009.01077.x

Lebold, K. M., Löhr, C. V., Barton, C. L., Miller, G. W., Labut, E. M., Tanguay, R. L., et al. (2013). Chronic vitamin E deficiency promotes vitamin C deficiency in zebrafish leading to degenerative myopathy and impaired swimming behavior. *Comp. Biochem. Physiol. C* 157, 382–389. doi: 10.1016/j.cbpc.2013.03.007

Lee, H., Kim, S.-H., Lee, J.-S., Yang, Y.-H., Nam, J.-M., Kim, B.-W., et al. (2016). Mitochondrial oxidative phosphorylation complexes exist in the sarcolemma of skeletal muscle. *BMB Rep.* 49, 116–121. doi: 10.5483/bmbrep.2016.49.2.232

Liu, L., Li, N., Zhao, Z., Li, W., and Xia, W. (2015). Novel WISP3 mutations causing spondyloepiphyseal dysplasia tarda with progressive arthropathy in two unrelated Chinese families. *Joint Bone Spine* 82, 125–128. doi: 10.1016/j.jbspin.2014.10.005

Luo, H., Shi, C., Mao, C., Jiang, C., Bao, D., Guo, J., et al. (2015). A novel compound WISP3 mutation in a Chinese family with progressive pseudorheumatoid dysplasia. *Gene* 564, 35–38. doi: 10.1016/j.gene.2015.03.029

Milenkovic, D., Blaza, J. N., Larsson, N.-G., and Hirst, J. (2017). The enigma of the respiratory chain supercomplex. *Cell Metab.* 25, 765–776. doi: 10.1016/j.cmet.2017.03.009

Miller, D. S., and Sen, M. (2007). Potential role of WISP3 (CCN6) in regulating the accumulation of reactive oxygen species. *Biochem. Biophys. Res. Commun.* 355, 156–161. doi: 10.1016/j.bbrc.2007.01.114

Miller, G. W., Labut, E. M., Lebold, K. M., Floeter, A., Tanguay, R. L., and Traber, M. G. (2012). Zebrafish (*Danio rerio*) fed vitamin E-deficient diets produce embryos with increased morphologic abnormalities and mortality. *J. Nutr. Biochem.* 23, 478–486. doi: 10.1016/j.jnutbio.2011.02.002

Mimaki, M., Wang, X., McKenzie, M., Thorburn, D. R., and Ryan, M. T. (2012). Understanding mitochondrial complex I assembly in health and disease. *Biochim. Biophys. Acta* 1817, 851–862. doi: 10.1016/j.bbabio.2011.08.010

Mittal, N., Babu, M. M., and Roy, N. (2009). The efficiency of mitochondrial electron transport chain is increased in the long-lived mrg19 Saccharomyces cerevisiae. *Aging Cell* 8, 643–653. doi: 10.1111/j.1474-9726.2009.00518.x

Moreno-Lastres, D., Fontanesi, F., García-Consuegra, I., Martín, M. A., Arenas, J., Barrientos, A., et al. (2012). Mitochondrial complex I plays an essential role in human respirasome assembly. *Cell Metab.* 15, 324–335. doi: 10.1016/j.cmet.2012.01.015

Nakamura, Y., Weidinger, G., Liang, J. O., Aquilina-Beck, A., Tamai, K., Moon, R. T., et al. (2007). The CCN family member Wisp3, mutant in progressive pseudorheumatoid dysplasia, modulates BMP and Wnt signaling. *J. Clin. Invest.* 117, 3075–3086. doi: 10.1172/JCI32001

Padhan, D. K., Sengupta, A., Patra, M., Ganguly, A., Mahata, S. K., and Sen, M. (2020). CCN6 regulates mitochondrial respiratory complex assembly and activity. *FASEB J.* 34, 12163–12176. doi: 10.1096/fj.202000405RR

Patra, M., Mahata, S. K., Padhan, D. K., and Sen, M. (2016). CCN6 regulates mitochondrial function. *J. Cell Sci.* 129, 2841–2851. doi: 10.1242/jcs.186247

Perbal, B. (2013). CCN proteins: a centralized communication network. *J. Cell Commun. Signal.* 7, 169–177. doi: 10.1007/s12079-013-0193-7

Percival, J. M., Siegel, M. P., Knowels, G., and Marcinek, D. J. (2013). Defects in mitochondrial localization and ATP synthesis in the mdx mouse model of Duchenne muscular dystrophy are not alleviated by PDE5 inhibition. *Hum. Mol. Genet.* 22, 153–167. doi: 10.1093/hmg/dds415

Rayavarapu, S., Coley, W., Kinder, T. B., and Nagaraju, K. (2013). Idiopathic inflammatory myopathies: pathogenic mechanisms of muscle weakness. *Skelet. Muscle* 3, 13. doi: 10.1186/2044-5040-3-13

Reed, B., and Jennings, M. (2010). *Guidance on the Housing and Care of Zebrafish (Danio rerio)*. London: Royal Society for the Prevention of Cruelty to Animals (RSPCA).

Repudi, S. R., Patra, M., and Sen, M. (2013). WISP3-IGF1 interaction regulates chondrocyte hypertrophy. *J. Cell Sci.* 126, 1650–1658. doi: 10.1242/jcs.119859

Scanziani, E. (1998). Immunohistochemical staining of fixed tissues. *Methods Mol. Biol.* 104, 133–140.

Schutze, N., Noth, U., Schneidereit, J., Hendrich, C., and Jakob, F. (2005). Differential expression of CCN-family members in primary human bone marrow-derived mesenchymal stem cells during osteogenic, chondrogenic and adipogenic differentiation. *Cell Commun. Signal.* 3, 5. doi: 10.1186/1478-811X-3-5

Sen, M., Cheng, Y.-H., Goldring, M. B., Lotz, M. K., and Carson, D. A. (2004). WISP3-dependent regulation of type II collagen and aggrecan production in chondrocytes. *Arthritis Rheum.* 50, 488–497. doi: 10.1002/art.20005

Shahi, P., Sehgal, A., Sudan, A., and Sehgal, S. (2020). Delayed-onset progressive pseudorheumatoid dysplasia with secondary synovial chondromatosis. *BMJ Case Rep.* 13, e234461. doi: 10.1136/bcr-2020-234461

Spinazzi, M., Casarin, A., Pertegato, V., Salviati, L., and Angelini, C. (2012). Assessment of mitochondrial respiratory chain enzymatic activities on tissues and cultured cells. *Nat. Protoc.* 7, 1235–1246. doi: 10.1038/nprot.2012.058

Stainier, D. Y. R., Raz, E., Lawson, N. D., Ekker, S. C., Burdine, R. D., Eisen, J. S., et al. (2017). Guidelines for morpholino use in zebrafish. *PLoS Genet.* 13:e1007000. doi: 10.1371/journal.pgen.1007000

Sun, J., Xia, W., He, S., Zhao, Z., Nie, M., Li, M., et al. (2012). Novel and recurrent mutations of WISP3 in two Chinese families with progressive pseudorheumatoid dysplasia. *PLoS One* 7:e38643. doi: 10.1371/journal.pone.0038643

Sunitha, B., Gayathri, N., Kumar, M., Keshava Prasad, T. S., Nalini, A., Padmanabhan, B., et al. (2016). Muscle biopsies from human muscle diseases with myopathic pathology reveal common alterations in mitochondrial function. *J. Neurochem.* 138, 174–191. doi: 10.1111/jnc.13626

Vincent, A. E., Ng, Y. S., White, K., Davey, T., Mannella, C., Falkous, G., et al. (2016). The spectrum of mitochondrial ultrastructural defects in mitochondrial myopathy. *Sci. Rep.* 6, 30610. doi: 10.1038/srep30610

Wittig, I., Braun, H.-P., and Schägger, H. (2006). Blue native PAGE. *Nat. Protoc.* 1, 418–428. doi: 10.1038/nprot.2006.62

Yang, Q., Yan, C., Wang, X., and Gong, Z. (2019). Leptin induces muscle wasting in a zebrafish kras-driven hepatocellular carcinoma (HCC) model. *Dis. Model. Mech.* 12, dmm038240. doi: 10.1242/dmm.038240

Yang, X., Song, Y., and Kong, Q. (2013). Diagnosis and surgical treatment of progressive pseudorheumatoid dysplasia in an adult with severe spinal disorders and polyarthropathy. *Joint Bone Spine* 80, 650–652. doi: 10.1016/j.jbspin.2013.03.006

Conflict of Interest: The authors declare that the research was conducted in the absence of any commercial or financial relationships that could be construed as a potential conflict of interest.

© 2016. Published by The Company of Biologists Ltd | Journal of Cell Science (2016) 129, 2841-2851 doi:10.1242/jcs.186247

RESEARCH ARTICLE

CCN6 regulates mitochondrial function

Milan Patra[1], Sushil K. Mahata[2,3], Deepesh K. Padhan[1] and Malini Sen[1,*]

ABSTRACT

Despite established links of CCN6, or Wnt induced signaling protein-3 (WISP3), with progressive pseudo rheumatoid dysplasia, functional characterization of CCN6 remains incomplete. In light of the documented negative correlation between accumulation of reactive oxygen species (ROS) and CCN6 expression, we investigated whether CCN6 regulates ROS accumulation through its influence on mitochondrial function. We found that CCN6 localizes to mitochondria, and depletion of CCN6 in the chondrocyte cell line C-28/I2 by using siRNA results in altered mitochondrial electron transport and respiration. Enhanced electron transport chain (ETC) activity of CCN6-depleted cells was reflected by increased mitochondrial ROS levels in association with augmented mitochondrial ATP synthesis, mitochondrial membrane potential and Ca^{2+}. Additionally, CCN6-depleted cells display ROS-dependent PGC1α (also known as PPARGC1A) induction, which correlates with increased mitochondrial mass and volume density, together with altered mitochondrial morphology. Interestingly, transcription factor Nrf2 (also known as NFE2L2) repressed CCN6 expression. Taken together, our results suggest that CCN6 acts as a molecular brake, which is appropriately balanced by Nrf2, in regulating mitochondrial function.

KEY WORDS: CCN6, Mitochondria, PGC1α, Nrf2

INTRODUCTION

CCN6, or Wnt-induced signaling protein 3 (WISP3), is a 354-amino-acid protein that can function both intracellularly and extracellularly (Brigstock et al., 2003; Davis et al., 2006; Miller and Sen, 2007; Pal et al., 2012; Perbal, 2013; Repudi et al., 2013). WISP3 gets its name from its sequence homology with other WISP (CCN)-family members that are induced by Wnt1 (Pennica et al., 1998; Sen et al., 2004). CCN6 appears to be the preferred name for WISP3, as suggested and published by the International CCN Society (Brigstock et al., 2003). A signal peptide at the N-terminus of CCN6 is followed sequentially by the insulin growth factor binding protein (IGFBP) domain, the Von Willebrand factor type C (VWC) repeat domain, the thrombospondin type I (THSP1) repeat domain and the cysteine knot domain (Hurvitz et al., 1999; Pennica et al., 1998). Although the IGFBP domain of CCN6 indicates possible interactions with IGF, the presence of other domains alludes to the occurrence of intermolecular interactions of a diverse nature through disulfide bridging and oligomerization (Engel, 2004; Hurvitz et al., 1999).

[1]Cancer Biology and Inflammatory Disorder Division, CSIR-Indian institute of Chemical Biology, 4-Raja S.C. Mullick Road, Jadavpur, Kolkata 700032, India. [2]Metabolic Physiology and Ultrastructure Biology Laboratory, University of California, San Diego, CA 92093-0732, USA. [3]Veterans Affairs San Diego Healthcare System, San Diego, CA 92161, USA.

*Author for correspondence (msen@iicb.res.in; senmalini@yahoo.com)

M.P., 0000-0001-6870-9938; D.K.P., 0000-0003-2159-5800; M.S., 0000-0001-5903-5943

Received 16 January 2016; Accepted 8 April 2016

Mutations within the CCN6 coding sequence are linked to a skeletal disorder termed progressive pseudo rheumatoid dysplasia (PPRD), which is characterized by progressive cartilage loss and irregularities in bone growth (Dalal et al., 2012; Ekbote et al., 2013; Garcia Segarra et al., 2012; Hurvitz et al., 1999; Liu et al., 2015; Luo et al., 2015; Yang et al., 2013). The several mutations associated with PPRD, identified thus far, span across the different domains of CCN6, implying that all the domains of CCN6 contribute to its overall function. On account of the established link of CCN6 with PPRD, a comprehensive characterization of its function at the molecular level is important. CCN6 has been shown to modulate both IGF1-induced as well as basal expression of cartilage hypertrophy markers, such as reactive oxygen species (ROS) (Miller and Sen, 2007; Repudi et al., 2013). Other functions of CCN6 that might be useful in the context of cartilage growth and/or maintenance remain to be deciphered.

Given its influence on total cellular ROS accumulation (Miller and Sen, 2007; Repudi et al., 2013), we wanted to investigate if CCN6 controls mitochondrial ROS by regulating the mitochondrial electron transport chain (ETC). Perhaps the loss of a functional cartilage and the aberrant matrix mineralization associated with CCN6 mutations in individuals with PPRD (Dalal et al., 2012; Ekbote et al., 2013; Garcia Segarra et al., 2012; Hurvitz et al., 1999; Liu et al., 2015; Luo et al., 2015; Yang et al., 2013) are due to an imbalance in cell differentiation and/or hypertrophy, arising partly from altered mitochondrial function. Accordingly, it is essential to estimate the influence of wild-type CCN6 on the activity of mitochondrial electron transport. It is also crucial to understand how CCN6 expression synchronizes with its function. Therefore, in the current study, we explored if and how CCN6 influences mitochondrial function, and examined regulation of CCN6 expression.

RESULTS

CCN6 controls the steady-state levels of mitochondrial ROS, ATP and Ca^{2+}

In the light of previous findings demonstrating CCN6 as regulating total cellular ROS (Miller and Sen, 2007; Repudi et al., 2013), we examined if CCN6 influences mitochondrial ROS accumulation in association with mitochondrial ATP synthesis and Ca^{2+} at the steady state. Our investigation was furthermore prompted by several reports documenting the interrelation of mitochondrial ROS, ATP and Ca^{2+} (Brookes et al., 2004; Lehninger, 1970).

Upon depletion of CCN6 in the chondrocyte line C-28/I2 through transfection of small interfering (si)RNAs (CCN6 siRNA), a moderately amplified mitochondrial ROS response was detected by using MitoTracker CMH_2Xros, as compared to control upon flow cytometry analysis (Fig. 1A). Depletion of CCN6 expression in CCN6-siRNA-transfected C-28/I2 cells was demonstrated by performing both reverse-transcriptase (RT)-PCR and immunoblotting analysis on RNA and protein harvested from

Journal of Cell Science (2016) 129, 2841-2851 doi:10.1242/jcs.186247

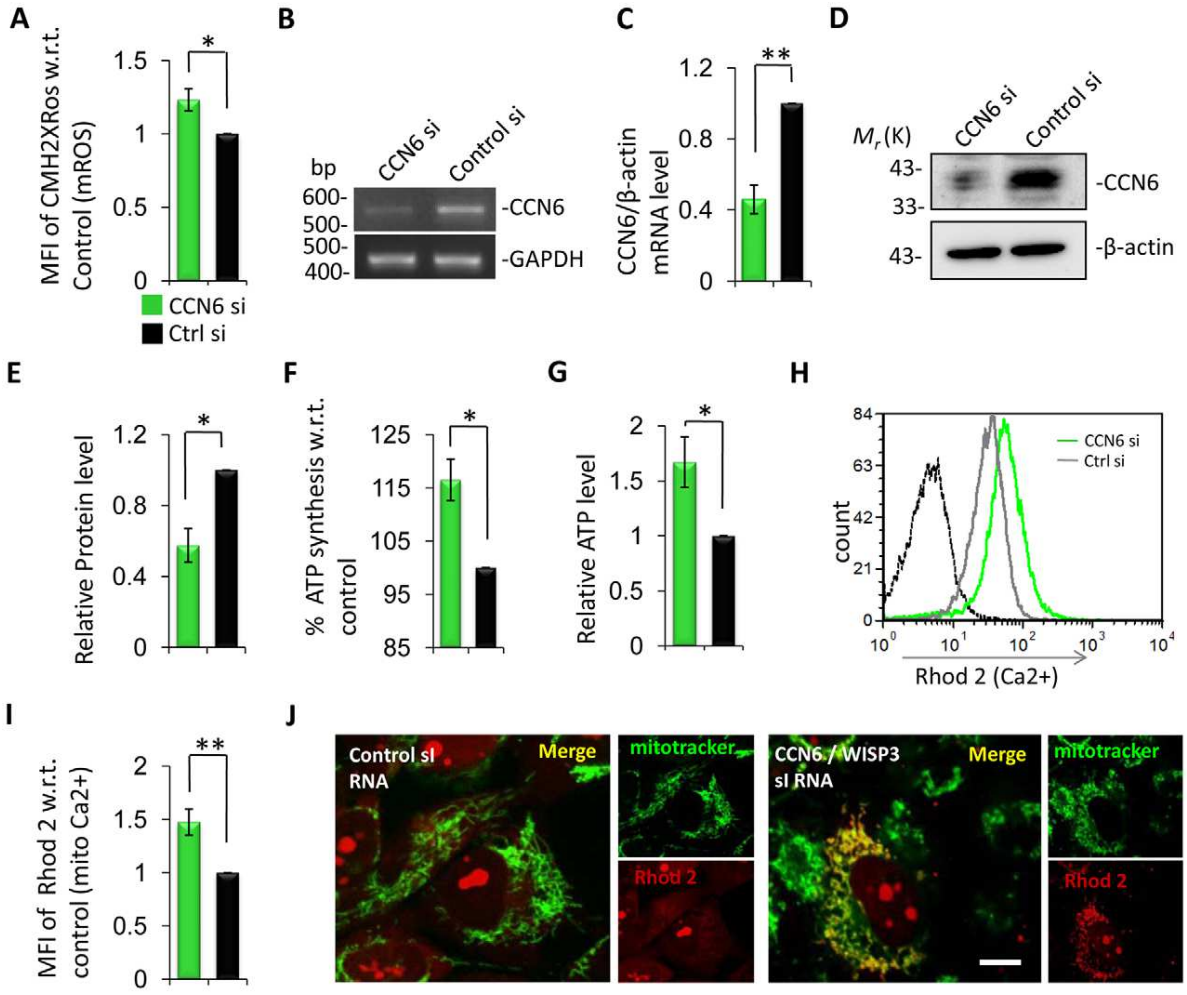

Fig. 1. Mitochondrial Ca^{2+}, ATP and ROS are regulated by CCN6. (A) Mitochondrial ROS (mROS) of CCN6-siRNA- (CCN6 si) versus control-siRNA (Ctrl si)-transfected cells as measured by FACS using CMH_2XRos (specific probe for mROS) (n=3). CCN6 knockdown depleted ~60% of CCN6, both at the RNA level relative to GAPDH (B,C) and protein level relative to β-actin (D,E) (n=3). (F) ATP synthesis within isolated mitochondria of CCN6-knockdown cells is higher than the control, as measured by using a luminometer and an ATP determination kit (n=4). (G) Total ATP is higher in CCN6-knockdown cells (n=4). (H) Histogram of FACS data shows right shift of Rhod 2 fluorescence in CCN6-knockdown cells (green line) compared to control (gray line) and unstained cells (dashed line). (I) Ca^{2+} uptake (Rhod2-bound cells) was significantly increased in CCN6-knockdown cells (n=6). (J) Confocal microscopy analysis reveals higher mitochondrial Ca^{2+} uptake, estimated through colocalization of Ca^{2+} (Rhod2, red) with mitochondria (MitoTracker Green FM, green). Data are represented as mean±s.e.m.; *P<0.05, **P<0.01 (unpaired Student's t-test); n represents the number of independent experiments. Key shown in A applies to all panels. MFI, mean fluorescence intensity. Scale bar: 10 µm.

the transfected cells (Fig. 1B–E). The increase in accumulated mitochondrial ROS in CCN6-depleted cells could be an outcome of electron leakage on account of increased ETC activity (Murphy, 2009). Increased mitochondrial basal metabolic output was additionally displayed in isolated mitochondrial fractions of CCN6-siRNA-transfected cells as an increased rate of ATP synthesis, as detected by luciferase activity (Fig. 1F). Mitochondrial ATP contributed, at least partly, to the twofold boost in the total cellular ATP levels of CCN6-depleted cells (Fig. 1G). Augmented mitochondrial ATP synthesis upon CCN6 depletion correlated with increased mitochondrial Ca^{2+} content, as judged by performing flow cytometry (Fig. 1H,I) and confocal microscopy (Fig. 1J). Increased mitochondrial Ca^{2+} in CCN6-depleted cells was validated through colocalization of Rhod 2 (Ca^{2+}) and MitoTracker Green (mitochondria) as detected with z-stack analysis (Movies 1, 2 and Fig. S1). CCN6-mediated regulation of mitochondrial ATP synthesis and Ca^{2+} content, as demonstrated here, indicates an important role for CCN6 in mitochondrial-Ca^{2+}-mediated matrix mineralization (Brighton and Hunt, 1978; Lehninger, 1970; Villa-Bellosta et al., 2013).

CCN6 regulates mitochondrial membrane potential

Increased mitochondrial ROS, ATP and Ca^{2+} levels in CCN6-depleted cells implies that CCN6 influences the activity of the mitochondrial ETC. Because the membrane potential of respiring mitochondria is a vital indicator of electron transport, we examined the mitochondrial membrane potential of CCN6-depleted cells as compared to that of the corresponding control cells, using both MitoTracker Red and Rhodamine 123. As evident from flow cytometry analysis, CCN6-siRNA-transfected cells harbored an increased proportion of MitoTracker-Red- and Rhodamine-123-sensitive respiring mitochondria as compared to the corresponding controls (Fig. 2A–C). The increase in mitochondrial membrane potential upon CCN6 depletion was

Journal of Cell Science (2016) 129, 2841-2851 doi:10.1242/jcs.186247

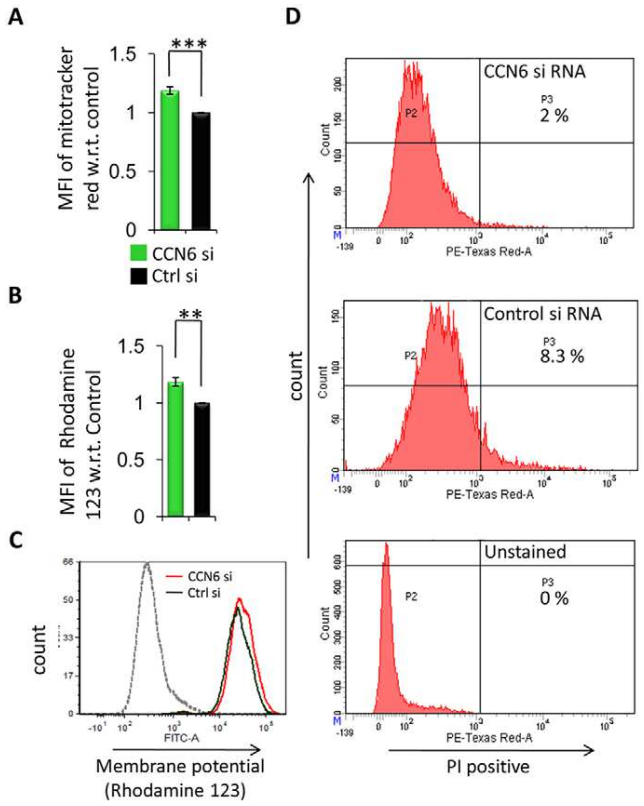

Fig. 2. CCN6-knockdown cells harbor more actively respiring mitochondria. (A) Flow cytometry analysis of cells loaded with MitoTracker Deep Red FM indicates that the amount of actively respiring mitochondria is significantly higher in CCN6-siRNA-transfected (CCN6 si) cells than in control scramble-siRNA-transfected (Ctrl si) cells (n=6). (B) Results of flow cytometry analysis using fluorescent probe Rhodamine 123, revealing a higher mitochondrial membrane potential of CCN6-siRNA-transfected cells compared to scramble-siRNA-transfected cells (n=3). (C) Histogram of Rhodamine 123 fluorescence (dashed line, unstained cells; red line, CCN6 siRNA; black line, scramble siRNA). (D) Propidium iodide (PI) exclusion assay. The propidium iodide exclusion assay was employed to measure dead cells both in CCN6-depleted and control cells (n=4). Data represent the percentage of the parent population – left quadrants (P2) are PI-negative (PE-Texas Red A channel) and right quadrants (P3) are PI-positive (PE-Texas Red A channel). Key shown in A also applies to B. MFI, mean fluorescence intensity. Data are represented as mean±s.e.m.; $^{**}P<0.01$, $^{***}P<0.001$ (unpaired Student's t-test); n represents the number of independent experiments.

modest enough to not cause any cell death as a result of necrosis or apoptosis, as assessed by both propidium iodide and annexin-V staining (Fig. 2D; Fig. S2A). The moderately increased membrane potential upon loss of CCN6 could be a reflection of a moderate increase in basal mitochondrial metabolism. Such augmentation in basal mitochondrial metabolism in CCN6-depleted cells might be conducive to protection from cell death, as demonstrated by the moderately improved survival in Fig. 2D. The effect of CCN6 depletion on cell proliferation was marginal (Fig. S2B).

Augmented mitochondrial ETC activity upon CCN6 depletion correlates with an increase in PGC1α expression and function

The transcriptional co-activator PGC1α [peroxisome-proliferator-activated receptor-γ coactivator-1α (PPARGC1A)] is inherently associated with mitochondrial function (Austin and St-Pierre, 2012; Spiegelman, 2007; Wenz, 2009). Thus, it was important to determine how increased mitochondrial ETC activity of CCN6-depleted cells correlates with PGC1α status. Accordingly, the PGC1α level in CCN6-siRNA-transfected cells was compared with that of controls. CCN6-depleted cells displayed increased levels of PGC1α both at the mRNA and protein levels (Fig. 3A,B). PGC1α expression has been previously correlated with increases in ROS (Austin and St-Pierre, 2012; Spiegelman, 2007; St-Pierre et al., 2006). Accordingly, we observed that the ROS quencher N-acetyl cysteine blocked the increase in PGC1α mRNA expression (Fig. 3C), suggesting that the increase in PGC1α expression in CCN6-depleted cells is ROS dependent. Elevated expression of the PGC1α-responsive oxidative phosphorylation (OXPHOS) gene *ATP5J* (Mootha et al., 2003) in CCN6-depleted cells, as demonstrated by both RT-PCR and immunoblot analyses, is furthermore suggestive of increased PGC1α function upon CCN6 depletion (Fig. 3D,E). Fig. 3F depicts the substantially increased levels of PGC1α and ATP5J protein in CCN6-depleted cells as compared to controls. Taken together, these results indicate that the elevated ROS levels that are, at least partly, contributed by augmented ETC activity might lead to increased PGC1α expression and function in CCN6-depleted cells. Considering the functional association of PGC1α with mitochondrial mass, we further checked for changes in mitochondrial mass in CCN6-siRNA-transfected cells by performing flow cytometry using MitoTracker Green. There was a consistent increase in mitochondrial mass in CCN6-siRNA-transfected cells compared to the corresponding controls (Fig. 3G). The increase in the intensity of MitoTracker Green of CCN6-siRNA-transfected cells was similar to the observed increase in the intensity of MitoTracker Red staining (Fig. 2A), indicating that CCN6 depletion increases the mass of respiring mitochondria (Zhou et al., 2011).

CCN6 is associated with mitochondria

In view of our experimental findings implicating CCN6 as a regulator of basal mitochondrial metabolism, it was necessary to check if CCN6 at least partially localizes to mitochondria. As depicted in Fig. 4A, subcellular fractionation of C-28/I2 cells followed by immunoblotting demonstrated the presence of CCN6 in mitochondrial fractions. COX-IV was used as a mitochondrial marker in these studies (Dolga et al., 2014). Proteinase K treatment of mitoplast preparations (Mick et al., 2012) and immunoblotting with antibodies to mitochondrial inner compartment marker proteins (NDUFS1 and ATP5A1) furthermore indicated that, although a considerable fraction of the CCN6 protein was accessible for proteinase K digestion, a notable fraction also remained resistant to it (Fig. 4B). Moreover, immunoblotting of the mitochondrial pellet and supernatant fractions, prepared separately from CCN6–Myc overexpressing cells in carbonate buffer (Mick et al., 2012; Zhou et al., 2008), with antibodies against Myc, Hsp60 (inner membrane and matrix marker) and TOM20 (outer membrane marker) indicated that, although most of the mitochondrial CCN6 was associated with the membrane, a portion was also present in the soluble fraction (De Vos et al., 2012; Sun et al., 2006) (Fig. 4C). Mitochondrial localization of CCN6 was also demonstrated through colocalization of endogenous, as well as overexpressed, CCN6 with MitoTracker Green by performing confocal microscopy (Fig. 4D). The extent of MitoTracker-Green–CCN6 colocalization, both at the endogenous level and after CCN6–Myc overexpression, was estimated by using a red, green and blue (RGB) profile plot (Fig. 4E endogenous CCN6, Fig. 4F overexpressed CCN6–Myc) and Pearson's coefficient (Fig. 4G).

Journal of Cell Science (2016) 129, 2841-2851 doi:10.1242/jcs.186247

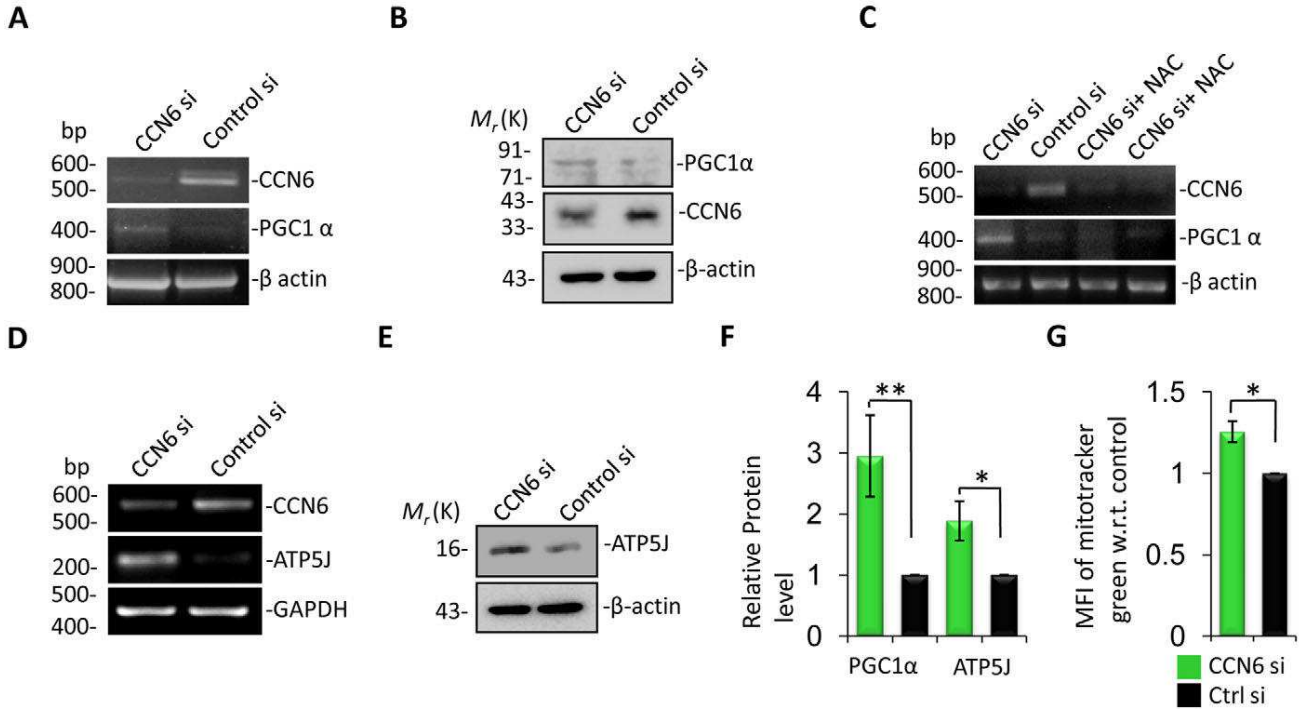

Fig. 3. Increased PGC1α expression and/or function in CCN6-knockdown cells, which is concomitant with an increase in mitochondrial content, is ROS dependent. Knockdown of CCN6 (CCN6 si) (~60% efficiency) with siRNA enhances PGC1α expression at the mRNA level (A) and protein level (B) (more than twofold). Control si, scramble control siRNA. (C) Treatment of CCN6-knockdown cells with ROS quencher N-acetyl cysteine (NAC) for 10 h reduced PGC1α expression level to baseline. An increase in PGC1α expression upon silencing of CCN6 increased expression of the PGC1α-responsive oxidative phosphorylation gene *ATP5J* at the RNA level (more than threefold) (D) and protein level (~threefold) (E). (F) Densitometry analysis of immunoblots reveals that PGC1α (*n*=4) and ATP5J (*n*=3) protein levels relative to β-actin were significantly higher in CCN6-knockdown cells than in control. (G) Flow cytometric analysis of MitoTracker green fluorescence in CCN6-knockdown C-28/I2 cells with respect to control (*n*=3). MFI, mean fluorescence intensity. *n* represents the number of independent experiments. Data are represented as mean±s.e.m.; **P*<0.05, ***P*<0.01 (unpaired Student's *t*-test).

Negative-control experiments for assessment of colocalization by using Pearson's coefficient were performed using isotype antibody and empty-vector-transfected cells (Fig. S3A,B). Presence of CCN6 in mitochondria was additionally substantiated by performing *z*-stacking analysis with confocal microscopy (Movie 3). These results suggest that the augmented ETC activity of CCN6-depleted cells might arise, at least partly, because of a lack of physical association of CCN6 with mitochondrial components. CCN6 might influence the activity of mitochondrial ETC components through intermolecular interactions, on account of the multimodular architecture of CCN6 (Engel, 2004; Hurvitz et al., 1999).

CCN6-depleted cells have altered mitochondrial morphology

Considering that CCN6 associates with mitochondria and that its depletion causes an increase in mitochondrial ETC activity and mass, it was important to examine whether CCN6 depletion correlates with altered mitochondrial morphology. Accordingly, transmission electron microscopy (TEM) analysis was performed, following similar procedures to those previously described (Pasqua et al., 2015), to evaluate the mitochondria of both CCN6-siRNA-transfected cells and the corresponding controls. TEM revealed an increased number of mitochondria together with elevated mitochondrial and cristae volume density {cristae volume density (%) = [sum of cristae area (μm^2) / mitochondrial area (μm^2)] × 100}, as well as crista area, in CCN6-depleted cells (Fig. 5A–H) as compared to controls. The red arrows in Fig. 5I indicate a possible site of mitochondrial fission in CCN6-depleted cells. The closer physical association of ER and mitochondria in CCN6-depleted cells as compared to controls (~27 nm vs ~52 nm) corroborates the observed mitochondrial Ca^{2+} influx that accompanies ATP synthesis (Fig. 5I–K). Alteration of mitochondrial shape and mass was furthermore evident upon depletion of CCN6 by using the CRISPR–Cas9 technique (Fig. S4). The efficiency of CCN6 depletion was demonstrated by using the SURVEYOR assay (Fig. S4C). The appearance of such features could correlate with the expression of chondrocyte hypertrophy markers, such as collagen X, which are associated with CCN6 depletion (Repudi et al., 2013). It will be interesting to investigate how CCN6 expression and mitochondrial morphology correlate with other cellular transformations that accompany hypertrophic differentiation (Buckwalter et al., 1986; Goldring et al., 2006).

Nrf2 regulates CCN6 expression

Given that CCN6 bears the potential to regulate mitochondrial respiration and ATP synthesis, it was important to understand how CCN6 itself is regulated. Previously, we have documented that CCN6 expression is enhanced by very low doses of ROS (Repudi et al., 2013). For an in-depth understanding of regulation of CCN6 expression, a bioinformatic approach was taken. Analysis of 10,000 bp upstream and downstream of the transcription start site revealed a binding site for the Nrf2 [nuclear factor erythroid 2 (NF-E2)-related factor 2 (NFE2L2)] transcription factor 4778 bp upstream of the transcription start site (Fig. 6A). Binding of Nrf2 to the region of the CCN6 promoter (designated Nrf2-binding site) identified by our bioinformatic search was confirmed by the

Journal of Cell Science (2016) 129, 2841-2851 doi:10.1242/jcs.186247

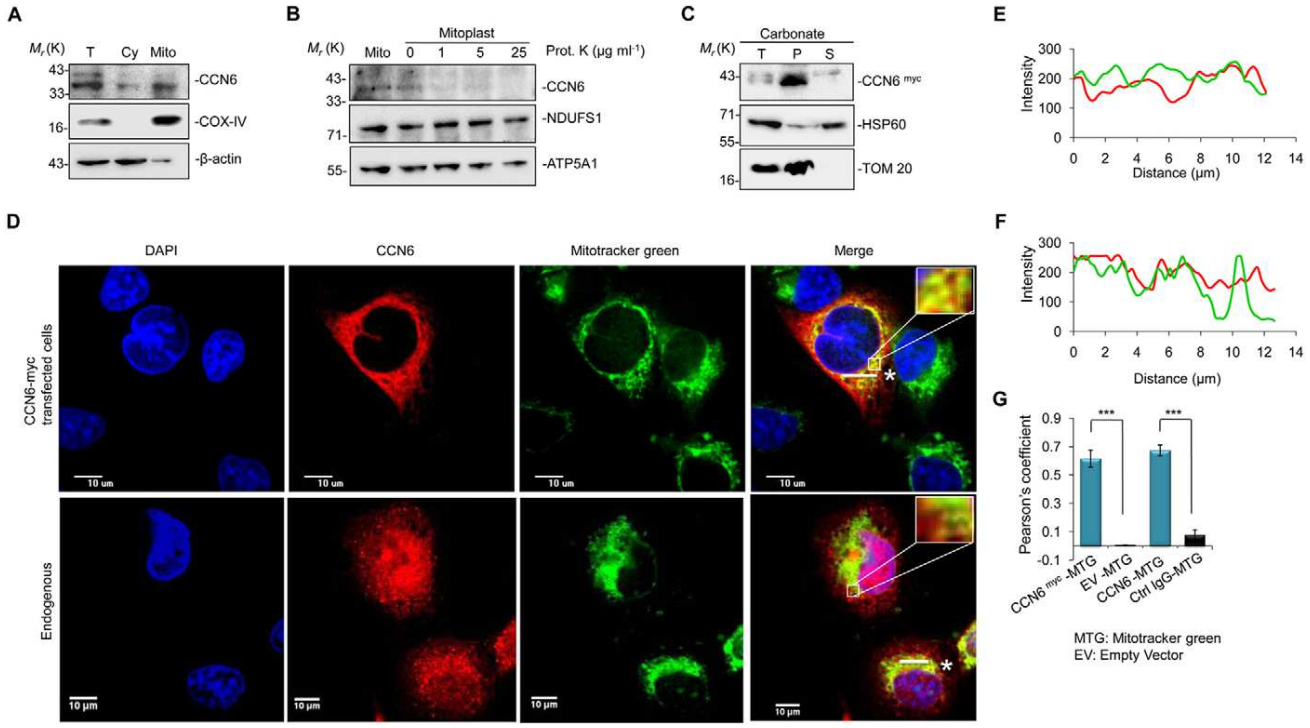

Fig. 4. CCN6 localizes to mitochondria. (A) Immunoblot demonstrating the presence of CCN6 in the mitochondrial fraction (Mito), cytosolic fraction (Cy) and whole-cell lysate (T) of C-28/I2 cells. COX-IV and β-actin were used as mitochondrial and cytosolic fraction loading controls, respectively. (B) Mitochondria from C-28/I2 cells were subjected to osmotic rupture for mitoplast preparation. Immunoblot of proteinase-K-digested (Prot. K) mitoplast corroborated localization of CCN6, which was associated with mitochondria. NDUFS1 and ATP5A1 were used as mitochondrial inner-compartment markers. (C) Immunoblot of a Na_2CO_3 (pH 11.5) preparation of isolated mitochondria from CCN6–Myc-transfected HEK293 cells, represented as total (T), membrane-rich pellet (P) and supernatant (S). TOM20 and HSP60 were used as references for mitochondrial outer membrane and mitochondrial inner membrane and matrix, respectively. (D) Confocal microscopy of C-28/I2 cells (endogenous) and CCN6–Myc-transfected C-28/I2 cells revealed colocalization of mitochondria (MitoTracker Green FM, green) with CCN6 (red). (E,F) RGB intensity plots of mitochondria (MitoTracker Green FM, green) and CCN6 (red) in C-28/I2 cells (endogenous, E; transfected with CCN6–Myc, F) depicting CCN6 localization in mitochondria. (G) Pearson's coefficient of colocalization between MitoTracker Green (MTG) and CCN6 was calculated from the confocal microscope data represented in panel D and Fig. S3. In calculating Pearson's coefficient for endogenous CCN6 (red) and MTG (green), confocal images of control IgG for CCN6 and MTG (Fig. S3A) were used as control. For calculation of Pearson's coefficient of colocalization in CCN6–Myc-transfected cells, confocal images of empty vector (EV)-transfected cells (Fig. S3B) were used as control (n=4). n represents the number of independent experiments. One way ANOVA followed by Bonferroni post-hoc test was performed to calculate the statistical significance of Pearson's coefficient; data are represented as mean±s.e.m., ***P<0.001.

luciferase activity of C-28/I2 cells that had been transfected with a luciferase reporter plasmid bearing the CCN6 promoter. In the presence of increasing concentrations of tert-butylhydroquinone (tBHQ), which promotes nuclear localization of Nrf2 (Nguyen et al., 2005), the reporter-plasmid-transfected C-28/I2 cells displayed progressively decreasing levels of luciferase activity, indicating that Nrf2 represses CCN6 expression (Fig. 6B). Nuclear translocation of Nrf2 upon tBHQ treatment and the concomitant decrease in CCN6 expression was substantiated separately using C-28/I2 cells (Fig. 6C,D). A chromatin immunoprecipitation (ChIP) assay further validated the binding of Nrf2 to the CCN6 promoter (Fig. 6E, top row). A similar ChIP assay that showed binding of RNA polymerase II (Fig. 6E, bottom row) established that the identified region was transcriptionally active. Interestingly, depletion of Nrf2 in chondrocytes through siRNA transfection led to an increase in CCN6 expression, both at the mRNA and protein levels, thus supporting that CCN6 expression is inhibited by Nrf2 (Fig. 6F,G). Considering that Nrf2 is a promoter of mitochondrial metabolism (Holmstrom et al., 2013; Ludtmann et al., 2014; Piantadosi et al., 2008), existence of a counter-regulatory CCN6–Nrf2 association that would appropriately control mitochondrial function seems plausible.

DISCUSSION

The involvement of CCN6 as an important player in mitochondrial respiration, Ca^{2+} accumulation and ATP synthesis brings a new dimension to our understanding of not only CCN6 function but also mitochondrial electron transport. The increased crista area and mitochondrial volume density along with closer mitochondria–ER association in CCN6-depleted cells as revealed by performing transmission electron microscopy (Fig. 5) are clearly indicative of an inverse relationship of mitochondrial metabolism and Ca^{2+} accumulation with CCN6 expression (Bravo et al., 2011; Rizzuto et al., 2009; Zampese et al., 2011). In view of the need of respiring mitochondria for release of mitochondrial Ca^{2+} during cell matrix mineralization (Brighton and Hunt, 1978; Lehninger, 1970; Villa-Bellosta et al., 2013), one can thus logically stipulate an important role of CCN6 in the regulation of mitochondrial electron transport and cell matrix calcification.

Mitochondrial localization of CCN6 and increased mitochondrial ATP synthesis in CCN6-depleted cells suggests that CCN6 could act as a brake for mitochondrial metabolism, thereby regulating cell growth. The regulation of ETC activity and its influence on cell growth and differentiation, although fundamental to biological systems, are far from being resolved. The potential involvement of

Journal of Cell Science (2016) 129, 2841-2851 doi:10.1242/jcs.186247

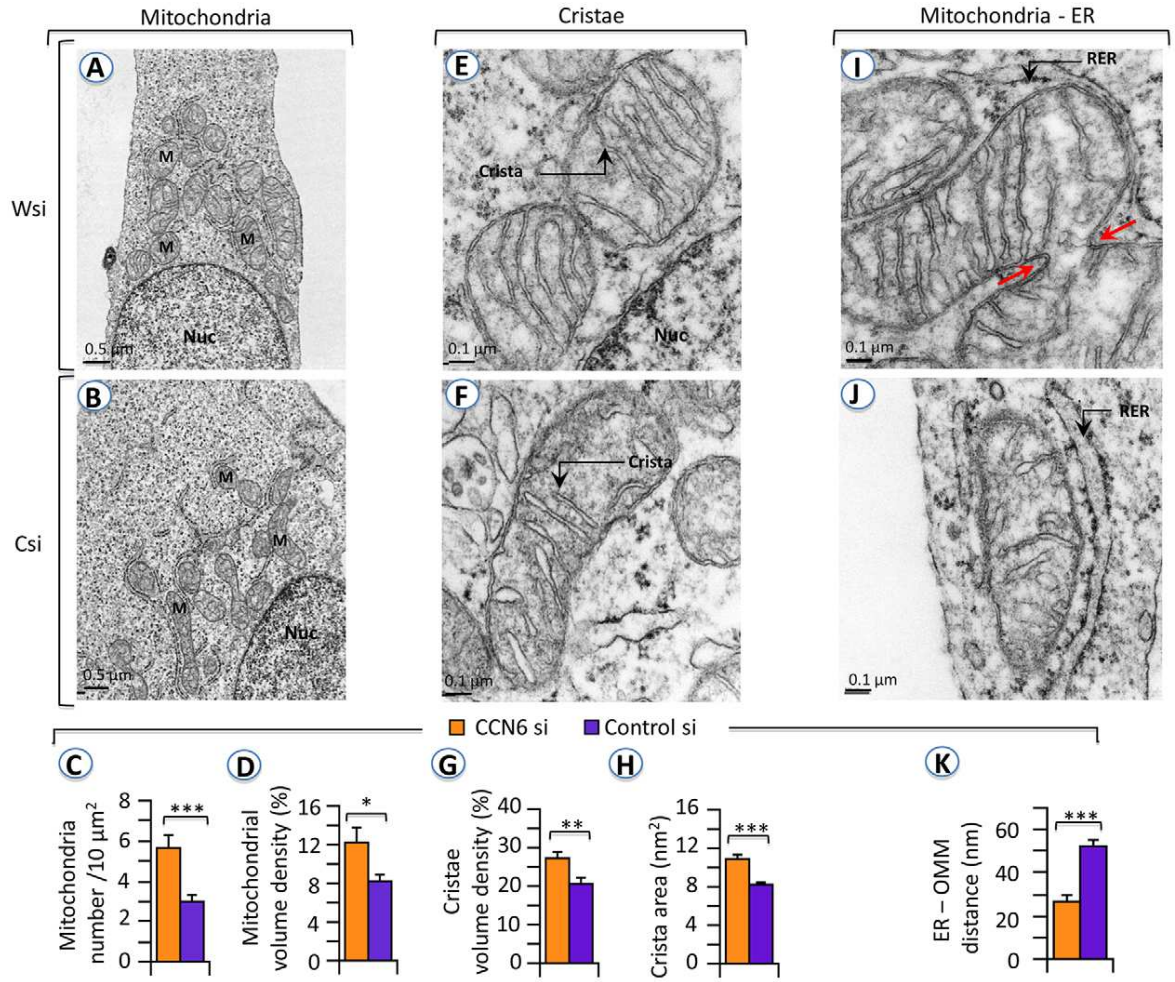

Fig. 5. Electron microscopy data showing mitochondrial morphology and ER–mitochondria juxtaposition in CCN6-knockdown vs control cells. Low magnification (2500×) electron microscopy images of CCN6 knockdown (Wsi, CCN6 si) (A) and control (Csi, control si) (B) cells. Morphometric analyses (*n*=25) show increased mitochondrial number (C) in Wsi cells and mitochondrial volume density (D) in Wsi cells compared to Csi cells. High magnification (15,000×) images of mitochondria in Wsi (E) and Csi (F). Morphometric analyses (*n*=100) show increased cristae volume density (G) and crista area (H) in Wsi cells compared to Csi cells. High magnification (15,000×) images of mitochondria and rough endoplasmic reticulum (RER) in Wsi (I) and Csi (J) cells showing the distance between mitochondria and ER. Morphometric analyses (*n*=25) revealed closer association of mitochondria and ER in Wsi cells to compared to in Csi cells (K). M, mitochondrion; Nuc, nucleus. Red arrows point to possible cleavage of mitochondria before complete fission. Data are represented as mean±s.e.m.; **P*<0.05, ***P*<0.01; ****P*<0.001 (unpaired Student's *t*-test with Welch's correction). *n* represents number of cells.

CCN6 therein could help to resolve the complex paradigm. In light of its multi-modular nature, CCN6 harbors an intrinsic potential for intermolecular interactions with other proteins. Therefore, it will be important to investigate whether the inhibitory influence of CCN6 on mitochondrial function is on account of its interactions with mitochondrial proteins. At the same time, it will be important to decipher if CCN6 uses any mitochondrial target sequence for mitochondrial entry or whether it is imported to mitochondria through an indirect mechanism (Doyle et al., 2013).

The present study demonstrates, for the first time, that the expression and function of PGC1α, the transcriptional co-activator that is essential for mitochondrial metabolism (Austin and St-Pierre, 2012; Spiegelman, 2007; Wenz, 2009), is modulated by the magnitude of CCN6-mediated effects on electron transport. PGC1α expression might be induced by the increased accumulation of ROS that results from augmented ETC activity in the absence of a fully functional CCN6 protein. Accumulated ROS perhaps promote the binding of CREB, MEF2, ATF2 and Foxo1 onto the PGC1α promoter (Fernandez-Marcos and Auwerx, 2011). PGC1α, once induced, could facilitate mitochondrial metabolism in a feed-forward mode. Thus, in the absence of a functional CCN6 protein, PGC1α could promote untimely cellular growth and hypertrophy through increased mitochondrial metabolism. The increased number and mass of mitochondria observed in CCN6-depleted cells (Figs 3G and 5C; Fig. S4F) could be partly facilitated by elevated PGC1α activity (Wu et al., 1999).

The documented inhibition of CCN6 expression by Nrf2 ushers in a new layer of coordination of mitochondrial dynamics through transcriptional regulation. CCN6 acts like a brake on ETC activity and ATP synthesis, whereas Nrf2, which is a facilitator of mitochondrial metabolism (Holmstrom et al., 2013; Ludtmann et al., 2014; Piantadosi et al., 2008), possibly coordinates with CCN6 by repressing its expression. The transcriptional co-activator PGC1α, which is turned on by accumulated ROS from enhanced ETC activity in a muted-CCN6 background, might be able to promote expression of Nrf2 through its influence on Notch

Journal of Cell Science (2016) 129, 2841-2851 doi:10.1242/jcs.186247

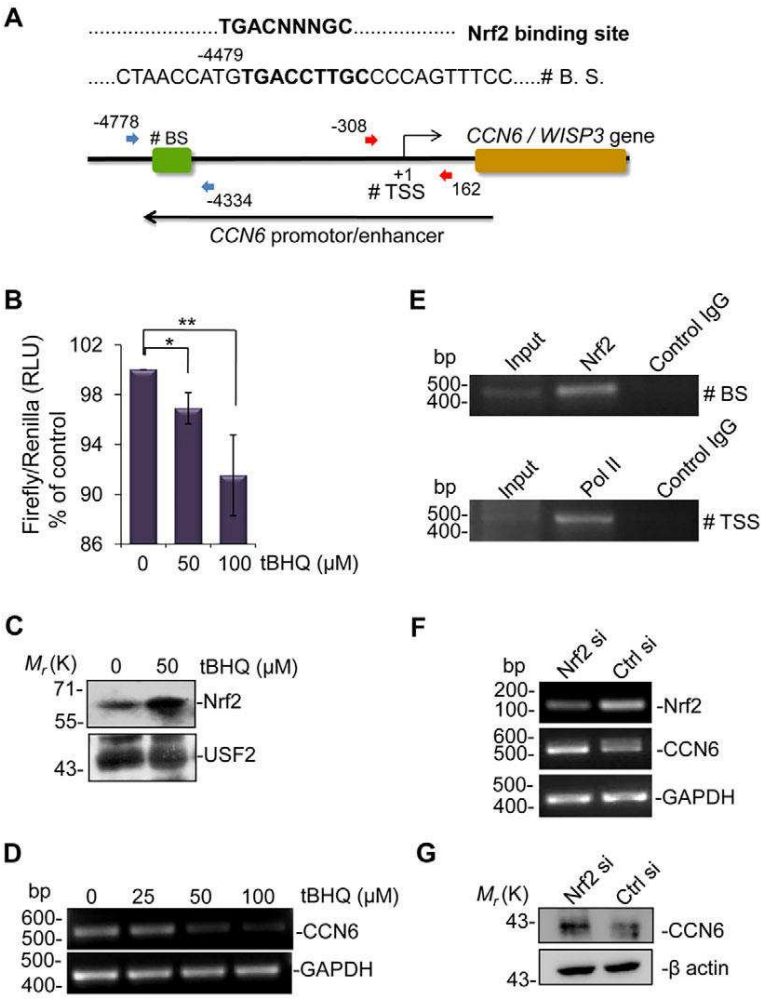

Fig. 6. Nrf2 binds to the CCN6 promotor and inhibits CCN6 expression. (A) The CCN6 promotor contains an Nrf2-binding site called anti-oxidant response element (ARE) represented as #B.S (Nrf2-binding site). N represents any nucleotide. (B) CCN6^{ARE}–Luc- and *Renilla*-co-transfected C-28/I2 cells that had been treated with the indicated concentration of tBHQ for 10 h showed a nuclear Nrf2-induced decrease in luciferase reporter activity. Treatment of C-28/I2 cells with indicated doses of tBHQ for 10 h enhanced Nrf2 nuclear translocation (~twofold) (C) and inhibited CCN6 expression (60% and 75% inhibition at 50 and 100 μM tBHQ, respectively; calculated using densitometry analysis with ImageJ) (D). USF2 was used as a nuclear loading control (C). (E) A ChIP assay confirmed Nrf2 binding to the CCN6 promotor (#BS) and RNA polymerase II (Pol II) binding to the transcription start site (#TSS). In Nrf2-knockdown cells (Nrf2 si) (~55% efficiency of knockdown), CCN6 expression was increased both at the RNA (~twofold) (F) and protein (~twofold) (G) levels. Data are represented as mean±s.e.m.; *P<0.05, **P<0.01 (unpaired Student's t-test); n=3 independent experiments. Ctrl si, control siRNA.

signaling (Sawada et al., 2014; Wakabayashi et al., 2014), and Nrf2 could repress CCN6 function furthermore.

The established link of CCN6 mutations with the development of the cartilage disease PPRD raises an important question. Given that CCN6 regulates mitochondrial respiration and ATP synthesis, why do specific phenotypes resulting from CCN6 mutations manifest primarily as loss of cartilage during puberty (Dalal et al., 2012; Ekbote et al., 2013; Garcia Segarra et al., 2012; Hurvitz et al., 1999; Liu et al., 2015; Luo et al., 2015; Yang et al., 2013)? Although it is true that the comprehension of CCN6-mutant phenotypes cannot be directly drawn through extrapolation of experimental findings related to wild-type CCN6, a clear knowledge of the function of the wild-type protein nevertheless could be required for a detailed analysis of the mutants. The functional significance of CCN6 expression at different developmental stages in different tissues is not clearly understood. But there is evidence that CCN6 plays an important role during cartilage growth and maintenance by sustaining expression of the extra cellular matrix (ECM) protein collagen II (Sen et al., 2004). Moreover, in view of the fact that CCN6 restricts mitochondrial metabolism, cartilage loss might result from premature chondrocyte hypertrophy that results from, at least in part, unregulated mitochondrial metabolism that is facilitated by a malfunctioning or nonfunctional CCN6 protein. Given that chondrocyte differentiation and ECM maintenance are crucial features of limb growth during puberty, cartilage could be most affected by mutant CCN6. A comprehensive characterization of the CCN6 protein and detailed evaluation of its significance in metabolic regulation and Ca^{2+} homeostasis could be useful in the functional analysis of PPRD-linked CCN6 mutants at the molecular level.

MATERIALS AND METHODS

Cell culture

C-28/I2 chondrocyte cells and HEK293 cells were maintained in Dulbecco's modified Eagle's medium (DMEM; Invitrogen) supplemented with 10% FBS, penicillin (1 unit ml^{-1}), streptomycin (1 μg ml^{-1}) and glutamine (2 mM) (Invitrogen) in a humidified incubator maintaining 37°C temperature and 5% CO_2 (Miller and Sen, 2007; Repudi et al., 2013). The C-28/I2 cell line was generated through retroviral infection of human juvenile costal cartilage with SV40 large T antigen (Goldring et al., 1994). The HEK293 cell line was purchased from American Type Culture Collection (ATCC). Both cell lines were tested for contamination.

Plasmids

Cloning of the CCN6 (WISP3) gene (GenBank AF100781) in between *Hind*III and *Xho*I restriction sites of the pSecTag2A vector to generate the CCN6–Myc construct has been described previously (Repudi et al., 2013). The Nrf2-binding site (anti-oxidant response element, ARE) between positions −4480 bp and −4471 bp was predicted upstream of CCN6 coding sequence from ensemble database. The sequence (−4492 bp to −4457 bp) was cloned between *Sal*I and *Bam*HI restriction enzyme sites in pGL3 luciferase vector to make the reporter construct (CCN6^{ARE}–Luc) (Repudi et al., 2013).

Journal of Cell Science (2016) 129, 2841-2851 doi:10.1242/jcs.186247

Transfection

The detailed transfection protocol has been reported previously (Repudi et al., 2013). Briefly, for plasmid expression studies, C-28/I2 chondrocyte cells were transfected with plasmid (2 µg) using Lipofectamine LTX transfection reagent (Invitrogen) and incubated for 48 h at 37°C in a humidified CO_2 cell culture incubator before harvesting for assays. For knockdown experiments, C-28/I2 chondrocyte cells were separately transfected with CCN6 siRNA (50 nM) or control siRNA (50 nM) (Dharmacon) and Nrf2 siRNA (25 nM) or control siRNA (25 nM) (Santa Cruz) using RNAiMAX transfection reagent (Invitrogen) as per the manufacturer's protocol and as described previously (Repudi et al., 2013). After 60–65 h of transfection, siRNA-transfected cells were analyzed.

RNA and cDNA preparation, and PCR

Total cellular RNA was isolated with the use of Trizol (Life Technologies) (Davis et al., 2006; Miller and Sen, 2007; Sen et al., 2004). The cDNA was prepared from RNA using cDNA synthesis kit (BioBharati Lifescience, India) as per the manufacturer's protocol. Gene expression was analyzed by performing PCR amplification of cDNA with specific primers: CCN6 (WISP3) forward 5′-ACCAAAGCTGGCTGGCAGTC-3′ and reverse 5′-TCTC CAGGTTCTCTGCAGTTTC-3′, GAPDH forward 5′-ACCACAGTCCATGCCATCAC-3′ and reverse 5′-TCCACCACCCTG TTGCTGTA-3′, PGC1α forward 5′-TGTGCTGCTCTGGTTGGTG-3′ and reverse 5′-GCTGAGTGTTGGCTGGTGC-3′, ATP5J forward 5′-GCACTTACCCTCCACTTCCT-3′ and reverse 5′-ATTCTTGCACTCAGTCCCGA-3′, β-actin forward 5′-ATCTGGCACCACA CCTTCTACAATGAGCTGCG-3′ and reverse 5′-CGTCATACTCCTGCTTGCTGATCC ACATCTGC-3′, and Nrf2 forward 5′-GAGAGCCCAGTCTTCATTGC-3′ and reverse 5′-TGCTCAATGTCCTGTTGCAT-3′.

Cell lysate preparation and immunoblotting

Whole-cell lysates were prepared using cell lysis buffer [20 mM Tris-HCl (pH 7.5), 500 mM NaCl, 1% Triton X-100, 1 mM EDTA, 50 mM dithiothreitol, 2 mM phenylmethylsulfonyl fluoride and 1% protease inhibitory cocktail (P8340, Sigma)] (Repudi et al., 2013). Total protein concentration was determined using the Bradford reagent (Bio-Rad). Subsequently, immunoblot analysis was performed by following a standard protocol (Repudi et al., 2013). Briefly, protein was transferred to PVDF membrane after SDS-PAGE and blocked for 2 h with either 5% BSA in TBST (Tris-buffered saline with 0.1% Tween-20) or 0.2% I-Block (Applied Biosystem). The blots were then incubated at 4°C overnight with separate primary antibodies using 1:1000 dilutions: anti-WISP3 (N-18) antibody (sc-8871, Santa Cruz) (Repudi et al., 2013; Tanaka et al., 2003), anti-PGC1α antibody (sc-13067, Santa Cruz) (Hong et al., 2011), anti-Nrf2 antibody (sc-13032, Santa Cruz) (Xiao et al., 2012), anti-USF2 antibody (sc-861, Santa Cruz) (Naskar et al., 2014), anti-ATP5A1 antibody (459240, Invitrogen), anti-COX-IV antibody (ab16056, Abcam), anti-NDUFS1 antibody (PA5-22309, Thermo Fisher), anti-HSP60 antibody (MA3-012, Thermo Fisher) and anti-ATP5J antibody (NBP1-88888, Novus Biologicals). Horseradish peroxidase (HRP)-conjugated secondary antibodies: anti-rabbit-IgG (A0545, Sigma), anti-mouse-IgG (A9044, Sigma) and anti-goat-IgG (A8919, Sigma) antibodies were used at a dilution 1:4000 for visualization with chemiluminescence reagent (Pierce and Millipore).

Subcellular fractionation

For isolation of mitochondria, C-28/I2 chondrocyte cells (6×10^8) were homogenized with a Dounce homogenizer in a buffer composed of 225 mM mannitol, 75 mM sucrose, 0.1 mM EGTA and 30 mM Tris-HCl (pH 7.4). Unbroken cells and nuclei were discarded by centrifuging the sample at 600 ***g*** for 5 min. Supernatant collected was further subjected to centrifugation at 7000 ***g*** for 10 min to obtain the mitochondrial pellet and cytosolic fraction. The mitochondrial pellet was washed with mitochondria wash buffer [225 mM mannitol, 75 mM sucrose and 30 mM Tris-HCl (pH 7.4)] and resuspended in mitochondrial resuspension buffer [250 mM mannitol, 0.5 mM EGTA and 5 mM HEPES (pH 7.4)] (Wieckowski et al., 2009).

To prepare nuclear and cytoplasmic extracts, C-28/I2 cells were incubated on ice in a hypotonic buffer [10 mM KCl, 1.5 mM $MgCl_2$, 10 mM HEPES (pH 7.9), 0.5 mM DTT, 1 mM PMSF and 1 mM Na_3VO_4] for 10 min. Cells were broken down with the addition of 0.5% NP-40. Centrifugation was carried out at 600 ***g*** for 5 min to obtain nuclear pellet and cytoplasmic supernatant. The nuclear pellet was sonicated in hypertonic buffer [1.5 mM $MgCl_2$, 420 mM NaCl, 20 mM HEPES (pH 7.9), 25% glycerol, 0.2 mM EDTA, 0.5 mM DTT, 1 mM PMSF, and 1 mM Na_3VO_4] for 15 s. Nuclear extract was obtained after centrifugation at 13,000 ***g*** for 15 min (Naskar et al., 2014).

Mitoplast preparation and mitochondrial fractionation with sodium carbonate buffer

Sub-mitochondrial localization of CCN6 was carried out by performing proteinase K protection assay. Mitochondria were osmotically ruptured by addition of MOPS buffer [10 mM MOPS and 1 mM EDTA, pH 7.2] to prepare mitoplasts (Mick et al., 2012). Mitoplast preparations of C-28/I2 cells were digested with increasing concentrations of proteinase K (1, 5 and 25 µg ml^{-1}). The effect of proteinase K digestion on mitoplast was blocked with 1 mM PMSF after 10–15 min of incubation on ice (Mick et al., 2012).

To isolate mitochondrial membranous and soluble sub-compartments, mitochondria from CCN6–Myc-transfected HEK293 cells were incubated for 30 min in carbonate buffer (100 mM Na_2CO_3, pH 11.5) and centrifuged for 45 min at 45,000 ***g*** (Mick et al., 2012; Zhou et al., 2008). The membranous part was mostly represented by a pellet, whereas the soluble part was represented by supernatant after centrifugation.

Flow cytometry

Total mitochondria, actively respiring mitochondria and membrane potential were measured by incubating cells for 20 min with 200 nM MitoTracker Green FM, Deep Red FM MitoTracker Red (Zhou et al., 2011) and Rhodamine 123 (Johnson et al., 1981) (Molecular Probes), respectively. Mitochondrial ROS (mROS) were analyzed by incubating cells with CMH_2XRos (200 nM) (Molecular Probes) for 25 min (Degli Esposti, 2002). Mitochondrial Ca^{2+} uptake was determined by treating cells with Rhod 2 (2 µM) (Molecular Probes) for 50 min (Hajnoczky et al., 1995; Mallilankaraman et al., 2012). Cells loaded with respective fluorescent dyes were trypsinized with 0.05% Trypsin EDTA (Invitrogen) and washed twice with PBS. The cells were finally resuspended in PBS at a concentration of 10^6 cells ml^{-1} and analyzed by using a BD FACS Calibur (BD Bioscience), taking 10,000 counts for each sample. For propidium iodide exclusion, siRNA-transfected C-28/I2 cells were trypsinized and washed with PBS. Propidium iodide solution (1 mg ml^{-1}) was added to cells before FACS analysis (Naskar et al., 2014). siRNA-transfected C-28/I2 cells were further analyzed for apoptosis or cell death by using an annexin-V–FITC and propidium iodide apoptosis detection kit (BD Biosciences), as per the manufacturer's protocol. To assess cell proliferation, C-28/I2 chondrocyte cells were incubated with carboxyfluorescein succinimidyl ester (CFSE) (5 µM) (Molecular Probes) for 20 min in PBS after 24 h of siRNA transfection (Lyons and Parish, 1994). CFSE fluorescence was measured after 65 h of siRNA transfection.

Measurement of mitochondrial ATP synthesis

Mitochondrial ATP synthesis was measured by incubating freshly prepared mitochondria (100 µg ml^{-1}) in respiration buffer [0.6 M sorbitol, 1 mM $MgCl_2$, 1 mM EDTA, 5 mM succinate, 1 mM ADP and 25 mM potassium phosphate pH 7.0] at 37°C for 15 min (Mittal et al., 2009; Mourier et al., 2014). Quantification of ATP was done by using an ATP determination kit (Molecular probes, Life Technologies) following the manufacturer's protocol. Luminescence for ATP measurement was recorded with a PerkinElmer VICTOR X3 luminometer.

Confocal microscopy

Confocal microscopy was performed using an Andor Revolution XD spinning disk microscope with an Andor ixon 897 EMCCD camera, and a Leica TCS SP8 microscope with PMT HyD detector. To check mitochondrial localization of CCN6 (WISP3), cells were first loaded with MitoTracker Green FM (200 nM) for 30 min, after which they were fixed with methanol, blocked with 2.5% BSA in PBS containing 0.1% Tween-20 (PBST) for 1 h, and incubated at 4°C overnight with either anti-WISP3

Journal of Cell Science (2016) 129, 2841-2851 doi:10.1242/jcs.186247

antibody (1:200) for localization in C-28/I2 cells or anti-Myc antibody (1:500) for localization in CCN6–Myc-transfected C-28/I2 chondrocytes. Cells were washed twice with PBST and incubated with secondary Alexa-Fluor-546-conjugated anti-goat antibody (1:2000) (Molecular Probes). DAPI was used to stain nucleus. For measurement of mitochondria-specific Ca^{2+} uptake, live-cell imaging was performed after treating the cells with MitoTracker Green FM (200 nM) for 30 min and Rhod 2 (μM) for 50 min (Hajnoczky et al., 1995; Mallilankaraman et al., 2012). Pearson's coefficient and RGB intensity plots of microscopy images for colocalization were performed using ImageJ (National Institutes of Health; NIH).

Electron microscopy

C-28/I2 chondrocyte cells were fixed with 2.5% glutaraldehyde and 2% paraformaldehyde in 0.15 M cacodylate buffer, and postfixed in 1% OsO_4 in 0.1 M cacodylate buffer for 1 h on ice. The cells were stained en bloc with 2–3% uranyl acetate for 1 h on ice. The cells were dehydrated in graded series of ethanol (20–100%) on ice followed by one wash with 100% ethanol and two washes with acetone (15 min each) and embedded with Durcupan. Sections were cut at 50 to 60 nm on a Leica UCT ultramicrotome, and picked up on Formvar and carbon-coated copper grids. Sections were stained with 2% uranyl acetate for 5 min and Sato's lead stain for 1 min. Grids were viewed using a JEOL 1200EX II (JEOL, Peabody, MA) transmission electron microscope and photographed using a Gatan digital camera (Gatan, Pleasanton, CA).

Morphometric analysis of mitochondria

Samples were anonymized, and morphometric measurements were made randomly from different cells as described previously (Pasqua et al., 2015). The line segment tool in NIH ImageJ 1.49 software was used to measure the distance between ER and mitochondria. The free-hand tool of the NIH ImageJ 1.49 software was used to manually trace around the cristae membrane, mitochondrial outer membrane area and cytoplasm area for determination of the mitochondrial and cristae volume density. The sum of the area of the total complement of cristae represented the cristae membrane surface area. To normalize the measurement, this sum was divided by the outer membrane area per mitochondrion. The sum of the area of the mitochondria was divided by the area of the cytoplasm and multiplied by 100 to determine the mitochondrial volume density (%). For determination of the cristae volume density (%), the sum of the area of the cristae was divided by the outer area of the mitochondria and multiplied by 100, as described previously (Pasqua et al., 2015). A 19×23-cm rectangular grid was overlaid on each image to count the number of mitochondria in each image, and the mitochondria number is presented per 10 μm^2 area of the cytoplasm.

Chromatin immunoprecipitation

The ChIP assay was performed by following standard protocols (Bernstein et al., 2005; Naskar et al., 2014). Briefly, C-28/I2 (~6×10^6) cells were incubated at 37°C for 10 min with 1% formaldehyde (Molecular Biology Grade, Calbiochem) to crosslink protein and DNA. Over-crosslinking was prevented with the addition of glycine to a final concentration 125 mM and incubation for 5 min. After lysis of cells in 1 ml SDS lysis buffer [50 mM Tris-Cl (pH-8.1), 10 mM EDTA and 1% SDS] sonication was performed to generate genomic DNA fragments of 100 bp to 500 bp in size. The sample was then diluted fivefold with ChIP dilution buffer [16.7 mM Tris-Cl (pH 8.1), 167 mM NaCl, 1.2 mM EDTA, 1.1% Triton X-100 and 1% SDS] and pre-cleared for 1 h with salmon sperm DNA and protein G agarose beads (Life Technologies). Subsequently, the sample was incubated overnight at 4°C with either 7 μg of anti-Nrf2 antibody (sc-13032X, Santa Cruz) or anti-RNA-polymerase-II antibody (sc-5943, Santa Cruz) (Naskar et al., 2014). In each case, rabbit IgG was used as control. The pulled down immune complex was sequentially washed with low-salt immune complex buffer (20 mM Tris-HCl, pH 8.1, 0.1% SDS, 1% Triton X-100, 150 mM NaCl), high-salt immune complex buffer (20 mM Tris-HCl, pH 8.1, 0.1% SDS, 1% Triton X-100, 500 mM NaCl), LiCl immune complex buffer (10 mM Tris-HCl, pH 8.1, 1 mM EDTA, 0.25 M LiCl, 1% deoxycholic acid, 1% Triton X-100) and Tris-EDTA (TE) buffer (10 mM Tris-HCl, pH 8.0, 1 mM EDTA). Reverse crosslinking was carried out by heating the sample with Chelex 100 (Bio-Rad) for 10 min on a dry bath. After proteinase K digestion, DNA from chromatin was purified by following standard phenol–chloroform extraction and isopropanol precipitation. Finally, the DNA was quantified by performing semi-quantitative PCR. Primers used were: ARE forward 5′-TCCTGCTACTGATCATGGTG-3′ and reverse 5′-AAGAGCTAACATTGGCCGA G-3′, and RNA polymerase II forward 5′-GCCTCCGAGAGAATCTGAG-3′ and reverse 5′-CTCTACCTCCCA-CACTACC-3′.

Luciferase assay

C-28/I2 cells were co-transfected with $CCN6^{ARE}$–Luc reporter construct and *Renilla* at a ratio of 50:1. After 48 h of transfection, cells were treated with 25, 50 and 100 μM of tBHQ for 6 h. The luciferase assay kit (Promega) was used to measure firefly and *Renilla* luciferase activity.

CCN6 CRISPR–Cas9 – C-28/I2 chondrocyte lines

High-quality guide RNA with a minimum of off-target effects and a high-quality score (89) was designed using CRISPR design tool (http://crispr.mit.edu) on all the exons of the CCN6 (WISP3) genomic region (RefSeq gene NG_011748.1). The guide RNA was cloned into pSpCas9 (BB) 2A-Puro vector (Addgene). The primer pair 5′-CACCGCCACGGTCCCAGCGACAT GC-3′ and 5′-AAACGCATGTCGCTGGGACCGTGGC-3′ was annealed, phosphorylated with polynucleotide kinase (Thermo Fisher) and ligated to the BbsI (Fermentus) digested vector using T7 ligase (NEB). The sequenced positive clone was used to transfect C-28/I2 cells using Lipofectamine LTX (Life Technologies). After 24–48 h of transfection cells, were subjected to puromycin selection (Ran et al., 2013). After 3–4 passages in growth medium without puromycin, cells were harvested for assays.

SURVEYOR assay

Insertion or deletion mutations in the genome were validated using SURVEYOR assay kit (IDT) (Ran et al., 2013). Isolated genomic DNA was subjected to PCR amplification using primer pair 5′-CTGCGAAGGC-AGGTTATTAG-3′ and 5′-GAAGCTCATGAACGAACACA-3′ flanking the target location. 400 ng of PCR products purified from wild-type C-28/I2 cells and CRISPR CCN6-knockout cells were melted and annealed in a buffer containing 10 mM Tris-HCl, pH-8.8, 50 mM KCl, 0.01% Tween-20 and 1.5 mM $MgCl_2$ to form a heteroduplex. The hybrid DNA was then incubated with 1 μl enhancer S, 1 μl nuclease S and 2 μl 0.15 M $MgCl_2$ at 42°C for 50 min as per the manufacturer's protocol. Cleaved products, which would arise only from heteroduplexes, were then analyzed in 2% agarose gel. Indel percentage was calculated by using the following the formula:

$$\text{Indel}\,(\%) = 100 \times [1 - \sqrt{\{1 - (b + c)/(a + b + c)\}}] \qquad (1)$$

(Ran et al., 2013).

In Eqn 1, a represents the band intensity of PCR product (529 bp) from nuclease-S-undigested duplex formed from genomic DNA of CCN6 WT cells and CRISPR CCN6 cells, whereas b and c represent the band intensities of nuclease-S-digested products of 211 bp and 318 bp, from the heteroduplex (529 bp), respectively.

Statistical analysis

GraphPad software was used for unpaired two-tailed Student's *t*-test analyses. Origin 8 software was employed for one way ANOVA followed by Bonferroni post-hoc test for comparison of Pearson's coefficients (DeGeer et al., 2015; Zhou et al., 2016). Data are represented as mean±s.e.m. Statistical significance was drawn by calculating *P*-values, which are represented as $*P<0.05$, $**P<0.01$ and $***P<0.001$.

Acknowledgements

We are grateful to Srinivasa Rao Repudi (The Hebrew University of Jerusalem, Jerusalem, Israel) for plasmids used in the study. We thank G. Ghosh, S. Kundu, S. Jati, S. N. Dey, T. Dalui and U. Ghosh for critical reading of the manuscript and useful comments. We thank D. Sarkar and S. Bhattacharya for help with confocal microscopy analysis. Transmission electron microscopy was conducted at the Cellular & Molecular Medicine Electron Microscopy core facility, University of California, San Diego.

Competing interests
The authors declare no competing or financial interests.

Author contributions
M.S. designed the research, organized experiments and wrote the paper. M.P. organized and performed experiments and helped in writing paper. S.K.M. performed TEM. D.K.P. performed some experiments.

Funding
This work is supported by a grant from the Department of Science and Technology, Ministry of Science and Technology [grant number SB/SO/BB-016/2014]; and institutional funding [grant number BSC0120]. M.P. and D.K.P. are supported by the Council of Scientific and Industrial Research (CSIR) fellowships, Government of India. A research career scientist award from the U.S. Department of Veterans Affairs supports S.K.M.

Supplementary information
Supplementary information available online at
http://jcs.biologists.org/lookup/suppl/doi:10.1242/jcs.186247/-/DC1

References

Austin, S. and St-Pierre, J. (2012). PGC1alpha and mitochondrial metabolism–emerging concepts and relevance in ageing and neurodegenerative disorders. *J. Cell Sci.* **125**, 4963-4971.
Bernstein, B. E., Kamal, M., Lindblad-Toh, K., Bekiranov, S., Bailey, D. K., Huebert, D. J., McMahon, S., Karlsson, E. K., Kulbokas, E. J., III, Gingeras, T. R. et al. (2005). Genomic maps and comparative analysis of histone modifications in human and mouse. *Cell* **120**, 169-181.
Bravo, R., Vicencio, J. M., Parra, V., Troncoso, R., Munoz, J. P., Bui, M., Quiroga, C., Rodriguez, A. E., Verdejo, H. E., Ferreira, J. et al. (2011). Increased ER-mitochondrial coupling promotes mitochondrial respiration and bioenergetics during early phases of ER stress. *J. Cell Sci.* **124**, 2143-2152.
Brighton, C. T. and Hunt, R. M. (1978). The role of mitochondria in growth plate calcification as demonstrated in a rachitic model. *J. Bone Joint Surg. Am.* **60**, 630-639.
Brigstock, D. R., Goldschmeding, R., Katsube, K.-I., Lam, S. C.-T., Lau, L. F., Lyons, K., Naus, C., Perbal, B., Riser, B., Takigawa, M. et al. (2003). Proposal for a unified CCN nomenclature. *Mol. Pathol.* **56**, 127-128.
Brookes, P. S., Yoon, Y., Robotham, J. L., Anders, M. W. and Sheu, S.-S. (2004). Calcium, ATP, and ROS: a mitochondrial love-hate triangle. *Am. J. Physiol. Cell Physiol.* **287**, C817-C833.
Buckwalter, J. A., Mower, D., Ungar, R., Schaeffer, J. and Ginsberg, B. (1986). Morphometric analysis of chondrocyte hypertrophy. *J. Bone Joint Surg. Am.* **68**, 243-255.
Dalal, A., Bhavani, G. S. L., Togarrati, P. P., Bierhals, T., Nandineni, M. R., Danda, S., Danda, D., Shah, H., Vijayan, S., Gowrishankar, K. et al. (2012). Analysis of the WISP3 gene in Indian families with progressive pseudorheumatoid dysplasia. *Am. J. Med. Genet. A* **158A**, 2820-2828.
Davis, L., Chen, Y. and Sen, M. (2006). WISP-3 functions as a ligand and promotes superoxide dismutase activity. *Biochem. Biophys. Res. Commun.* **342**, 259-265.
De Vos, K. J., Morotz, G. M., Stoica, R., Tudor, E. L., Lau, K.-F., Ackerley, S., Warley, A., Shaw, C. E. and Miller, C. C. (2012). VAPB interacts with the mitochondrial protein PTPIP51 to regulate calcium homeostasis. *Hum. Mol. Genet.* **21**, 1299-1311.
DeGeer, J., Kaplan, A., Mattar, P., Morabito, M., Stochaj, U., Kennedy, T. E., Debant, A., Cayouette, M., Fournier, A. E. and Lamarche-Vane, N. (2015). Hsc70 chaperone activity underlies Trio GEF function in axon growth and guidance induced by netrin-1. *J. Cell Biol.* **210**, 817-832.
Degli Esposti, M. (2002). Measuring mitochondrial reactive oxygen species. *Methods* **26**, 335-340.
Dolga, A. M., de Andrade, A., Meissner, L., Knaus, H.-G., Höllerhage, M., Christophersen, P., Zischka, H., Plesnila, N., Höglinger, G. U. and Culmsee, C. (2014). Subcellular expression and neuroprotective effects of SK channels in human dopaminergic neurons. *Cell Death Dis.* **5**, e999.
Doyle, S. R., Kasinadhuni, N. R. P., Chan, C. K. and Grant, W. N. (2013). Evidence of evolutionary constraints that influences the sequence composition and diversity of mitochondrial matrix targeting signals. *PLoS ONE* **8**, e67938.
Ekbote, A. V., Danda, D., Kumar, S., Danda, S., Madhuri, V. and Gibikote, S. (2013). A descriptive analysis of 14 cases of progressive-psuedorheumatoid-arthropathy of childhood from south India: review of literature in comparison with juvenile idiopathic arthritis. *Semin. Arthritis Rheum.* **42**, 582-589.
Engel, J. (2004). Role of oligomerization domains in thrombospondins and other extracellular matrix proteins. *Int. J. Biochem. Cell Biol.* **36**, 997-1004.
Fernandez-Marcos, P. J. and Auwerx, J. (2011). Regulation of PGC-1alpha, a nodal regulator of mitochondrial biogenesis. *Am. J. Clin. Nutr.* **93**, 884S-890S.
Garcia Segarra, N., Mittaz, L., Campos-Xavier, A. B., Bartels, C. F., Tuysuz, B., Alanay, Y., Cimaz, R., Cormier-Daire, V., Di Rocco, M., Duba, H.-C. et al. (2012). The diagnostic challenge of progressive pseudorheumatoid dysplasia (PPRD): a review of clinical features, radiographic features, and WISP3 mutations in 63 affected individuals. *Am. J. Med. Genet. C Semin. Med. Genet.* **160C**, 217-229.
Goldring, M. B., Birkhead, J. R., Suen, L. F., Yamin, R., Mizuno, S., Glowacki, J., Arbiser, J. L. and Apperley, J. F. (1994). Interleukin-1 beta-modulated gene expression in immortalized human chondrocytes. *J. Clin. Invest.* **94**, 2307-2316.
Goldring, M. B., Tsuchimochi, K. and Ijiri, K. (2006). The control of chondrogenesis. *J. Cell. Biochem.* **97**, 33-44.
Hajnoczky, G., Robb-Gaspers, L. D., Seitz, M. B. and Thomas, A. P. (1995). Decoding of cytosolic calcium oscillations in the mitochondria. *Cell* **82**, 415-424.
Holmstrom, K. M., Baird, L., Zhang, Y., Hargreaves, I., Chalasani, A., Land, J. M., Stanyer, L., Yamamoto, M., Dinkova-Kostova, A. T. and Abramov, A. Y. (2013). Nrf2 impacts cellular bioenergetics by controlling substrate availability for mitochondrial respiration. *Biol. Open* **2**, 761-770.
Hong, T., Ning, J., Yang, X., Liu, H.-Y., Han, J., Liu, Z. and Cao, W. (2011). Fine-tuned regulation of the PGC-1alpha gene transcription by different intracellular signaling pathways. *Am. J. Physiol. Endocrinol. Metab.* **300**, E500-E507.
Hurvitz, J. R., Suwairi, W. M., Van Hul, W., El-Shanti, H., Superti-Furga, A., Roudier, J., Holderbaum, D., Pauli, R. M., Herd, J. K., Van Hul, E. V. et al. (1999). Mutations in the CCN gene family member WISP3 cause progressive pseudorheumatoid dysplasia. *Nat. Genet.* **23**, 94-98.
Johnson, L. V., Walsh, M. L., Bockus, B. J. and Chen, L. B. (1981). Monitoring of relative mitochondrial membrane potential in living cells by fluorescence microscopy. *J. Cell Biol.* **88**, 526-535.
Lehninger, A. L. (1970). Mitochondria and calcium ion transport. *Biochem. J.* **119**, 129-138.
Liu, L., Li, N., Zhao, Z., Li, W. and Xia, W. (2015). Novel WISP3 mutations causing spondyloepiphyseal dysplasia tarda with progressive arthropathy in two unrelated Chinese families. *Joint Bone Spine* **82**, 125-128.
Ludtmann, M. H. R., Angelova, P. R., Zhang, Y., Abramov, A. Y. and Dinkova-Kostova, A. T. (2014). Nrf2 affects the efficiency of mitochondrial fatty acid oxidation. *Biochem. J.* **457**, 415-424.
Luo, H., Shi, C., Mao, C., Jiang, C., Bao, D., Guo, J., Du, P., Wang, Y., Liu, Y., Liu, X. et al. (2015). A novel compound WISP3 mutation in a Chinese family with progressive pseudorheumatoid dysplasia. *Gene* **564**, 35-38.
Lyons, A. B. and Parish, C. R. (1994). Determination of lymphocyte division by flow cytometry. *J. Immunol. Methods* **171**, 131-137.
Mallilankaraman, K., Doonan, P., Cárdenas, C., Chandramoorthy, H. C., Müller, M., Miller, R., Hoffman, N. E., Gandhirajan, R. K., Molgó, J., Birnbaum, M. J. et al. (2012). MICU1 is an essential gatekeeper for MCU-mediated mitochondrial Ca(2+) uptake that regulates cell survival. *Cell* **151**, 630-644.
Mick, D. U., Dennerlein, S., Wiese, H., Reinhold, R., Pacheu-Grau, D., Lorenzi, I., Sasarman, F., Weraarpachai, W., Shoubridge, E. A., Warscheid, B. et al. (2012). MITRAC links mitochondrial protein translocation to respiratory-chain assembly and translational regulation. *Cell* **151**, 1528-1541.
Miller, D. S. and Sen, M. (2007). Potential role of WISP3 (CCN6) in regulating the accumulation of reactive oxygen species. *Biochem. Biophys. Res. Commun.* **355**, 156-161.
Mittal, N., Babu, M. M. and Roy, N. (2009). The efficiency of mitochondrial electron transport chain is increased in the long-lived mrg19 Saccharomyces cerevisiae. *Aging Cell* **8**, 643-653.
Mootha, V. K., Lindgren, C. M., Eriksson, K.-F., Subramanian, A., Sihag, S., Lehar, J., Puigserver, P., Carlsson, E., Ridderstråle, M., Laurila, E. et al. (2003). PGC-1alpha-responsive genes involved in oxidative phosphorylation are coordinately downregulated in human diabetes. *Nat. Genet.* **34**, 267-273.
Mourier, A., Ruzzenente, B., Brandt, T., Kuhlbrandt, W. and Larsson, N.-G. (2014). Loss of LRPPRC causes ATP synthase deficiency. *Hum. Mol. Genet.* **23**, 2580-2592.
Murphy, M. P. (2009). How mitochondria produce reactive oxygen species. *Biochem. J.* **417**, 1-13.
Naskar, D., Maiti, G., Chakraborty, A., Roy, A., Chattopadhyay, D. and Sen, M. (2014). Wnt5a-Rac1-NF-kappaB homeostatic circuitry sustains innate immune functions in macrophages. *J. Immunol.* **192**, 4386-4397.
Nguyen, T., Sherratt, P. J., Nioi, P., Yang, C. S. and Pickett, C. B. (2005). Nrf2 controls constitutive and inducible expression of ARE-driven genes through a dynamic pathway involving nucleocytoplasmic shuttling by Keap1. *J. Biol. Chem.* **280**, 32485-32492.
Pal, A., Huang, W., Li, X., Toy, K. A., Nikolovska-Coleska, Z. and Kleer, C. G. (2012). CCN6 modulates BMP signaling via the Smad-independent TAK1/p38 pathway, acting to suppress metastasis of breast cancer. *Cancer Res.* **72**, 4818-4828.
Pasqua, T., Mahata, S., Bandyopadhyay, G. K., Biswas, A., Perkins, G. A., Sinha Hikim, A. P., Goldstein, D. S., Eiden, L. E. and Mahata, S. K. (2015). Impact of Chromogranin A deficiency on catecholamine storage, catecholamine granule morphology, and chromaffin cell energy metabolism in vivo. *Cell Tissue Res.* **363**, 693-712.
Pennica, D., Swanson, T. A., Welsh, J. W., Roy, M. A., Lawrence, D. A., Lee, J., Brush, J., Taneyhill, L. A., Deuel, B., Lew, M. et al. (1998). WISP genes are members of the connective tissue growth factor family that are up-regulated in wnt-

1-transformed cells and aberrantly expressed in human colon tumors. *Proc. Natl. Acad. Sci. USA* **95**, 14717-14722.
Perbal, B. (2013). CCN proteins: a centralized communication network. *J. Cell Commun. Signal.* **7**, 169-177.
Piantadosi, C. A., Carraway, M. S., Babiker, A. and Suliman, H. B. (2008). Heme oxygenase-1 regulates cardiac mitochondrial biogenesis via Nrf2-mediated transcriptional control of nuclear respiratory factor-1. *Circ. Res.* **103**, 1232-1240.
Ran, F. A., Hsu, P. D., Wright, J., Agarwala, V., Scott, D. A. and Zhang, F. (2013). Genome engineering using the CRISPR-Cas9 system. *Nat. Protoc.* **8**, 2281-2308.
Repudi, S. R., Patra, M. and Sen, M. (2013). WISP3-IGF1 interaction regulates chondrocyte hypertrophy. *J. Cell Sci.* **126**, 1650-1658.
Rizzuto, R., Marchi, S., Bonora, M., Aguiari, P., Bononi, A., De Stefani, D., Giorgi, C., Leo, S., Rimessi, A., Siviero, R. et al. (2009). Ca(2+) transfer from the ER to mitochondria: when, how and why. *Biochim. Biophys. Acta* **1787**, 1342-1351.
Sawada, N., Jiang, A., Takizawa, F., Safdar, A., Manika, A., Tesmenitsky, Y., Kang, K.-T., Bischoff, J., Kalwa, H., Sartoretto, J. L. et al. (2014). Endothelial PGC-1alpha mediates vascular dysfunction in diabetes. *Cell Metab.* **19**, 246-258.
Sen, M., Cheng, Y.-H., Goldring, M. B., Lotz, M. K. and Carson, D. A. (2004). WISP3-dependent regulation of type II collagen and aggrecan production in chondrocytes. *Arthritis Rheum.* **50**, 488-497.
Spiegelman, B. M. (2007). Transcriptional control of mitochondrial energy metabolism through the PGC1 coactivators. *Novartis Found Symp.* **287**, 60-63; discussion 63-69.
St-Pierre, J., Drori, S., Uldry, M., Silvaggi, J. M., Rhee, J., Jäger, S., Handschin, C., Zheng, K., Lin, J., Yang, W. et al. (2006). Suppression of reactive oxygen species and neurodegeneration by the PGC-1 transcriptional coactivators. *Cell* **127**, 397-408.
Sun, F.-C., Wei, S., Li, C.-W., Chang, Y.-S., Chao, C.-C. and Lai, Y.-K. (2006). Localization of GRP78 to mitochondria under the unfolded protein response. *Biochem. J.* **396**, 31-39.
Tanaka, S., Sugimachi, K., Maehara, S.-I., Shimada, M. and Maehara, Y. (2003). A loss of function mutation in WISP3 derived from microsatellite unstable gastric carcinoma. *Gastroenterology* **125**, 1563-1564.
Villa-Bellosta, R., Rivera-Torres, J., Osorio, F. G., Acin-Perez, R., Enriquez, J. A., Lopez-Otin, C. and Andres, V. (2013). Defective extracellular pyrophosphate metabolism promotes vascular calcification in a mouse model of Hutchinson-Gilford progeria syndrome that is ameliorated on pyrophosphate treatment. *Circulation* **127**, 2442-2451.
Wakabayashi, N., Skoko, J. J., Chartoumpekis, D. V., Kimura, S., Slocum, S. L., Noda, K., Palliyaguru, D. L., Fujimuro, M., Boley, P. A., Tanaka, Y. et al. (2014). Notch-Nrf2 axis: regulation of Nrf2 gene expression and cytoprotection by notch signaling. *Mol. Cell. Biol.* **34**, 653-663.
Wenz, T. (2009). PGC-1alpha activation as a therapeutic approach in mitochondrial disease. *IUBMB Life* **61**, 1051-1062.
Wieckowski, M. R., Giorgi, C., Lebiedzinska, M., Duszynski, J. and Pinton, P. (2009). Isolation of mitochondria-associated membranes and mitochondria from animal tissues and cells. *Nat. Protoc.* **4**, 1582-1590.
Wu, Z., Puigserver, P., Andersson, U., Zhang, C., Adelmant, G., Mootha, V., Troy, A., Cinti, S., Lowell, B., Scarpulla, R. C. et al. (1999). Mechanisms controlling mitochondrial biogenesis and respiration through the thermogenic coactivator PGC-1. *Cell* **98**, 115-124.
Xiao, Y., Karnati, S., Qian, G., Nenicu, A., Fan, W., Tchatalbachev, S., Höland, A., Hossain, H., Guillou, F., Lüers, G. H. et al. (2012). Cre-mediated stress affects sirtuin expression levels, peroxisome biogenesis and metabolism, antioxidant and proinflammatory signaling pathways. *PLoS ONE* **7**, e41097.
Yang, X., Song, Y. and Kong, Q. (2013). Diagnosis and surgical treatment of progressive pseudorheumatoid dysplasia in an adult with severe spinal disorders and polyarthropathy. *Joint Bone Spine* **80**, 650-652.
Zampese, E., Fasolato, C., Kipanyula, M. J., Bortolozzi, M., Pozzan, T. and Pizzo, P. (2011). Presenilin 2 modulates endoplasmic reticulum (ER)-mitochondria interactions and Ca2+ cross-talk. *Proc. Natl. Acad. Sci. USA* **108**, 2777-2782.
Zhou, C., Huang, Y., Shao, Y., May, J., Prou, D., Perier, C., Dauer, W., Schon, E. A. and Przedborski, S. (2008). The kinase domain of mitochondrial PINK1 faces the cytoplasm. *Proc. Natl. Acad. Sci. USA* **105**, 12022-12027.
Zhou, R., Yazdi, A. S., Menu, P. and Tschopp, J. (2011). A role for mitochondria in NLRP3 inflammasome activation. *Nature* **469**, 221-225.
Zhou, H., Zheng, C., Su, J., Chen, B., Fu, Y., Xie, Y., Tang, Q., Chou, S.-H. and He, J. (2016). Characterization of a natural triple-tandem c-di-GMP riboswitch and application of the riboswitch-based dual-fluorescence reporter. *Sci. Rep.* **6**, 20871.

The FASEB Journal / Volume 34, Issue S1 / p. 1-1

Biochemistry and Molecular Biology | Free Access

CCN6 REGULATES MITOCHONDRIAL RESPIRATORY COMPLEX ASSEMBLY AND ACTIVITY

Deepesh Kumar Padhan, Archya Sengupta, Milan Patra, Sushil Kumar Mahata, Ananya Ganguly, Malini Sen

First published: 20 April 2020
https://doi.org/10.1096/fasebj.2020.34.s1.02868

Abstract

Background

CCN6 is a multidomain protein of mesenchymal origin. Mutations in CCN6 lead to PPRD (Progressive Pseudo Rheumatoid Dysplasia), which is associated with cartilage loss, muscle wasting and restricted skeletal development. Mechanism of PPRD pathogenesis and its connection with CCN6 is unclear. Previously we documented that CCN6 localizes to mitochondria and regulates ATP production. Here we have investigated the molecular mechanism of this regulation in context of PPRD.

Objective

1. To check whether CCN6 regulates mitochondrial respiratory complex assembly and activity.
2. To check if engineering PPRD causing CCN6 mutations alters the function of the mitochondrial respiratory complex.

Methods

CCN6 expression was depleted by siRNA transfection in C28/I2 chondrocyte cell line. CCN6 mutants were generated by CRISPR-Cas9 technology. CCN6 association with respiratory complex was assessed by 2D BN/SDS PAGE & size-exclusion chromatography. Mitochondrial respiratory complex activity/assembly was assessed spectrophotometrically and by BN-PAGE in-gel assay. Transmission electron microscopy (TEM) was used to study mitochondrial morphology.

Results

Size-exclusion chromatography and 2D BN/SDS PAGE of mitochondria reveals that CCN6 is associated with Complex I/Super complexes of mitochondrial electron transport chain. Partial depletion of CCN6 by siRNA shows close association of RER with mitochondria and alteration of its mitochondrial distribution relative to cytosol, thereby resulting in increased Complex I activity and

assembly. CCN6 mutation (truncation in exon 5, similar to PPRD linked mutation), however, results in disrupted complex I activity and assembly. CCN6 mutation also correlates with distorted mitochondria and mitophagy.

Conclusion

CCN6 is required for the regulation of mitochondrial respiratory complex activity/assembly in chondrocytes, which involves controlled juxtaposition of RER-mitochondria. Mutations in CCN6 disrupt respiratory complex activity/assembly and cause mitophagy.

Support or Funding Information

This work is supported by a grant from the Department of Science and Technology, Grant No-SB/SO/BB-016/2014 and Department of Biotechnology, Grant No-BT/PR24244/MED/12/764/2017, Ministry of Science and Technology, Government of India. D.K.P. is supported by the Council of Scientific and Industrial Research (CSIR) fellowship, A.S is supported by DBT-RA programme and A.G is supported by University Grant Commission (UGC), Government of India.

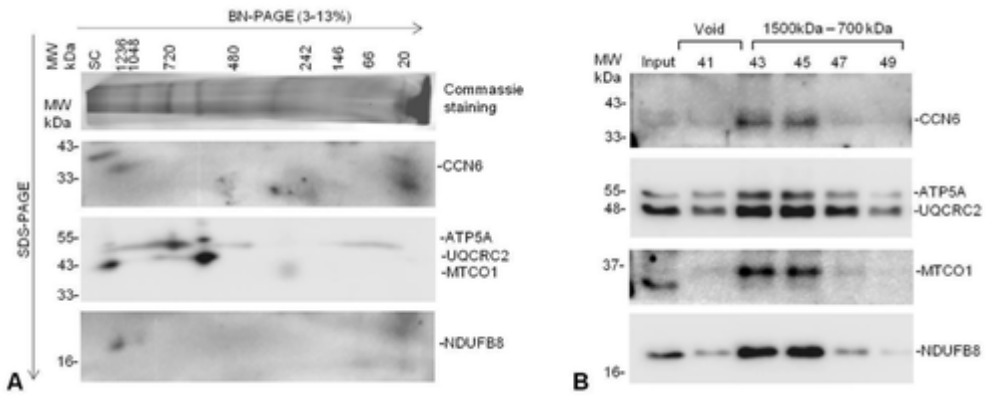

Figure 1

Open in figure viewer | PowerPoint

CCN6 migrates as a high molecular weight complex with mitochondrial respiratory complex proteins.

CCN6 remains as high molecular weight complex in mitochondria along with subunits of mitochondrial electron transport chain including complex I subunit NDUFB8 as shown by 2D BN-PAGE/SDS-PAGE **(A)** and size exclusion chromatography **(B)** of mitochondrial lysate from C28/I2 cells (chondrocyte line).

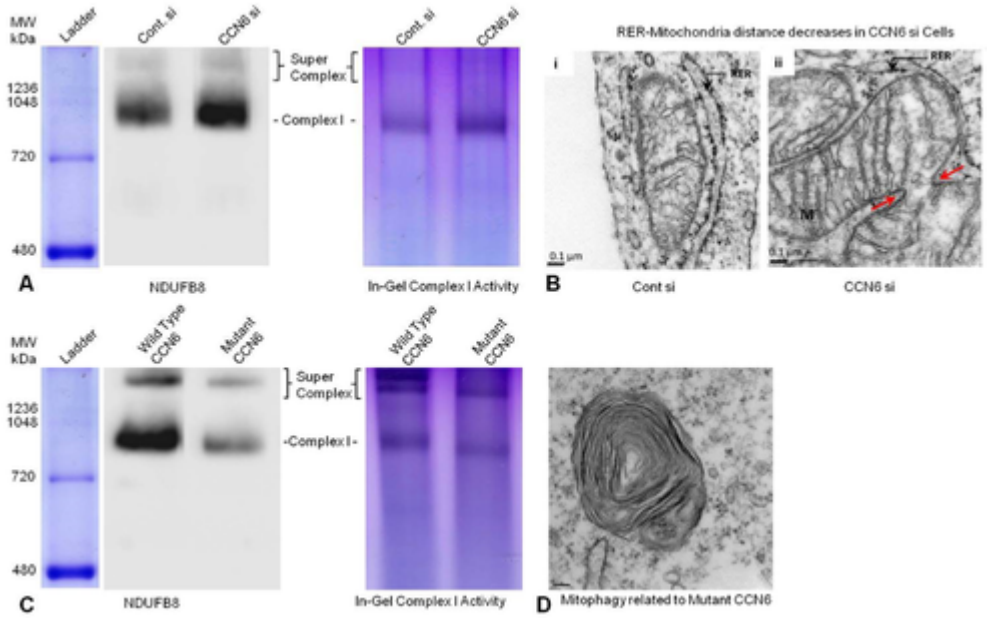

Figure 2

Open in figure viewer | PowerPoint

CCN6 regulates mitochondrial respiratory complex assembly and activity.

(A) Increased Complex I assembly and activity was documented by BN-PAGE western blot with NDUFB8 (Complex I subunit) antibody and in-gel Complex I activity assay in CCN6 siRNA transfected (CCN6 partially depleted) C-28/I2 cells (CCN6 si) as compared to control cells (Cont.si). **(B)** Transmission Electron Microscopy (TEM) micrographs showing decreased RER-Mitochondria distance in CCN6 siRNA transfected cells. **(C)** BN-PAGE western blot with NDUFB8 antibody and in-gel Complex I activity of CRISPR Cas9 mediated PPRD causing CCN6 mutants shows reduced Complex I/Super complex assembly and activity. **(D)** TEM micrographs shows presence of mitophagy in CCN6 mutant cells.. RER: Rough endoplasmic reticulum. M: Mitochondria